SPACE STATION TRACKING REQUIREMENTS FEASIBILITY STUDY

Final Report
Volume I

Contract No. NAS9–17414

Prepared for

NASA Lyndon B. Johnson Space Center
Houston, TX 77058

Technical Monitor: Sid Novosad

Prepared by

Sergei Udalov
James Dodds

Contributions by

Dr. Gaylord K. Huth
Dr. K. T. Woo
Dr. Robert Scholtz
Dr. Unjeng Cheng
Richard Austin

Axiomatix
9841 Airport Boulevard
Suite 1130
Los Angeles, CA 90045

Axiomatix Report No. R8807-3
July 27, 1988

TABLE OF CONTENTS

VOLUME I

1.0 INTRODUCTION AND OVERVIEW

The objective of this feasibility study was to determine analytically the accuracies of various sensors which are being considered as potential candidates for Space Station use. Specifically, the feasibility studies were performed to determine whether or not the candidate sensors are capable of providing the required accuracy, or if alternate sensor approaches should be investigated. Other topics related to operation in the Space Station environment were considered as directed by NASA-JSC.

The following topics were addressed in the report:

- Space Station GPS
- Space Station Radar
- Docking Sensors
- Space Station Link Analysis
- Antenna Switching, Power Control, and AGC Functions for Multiple Access
- Multi-Channel Modems
- FTS / EVA Emergency Shutdown
- Space Station Information Systems (SSIS) Coding
- Wanderer Study
- Optical Communications System Analysis.

The following sections present brief overviews of the above-mentioned topics. Wherever applicable, the appropriate appendices provide detailed technical analysis of these topics.

This report is presented in two volumes. Volume I contains the main body and Appendices A through J. Volume II contains Appendices K through U.

2.0 SPACE STATION GPS

2.1 Background Information

The Space Station System consists of unmanned space platforms, free-flying satellites, orbital transfer vehicles (OTV), and orbital maneuvering vehicles (OMV) that interact with the manned Space Station, along with the Space Transportation System (STS), in orbit [2.1]. In addition, the Space Station System is aided by the TDRSS (Satellites and Whitesands Ground Terminal) and ground control stations (Network Control Center NCC and Mission Control Center MCC). Figure 2.1-1 illustrates the Space Station System graphically. Table 2.1-1 summarizes the number of vehicles and their expected ranges from the Space Station.

For efficient utilization of these vehicular elements, many detached operations will be performed in parallel. This will require the Space Station to have a traffic control system to monitor and coordinate these related operations. The relative positions of the Space Station and the vehicles must be determined continuously. In other words, both the Space Station and the detached vehicles must be tracked.

In order to facilitate and standardize the Space Station tracking and traffic control operations, and "Operational Control Zone" (OCZ) concept was described in [2.1], which segments the Space Station's Communication and tracking requirements into coverage "zones" according the functions. Figure 2.1.2 illustrates the Operational Control Zones as described in [2.1].

Considering both the vehicle range requirements and the OCZ's illustrated in Figure 2.1-2, the Space Station Tracking Performance Requirements are summarized in Table 2.1-2, which divides tracking requirements into four categories: Long Range Tracking, Short Range Tracking, Proximity Operations Tracking, and Docking Sensors [2.2].

One of the objectives of this study was to investigate the feasibility of using the NAVSTAR Global Positioning System (GPS) or a GPS-based system for Space Station

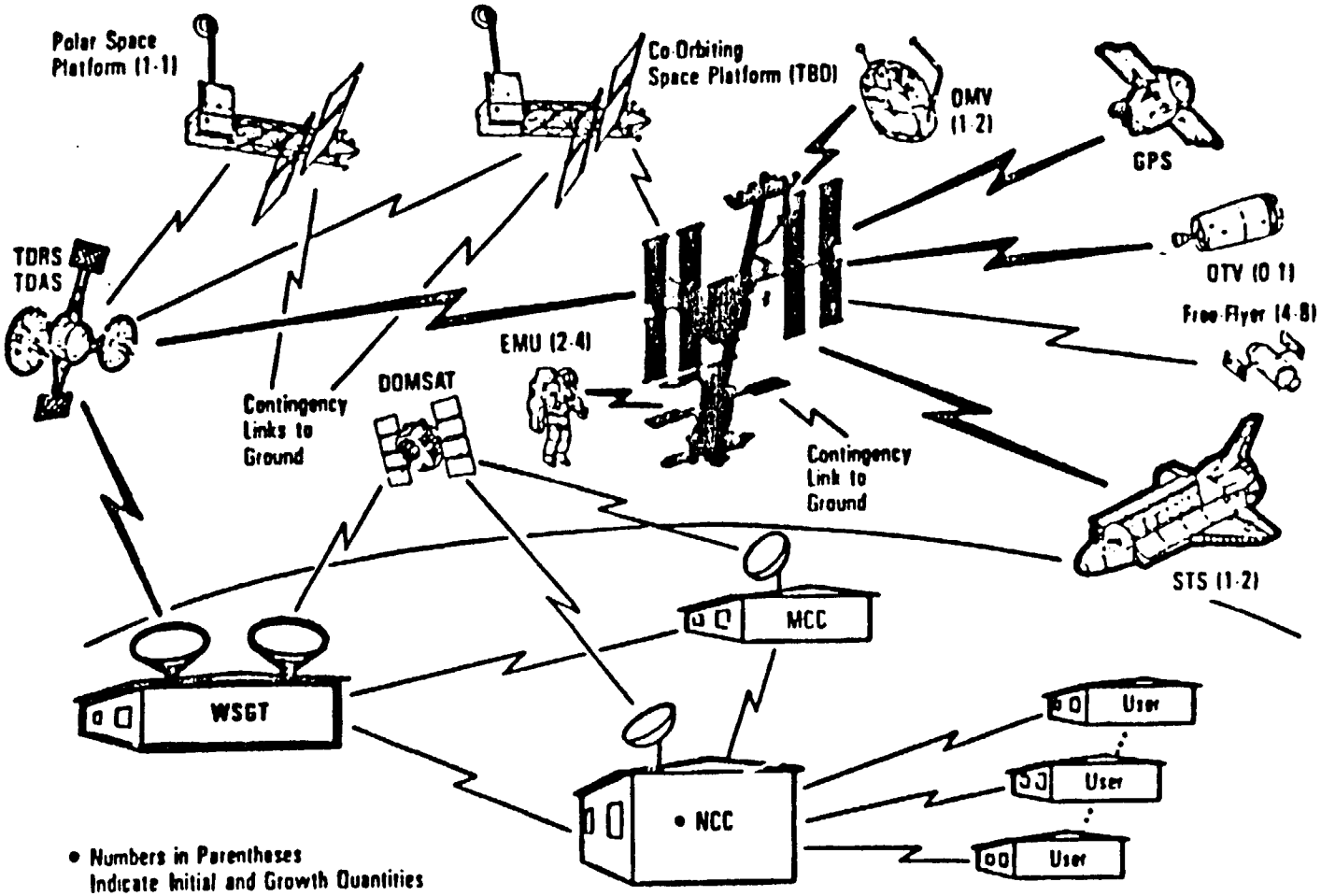

Figure 2.1-1. Vehicle Tracking Requirements in the Space Station System.

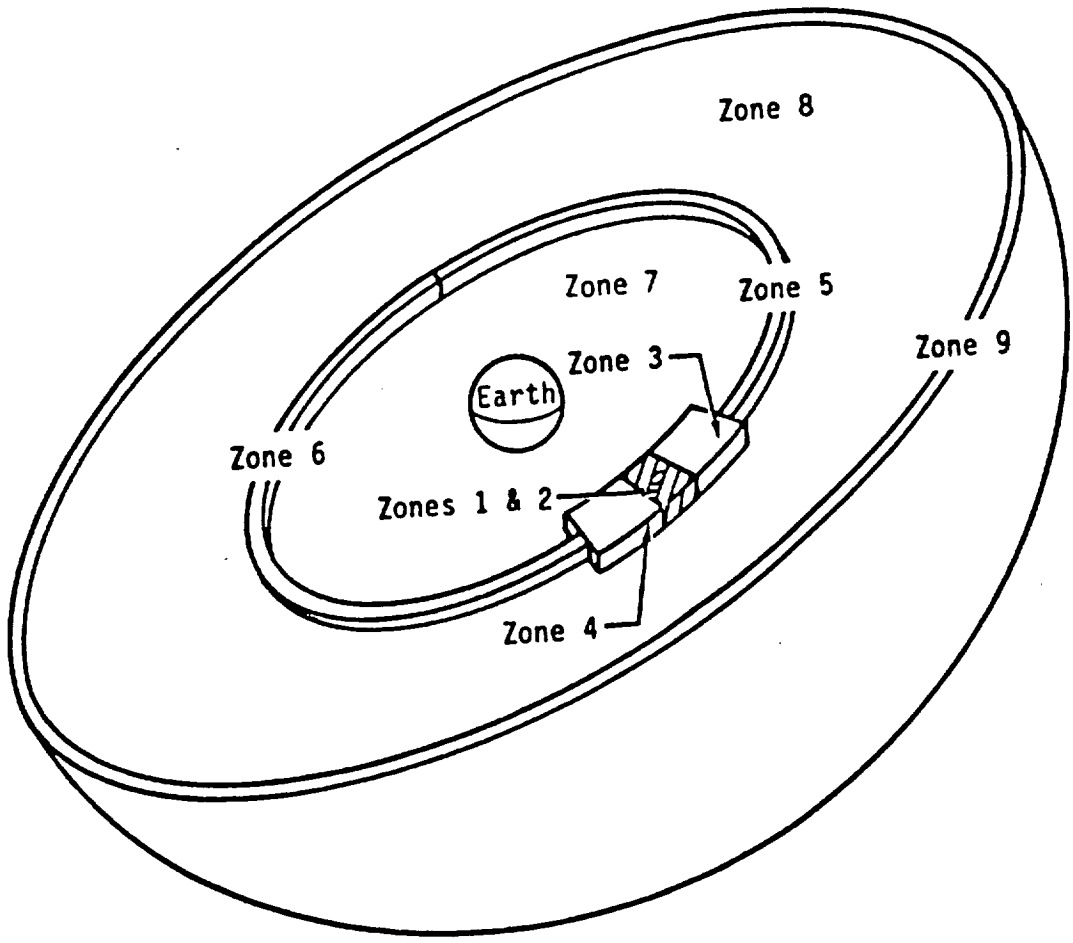

Figure 2.1-2. Cutaway view of operational control zones (hemispherical cutaway) for Space Station Tracking and Traffic Control (from [1]).

tracking. In particular, the short range, long range, and proximity operations tracking requirements listed in Table 2.1-1 are of special interest here because the accuracy requirements of these three types of Space Station Tracking objectives are approximately within the capability of an appropriately designed GPS based system.

There are at least three known approaches in using GPS transmissions for radio-navigation and user position determination:

(1) standard GPS using P-code or C/A code,

(2) differential GPS using P-code or C/A code,

(3) radio-interferometry using SERIES-X (Satellite Emission Range Inferred Earth Surveying) type of techniques which does not require the knowledge of either the P or the C/A codes [2.3], [2.4], [2.5].

The standard GPS approach has the advantage of not requiring a cooperative reference station whose location is required to be known. However, it has some drawbacks. With GPS's Selective Availability Plan, the accuracy of a C/A code user is degraded. The P-code user can achieve good accuracy. However, P-code is classified and its access requires Department-of-Defense permission.

Differential GPS (DGPS) and the SERIES type of approaches can offer better accuracy than the standard GPS since they are differential approaches and have the capability of cancelling error sources which are common to both the user and the reference station. This capability also allows them to mitigate the effect of denial of accuracy created by the GPS's Selective Availability Plan. Being differential approaches, they both will, however, require cooperative reference stations whose locations are surveyed and known. Another drawback of the differential approaches is that there will be an error contribution, due both to the distance between the reference and the user and the uncertainty in the knowledge of the ephemeris of the GPS satellite. When the distance between the user and

Table 2.1-1. Number of Vehicles and Ranges from the Space Station.

Vehicle Type	Quantities	Ranges
Free Flyers	4 – 8	2000 km
Space Shuttle Orbiters	1 – 2	37 km
Orbital Transfer Vehicles (OTV)	1	185 km
Orbital Maneuvering Vehicles (OMV)	1 – 2	185 km
Extravehicular Mobility Units (EMU)	2 – 4	1 km

Table 2.1-2. Summary of Space Station Tracking Requirements.

Function	Performance Requirement
Long Range Tracking	Max Range: 1080 m Coverage: Limited to comm data link coverage Accuracy: (GPS position) ±15 m (49.2 ft.)
Short Range Tracking	Max Range: 20 nm Coverage: 4 PI steradians Accuracies: Angle: ±10 MRad (0.57 deg.) Range: ±100 m (328 ft.) or 1% Velocity: .3 m/sec (1 fps) or 1 %
Proximity Operations Tracking	Max Range: 1000 ft. Coverage: Limited to comm data coverage Accuracy: (GPS position) ±1m (3.3 ft.)
Docking Sensors	Max Range: 1000 ft. Coverage: 20 deg. cone Accuracies: Angle: ±0.5 cm (.02 ft.) Range: ±2 MRad (0.1 deg.) Velocity: 1.0 cm/sec (0.03 fps) Attitude: ±10 MRad (0.57 deg.)

M = meter
m = milli

the reference station is large, this error can be significant, and may destroy the performance advantages of the differential approaches over the standard approach.

In this section, only the achievable accuracies of Standard GPS with respect to the Space Station requirements are summarized. The performance with DGPS and SERIES type of arrangements is discussed in sections 2.2. and 2.3, respectively.

References

[2.1] Nader, B.A. and Dupont, A.L., "Space Station Operations Operational Control Zones," Report No. 84-FM-62/JSC-20235, published by Mission Planning and Analysis Division, NASA-JSC, May 1985.

[2.2] Draft Statement of Work on "Space Station Tracking Requirements Feasibility Study," issued by NASA-JSC, May 1985.

[2.3] P. F. MacDoran, R. B. Miller, L. A. Buennagel, H. G. Fliegel, and L. Tanida, "Codeless GPS Systems for Positioning of Offshore Platforms and 3D Seismic Surveys," Journal of the Institute of Navigation, Summer 1984.

[2.4] Ondraski, V.J. and Wu, S.C., "A Simple and Economical Tracking System with Subdecimeter Earth Satellite and Ground Receiver Position Determination Capabilities," 3rd International Symposium on the Use of Artificial Satellites for Geodesy and Geodynamics, Ermioni, Greece, September 20 – 24, 1982.

[2.5] Crow, R.B., et al., "SERIES-X Final Engineering Report," NASA-JPL Report JPL-D-1476, August 1984.

2.2 Space Station Tracking with Standard GPS

Based on the C/A and P-code positioning results derived in Appendix A, the following conclusions can be made:

(1) A 9-M positioning accuracy is achievable using the GPS L1-P-code signal in the Space Station altitude of 500 km. P-code performance using the standard GPS navigation solution is relatively insensitive to the receiver noise figure (noise figures in the range from 1 to 5 dB will be acceptable). This will meet the Space Station's short and long range tracking requirements of 100 M and 15 M positioning accuracies, respectively.

(2) C/A code positioning accuracy will be degraded to 100 M under accuracy denial according to the current DOD Selective Availability Plan. Without accuracy denial, the L1-C/A code positioning accuracy in the Space Station altitude is expected to be ≈12 M and 10 M for receivers with 5 dB and 1 dB noise figure, respectively. The Selective Availability Plan is expected to be in effect in the operational GPS. Thus, it can be concluded that the C/A code users, utilizing the standard GPS navigation solution, can only meet the short range tracking requirement of the Space Station.

(3) Lowering the receiver noise figure to 1 dB (from 5 dB) does not provide significant performance improvements for the standard GPS using either P or C/A codes. The dominating error sources in standard GPS are errors in the GPS Space and Control Segments. They cannot be eliminated unless some forms of differential GPS are used.

It is expected that either the Differential GPS (DGPS) or the SERIES-X types of radio positioning, both of which are capable of mitigating the effects of the denial of accuracy and the errors common to the user and the reference station (such as GPS Space and Control Segment errors), will have better achievable positioning accuracies than the

standard GPS results. However, these differential schemes will require cooperative reference stations whose locations are surveyed, and communication links between the reference station and the users. The performance of DGPS and the SERIES-X types of positioning techniques will be discussed in forthcoming reports.

The estimated positioning accuracies using L1,C/A or P-code signals with Standard GPS navigation positioning algorithms are summarized in Table 2.2-1 for easy reference.

2.3 Performance of Differential GPS for Space Station Tracking and Traffic Control

2.3.1 General Considerations

Performance of Space Station tracking with standard GPS was discussed in Section 2.2. It was estimated that in the Space Station environment the positioning accuracies of the Space Station and the detached vehicles using standard GPS P-code ranging can be as good as ≈9 M (1-σ). This is appreciably more accurate than the commonly budgeted P-code position accuracy of 15 M. There are two justifications for this expected improvement: (i) the tropospheric delay error is negligible at the Space Station's 500 KM altitude; and (ii) the multipath error can be appreciably smaller than surface users by careful design and placement of the GPS antennas.

While the 9 M position accuracy can meet the long range and short range tracking requirements (± 15 M and ± 100 M, respectively) of the Space Station, it does not meet the proximity operation requirement of ± 1 M. In order to meet the accuracy requirement of proximity operations, it is necessary to apply some form of differential GPS (DGPS) measurement rather than the standard GPS method of position determination. In the DGPS process, the common error sources such as satellite clock error, satellite ephemeris prediction errors, and denial of accuracy effects, which are observed simultaneously by the Space Station and the detached vehicles, can be eliminated. This results in improved relative positioning accuracy between the Space Station and the detached vehicles. The

Table 2.2-1. Summary of Positioning Accuracy.*

RECEIVER NOISE FIG.	BEFORE OR AFTER FILT.	C/A CODE WITH ACCURACY DENIAL	C/A CODE WITHOUT ACCURACY DENIAL	P CODE WITH SELECTIVE AVAILABILITY
5 dB (28 dB°K)	BEFORE FILTERING	100 M	27.4 M	13.0 M
	AFTER FILTERING	100 M	11.9 M	8.8 M
1 dB (18.76 dB°K)	BEFORE FILTERING	100 M	18.9 M	12.3 M
	AFTER FILTERING	100 M	9.9 M	8.6 M

* L1 Link with PDOP = 3.0 are assumed for all cases here.

various error sources in DGPS position determination and the achievable accuracies are discussed in Appendix B. It should be noted here that in the proposed DGPS approach relative positions are determined rather than absolute positions. This, however, should not have any significant negative impacts on traffic control since relative positions between the Space Station and the detached vehicles are more important than their respective absolute positions for this application.

It is deemed necessary, however, to have both standard GPS and differential GPS navigation capabilities for Space Station tracking although DGPS can provide better accuracies in relative position determination than standard GPS. The reasons for requiring standard GPS capabilities are the following:

(1) DGPS requires the Space Station and the detached vehicles to be in view of the same set of four GPS satellites. This may not be possible for some detached vehicles in certain orbital conditions (e.g., the Space Shuttle during ascent). For those situations standard GPS will be useful for relative tracking.

(2) In order to achieve high relative positioning accuracy, the pseudorange measurements made by the Space Station and the detached vehicles must be accurately time-tagged and compared. Due to high orbital velocities, time-tagging should be performed with user clocks which are properly aligned with GPS system time by the GPS Time-Transfer Approach. This requires standard GPS receivers for time-transfer operations, which can result in time-transfer errors of the order of ≤ 1 μs.

With a low-noise (1-dB noise figure) receiver design, proper antenna configuration to minimize multipath, and accurate system timing to minimize time-tagging error, our analysis shows that DGPS can provide relative position accuracies of $\approx$ 1.01 M and 1.3 M, respectively, for the Space Station proximity operations and short range tracking

requirements. Long range tracking, if needed, can be provided by standard GPS which can achieve position accuracies of 9 M. In both cases P-code is assumed available.

2.3.2 Conclusions

Two main conclusions that come as a result of this study are:

(1) With careful receiver design and environmental control for multipath, it is expected that P-code DGPS can meet the relative positioning accuracy requirements for space station traffic control. C/A code DGPS will meet the long and short range tracking requirements; however, it falls short of meeting the proximity operation requirement (accuracy = 1.6 M instead of 1.0 M). The design constraints can be summarized as follows:

- Low noise receiver design (NF = 1 dB)
- Narrow code loop bandwidth (0.5 to 1 Hz)
- Fine code loop NCO resolution (1/64 for P, 1/512 for C/A)
- Careful placement and design of GPS antennas (0.2 M for P-code, 0.5 M for C/A code).
- Small Kalman filter mechanization error ($\leq$ 0.2 M)
- Minimum time tagging errors in differential ranges
- Position locations are relative to reference station (i.e., not absolute location determination).

(2) Both DGPS and standard GPS should be valid sensors for Space Station traffic control tracking. DGPS will be needed for short range and proximity operations tracking because of accuracy requirements for close range applications. Standard GPS will be required for time transfer to allow clock alignments for the purpose of time-tagging. It will also be needed for some long range tracking operations where the detached vehicle and the Space Station cannot both see the same set of four GPS satellites. Table 2.3.2-1 summarizes these conclusions.

BOTH STANDARD GPS AND DGPS SHOULD BE VALID SENSORS FOR SPACE STATION TRACKING , WITH OVERLAPPING REGIONS OF COVERAGE.

TECHNIQUE	APPLICATIONS	ESTIMATED PERFORMANCE
STANDARD GPS	LONG RANGE AND SHORT RANGE TRACKING, ESPECIALLY WHEN THE SPACE STATION AND THE DETACHED VEHICLE CANNOT SEE THE SAME 4 GPS SATELLITES	$1-\sigma$ POSITION ERRORS (PDOP =3): P-CODE = 8.6 - 8.8 m C/A CODE WITHOUT ACCURACY DENIAL =12.5 -18 m C/A CODE WITH ACCURACY DENIAL = 100 m
DGPS	SHORT RANGE AND PROXIMITY OPERATION TRACKING (AND POSSIBLY LONG RANGE TRACKING), WHEN SPACE STATION AND DETACHED VEHICLE CAN SEE THE SAME 4 GPS SATELLITES, ALSO WHEN HIGH TRACKING ACCURACIES ARE REQUIRED.	$1-\sigma$ RELATIVE POSITION ERRORS (PDOP =3): P-CODE = 1.01 m (PROXIMITY) 1.31 m (SHORT RANGE) C/A CODE: 1.60 m (PROXIMITY) 1.81 m (SHORT RANGE)

Table 2.3.2-1. Preliminary Conclusions.

2.4 Codeless Tracking of GPS Signals Using a SERIES Receiver

Most GPS receivers employ a despreading operation which consists of cross-correlating the received wideband signal (C/A or P channel) with a locally generated replica of the spread-spectrum code signal to measure time-of-arrival and demodulate the data needed for navigation calculations. These techniques require knowledge of the appropriate code, a code generator, and code synchronization circuitry in the receiver for each GPS satellite signal to be received, with a complexity dependent on the choice of serial or parallel processing of GPS satellite signals.

A technique, which avoids the need for any code information and in fact does not even require the satellite orbit and clock data (a priori), was developed at the jet Propulsion Laboratory by Peter MacDoran in late 1970's [2.6] – [2.10]. MacDoran retained the commercial rights to the system, called SERIES (Satellite Emission Range Inferred Earth Surveying), and left JPL to form ISTAC, Inc., (International Series Technology Applications Corporation). The authors visited ISTAC, Inc., on September 5, 1985, viewed a demonstration of the SERIES receiver in operation, and discussed the system's capabilities with MacDoran. MacDoran feels that the Space Stations navigation specifications can be met by ISTAC's present tested technology, and noted in passing that ISTAC is willing to perform funded demonstrations for interested parties.

The purpose of this section is to give our impressions of the modus operandi of a receiver with SERIES capability and, in particular, how such a receiver replaces the information which could have been attained with knowledge of the C/A and/or P codes.

One possible receiver processing is described in [2.10], in which:

(1) The received GPS signals are simultaneously received and passed through a "spectral" compressor" which creates a set of pure tones at the received C/A clock rate, P clock rate, 2 x L_2 carrier frequency, etc.

(2) The phases of these tones are measured relative to local clocks at two receivers, with tones from different satellites being sorted by doppler shift characteristics.

(3) Phase measurement differencing of a single tone between two receivers and between two satellites is used to eliminate most large error sources, including local clock uncertainties, etc., leaving a doubly differenced phase measurement known modulo 2π. Signals from four satellites must be processed in this manner to supply enough data for navigation.

(4) The phase 2π ambiguities in the measurements of (3) are resolved sequentially first for the longest wavelength tone, then the next longest, etc., with the unambiguous phase tracking accuracy of each tone being sufficient to unambiguously resolve the phase of the next higher frequency tone.

(5) Satellite ephemeris data can be developed from direct observation of the satellite signals over a period of time [2.7], from a cold system start, presumably by observations of GPS signal doppler and doppler rate by stations at known locations.

It is worth noting that the system can be jammed by large numbers of in-band tones, or by jamming the data link between the two user receivers which are carrying out differential measurements. hence, communication security cannot be guaranteed.

The spectral compressor described in (1) above could be a delay-and-multiply operation [2.10] carried out on the wideband GPS signal with filtering following multiplication. The adverse signal-to-noise ratio at the input to the compressor, because of the wide bandwidth of the GPS signal, means that a low-noise receiver and very narrow post-multiplication filtering are necessary. (MacDoran indicated to us that the ISTAC equipment used a 60°K amplifier and 0.1 Hz bandwidth FFT filters.)

The above comments should indicate that codeless GPS precise positioning is possible, suggest a method, and name one commercial supplier.

Appendix C describes a study of a method for spacecraft position location based on observations of the Global Positioning System (GPS) satellites' signals. In the "codeless technique" described these, the user does not require access to the P-code information used in standard GPS receivers to demodulate the wideband GPS signal with a correlation detector. Instead, the user develops a set of Doppler-shifted tones from each satellite's wideband signal, and derives its location via Doppler navigation and tone-ranging techniques.

Our further study of this technique was terminated when it was determined that P-code assess would be granted to Space Station users.

References

[2.6] P. F. MacDoran, J. H. Whitcomb, and R. B. Miller, "Codeless GPS Positioning Offers Sub-Meter Accuracy," Sea Technology, October 1984.

[2.7] P. F. MacDoran, R. B. Miller, L. A. Buennagel, H. G. Fliegel, and L. Tanida, "Codeless GPS Systems for Positioning of Offshore Platforms and 3D Seismic Surveys," Journal of the Institute of Navigation, Summer 1984.

[2.8] P. F. MacDoran, J. H. Whitcomb, R. B. Miller, and L. A. Buennagel," Codeless GPS Systems for Marine Positioning and Navigation," Proceedings of the Offshore Technology Conference, 1985.

[2.9] P. F. MacDoran, R. B. Miller, L. A. Buennagel, and J. H. Whitcomb," Codeless Systems for Positioning with NAVSTAR-GPS," presented at the First International Symposium on Precise Positioning with the Global Positioning System, Rockville, MD, 15 – 19 April 1985.

[2.10] T. P. Yunck, "An Introduction to SERIES-X," JPL Notes, November 1982.

25 Space Station GPS Navigation Simulation

To provide for analytical support and simulation of GPS related problems, Axiomatix had to consider various analytical assumptions upon which to base our quantitative investigations. We have summarized the related background and procedures in a special report which constitutes Appendix D.

The material presented in Appendix D constitutes theoretical background information used for simulation of GPS navigation by the Space Station. Section 1 deals with the computation of the satellite position in its respective orbit. Section 2 addresses an important issue of GPS satellite visibility by a user. In Section 3, the concepts GDOP and PDOP are defined analytically. Kalman filtering for pseudorange and delta pseudorange is summarized mathematically in Section 4. Finally, in Section 5, the steps involved in simulation of GPS navigation are summarized.

3.0 SPACE STATION RADAR CONSIDERATIONS

In this section, we provide a brief summary of our effort in the area of Space Station radar sensors. Although as the result of NASA "scrub," the requirement for a radar was eliminated from the IOC phase, the material presented here reflects our thinking during the earlier phases of the study. Basically, we have considered two types of radar: (1) long range radar capable of operating up to 2000 km and (2) control zone radar operating up to 37 km. The first case reflects some of our original thinking on the subject. The second case deals with the performance of an unmodified shuttle Ku-Band radar and the comparison of this radar to a phased-array multi-target radar proposed by RCA, a Phase B contractor.

3.1 Long Range Tracking Radar

3.1.1 Functions and Applications

The justification for a long range radar capability for the Space Station is predicated upon the existence of several applications where the long range radar can either perform certain unique function or can significantly augment the operation of another type of tracking service such as can be provided either by GPS or, at least in part, by a communications transponder. Among the areas where the long range radar can be utilized, the following functions and/or application have been identified so far for the 185 km to 2000 km range:

(1) Augment the tracking service provided by relaying of GPS positional data to Space Station (SS).

(2) Providing tracking data to the space traffic control system.

(3) Serving as a part of orbital control in the range of 185 km to 2000 km.

(4) Aiding in detecting users at maximum range of 2000 km and providing angular information for pointing high gain SS comm link antennas.

(5) Provide tracking information for hand-over from co-orbiting (zones 5 and 6) to rendezvous zones 3 and 4, the latter having their outer limits at 185 km.

Additional arguments supporting these potential applications are presented below.

The use of GPS received on co-orbiting vehicles and the telemetering of the GPS positional data to SS via a communication link has been baselined as a primary mode of long range tracking [3.1]. However, this baseline raises an issue of requiring a GPS receiver on all free flyers. There also is the issue of requiring a GPS receiver on all free flyers. There also exists an argument that a secondary source of tracking/navigation information can be supplied by communication system auto-tracking.

Regardless of the validity of either of the arguments, the fact remains that both of the methods require the communication link and thus are not autonomous. Beacon-aided radar/tracking, therefore, can provide for a true back-up capability for long range navigation and tracking.

Autonomous radar-based system can provide the Space Station with capability of tracking free flyers and other vehicles without dependence on the comm link or any other means such as ground track. This autonomy may be of great value to space traffic control and to the orbital control functions.

Another function which long range tracking can provide is to supply angular information for pointing high directivity antennas of the SS for establishing a high rate comm link at long ranges. This function, however, is predicated on the existence of the requirement for such high rate comm links up to 2000 km and it should thus not be the primary reason for long range radar.

3.1.2 Technical Issues

In this section, we consider some key issues which are involved in regards to the feasibility of having a radar operation up to the extreme tracking range of 2000 km.

Although formally there is no radar coverage requirement for the coorbiting satellite zones 5 (leading) and 6 (trailing), several advantages of providing radar coverage within these zones should be considered. In determining any potential advantages and the associated trade-offs, one should consider following factors:

(1) Function / Application

(2) Coverage Requirement

(3) Accuracy Requirements and Trade-Offs

and (4) Design Implementations

In addition to these general factors, such specific issues as passive (reflector) versus active (transponder-aided) radar operation must be addressed.

Although not all of the issues have been resolved to date, particularly that of coverage and accuracy requirements, the following conclusions can be reached based on range equation for radar target detection at 2000 km:

(1) Detection of a skin return from a 1 m^2 target requires megawatts of peak power and tens of kilowatts of average power.

(2) Equipping the target with a passive reflector such as a corner reflector (1 meter on a side) reduces the peak power requirement to tens of kilowatts and the average power to much less than one kilowatt.

(3) Use of FM/CW radar with a corner reflector, although requiring transmitter signal leakage cancellation, can reduce both the peak and CW power (they are same) requirements to 50 watts. This value of power represents the capability of the Ku-Band radar / communication system presently used on the Shuttle Orbiter.

(4) Use of a cooperative active transponder on the target also reduces peak power requirement to about 50 watts, thus providing for a potential utilization of the Ku-Band system presently used onboard Shuttle Orbiter

At this point, consequently, the main issues center on the following:

(a) Passive reflector vs. beacon (transponder) radar system.

(b) Implementation trade-offs for systems listed in (a) above.

and (c) Accuracy required and achievable with either a passive or an active (beacon) system.

The considerations above pertain to the operation in the 185 km to 2000 km range, with particular emphasis on acquisition at 2000 km.

Appendix E contains analytical support for the conclusions expressed above.

3.2 Short Range Radar Considerations

Prior to the NASA scrub, there was a requirement for a radar to provide the coverage up to 37 km from the Space Station. The main purpose of this radar was to provide a traffic control capability within the command and control zone (zone 2). Table 3.2-1 shows the specifications pertaining to the radar performance in this zone. The table also shows some of the parameters suggested by RCA, one of the Phase B contractors.

RCA proposed a phased array, multi-target radar. The proposed radar would consist of two units, each having 3 "faces" to provided the required coverage. Figure 3.2-1 shows the direction of the coverage provided by each unit and the corresponding array face. Figure 3.2-2 shows the proved locations of the two phased array radar units on the Space Station. Also, Figure 3.2-3 shows the actual coverage of the phased array radar proposed by RCA.

Axiomatix has considered the alternative, namely the use of Shuttle Ku-Band radar to meet the requirements of the Space Station radar. Figure 3.2-4 shows the proposed

Table 3.2-1. Space Station Radar Requirements.**

	SPACE STATION SPECIFICATIONS	CONTRACTOR SUGGESTED VALUES
MAXIMUM RANGE	20 NM (37 km)	
MINIMUM RANGE	1640 FT. (500 m)	
ANGULAR COVERAGE	4 PI STERADIANS	
REQUIRED FUNCITONS : (A) SEARCH AND ACQUISITION (B) TRACKING		
TARGET TYPES:		
NON-COOPERATIVE TARGETS MINIMUM RADAR CROSS SECTION	1 SQ. METER	
*SEARCH TIME (2 PI STERADIANS)		1 MINUTE
*TRACKING UPDATE RATE		10 Hz
NO. SIMULATIONS TRACKS/HEMISPHERE	4	
RANGE ACCURACY (ONE SIGMA)	328 FT. OR 1%	
RANGE RATE ACCURACY (ONE SIGMA)	1 FT./SEC. OR 1%	
ANGLE ACCURAGY (ONE SIGMA)	10 MILS	
* PROBABILITY OF DETECTION (SINGLE DWELL)		0.9
*EXPECTED FALSE ALARMS/MINUTE		20
GROWTH CAPABILITY (TARGETS/HEMISPHERE)	8	

*ALL REQUIREMENTS, EXCEPT THESE, TAKEN FROM RFP OR REFERENCE CONFIGURATION DESCRIPTION. THESE REQUIREMENTS ADDED, CONSISTENT WITH RFP AND RCD, TO PROVIDE COMPLETE SET OF REQUIREMENTS FOR TRADEOFF ANALYSIS.

**Prior to scrub

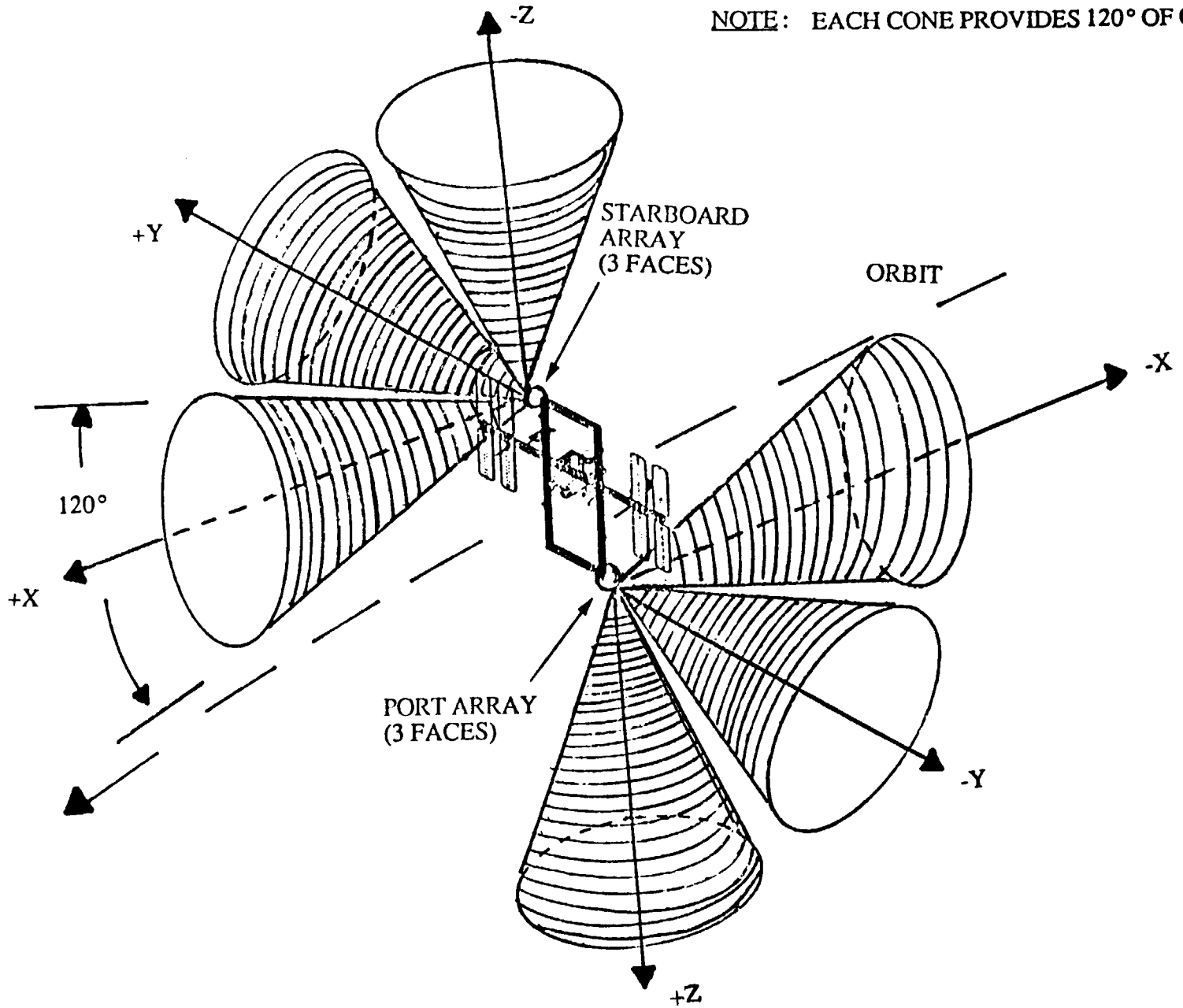

Figure 3.2-1. Space Station Phased Arrary Radar Coverage.

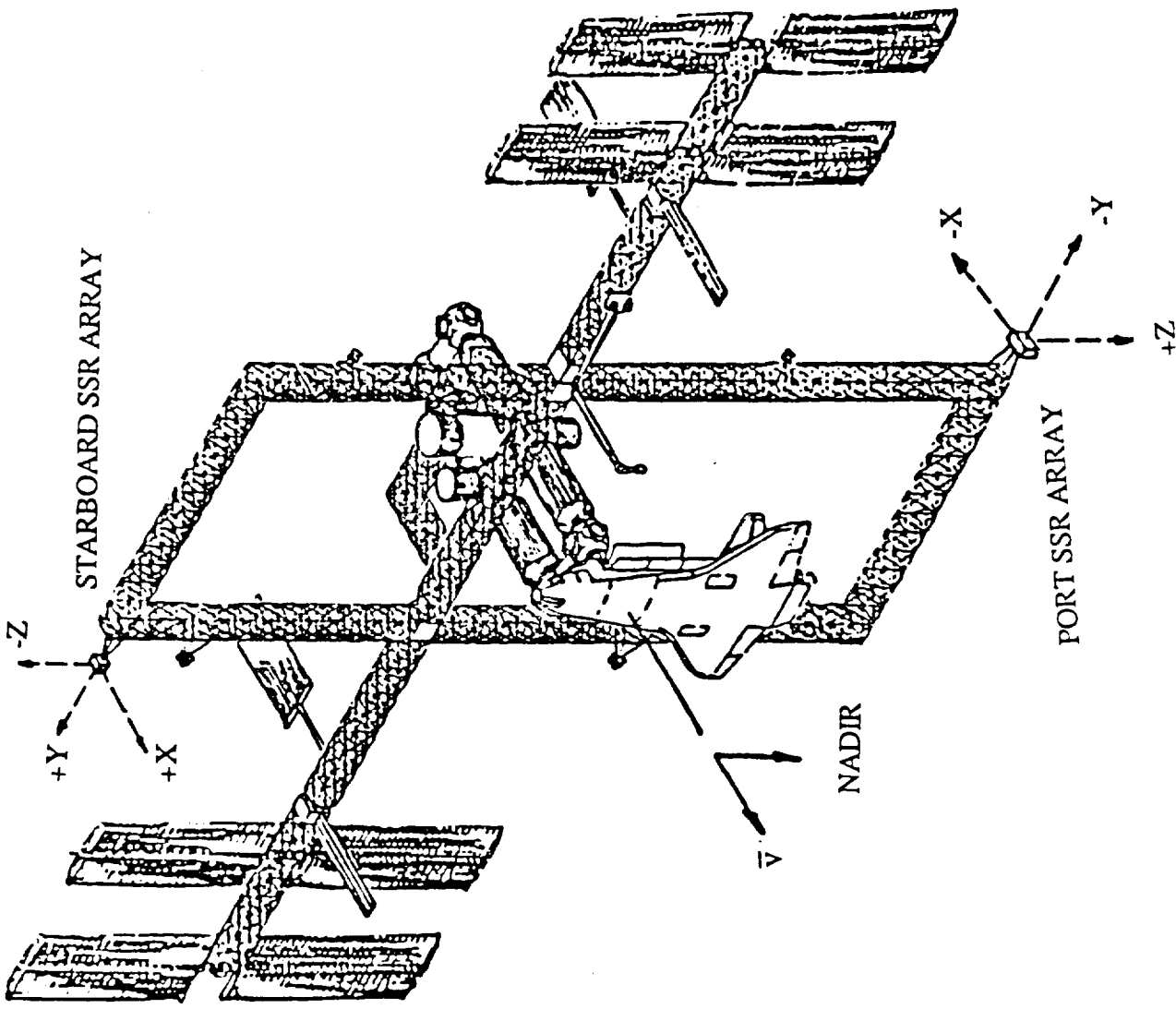

Figure 3.2-2. Candidate Location of Space Station Radar Array Faces on Space Station.

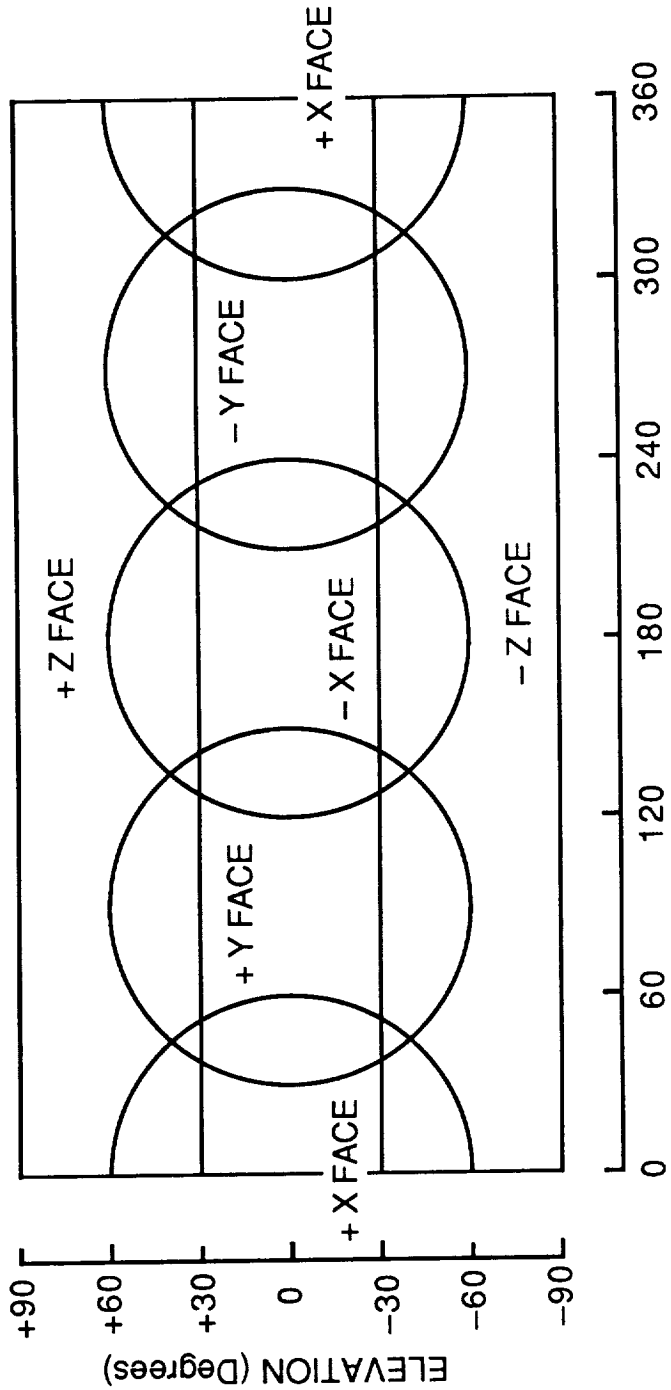

Figure 3.2-3. Space Station Six-Face Phased Array Coverage.

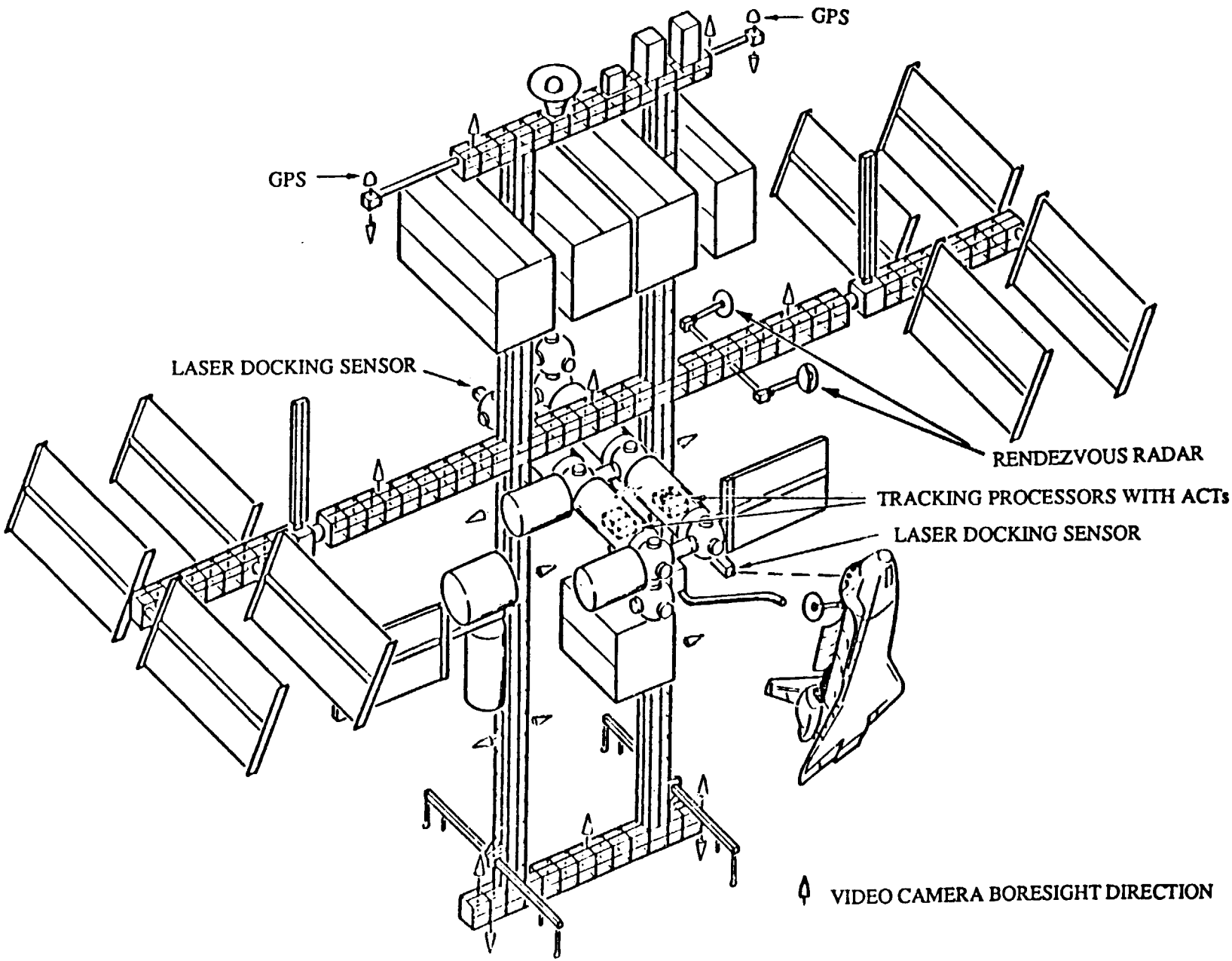

Figure 3.2-4. Ku-Band Rendezvous Radar Location on Space Station.

location of two Ku-Band radars which can provide a near hemispherical coverage shown in Figure 3.2-5.

Axiomatix has also performed an analysis of an unmodified Shuttle Ku-Band radar to determine its performance relative to the requirements and the RCA radar. Table 3.2-2 provides a comparison of the two radars. Based on the results shown in the table, the following conclusions can be reached:

(1) With the exception of longer acquisition time, the Ku-Band radar meets required tracking accuracy in range, range rate and angle in its unmodified state.

(2) Longer acquisition time may not be a limitation for Space Station radar because of slow relative target motion.

(3) Antenna slew time will be the limiting factor for the track data update time for the Ku-Band radar.

The following technical issues still remain:

(1) Ku-Band antenna gimbal performance and reliability under the requirement to move from target to target while tracking.

(2) Comparative performance of the two candidates (phased array vs. Ku-Band) with maneuvering targets.

The supporting material for Axiomatix's conclusions are present in Appendices F, G, and H.

Reference

[3.1] Space Station Reference Configuration Description; JSC-19989, Systems Engineering and Integration Space Station Program office/JSC, August 1984.

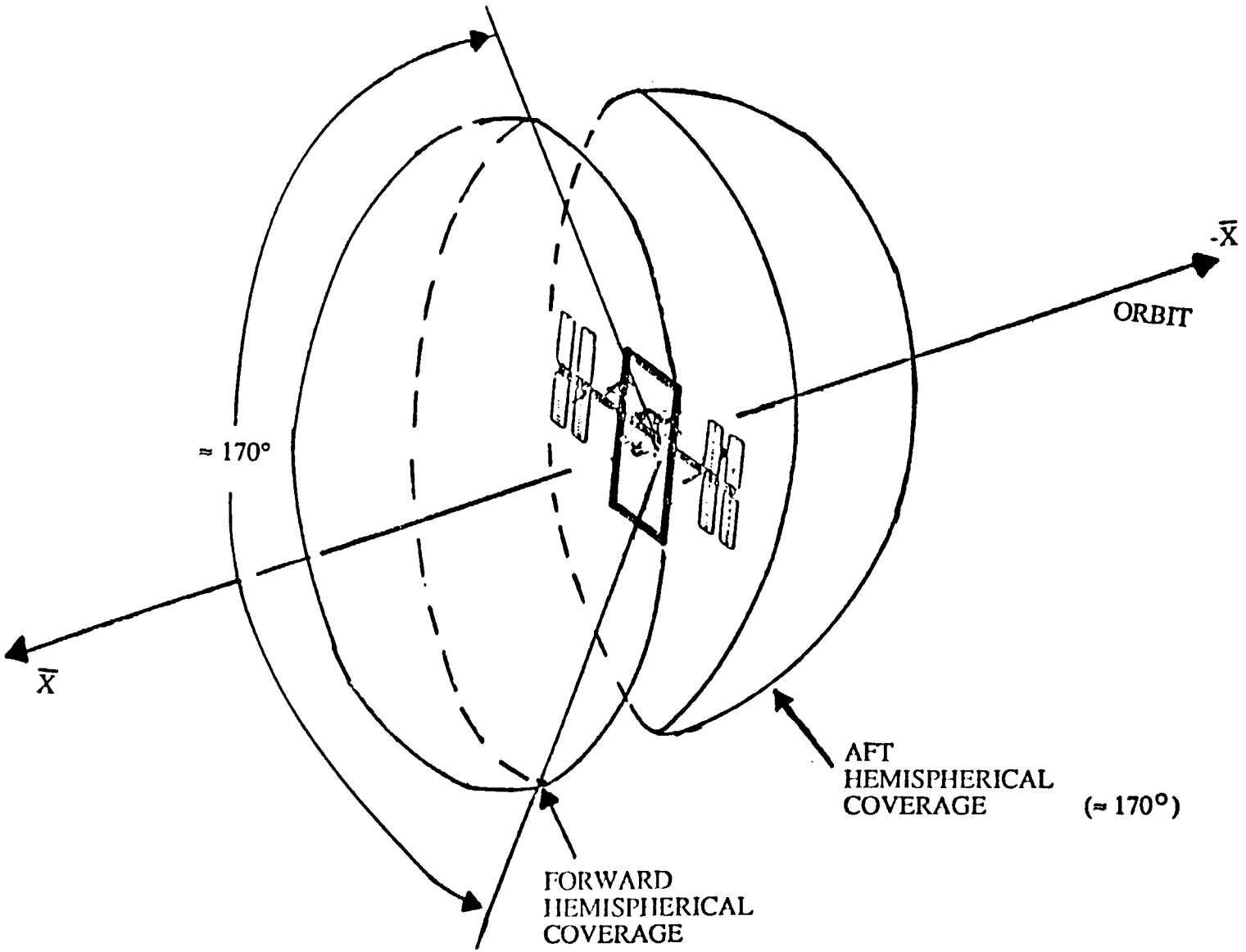

Figure 3.2-5. Modified Shuttle Ku-Band Radar Coverage for Space Station.

CHARACTERISTIC	PHASED ARRAY RADAR S-BAND	C-BAND	X-BAND	UMODIFIED SHUTTLE RADAR KU-BAND[2]
OPERATING FREQUENCY (GHz)	3.1–3.5	5.2–5.6	9.8–10.2	13.9
ANTENNA DIAMETER (FT.)	3.2	2.77	2.2	3
NO. ARRAY ELEMENTS/FACE	256	512	1024	N/A
ANTENNA BEAMWIDTH (DEG.)	6.4	4.5	3.2	1.7
ANTENNA DIRECTIVE GAIN (dBI)	28	31	34	37.7
SYSTEM NOISE FIGURE (dB)	4.2	4.5	4.8	7.9
TRACK LOSS (dB)	14	15	15.7	15.1
PEAK POWER (WATTS)	647	543	517	50
AVERAGE POWER (WATTS)	150	126	120	9.85
OPERATING WAVELENGTH (M)	0.091	0.056	0.030	0.021
SEARCH TIME/HEMISPHERE (SEC)	51	102	220	820
RANGE ACCURACY (FT.)[1]	18.4	18.4	18.4	67
RANGE RATE ACCURACY (FT/SEC)[1]	1	0.66	0.33	0.56[3]
ANGLE ACCURACY (mrad)[1]	4	3.1	2	1.57[3]

NOTE 1: ONE-SIGMA VALUE AT MAXIMUM RANGE.

NOTE 2: TWT TRASMITTER AT KU-BAND

NOTE 3: $B_N = 0.4$Hz

Table 3.2-2. Comparison of Phased Array and Shuttle Ku-Band Radar Performance.

4.0 Active Electromagnetic Docking Scheme

4.1 Background

Axiomatix has studied some optical docking proposals for the Space Station, and, noting the complexity of their design, investigated other techniques which may be applicable in solving the optical docking problem. The key issue for one proposal, it appears, is the spectral analysis of minute quantities of retroreflected light from a distant vehicle. Another is the multiple ranging to three retroreflectors to define a plane in space. Rather than follow the retroreflected light approach, a more direct method was conceived by Axiomatix, one which would actively align a docking vehicle to a desired attitude and bearing and accurately monitor the closing rate during the docking maneuver. Remote control can be maintained by modulating (e.g., amplitude modulation) the same laser beam used to align and move the docking vehicle to send simple commands. Many of these techniques are readily compatible with similar RF techniques and therefore can be developed using comparable millimeter and submillimeter quasi-optic systems.

4.2 Summary of the Active Optical Docking Scheme Conceived by Axiomatix

Initial acquisition of the docking vehicle is readily achieved by video means. Once acquired, the docking station aims a laser beam at a retroreflector on the docking vehicle, and photoconductive tracking sensors monitoring the retroreflected beam at the laser provides continuous tracking of the retroreflector. The laser beam is reflected off of a conical reflector to create a circularly symmetric beam of light to define a plane in space and illuminates a number of photodetector arrays. The illumination position on these photodetector arrays completely characterizes the alignment of the docking vehicle to the incident laser beam since it measures the degree of misalignment. This information in turn may be used to align the docking vehicle using an onboard computer.

However, it is also possible to dynamically correct this misalignment by an active technique that senses the direction of misalignment and uses the attitude control subsystem of the docking vehicle to immediately align itself to the laser beam. This novel technique uses a complementary photoconductive pair of strips to provide the driving voltages to allow the attitude control system of the docking vehicle to align itself orthogonally to the incident laser beam. The laser beam, if normal to the plane of the docking vehicle, is reflected off the conical reflector to form a circular pattern centered on these photoconductive tracking sensors. If the docking vehicle is not orthogonal to the laser beam, the misalignment causes the reflected laser light to become offset from the centered position on the photoconductive tracking sensors, which in turn generate corrective driving voltages which realign the docking vehicle.

Furthermore, this same concept allows for the movement of the docking vehicle to follow the laser beam into the desired docking position by sensing the laser beam motion. The laser beam (increased in diameter by a beam expander) is larger than the conical reflector, and this spillover radiation incident on photoconductive tracking sensors can similarly drive the docking vehicle in the direction of movement of the laser beam.

The roll attitude can be measured precisely, although with a 180 degree ambiguity, by exploiting the linear polarization of the incident laser beam and using polarization cancellation to establish two ambiguous roll positions accurately. This ambiguity may be visually resolved or other techniques used to differentiate the correct position. This roll position can either be measured directly on the docking vehicle by using a photodetector behind a fixed crossed polarizer. On the docking station the roll attitude is determined by measuring the polarization of the reflected light from a flat mirror surrounding the conical reflector, once alignment is achieved, which retains the original polarization orientation. By incorporating a polarization rotator on the laser which effectively rotates the linear polarization (effectively rotating the laser), the polarization cancellation position and therefore the roll attitude can be established.

Active roll attitude control can be implemented such that the docking vehicle rolls with the orientation of linear polarization. If a tracking sensor is placed behind two adjacent polarizers oriented at + and –45 degrees to the laser beam polarization, the incident illumination on both photoconductive sensors are identical and therefore balanced. Any deviation from this condition will generate driving voltages which will cause the docking vehicle to follow the orientation of linear polarization of the laser.

The accurate measurement of the closing rate is very crucial in a docking maneuver. A scheme has been developed to to measure the relative velocity, both on the docking vehicle and docking station, extremely accurately using interferometric techniques such that the resolution is of the order of the wavelength of the laser light.

Remote command capabilities may be incorporated into this active docking scheme by simply modulating the laser beam. Amplitude modulation, for example, can use the same laser beam to communicate commands which are received by a photodetector demodulation subsystem. FM may be considered for a similar millimeter wave system.

Thus, it is possible to have an active laser beam control system (or comparable active control system using millimeter waves) on the Space Station which can completely control the attitude and bearing of a docking vehicle, monitor the closing velocity, and remotely command the docking vehicle independent of a separate communications link. A detailed explanation of Axiomatix's technique is given in Appendix I.

5.0 SPACE STATION LINK ANALYSIS

During the earlier stages of the contract, Axiomatix was asked by NASA to provide the baseline concept for some of the special cases of the Space Station links. As the result, several analyses have been carried out and summarized in the appropriate reports. Specific topics addressed by Axiomatix were

(1) MSCS Link Design Considerations.

(2) Shuttle Orbiter/Space Station Links.

(3) Shuttle Ku-Band Radar Interference to Space Station Links.

In the following sections, these topics are overviewed. The details are presented in the appropriate appendices.

5.1 MSCS Links Design Considerations

This technical report considered the radio frequency (RF) links for the Mobile Service Center System (MSCS) formerly referred to as Mobile Remote Manipulator System (MRMS). The links analyzed are those between the MSCS and the Orbiter and also between the MSCS and the Space Station. It is assumed that only one link is active at any time.

The links considered are S-band links and Ku-band links. For the S-band case, we have assumed that, for IOC phase, the MSCS commands and telemetry requirements can be satisfied by treating the MSCS as a payload, thus allowing for utilization of the Payload Interrogator (PI) equipment on the Shuttle. We have also assumed that at S-band the 2.25 GHz Shuttle FM link frequency can be used for transmission of one TV channel in either an analog (FM) or in a digital (PSK or QPSK) format. For the Ku-band case, we are assuming that the multiple access (MA) Space Station equipment will be used ultimately for the MSCS as well as for the Shuttle/Space Station links.

The S-band and Ku-band link budgets for digital (22 Mbps) single channel TV transmission indicate that with a 1-watt transmitter and "omni" antennas at both ends,

adequate margin exists for either frequency. There is, of course, a significant margin advantage for the S-band link, because of the larger aperture of the S-band antennas (i.e., frequency dependence). But, this theoretical advantage of about 16 dB is offset by about 5dB due to excessive receive circuit losses at S-band.

In this report, we also address the problem of handling more than one TV channel at either band. The 'brute force" approach to this problem would be to utilize more RF channels for TV transmission. At S-band, however, this may be quite a problem because of frequency band limitation. At Ku-band, the problem may be less severe but still not trivial.

One way to reduce the total RF bandwidth required to transmit more than one channel (may be up to 5 channels) is to use video data compression on each channel. This, however, may not be acceptable from the standpoint of picture quality. Thus, methods which operate on a total bit stream of up to 5 digitized channels may have to be considered. Two possible methods are:

(1) Adaptive Bit Sampling Multiplexing (ABSMUX)

and (2) Multi-level, bandwidth conserving modulation such as M-ary PSK.

The first method (ABSMUX) takes advantage of picture statistics averaged over several channels. For example, if there is high activity in only one channel, and relatively low activity (i.e., little motion) in others, the total bit stream required for transmission may be far less than if the same constant bit rate was assigned to each channel. Note, however, that the bit rate is always higher than the bit rate of a single channel. Consequently, the RF bandwidth required is more than that required to transmit one digital TV channel. Furthermore, a considerable amount of video signal processing is required at both ends of the ABSMUX link.

The second method, i.e., multi-level modulation such as M-ary PSK (MPSK), permits several digital data streams to be multiplexed into one RF channel having the

bandwidth of a single channel. The penalty paid for such bandwidth conservation is, of course, the increased transmitter power. Because the use of MPSK falls into category of RF transmission, we have considered a possibility of using such modulation for the MSCS link to Space Station.

Table 5.1-1 shows the summary of the link budgets.[1] From this table, it is evident that very good link margins exist for the command and telemetry links at all bands. For those telemetry links which are at Ku-band and which may be multiplexed with multi-channel digital TV, the margins were not computed, but it is assumed here that they (i.e., margins) are not worse than the margins for the multi-channel digital TV links.

The most significant comparison of the S-band and Ku-band operation of the 5-channel links is that the larger aperture of the S-band omni antennas provides a significant transmitter power saving when compared to Ku-band operation. Specifically, it takes 5 watts of transmitter power at S-band with an omni antenna and 50 watts at Ku-band with an omni antenna.

This implies that for Ku-band operation either antenna gains have to be increased with concomitant directivity problems or the transmitter power has to increase accordingly if the 32-level MPSK approach is to be adopted for simultaneous transmission of 5 digital TV channels. But, 50 watts of Ku-band power is already equal to the capability of the TWTA which is currently used with the Orbiter Ku-band radar/communication system. Thus, requiring more power at Ku-band does not seem like a feasible approach.

The key remaining issue is the implementation of multi-channel digital TV links between MSCS and Space Station. We have baselined here an innovative approach, i.e, a 32-level MPSK for multiplexing of five digital TV channels within the bandwidth of a single 25 Mbps channel. We realize that we have to pay the penalty in power to stay within the bandwidth of a single channel. Such a trade-off is of particular importance for S-band

[1]At maximum range of 100 meters.

Link	Band	Signal Transmitted	Origin	Destination	Rate	EIRP (dBm)	Link Margin (dB)	Comments
MSCS/ Shuttle Orbiter (SO)	S	CMD	SO	MSCS	2 kbps	30.4	64.5	Payload Interrogator Link
		TLM	MSCS	SO	16 kbps	15	37.8	Payload Interrogator Link
		Analog FM TV	MSCS	SO	Analog	25	15.8	Analog FM Receive
		Digital TV	MSCS	SO	25 Mbps	25	18.6	Requires Special Tx and Rx Equipment
	Ku	CMD	SO	MSCS	100 kbps	15	19.9	
		TLM	MSCS	SO	100 kbps	15	20.2	
		Digital TV	MSCS	SO	25 Mbps*	25	6.2	Single-Channel Digital TV
MSCS/ Space Station (SS)	S	CMD	SS	MSCS	2 kbps	30.4	64.5	
		TLM	MSCS	SS	16 kbps	15	37.9	
		Digital TV	MSCS	SS	25 Mbps*	32	9.6	5 Channels @ 25 Mbps via 32-level MPSK
	Ku	CMD	SS	MSCS	100 kbps	15	19.9	
		TLM	MSCS	SS	100 kbps	15	20.2	
		Digital TV	MSCS	SS	25 kbps	25	6.2	Single-Channel Digital TV
		Digital TV	MSCS	SS	25 Mbps*	42**	3.3	5 Channels @ 25 Mbps via 32-level MPSK

*Telemetry is assumed to be a small fraction of TV data rate, thus the multiplexing of TLM data stream with TV data is negligible on the link margin.

**Requires a 50 watts transmitter at Ku-band

Table 5.1-1. Link Budget Summary for MSCS/Orbiter and MSCS/Space Station Links (Range = 100 meters)

utilization of multi-channel digital TV transmission if such utilization is considered as the only feasible alternative for multi-channel TV transmission. Also, if MPSK is to be adopted as a possible approach, there remains such technical issues as the effect of multi-path and the complexity of the equipment. Furthermore, MPSK equipment is different from the "baseline" Ku-band equipment, and thus the extra development cost must be considered. Consequently, further trade-offs are necessary to determine the most feasible approach to implementing simultaneous multi-channel digital TV transmission from MSCS.[2] Appendix J contains the details of this link study.

5.2 Shuttle Orbiter/Space Station Links

This report considers possible implementations of the RF links for command, telemetry, and voice communication between the Shuttle Orbiter (SO) and the Space Station (SS). For these links, there are three implementable and realistic candidates. These are:

1) All S-band link
2) All Ku-band link

and 3) Hybrid S-band/Ku-band Link

Another possibility would involve the use of UHF for voice communication, but this approach was not considered here because of potential frequency utilization problem.

Table 5.2-1 shows link margin summary for Shuttle/Orbiter RF link implementations at either S-band or Ku-band.[3] The table indicates that the Ku-band implementation has significantly higher margins than the S-band implementation. This is due primarily to the use of high gain (24 dB) antennas on the Space Station end of the link.

---

[2] The actual MSCS requirement has been subsequently reduced to only 3 channels. For this, Axiomatix has developed a concept of an 8-PSK modem described in Section 7.1 of this report.

[3] Hybrid use of S- and Ku-bands would involve same link margins, therefore, no listing is given for a "hybrid" approach.

Link	Band	Signal Transmitted	Origin	Destination	Rate	EIRP (dBm)	Link Margin (dB)	Comments
Shuttle Orbiter (SO) to Space Station (SS)	S	CMD	SO	SS	2 kbps	30.7	7.9	PI Link
		VOICE			16 kbps		7.8	PI Link
	Ku	CMD			2 kbps	28	16.4	Ku-band MA Link
		VOICE			16 kbps		16.4	Ku-band MA Link
Space Station (SS) to Shuttle Oribter(SO)	S	TLM	SS	SO	16 kbps	33	3.4	PI/Transponder link
		VOICE			16 kbps		2.5	PI/Transponder link
	Ku	TLM			16 kbps	52.4	13.9	Ku-band MA Link
		VOICE			16 kbps		13.9	Ku-band MA Link

Table 5.2-1. Link Margin Summary for Shuttle Orbiter/Space Station S-Band and Ku-Band Link at 37 Km

The advantage of larger antenna apertures provided by S-band is offset by the fact that only 0 dB antenna gain is assumed at the Space Station end for the S-band operation. This assumption is very conservative and it results rather low margins for the S-band link which carries the telemetry and voice from the Space Station to the Orbiter. If the Space Station antenna gain at S-band is increased to 3 dB, then the margins improve accordingly. At this point, we do not see any reasons why such antenna gain increase could not be acceptable if the decision is made to operate at S-band.

The unique feature of the S-band implementation considered in this report is technique for transmitting two-way 16 kbps delta-modulation voice between the Shuttle and the Space Station at the maximum range of 37 km. This approach, as proposed by Axiomatix, uses the existing standard subcarriers for communicating digital voice. For the Shuttle/Space Station link, the subcarriers in the range from 65 KHz to 95 KHz are considered as possible candidates. These subcarriers are typical of CIE and/or CIU equipment and are readily handled by the payload interrogator (PI). For the Space Station/Shuttle link, the standard 1.7 MHz subcarrier can be used for digital (16 kbps) voice. Consequently, by modulating the appropriate subcarriers at both ends of the S-band link a viable method for a two-way voice communication can be provided.

From the S-band and Ku-band link budgets considered, it appears that either implementation alone, or the combination of the two, can meet the requirements for the Shuttle Orbiter/Space Station link. Furthermore, as described in this report, there appears to be a possibility of adapting some of the existing S-band payload link equipment for providing two-way voice capability to the link. This capability will permit the Orbiter to satisfy the voice link requirements without actually using the Ku-band MA system.

From the standpoint of the Orbiter, this appears to be relatively low cost solution, requiring only minor baseband modifications to CIE or similar equipment and the corresponding transponder. Neither RF nor any antenna modifications will be required. However, remaining at S-band beyond the IOC capability will impose dual-band (S- and

Ku-bands) operation requirement on the Space Station. The impact of the latter requirement remains to be addressed.

The reference made above to the CIE is not to the actual CIE which is a part of DOD's SGLS network. What is meant here is simply an equipment which is "CIE-like" in design, i.e., it has more than one subcarrier on the link to the payload. In fact, it could possible be a modified PSP. Whatever equipment it may be, the main requirement is that the 16 kbps digital voice can be "patched in" into it at the Orbiter and also be recovered and separated from telemetry for on-board use. Commands, however, could originate either on the ground or on-board.

Appendix K provides a detailed description of the implementations and the trade-offs associated with the shuttle orbiter/Space Station links

5.3 Shuttle Ku-Radar Interference to Space Station Links

5.3.1 Ku-Band Radar Interference Scenario

The problem of radar interference arises when the Shuttle rendezvous with the Space Station using its Ku-band radar which frequency hops between five frequencies in the range from about 13.8 GHz to 14.0 GHz. This interference has potential impact on

(1) Ku-Band forward link (SGL) from TDRS to Space Station

and (2) Multiple Access return links from Ku-band users.

Figure 5.3.1-1 shows the Ku-band radar interference scenario and Figure 5.3.1-2 provides spectral representation of the problem. As can be seen from Figure 5.3.1-2, the primary problem in the interference of the 13.779 GHz radar line to 13.775 GHz TDRS down link. Interference to the MA link is of far less problem.

Figure 5.3.1-2. Relative Spectral Density of Ku Radar and SS Communication Links.

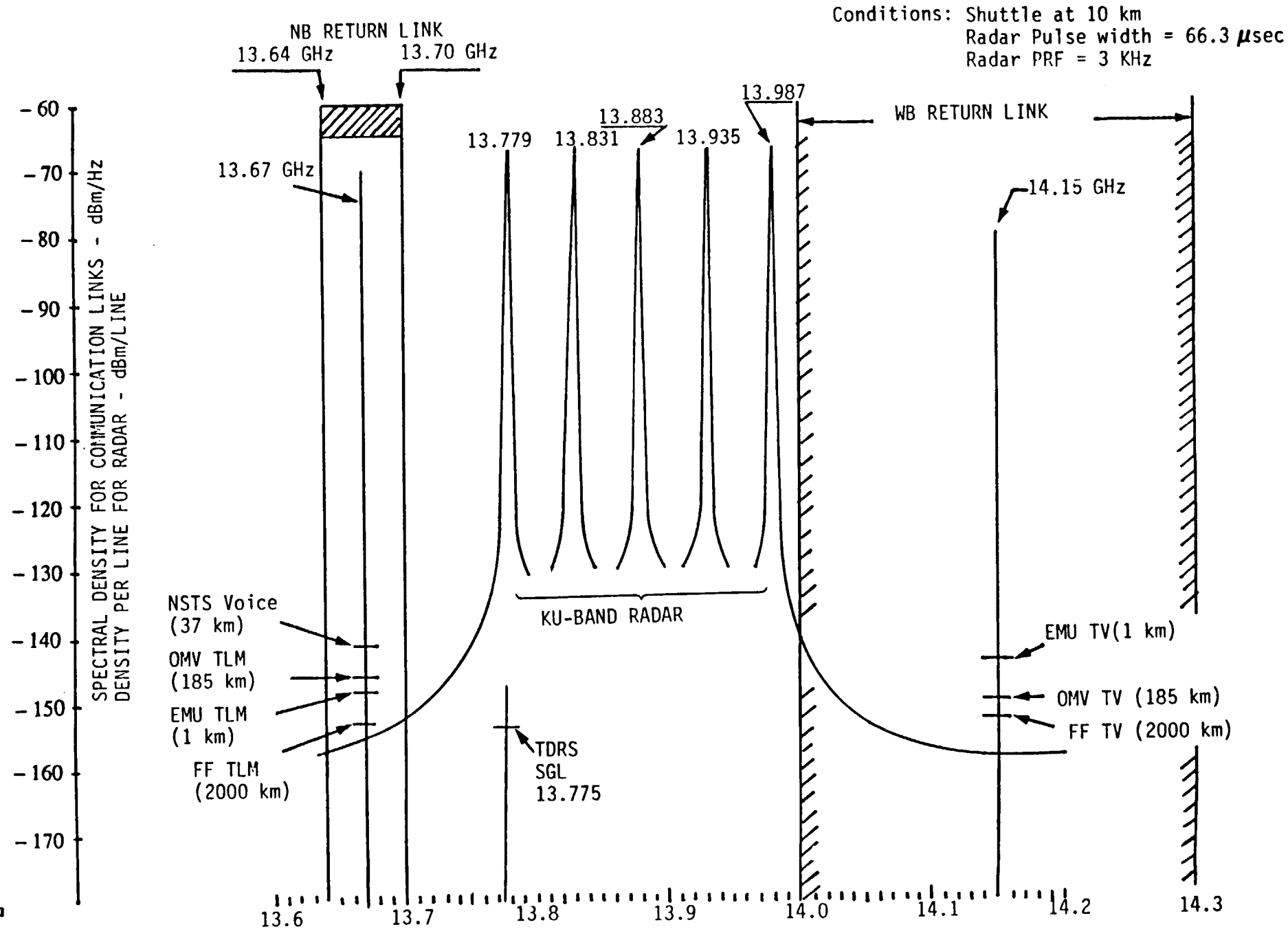

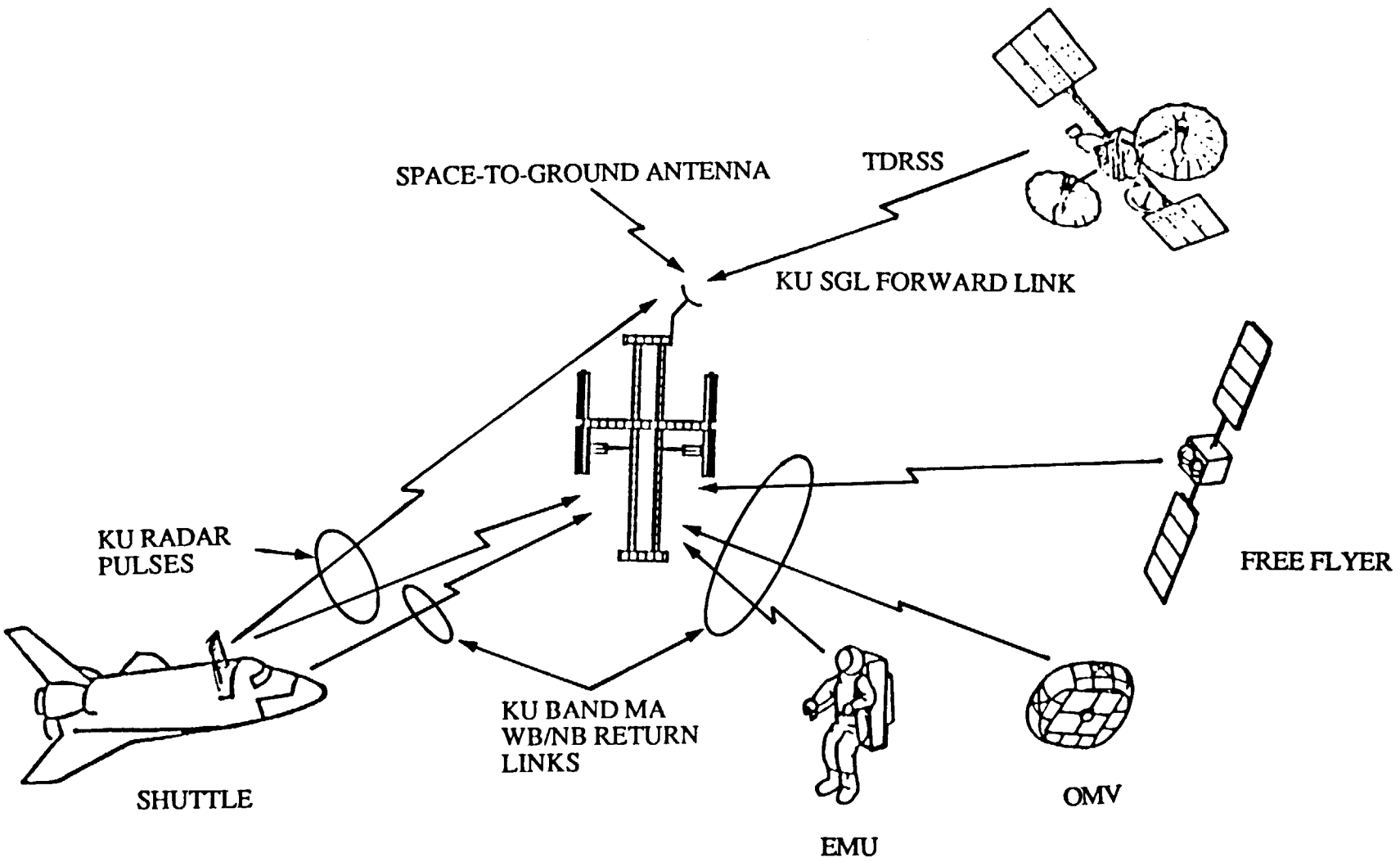

Figure 5.3.1-1. Shuttle Ku-Band Radar Interference to Space Station Receive Links.

5.3.2 Potential Fixes for Ku Radar Interference to SGL

The following fixes were considered by Axiomatix in addition to fixes already considered by other Space Station contractors:

Operational Fix

- Use Ku-band radar beacon mode at unhopped frequency of 13.883 GHz with appropriate passive reflector at SS to provide for CP[4] return.

RF and Receiver Fixes

- Antenna sidelobe canceller
- Pulse estimator canceller
- Hard limiter canceller
- Baseband canceller

Preferred Approach

- Use of active mode center frequency (without beacon) provides lowest cost solution—no modifications to Space Station systems.
- Requires investigation of Space Station radar cross section with CP waves.
- Requires more thorough test of Ku-band radar active mode performance.
- May require passive radar enhancement device.
- May restrict Shuttle approach vectors if directional radar enhancement device is required.

Alternate Approaches

- Cancellation methods provide alternate solution but they require development of additional hardware.
- Cancellation may provide for unrestricted approach direction.

---

[4] Circularly Polarized

5.3.3 Ku Radar Interference to MA Links—Summary

- Analysis indicates that there may be about 1.5 dB margin degradation to reception of wideband video signals from FF and OMV when these vehicles are at their maximum ranges of 2000 km and 185 km, respectively.

- The margin degradation of 1.5 dB is based on worst case assumption of Ku Radar being in the beam of high gain antennas servicing FF and OMV video links. Nevertheless, there still is a remaining margin for these links.

- Other links do not exhibit degradation neither in the NB nor in the WB return links.

Appendix L contains a detailed examination of the Ku-Band interference problem and it presents detailed explanation of the fixes proposed.

6.0 ANTENNA SWITCHING, POWER CONTROL, AND AGC FUNCTIONS

6.1 Overview

During the course of this study, NASA requested that Axiomatix provide considerations for antenna switching, power control, and AGC functions for the Space Station's multiple-access (MA) system. The background for the general requirements for these functions is given below.

Antenna Switching

Antenna switching will be required to provide for optimum link conditions despite the relative movement of the MA system users with respect to the Space Station (SS). For movement within the proximity operations zone, several omni antennas located at various points of the Space Station will provide for near-spherical coverage, but some criteria for selecting the proper antenna are required. Also, the quality of the received signal must be sampled to determine when to switch from an omni to a medium gain antenna and vice versa, the latter scenario being a part of power control.

Power Control

The users of the Space Station's MA system transmit signals at two widely separated rates. For example, the telemetry rate is about 100 Kbps and the video rate is about 22 Mbps. Also, the range to a user may be from about a few meters (EMU) to about 37 km (OMV, NSTS). This creates a potential problem of interchannel interference and receiver overloading. Thus, means of controlling EIRP of users to reduce the Min/Max signal differential at Space Station's receivers is required.

AGC Function

The multiple access system of the Space Station receives Ku-band signals from several users. These signals are picked up by antennas placed at various locations of the SS. The signals are amplified, filtered and supplied via a bus (IF or Fiber-Optical) to the

programmable signal processors (PSP) for data demodulation. The type and distribution of the AGC function has to be identified.

The role of Axiomatix in dealing with these requirements can be summarized as follows:

1) Identify key issue in each of these tasks,

2) Analyze tradeoffs between available alternatives,

and 3) Recommend baseline approaches.

A more detailed overview of our ideas on these subjects is given in Appendix M. The view presented these reflect our thinking at the time of the preparation of the report presented in Appendix M. Some of the views presented there have been modified as the result of our subsequent analyses and also as the result of the Phase C award.

6.2 Power Control

The motivation for the power control arises due to the following three factors: (1) the FDMA configuration of the return links, (2) the near/far problem, and (3) the dynamic range limitation of the Space Station's RF receiving and the IF distribution components. Figure 6.2-1 shows the power control function scenario.

Two receiver architectures were examined for their ability to handle the FDMA signals. These architectures are: (1) a wideband receiver proposed by the McDonnel Douglas team and (2) a channelized receiver proposed by the Rockwell International team.

The salient feature of the first approach is a single wideband downconversion of the entire return link band (300 MHz wide) to a wideband IF. Thus, each antenna of an antenna group is connected to a separate receiver which then connects to its own FO cable driver. The main advantage of this approach is the simplicity of the Ku-Band receivers. With a channelized approach a group of antenna receivers has a capability to amplify selectively the individual channels of the return link band. Although this approach is more

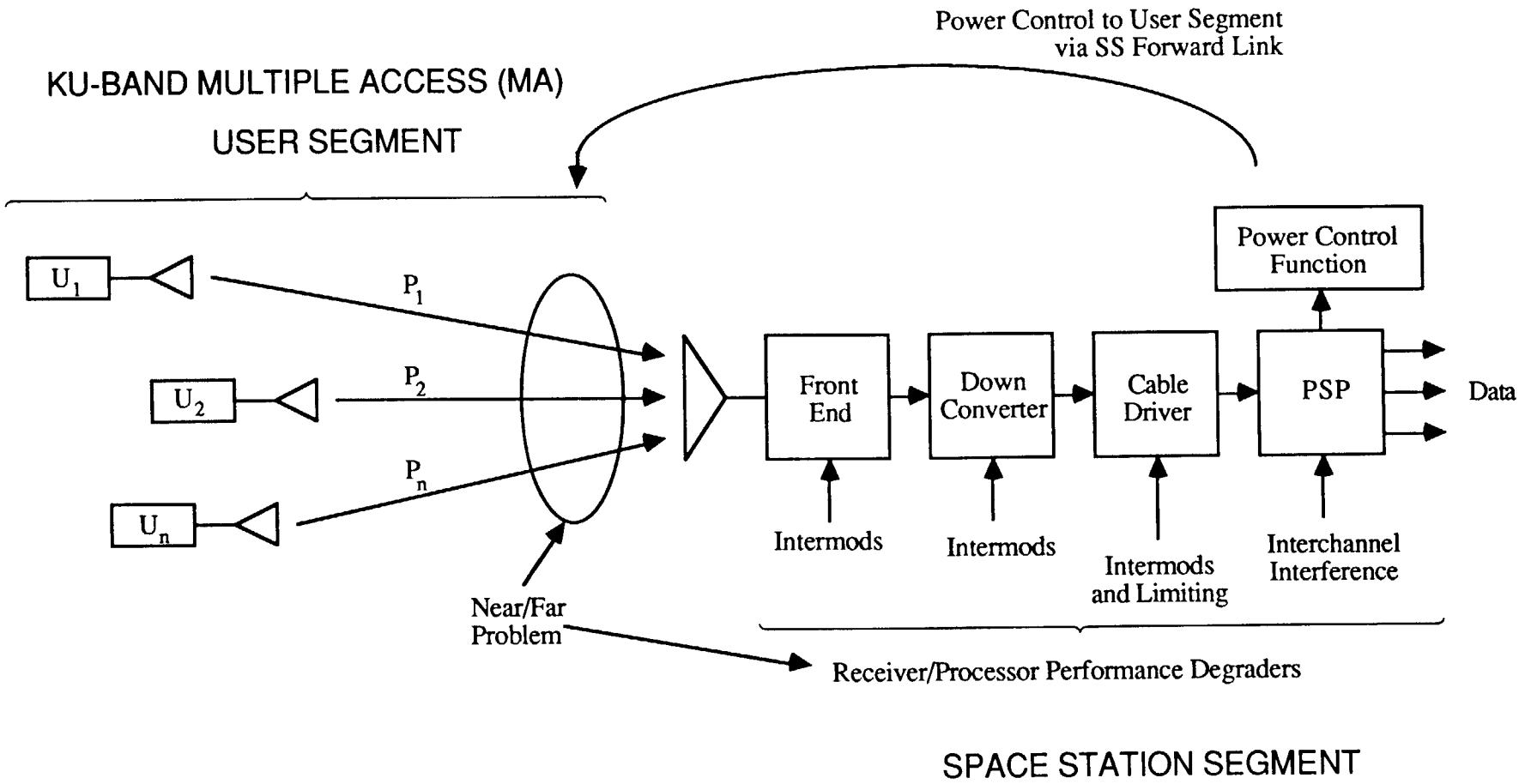

Figure 6.2-1. Power Control Functional Scenario.

complicated than the wideband approach it provides for a channel-dedicated AGC function within each receiver.

Figure 6.2-2 presents a side by side comparison of our estimates for the third order intermodulation behavior of the two receiver architectures. The bandwidth assumed is that of a digital video link, i.e., 25 MHz. As indicated in the figure, the origins of the third order intercepts are different for the two receiver architectures. It can also be seen from this figure that a channelized receiver can, at least in principle, accommodate a 20 dB higher level of the input signals before the internal generation of the third-order intermods. This capability is due to the channelized AGC available with a channelized receiver.

Because of the potential advantages of the channelized receiver, this configuration was adapted as a baseline for subsequent analysis to determine the power control window capabilities and limitations of the Space Station receiving system. Of particular significance was the analysis of the FO cable link capabilities.

Based on a practical model of an FO cable link, it was established that the basic limitation for the power control window is the FO cable loss which causes the degradation in the system SNR at the optical receiver. In view of this degradation, it is estimated that a power window for the high SNR users, such as EMU and MSC-3,* may be limited to 10 dB. For the lower SNR users, such as FF and OMV, the power control window of up to 15 dB appears feasible. Figures 6.2-3 and 6.2-4 show how the FO cable loss affects the system SNR transfer curve.

However, a conservative recommendation is a 6 dB ± 3 dB power control window with a channelized receiver. The "flattening" of the curve at the higher input SNR means that it is more difficult to estimate with accuracy the large SNR values which are the result of the increasing signals due to the range closure. This is based on a baseline assumption

* A three channel 8-PSK system.

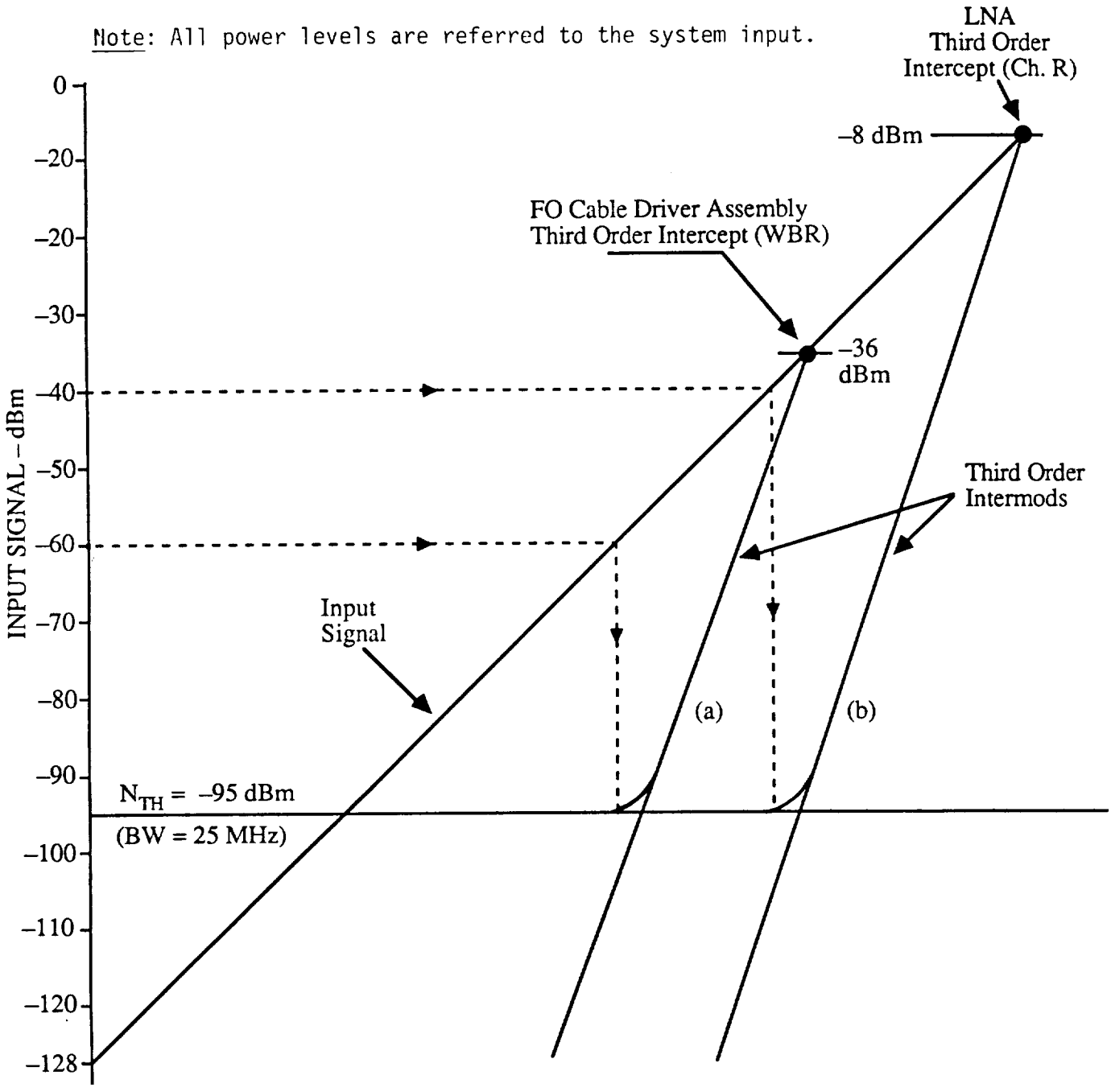

Figure 6.2-2. Third Order Intermods for (a) Wideband Receiver and (b) Channelized Receiver.

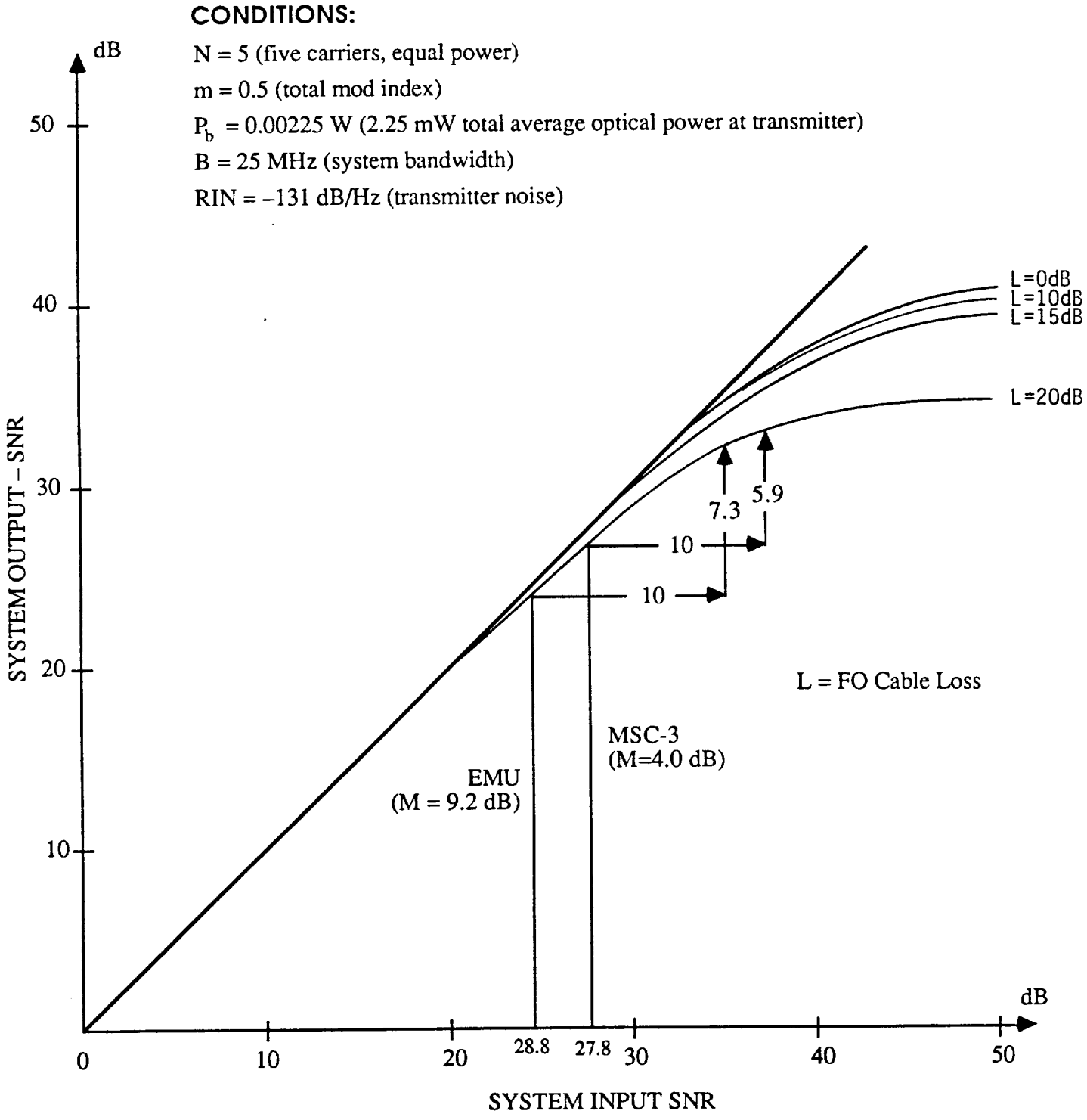

Figure 6.2-3. System SNR Transfer Curve as Function of FO Cable Loss (EMU and MSC-3 Power Control Window of 10 dB).

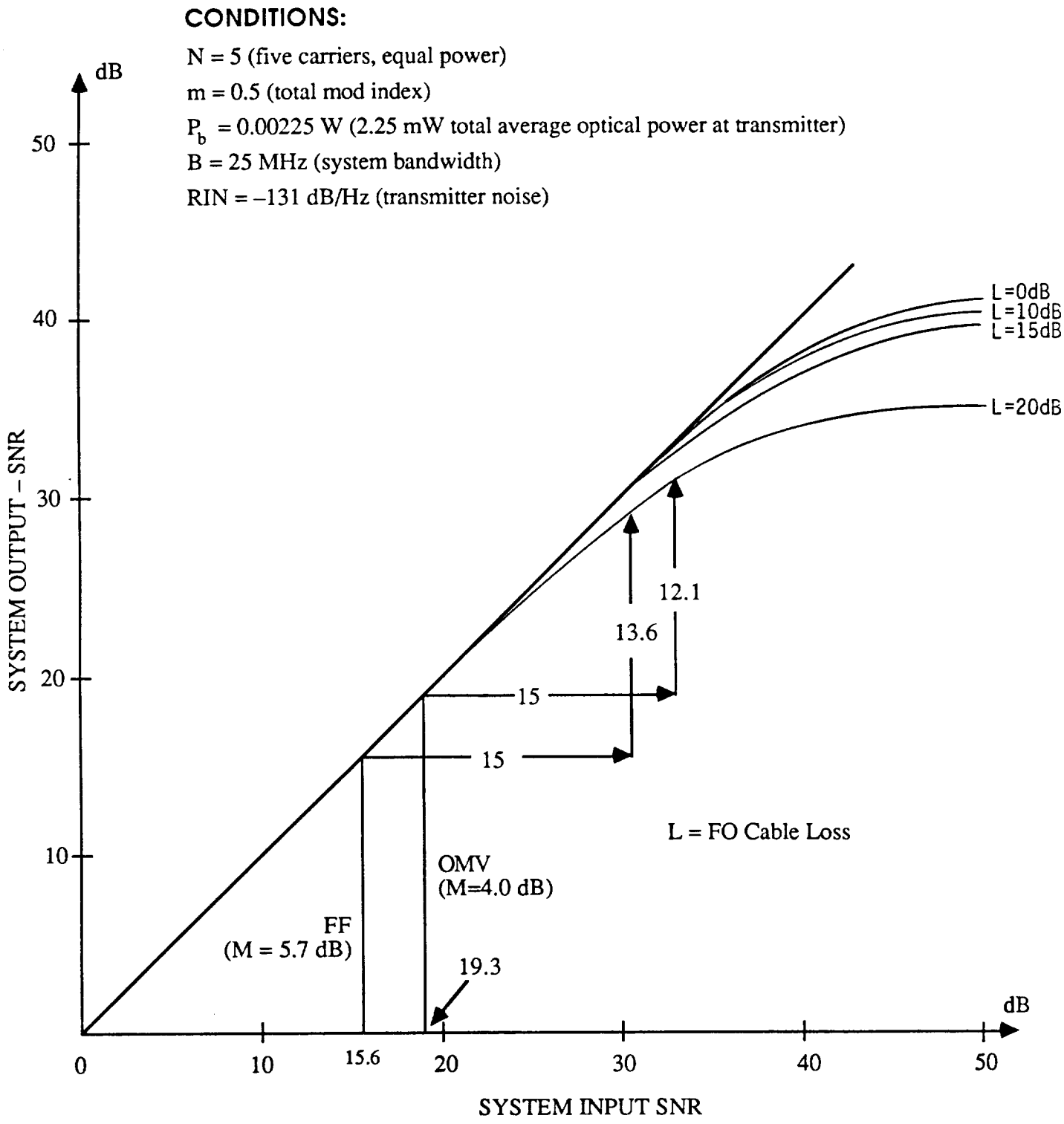

Figure 6.2-4. System SNR Transfer Curve as Function of FO Cable Loss (FF and OMV Power Control Window of 15 dB).

that the power control signal is developed at the coherent demodulators located at the receiving end of the FO cable link.

The possibility of using a PIN diode to control the power input to the user's transmitter, and thus control the output EIRP, was examined. It was determined that 60 dB of power control can be obtained in this manner without antenna switching. Figure 6.2-5 shows a functional block diagram for this viable concept.

In Appendix N, various technical aspects of implementing the power control for the Space Station Multiple Access (MA) system are addressed. Particular emphasis is placed on the RF/IF processing of the Ku-Band MA signals received by the station. A fiber optic (FO) cable link is assumed to be carrying the IF signals between the boom locations of the receiver/transmitter (R/T) units and the central processing unit located in the habitat module. Capabilities and limitations of using an FO cable link as a subunit of the power control function are examined.

6.3 Antenna Switching

Antenna switching will be required to provide for optimum link conditions despite the relative movement of the MA system users with respect to the Space Station. For the movement within the proximity operation zone, several omni antennas located at various points of the Space Station can provide for near-spherical coverage, but some criteria for selecting the proper antenna are required. Also, the quality of the received signal must be sampled to determine when to switch from an omni to a medium gain antenna and vice versa. The McDonnel Douglas team proposed the use of a dedicated receiver to sample the levels of the signals received by various antennas. Axiomatix believes that this is a reasonable approach considering the complexity of the antenna coverage requirement. Provided below are some of our current thoughts on the use of a sampling receiver to provide the information for antenna switching.

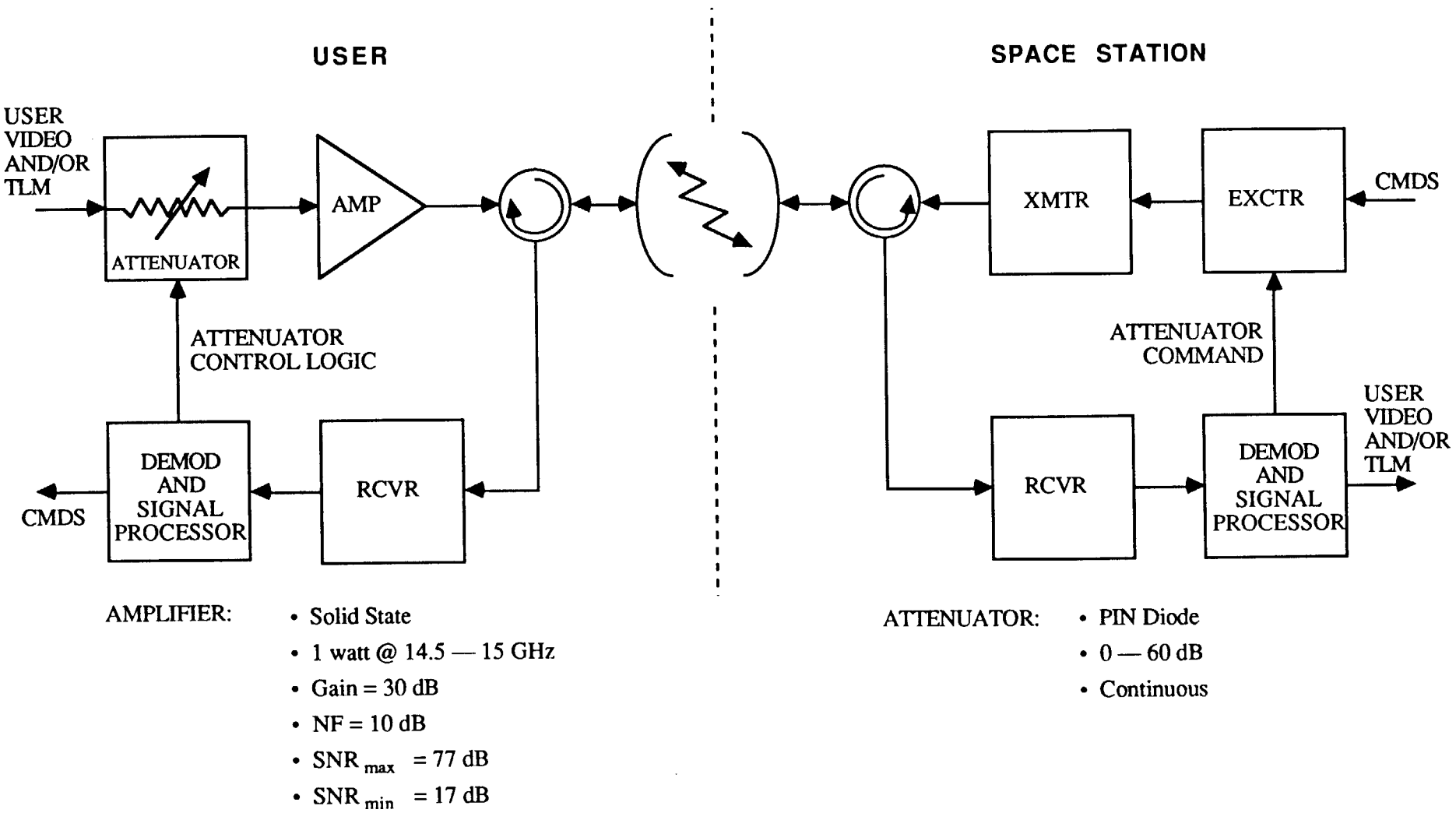

Figure 6.2-5. Functional Block Diagram for User Power Control.

Figure 6.3-1 shows how such sampling receiver can be connected to the IF distribution system. As shown in the figure, the baseline system consists of four hemis, four medium gain antennas and two air lock antenna assemblies. This provides for a total of ten IF inputs to a 10 x 6 IF switch matrix. Four of the matrix's outputs go four "active" channel receivers, one goes to order wire/ranging receiver and one goes to antenna signal level receiver.

Figure 6.3-2 provides a qualitative indication of how the antenna signal level receiver can provide information for predicting signal level trends. This "prediction" feature can be implemented by considering a "history" of samples rather than one sample at a time.

The advantage of prediction is that one may obtain the information on the next "optimum" antenna position before the signal at the "current" antenna falls below the acceptable level threshold (ALT).

The prediction algorithm will be most effective if the antenna sampling rate is several times faster than the motion components of the user. Considering the fact than only one sampling receiver is available, and that this receiver must typically sample four channels at each antenna, the time it takes the sampling receiver to "settle" on a given sample becomes an important system parameter. One of the tasks of the future Space Station contract is to consider some of the methods for establishing valid indicators of signal "quality" provided at the output port of the sampled antenna.

6.4 AGC Considerations

In considerations pertaining to the AGC function, there arises a question of whether a certain portion of the gain control be assigned to the front end. This is particularly true for the case of the MA system where all of the FDM channels may be amplified by a single wideband (approximately 300 MHz wide) low noise amplifier (LNA). Figure 6.4-1 shows a functional block diagram of such a front end. As shown in Figure 6.4-1, a multi-user

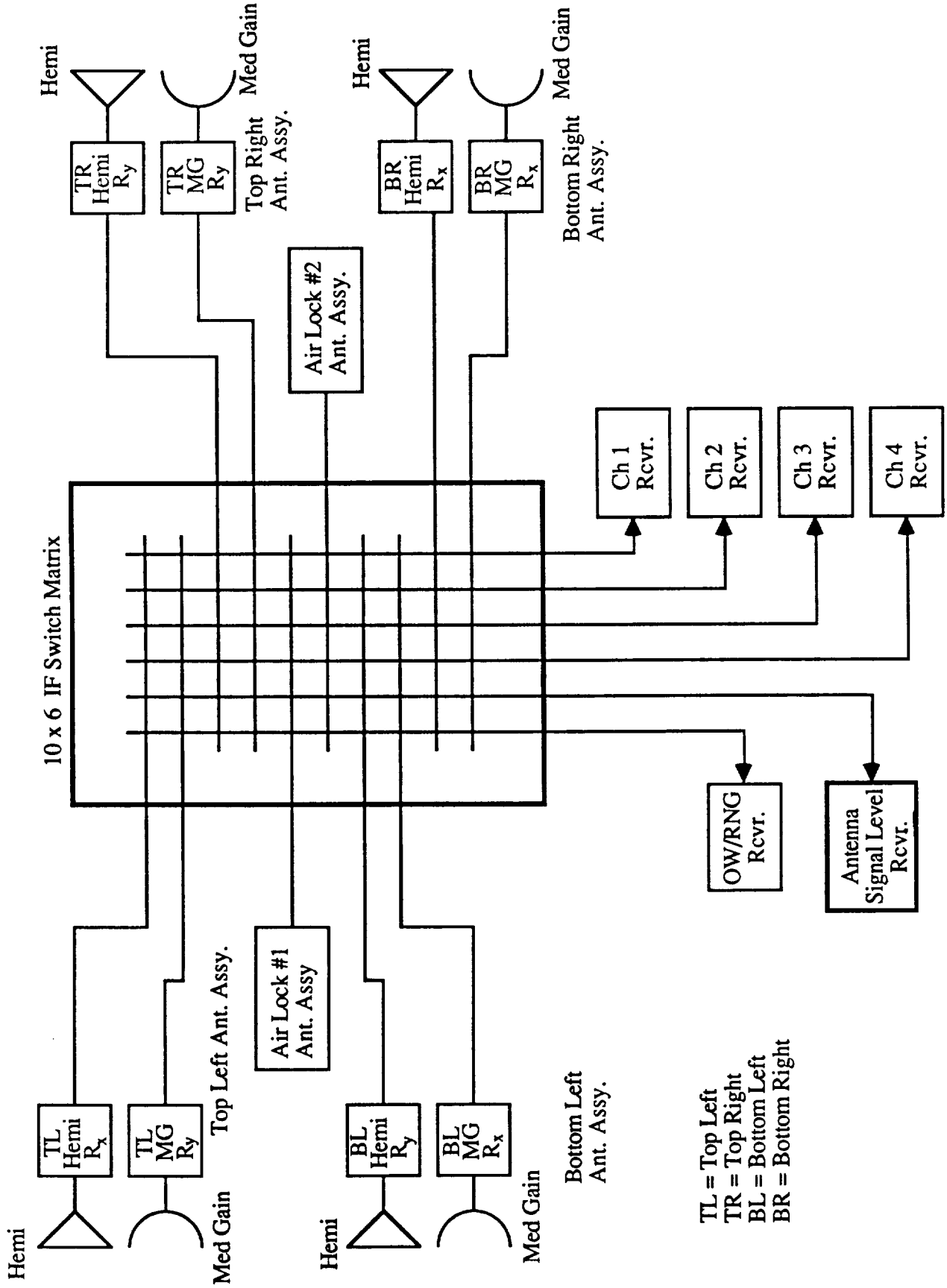

Figure 6.3-1. Antenna Signal Level Receiver Connection.

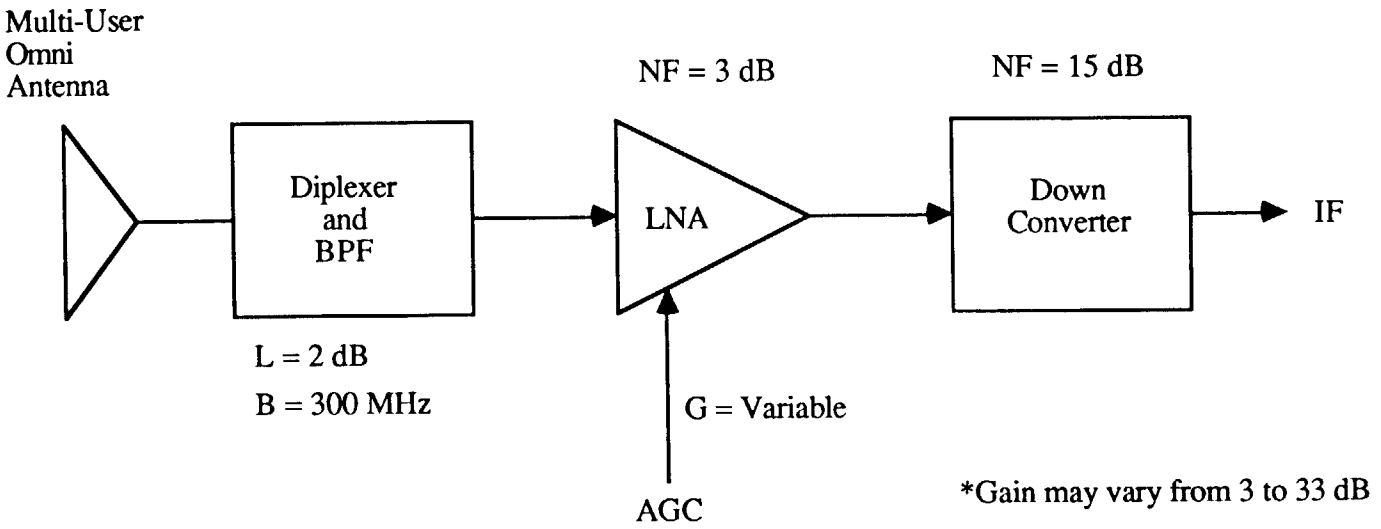

Figure 6.4-1. Functional Block Diagram of a Variable Gain, Wideband Front-End.

antenna, such as an omni, connects to a diplexer and a bandpass filter. The signals picked up by the antenna are received from various users which may be at various distances from the antenna. The signals are amplified by the LNA and applied to the downconverter. The downconverter translates the FDMA signals to either a wideband or a channelized IF amplification chain. The baseline estimates for the losses, the noise figures and the gains are shown in the block diagram.

Although it is assumed that some form of power control is in effect and thus the powers received should be within an aperture of 6 to 10 dB from each other, there may arise a situation when one of the users may be not under the power control and thus dominate the front end. In this case it may be beneficial to lower the gain of the LNA to reduce the possibility of the intermods developing in the front end. Within the framework of the baseline assumptions indicated in Figure 6.4-1, we have computed the noise floor degradation which may result from reducing the gain of the LNA. This degradation is shown in Figure 6.4-2. It can be seen in Figure 6.4-2 that there is a trade-off between the amount of gain reduction and the noise degradation. Specifically, the higher the gain reduction the worse is the noise degradation. To improve this situation, one can increase the LNA gain to about 50 dB and control the gain down from 50 dB to 20 dB (but not below) in order to minimize the noise floor degradation due to AGC action. An alternative is to reduce the effective noise figure of the downconverter.

6.5 RF vs. Optical Cable Trade-Offs

In Section 6.2, the use of a Fiber Optical (FO) cable was assumed in our examination of the power control. Subsequently, NASA has requested as to consider some trade-offs between the use of FO vs. RF cable for the distribution system. Presented below are some of our considerations on the subject.

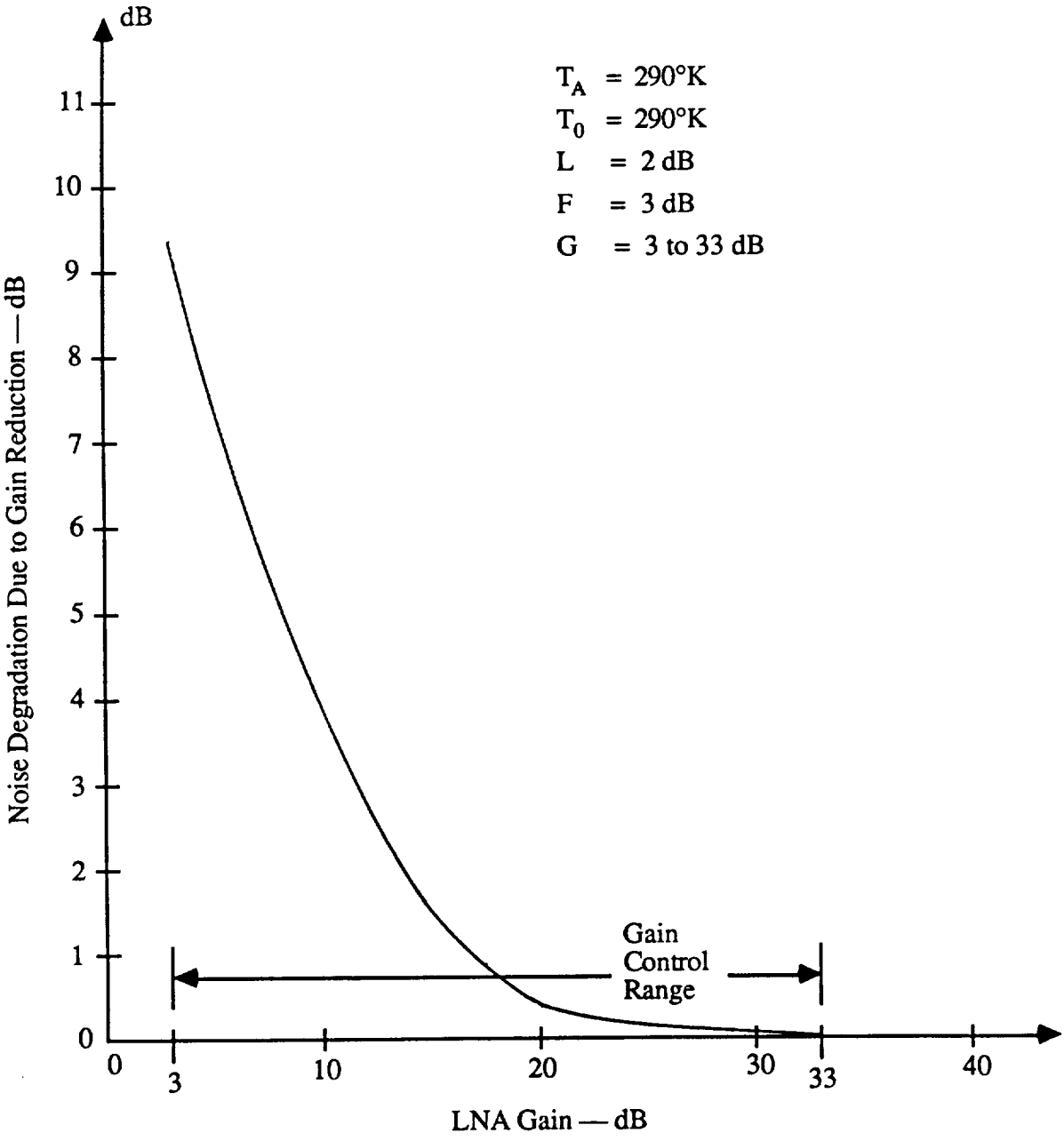

Figure 6.4-2. Noise Degradation as Function of LNA Gain.

6.5.1 Background Information

The following questions were addressed to Axiomatix:

(1) Is there really any advantage in using the FO cables, considering the cost and the current level of the technology, or will the conventional RF cable be sufficient?

(2) Considering the complexity of a channelized approach for the amplification prior to the FO (or RF) cable driver, is this approach warranted in view of the fact that a wideband IF amplification shows promising results?

(3) If one does consider the FO cable approach, what are the advantages of going to the 1300 nm operation?

As the result of these questions, we have reviewed the technical data available to us so far. Also, we have requested additional information from NASA so that we can be brought up to date on the latest developments and trends.

We have also examined the fiber optic vs. coaxial link ranking table presented in Appendix A (p. A-140) of the McDonnel Douglas, Phase B Study Report of December 1985.

From this table we have extracted the data which pertains to the rating of the cable network for the Ku-Band MA system. In addition to the ranking factors already given in the table, we have provided an "importance factor" value and weighted the ranking factors by the appropriate values of this importance factor. Table 6.5.1-1 shows the results. It is interesting to note that despite the importance factor weighing, there is only a marginal advantage indicated in favor of the coaxial cable. We admit, of course, that our rating according to the importance factor is subjective and more fact finding has to be performed.

Table 6.5.1-1. Fiber Optic vs. Coaxial Link Ranking.[1], [2]

	Importance Factor	ILD-PIN/FET FO Link 750 MHz Max	Points	COAX CABLE Link[3]	Points
Weight	3	5	15	1	3
Power/Thermal	1	4	4	5	5
RFI/EMP	2	5	10	1	2
Intermod/Linearity	1	3	3	5	5
Reliability	3	3	9	5	15
Maintainablity	2	4	8	5	10
Commonality	1	4	4	5	5
Growth Potenial	2	5	10	4	8
Interface/Assy	1	5[4]	5	5	5
Cost	2	2	4	5	10
Risk	3	3	9	5	15
Total Unweighed Points		43		46	
Total Weighed Points			81		83

(1) Ranking is from POOR (1) to BEST (5)

(2) Based on a cable lenght of 500 ft.

(3) Based on 1/4 inch Heliax coaxial cable.

(4) Can have many optical fibers in a small cable.

Importance factor: 3 = highest

6.5.2 Some Specific Comparison Criteria

We have continued our examination of the performance comparison of co-axial vs. fiber optic IF link. The data available to us is that contained in the RCA report [1] on the Proof of Concept (POC) breadboard. The specific data which we are examining is contained in Appendix A11 of this report. Figure 6.5.2-1 is the performance comparison of the two approaches, i.e., co-ax vs. fiber cable IF transmission. We have used the third-order intermodulation data given in this figure for the prediction of the effect of the intermods on the power control window. In our last monthly report, we have commented on the fact for a 10 dB power control window sufficient margin exists between the thermal noise of the "weak" signal and the third order intermods generated by strong signals.

It is our understanding that the intermod data provided by RCA (see tables in Figure 6.5.2-1) is based on actual experimental data. We have been also assuming that the third order intermodulation is of the 2A-B (or 2B-A) type which is the case for two signals. If this indeed is the case than we can expect that the intermodulation of the A + B – C type (i.e., a case of three signals) will be about 6 dB higher than that due to 2A – B type. However, even if this is the case, the intermods are still at least 20 dB below the noise level of a "weak" signal, i.e., the signal which is 10 dB below the other, stronger signals. Therefore, from this point of view there is no obvious disadvantage for either of the approaches.

With respect to the dynamic range capabilities of the coax and the fiber cable implementations, Figure 6.5.2-1 shows that for both of these systems the smallest gap between the signal and the third intermod intercept point occurs at the output of the second down converter stage, i.e., stage 12 in Figure 6.5.2-1. For this stage the signal is a –31 dBm and the third IM intercept point is at 0 dBm. If we assume that the 1 dB compression point is about 10 dB below the 3 IM intercept, than there is about 21 dB margin before the signals begin to clip. Thus, if we assume that one of the signals is 10 dB stronger than –31 dBm than we still have about 11 dB of margin before clipping. The only fact which is not

SYSTEM NF AND IM PRODUCT LEVELS

STAGE #	NF (DB)	GAIN (DB)	INTCPT (DBM)	SIGNAL (DBM)	SYS NF (DB)	IM PROD (DBS)
INPUT	-	-	-	-60.0	3.66	200.0
1	1.0	-1.0	100.0	-61.0	2.66	200.0
2	2.5	33.0	24.0	-28.0	21.27	104.0
3	10.0	-10.0	5.0	-38.0	11.27	85.0
4	4.0	14.0	24.0	-24.0	24.38	82.8
5	4.0	12.0	32.0	-12.0	36.35	79.0
6	30.0	-30.0	200.0	-42.0	6.35	79.0
7	4.0	15.0	30.0	-27.0	17.63	78.9
8	12.0	-12.0	40.0	-39.0	5.63	78.8
9	4.0	14.0	24.0	-25.0	14.72	77.9
10	9.0	-9.0	100.0	-34.0	5.72	77.9
11	4.0	14.0	24.0	-20.0	15.00	75.6
12	11.0	-11.0	0.0	-31.0	4.00	60.3
13	4.0	14.0	24.0	-17.0	0.00	59.7

COAX

SYSTEM NF AND IM PRODUCT LEVELS

STAGE #	NF (DB)	GAIN (DB)	INTCPT (DBM)	SIGNAL (DBM)	SYS NF (DB)	IM PROD (DBS)
INPUT	-	-	-	-60.0	4.08	200.0
1	1.0	-1.0	100.0	-61.0	3.08	200.0
2	2.5	33.0	24.0	-28.0	27.08	104.0
3	10.0	-10.0	5.0	-38.0	17.08	85.0
4	4.0	14.0	24.0	-24.0	30.87	82.8
5	4.0	12.0	32.0	-12.0	42.86	79.0
6	40.0	-35.0	-15.0	-47.0	5.96	62.6
7	4.0	15.0	30.0	-32.0	16.65	62.6
8	12.0	-12.0	40.0	-44.0	4.65	62.6
9	4.0	15.0	30.0	-29.0	11.42	62.6
10	6.0	-6.0	100.0	-35.0	5.42	62.6
11	4.0	15.0	30.0	-20.0	15.00	62.4
12	11.0	-11.0	0.0	-31.0	4.00	56.2
13	4.0	14.0	24.0	-17.0	0.00	55.8

FIBER

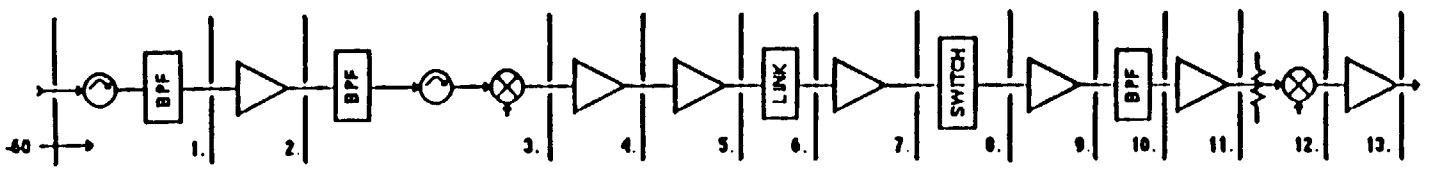

Figure 6.5.2-1. Receive Link Performance Coax vs. Fiber Comparison [6.1]

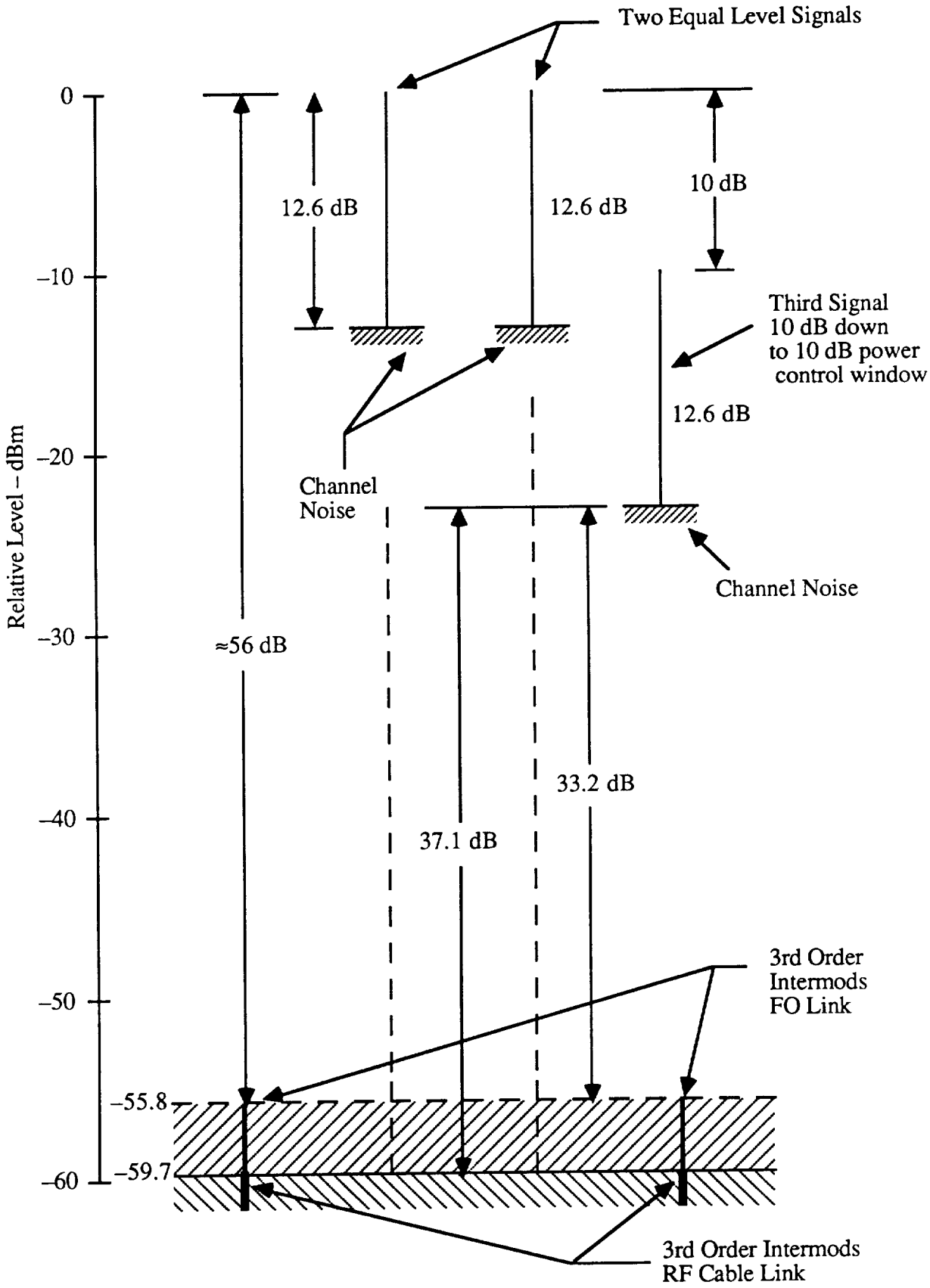

Figure 6.5.2-2. Projected 3rd Order Intermods for FO and RF Cable Links.

obvious to us is whether the –31 dBm level refers to one signal of a group of several signals or to a group of several signals. We are examining some of these variations and the possible effect of these on the power window tolerance.

To use the up-to-date model of the Space Station receiving chain, we have examined the RCA report on the Proof of Concept (POC) breadboard. Figure 6.5.2-2 shows the projected 3rd order intermods (two-signal case) for both the FO and the RF cable links. As the figure shows the intermods are at –55.8 dB and –59.7 dB, respectively.

We also show the level of channel noise for the two signals. The channel SNR of 12.6 dB is shown. This SNR corresponds to uncoded 44 Mbps transmission from MSC at 200 m, and uncoded EVA links at 200 m and 1 km.

We can see that the 3rd order IM noise is at least 43 dB below the level of the channel noise.

We also show a third signal which is 10 dB down with respect to the two main "reference" signals. This 10 dB down condition may be representative of a signal at the low extreme of the power control window. It can be seen that for this case the 3rd order intermods are still at least 33 dB (FO link) down. Although this 33 dB "margin" may not be accurate, because the presence of the third signal does contribute additional intermods, it is reasonable to assume that the margin will not be degraded significantly. This means that with respect to the 3rd order IM products either system will perform adequately with a 10 dB power window.

REFERENCE

[6.1] RCA, "Space Station Communications and Tracking Multiple Access Communications System Proof of Concept Breadboard," Final Report, MA-219T, August 1987.

7.0 MULTI-CHANNEL MODEM CONSIDERATIONS

7.1 Introduction and Overview

Although the present concept of the return links can be satisfied by a conventional 4-PSK (i.e., QPSK) modulation providing either two independent channels, or one channel coded at rate 1/2, the motivation to consider the 8-PSK mode results from the MSC requirement for 3 digital television channels. Thus, the idea expressed in this report is that a 4-PSK modem design baselined for the major portion of users can be expanded to include an 8-PSK capability at a reasonable cost in increased complexity. In other words, the intent here is to assume a 4-PSK design as a baseline which is easily expanded to include an 8-PSK capability. Ideally, the component partitioning would be such that a major portion of the modem will consist of the 4-PSK capability, with the 8-PSK capability provided in the form of plug-in modules for the MSC user as well as for other users which may require 3 digital TV channels in the future.

The design considerations for a multi-channel modem are driven by the requirement to transmit and receive digital TV signals at rates up to 22 Mbps – 25 Mbps per channel. Thus, circuit configurations which can be implemented by high speed circuitry must be given primary consideration.

7.2 Modem Requirements

The return link requirements for Ku-band MA users are summarized in Table 7.2-1. From the table, it can be seen that there are basically two return rates; one at about 100 kbps and the other at about 22 Mbps. Although, as shown in the table, the two Phase B contractors established slightly different requirements for these two rates, the implementation driver for the modem is still the upper rate which may be as high as 25 Mbps according the RI estimate.

The functional goals which are the motivators for considering an 8-PSK modem to meet the MSC requirement for 3 simultaneous digital TV channels are as follows:

User	Requirement Rates				Comments
	TLM/Voice (kbps)		Video (Mbps)		
	MCDD	RI	MCDD	RI	
MSC	160	128	22	25	Three simultaneous video signals are required.
EVA	100	128	22	25	
NSTS	100	128	N/A	N/A	
OMV/OTV	100	128	22	25	
FF/COP	100	128	22	25	

MCCD = Requirement established by McDonnell Douglas Corp. team [1].
RI = Requirement established by Rockwell International team [2].

Table 7.2-1. Return Link Requirements for Ku-band MA-Users.

1) Addition of the three-channel capability must not increase RF channel bandwidth significantly beyond that for the two-channel mode.

2) Modulation method should not change drastically when the modem switches from 2-channel to 3-channel mode.

3) The modem must have as much hardware commonality as possible between the 2-channel and the 3-channel modes.

Figure 7.2-1 shows a functional diagram of a 4/8-PSK multi-channel modem utilization within the Ku-band MA system. As indicated, the 4-PSK (i.e., QPSK) mode is the baseline, and the 8-PSK mode is considered as a multi-channel capability. This diagram is responsive to the goals stated above. One of the salient features of the concept shown in Figure 7.2-1 is that a constant envelope signal is provided by the 8-PSK operation making it fully compatible with the RF amplification equipment used with the 4-PSK mode.

Figure 7.2-2 shows a functional hardware partitioning for the proposed 4/8-PSK modulator and the corresponding demodulator. The main idea expressed in Figure 7.2-2 is that the 4-PSK mode is the baseline mode for the modem and that the 8-PSK mode is a hardware "add-on" to be utilized by such users as the MSC. Such partitioning requirement determines the modem implementation/configuration design described in the subsequent section of this report.

Appendix O contains detailed description of the implementation for a multi-channel modem. Because the subject matter presented there deals mainly with the implementation of the modulation/demodulation functions of the proposed modem, we do not address the issues of an IF frequency at which the actual modem implementation should take place. It suffices to state, however, than an IF frequency in the range of 150 MHz to 700 MHz is envisioned. The final selection of the IF frequency will be determined by the frequency plan of a particular Ku-band MA system selected for the Space Station/user application.

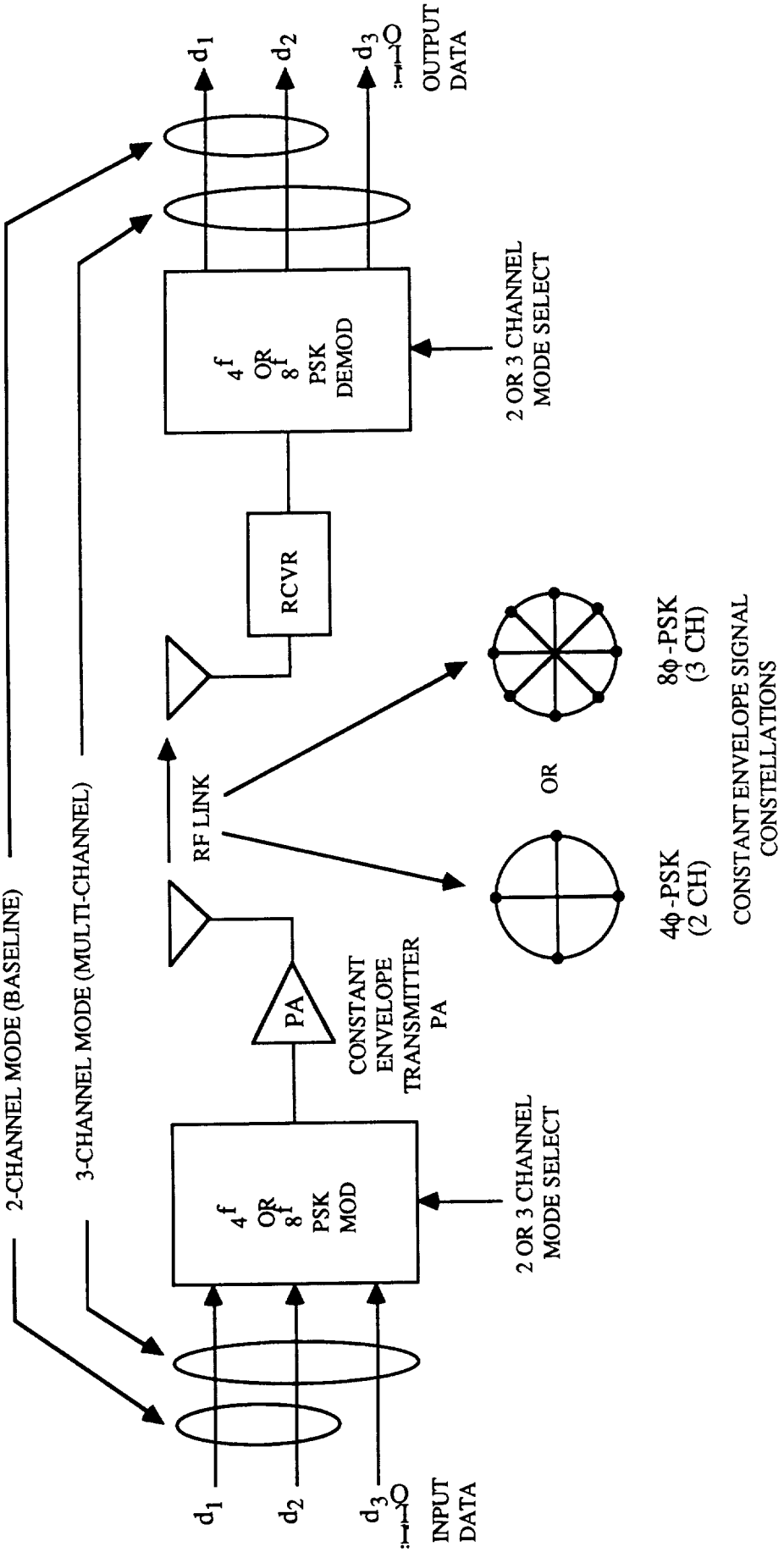

Figure 7.2-1. Functional Diagram of a Multi-Channel 4/8-PSK Modem System.

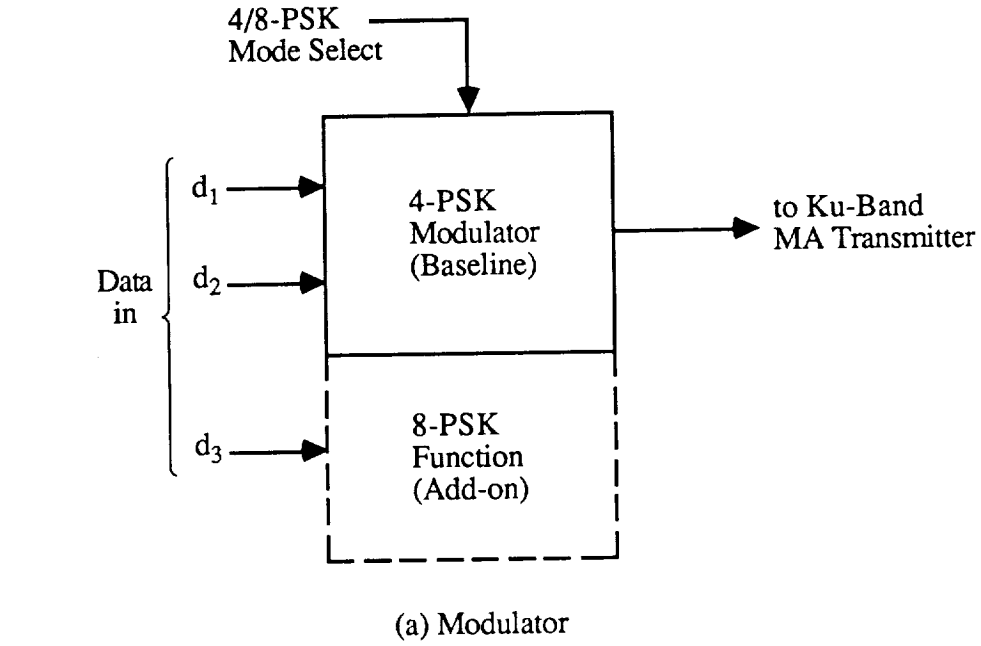

(a) Modulator

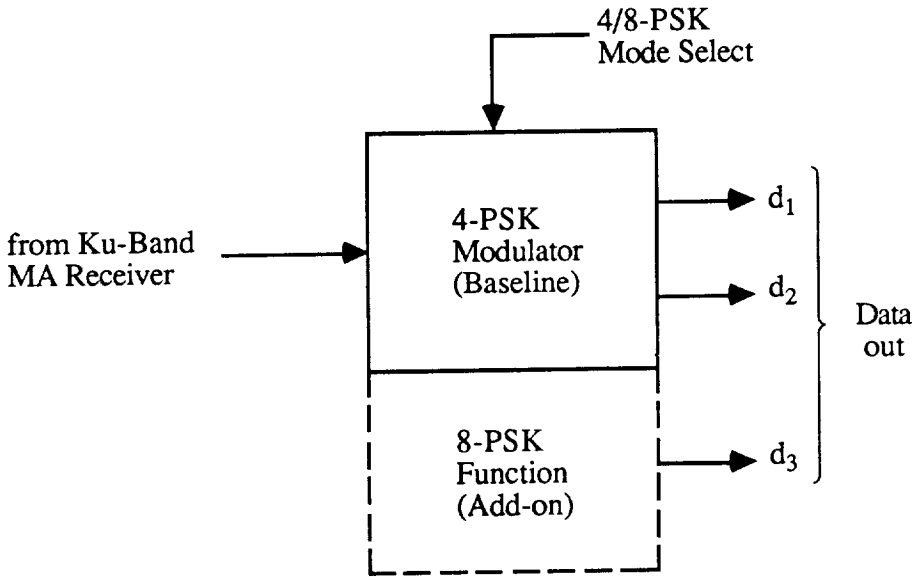

(b) Demodulator

Figure 7.2-2. Functional Hardware Partitioning for the 4/8 PSK Modulator (a) and Demodulator (b).

7.3 Multi-Channel Modem for FTS

7.3.1 Introduction and Overview

The motivation to consider an 8-PSK modem for FTS results from the FTS requirement for 4 digital television channels and one high data rate channel. Thus, the idea expressed here is that a 4-PSK modem design baselined for the major portion of the Space Station users can be expanded to include an 8-PSK capability at a reasonable cost and with only moderate increase in complexity. In other words, the intent here is to assume a 4-PSK design as a baseline which is easily expanded to include an 8-PSK capability. Ideally, the component partitioning would be such that a major portion of the modem will consist of the 4-PSK capability, with the 8-PSK capability provided in the form of plug-in modules for the FTS user as well as for other users (MSC, for example) which may require multiple high digital rate channels in the future.

The modem design considerations are driven by the requirement to transmit and receive up to three (3) digital data streams at rates up to 22 Mbps – 25 Mbps per channel. Thus, circuit configurations which can be implemented by high speed circuitry are given primary consideration.

7.3.2 Modem Requirements

The return link requirements for the FTS are summarized in Table 7.3.2-1. As shown, there are four channels of digital data required. One channel is a full motion channel digitized to data rate of 22 Mbps. The other three channels carry 10 Mbps. The other three channels carry 10 Mbps digital video which is a reduced motion video data. The remaining channel is a high data rate channel. The total throughput rate to be accommodated by the modem is 62 Mbps.

Considering the fact that each wideband channel of the MA system can accommodate 22 to 25 Mbps rate, three such channels can provide the required throughput.

An 8-PSK modem provides the capacity to carry three 22 to 25 Mbps channels simultaneously within the RF bandwidth of a single channel.

To convert the five channels listed in Table 7.3.2-1 into three channels which are compatible with an 8-PSK modem, a multiplexer is required. Part (a) of Figure 7.3.2-1 shows a functional block diagram for such multiplexer (MUX). The corresponding demultiplexor is shown in part (b). The MUX/DEMUX equipment is unique to the FTS requirement and thus should be a part of the FTS interface. The 8-PSK function can be a part of the "standard" add-on to the MA baseline equipment. In other words, the 8-PSK add-on can be used by other potential users of the MA system. The MSC is an example of such potential user.

The actual modem implementation is identical to the one described in Section 7.2 and covered in detail in Appendix O.

Channel	Signal Type	Data Rate (Mbps)	Comments
1	TV	10	Reduced motion
2	TV	10	Reduced motion
3	TV	10	Reduced motion
4	TV	22	Full motion TV
5	Data	10	High data rate
		62	Total throughput

Table 7.3.2-1. FTS Return Link Requirements.

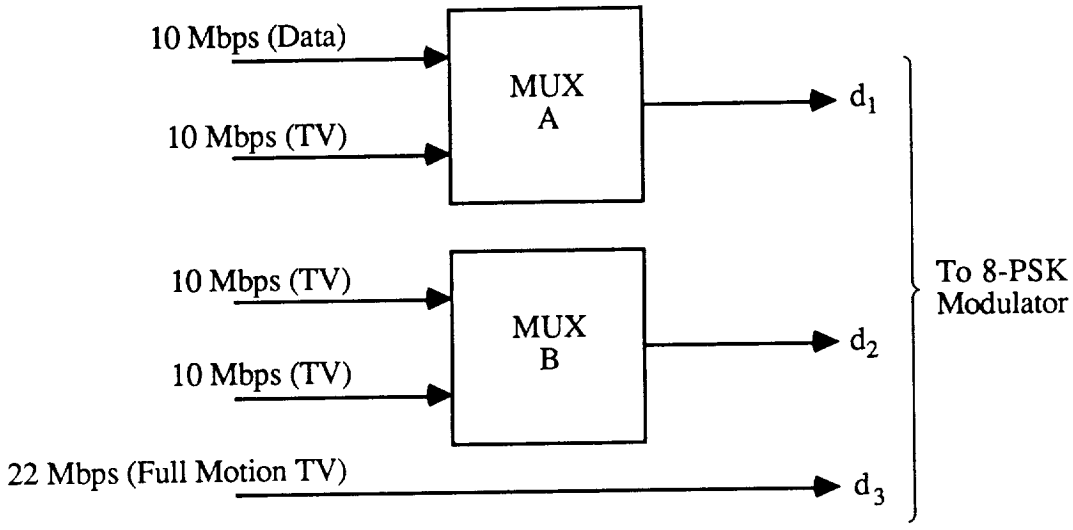

(a) Modulator MUX

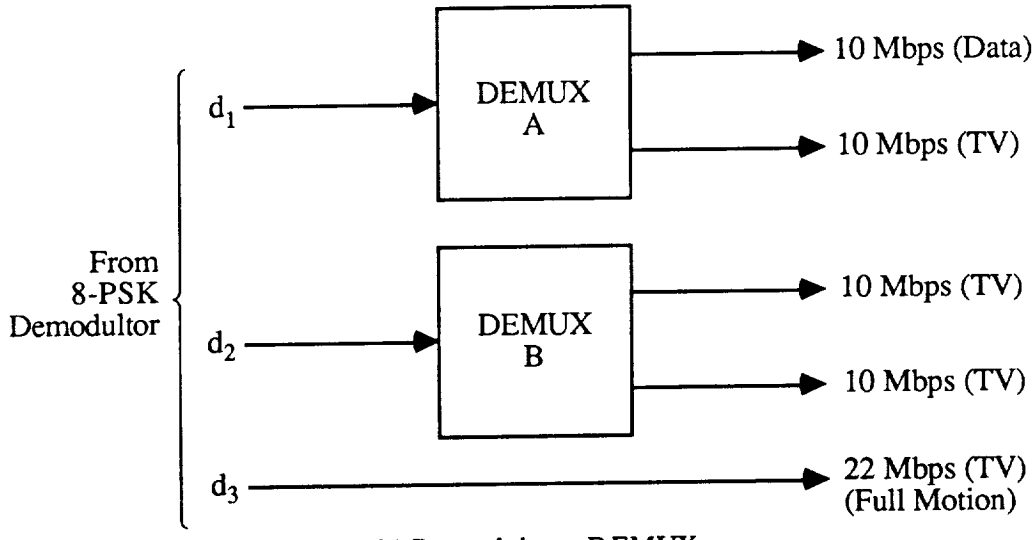

(b) Demodulator DEMUX

Figure 7.3.2-1. MUX/DEMUX Functional Requirements for FTS 8-PSK Modem.

8.0 FTS/EVA EMERGENCY SHUTDOWN LINK

8.1 Overview of the Concept

The purpose of the link is provide the EVA's with the capability to shutdown the FTS in case the latter endangers the activity of the EVA or EVA's. Figure 8.1-1 shows the basic concept developed to date by Axiomatix and NASA. The concept operates as follows:

(1) EVA's send low duty cycle signals to FTS. The purpose of these signals is to test the quality of the links between the EVA's and FTS.

(2) FTS detects the low duty cycle EVA signals, monitors the quality of these signals, and reports the quality to the Space Station via the "normal" FTS/SS link which can be either at Ku-Band or hardwire.

(3) Space Station reports to the EVA's any malfunction of the EVA/FTS links. This reporting is via the "normal" SS/EVA forward links.

(4) For FTS safety action the appropriate EVA transmits a coded, high duty cycle signal directly to the FTS to disable it.

8.2 Modulation Trade-Offs and Link Budgets

Axiomatix has considered three modulation types for the FTS/EVA emergency shutoff link. These modulation types were: (1) pulsed AM with a coded tone sequence, (2) pulsed FM/FSK with a coded tone sequence, and (3) spread spectrum PN sequence modulation. The advantages of both the pulsed AM and the pulsed FM/FSK are the availability of proven technology, relatively simple implementation and independence from requiring complicated sync procedures. The disadvantage of these two simple techniques is that they inherently lack signal processing/interference rejection capability. However, Axiomatix is proposing a signal encoding technique [8.1] which will provide either the pulsed AM or the pulsed FM/FSK transmissions with powerful interference rejection capabilities. This coding technique will not only provide signal immunity from spurious

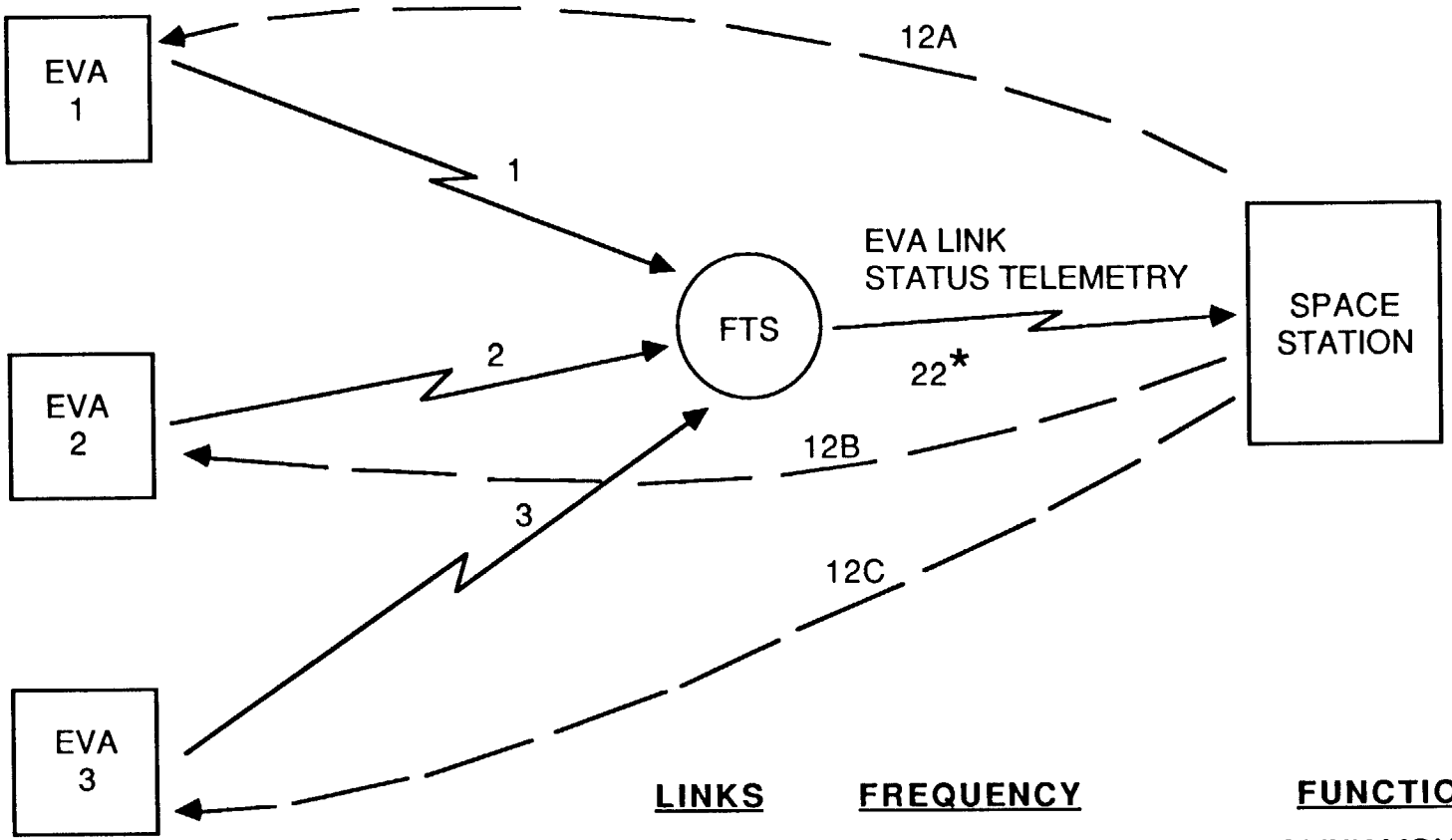

LINKS	FREQUENCY	FUNCTION
1, 2, 3	TBD	PROVIDE LINK MONITOR STATUS SIGNAL AND FTS SHUT DOWN
22	KU-BAND	REPORT EVA/FTS STATUS TO SS STATION VIA FTS/SS RETURN LINK
12A,12B,12C	KU-BAND	REPORT TO EVA THE STATUS OF THE EVA/FTS LINK

* THIS MAY BE A HARDWIRE LINK

Figure 8.1-1. FTS Safety Link Concept.

interference from the earth-based transmitters but it will also provide a capability for several EVA's to share a single RF channel without generating mutual interference.

From the standpoint of providing good interference immunity the spread spectrum technique based on pseudo-noise (PN) sequence modulation would be highly desirable. Furthermore, with this techniques code multiplexing can be used to allow for sharing by several EVA's of a single RF channel. However, from the standpoint of complexity, the PN spread spectrum technique may not be desirable. First, the technology involved is rather complicated and thus may require considerable power consumption. Second, the frequent signal fades which may occur in an operational EVA scenario may present problems in reacquiring either the carrier or the code, or both, of a PN signal. The time delays which may result in from such reacquisitions are not desirable for the application on hand. Third, a PN sequence modulation is not easily adaptable to working with low duty cycle signals which are required for the link status test transmissions.

For the reasons stated above, we decided to rule out the use of spread spectrum modulation for the FTS/EVA emergency shutoff link. Instead, we decided to examine in detail the possibilities of either the pulsed AM or the pulsed FM/FSK modulations. Table 8.2-1 summarizes the results of our modulation trade-off considerations.

To accommodate the single-channel technique proposed by Axiomatix, a minimum data rate of 1000 bps is required. Thus, we have re-worked our earlier link budgets, which were based on 100 bps to provide for the 1000 bps capability.

Figure 8.2-1 shows the demodulation model for the 1000 bps AM link. Table 8.2-2 provides the link budget for this link.

Figure 8.2-2 shows the demodulation model for the 1000 bps FSK link. The corresponding link budget is shown in Table 8.2-3.

MODULATION	ADVANTAGES	DISADVANTAGES
1) PULSED AM WITH CODED TONE SEQUENCE	1. PROVEN TECHNOLOGY 2. SIMPLE IMPLEMENTATION 3. NO COMPLICATED SYNC PROCEDURE REQUIRED	1. VULNERABLE TO INTERFERENCE *
2) PULSED FSK WITH CODED SIGNAL SEQUENCE	1. PROVEN TECHNOLOGY 2. SIMPLE IMPLEMENTATION 3. NO COMPLICATED SYNC PROCEDURE REQUIRED	1. VULNERABLE TO INTERFERENCE *
3) SPREAD SPECTRUM PN SEQUENCE MODULATION	1. PROVIDES GOOD INTERFERENCE IMMUNITY 2. CODE MULTIPLEXING CAN BE USED TO PROVIDE FOR A SINGLE RF CHANNEL OPERATION	1. COMPLEX TECHNOLOGY 2. CODE AND CARRIER RE-SYNC MAY BE REQUIRED AFTER SIGNAL FADES 3. MAY NOT BE ADAPTABLE TO PULSED OPERATION WHICH MAY BE REQUIRED TO KEEP THE DUTY CYCLE LOW DURING NON-EMERGENCY SITUATION

* Vulnerability to interference can be alleviated by means of special modulation/coding technique proposed by Axiomatix.

Table 8.2-1. FTS Safety Link Modulation Trade-Offs.

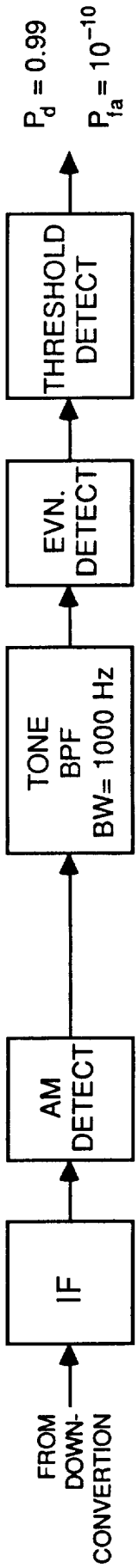

Figure 8.2-1. FTS Safety Link AM Demodulation Model for 1000 bps Rate.

Number of AM tones	1	
Transmitter Power (watts)	0.001	1 mw
Transmitter power (dBw)	–30.0	
Transmit circuit loss (dB)	–0.5	
Transmit antenna gain (dB)	–20.0	85% spherical coverage
Transmit pointing loss (dB)	–3.0	
EIRP (dBm)	–53.5	
Path Loss (dB)	–62.0	100 m, 300 MHz
Receive antenna gain (dB)	–20.0	85% spherical coverage
Receive pointing loss (dB)	–3.0	
Polarization loss (dB)	–3.0	Estimate
Receive circuit loss (dB)	–0.5	
Received signal power (dBw)	–142.0	
System noise density (dBw/Hz)	–199.0	NF = 5 dB
Carrier to noise density (dB-Hz)	57.0	
Modulation loss (dB)	–4.8	
Detection Bandwidth (dB-Hz)	–30.0	1000 Hz Bw
Receive SNR (dB)	22.2	
Theoretical SNR (dB)	16.1	$P_d = 0.99$, $P_{FA} = 10^{-10}$
Implementation loss (dB)	2.0	
Required SNR (dB)	18.1	
Link Margin (dB)	4.1	

Table 8.2-2. Link Budget for AM FTS Safety Link at R = 100 m (Data Rate 1000 bps).

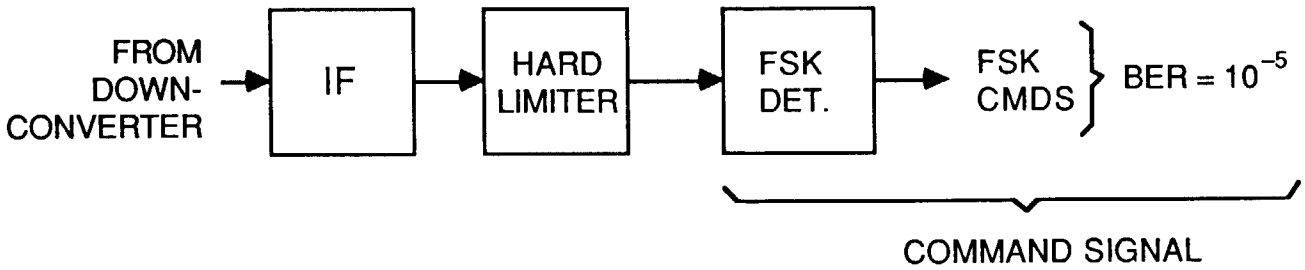

Figure 8.2-2. FTS Safety Link FSK Demodulation Model for Data Rate of 1000 bps.

Transmitter power (w)	0.001	1 mw
Transmitter power (dBw)	–30.0	
Transmit circuit loss (dB)	–0.5	
Transmit antenna gain (dB)	–20.0	85% spherical coverage
Transmit pointing loss (dB)	–3.0	
EIRP (dBm)	–53.5	
Path Loss (dB)	–62.0	100 m, 300 MHz
Receive antenna gain (dB)	–20.0	85% spherical coverage
Receive pointing loss (dB)	–3.0	
Polarization loss (dB)	–3.0	Estimate
Receive circuit loss (dB)	–0.5	
Received signal power (dBw)	–142.0	
System noise density (dBw/Hz)	–199.0	NF = 5 dB
Carrier to noise density (dB-Hz)	57.0	
Modulation loss (dB)	–1.0	Estimate
Data rate (dB-Hz)	–30.0	1000 bps
Receive E_b/N_0 (dB)	26.0	
Theoretical E_b/N_0 (dB)	13.4	FSK, BER = 10^{-5}
Implementation loss (dB)	2.0	
Required E_b/N_0 (dB)	15.4	
Link Margin (dB)	10.6	

Table 8.2-3. Link Budget for FSK Modulated FTS Safety Link Command at R = 100 m and Data Rate of 1000 bps.

8.3 Equipment Configurations

The requirement for the FTS/EVA emergency shutoff link calls for a relatively simple, small, light weight, and low power consumption transmitter at the EVA end of the link. The requirement at the FTS end of the link calls for receiver capable of receiving simultaneously the transmissions from several EVA's. The descriptions given below pertain to EVA transmitting and FTS receiving equipment.

8.3.1 EVA Transmitter

Figure 8.3.1-1 shows a functional block diagram for an EVA transmitter. As shown, the modulator and the coder develop appropriate signals for link status test (low duty cycle) and emergency shutdown command. Then signals are developed at an IF which may typically be 10.7 MHz or any other frequency in the 5 to 20 MHz range. The IF signal is the upconverted by a balanced mixer and the appropriate frequency term is filtered by a BPF. This signal is then amplified, filtered, and applied to EVA antenna. The nominal transmission frequency may be about 300 MHz.

8.3.2 Frequency Division Multiplexing FTS Receiver

Figure 8.3.2-1 shows a functional block diagram for a multi-channel FTS receiver. The frequency division feature is provided by using several IF amplifiers, each tuned to a different frequency. The bandwidth of each of these IF amplifier may be approximately 10 KHz. The features of this type of receiver are summarized in Table 8.3.2-1.

The remaining issues pertaining to the use of this type of a receiver are summarized in Table 8.3.2-1. Axiomatix believes, however, that a single channel receiver described in the next section is more suitable for the type of coding/modulation proposed for the EVA/FTS link.

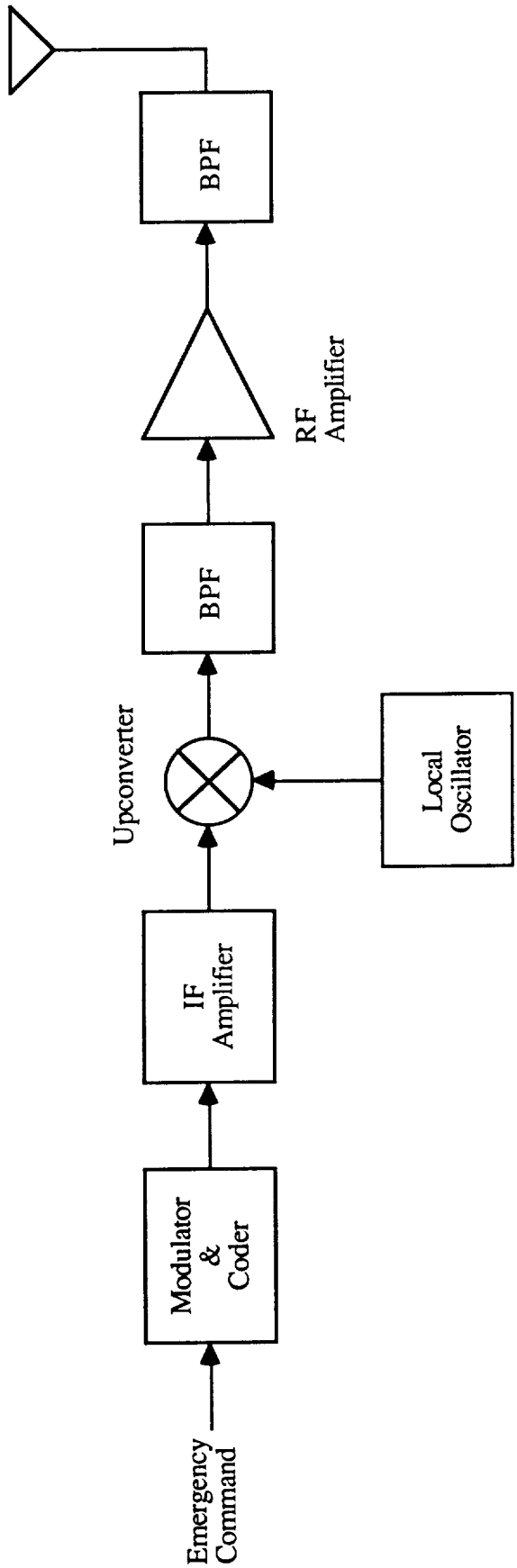

Figure 8.3.1-1. Functional Block Diagram of EVA Transmitter.

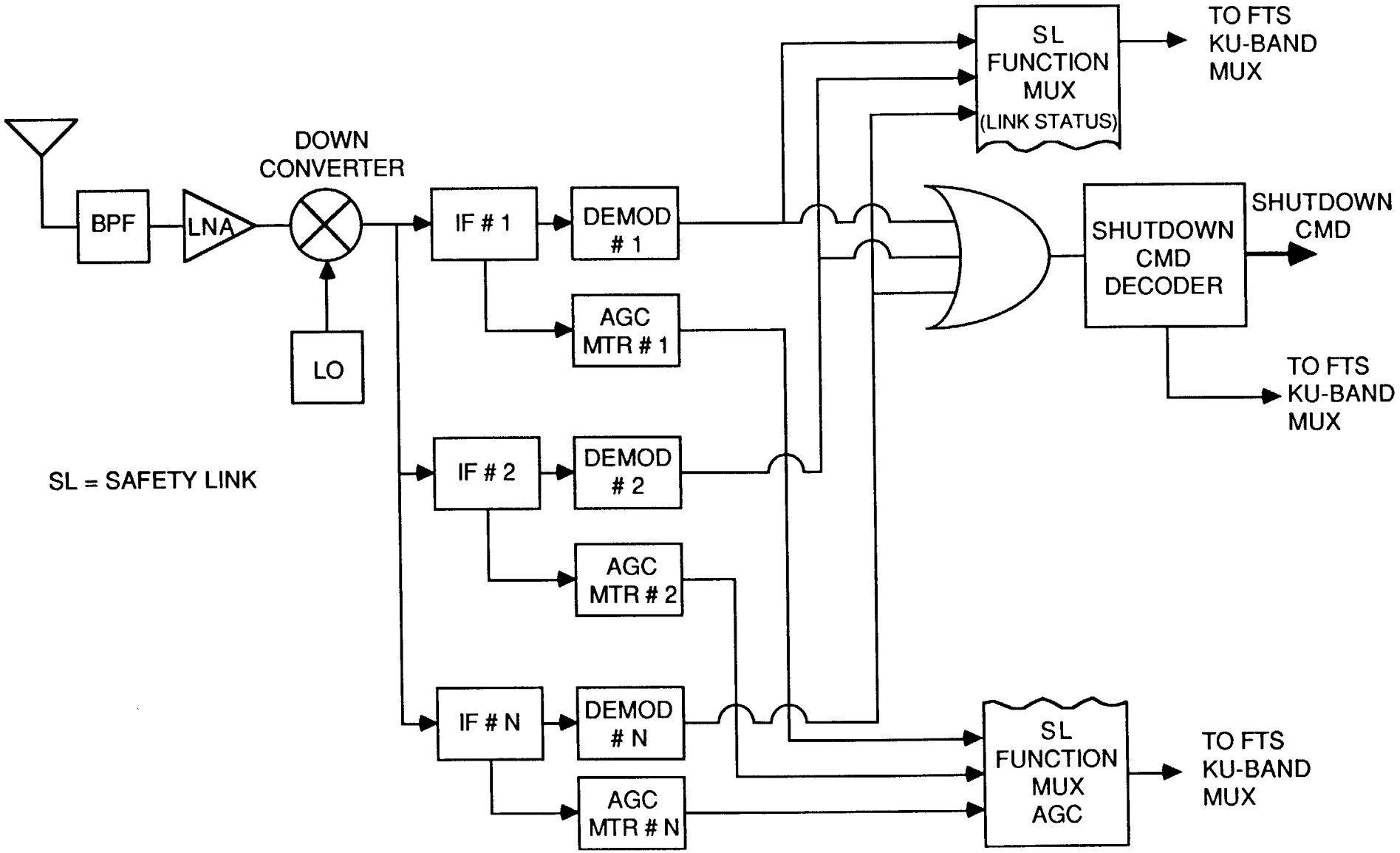

Figure 8.3.2-1. Multi-Channel FTS Safety Link Receiver – Functional Block Diagram (AM or FM).

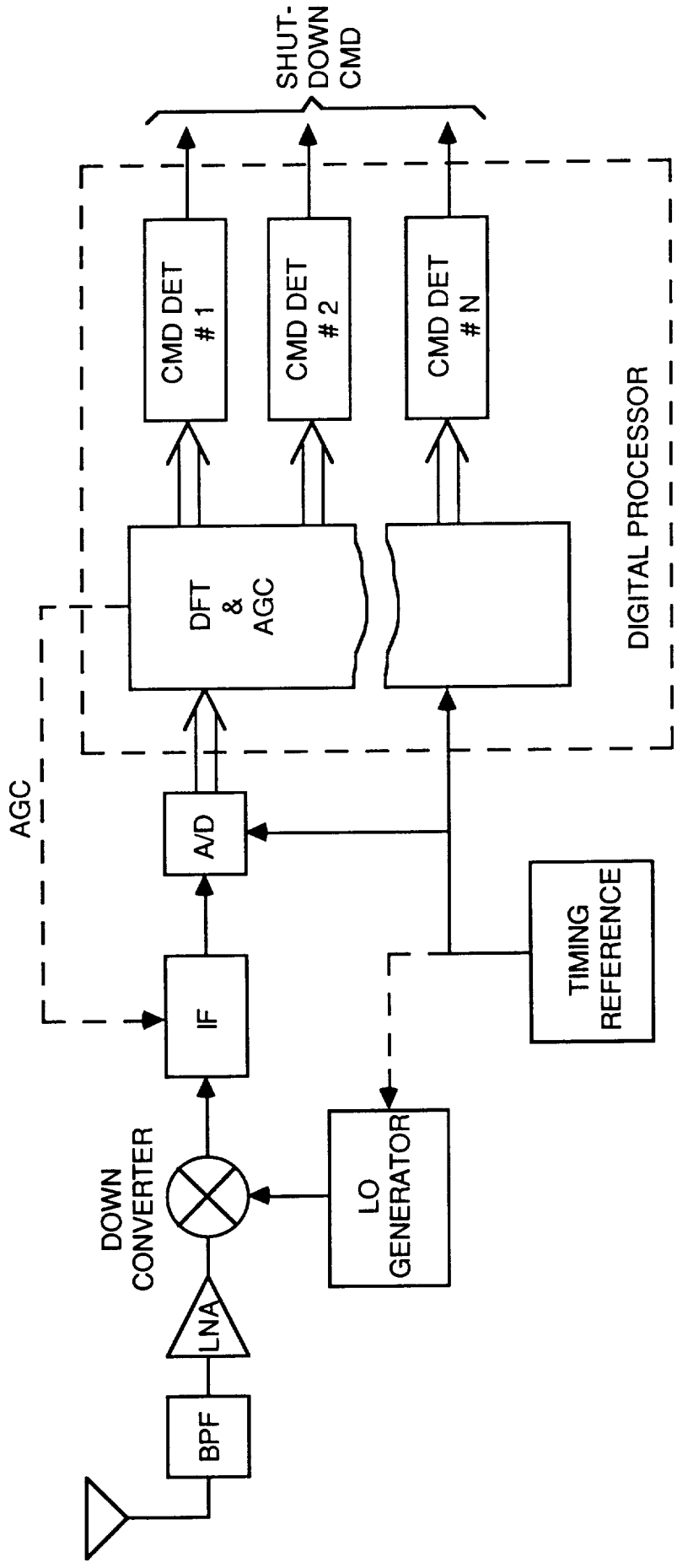

Figure 8.3.3-1. FTS Safety Link Single RF Channel Receiver (AM or FM) Functional Block Diagram.

- SIMPLE FRONT END CONSISTS OF A BPF AND AN LNA. BPF COVERS 3 (OR MORE) CHANNELS OF EVA SL TRANSMISSIONS.*

- SINGLE CONVERSION RECEIVER WITH SEVERAL IF'S, EACH TUNED TO A SPECIFIC EVA SL CHANNEL.*

- EITHER ONE OF EVA SL TRANSMISSIONS CAN BE DECODED (A SINGLE SHUT-DOWN CMD DECODER IS USED).*

- LINK STATUS IS MONITORED AND TRANSMITTED TO SS VIA A "NORMAL" KU-BAND RETURN LINK.

- AN ADDITIONAL FEATURE IS AGC MONITORING AND TRANSMISSION TO SS FOR THE PURPOSE OF PROVIDING COARSE INFORMATION ON EVA RANGES TO FTS.

* DEPENDING ON SIGNAL DESIGN THESE FEATURS MAY BE EITHER SIMPLIFIED OR MODIFIED.

Table 8.3.2-1. Multi-Channel FTS Safety Link Receiver (AM or FM) Features.

- COMMON VS. INDIVIDUAL SHUT-DOWN COMMAND DECODER(S).
- AGC DESIGN FOR RECEIVED SIGNAL HAVING VARYING DUTY CYCLES.
- ADDITIONAL COMPLEXITY REQUIRED TO PROVIDE AGC MONITORING LINK TO SS. (IS AGC MONITORING DESIRED?)
- RECEIVER FREQUENCY PLAN CONSIDERATIONS (SELECTIVITY VS. COMPLEXITY).

Table 8.3.2-2. Multi-Channel FTS Safetly Link Receiver (AM or FM) – Remaining Issues.

8.3.3 Single Channel Receiver

Figure 8.3.3-1 shows a functional block diagram for a single channel receiver. The salient features of this receiver configuration are summarized in Table 8.3.3-1. This receiver is for the type of modulation/coding described in Reference 1. The design issues pertaining to the single channel receiver are summarized in Table 8.3.3-2. These issues will be resolved during the subsequent phases of the program.

REFERENCE

[8.1] J. Dodds, S. Udalov, "FTS/EVA Emergency Link Analysis," Axiomatix Report No. R8805-6, May 26, 1988.

Table 8.3.3-1. FTS Safety Link Single RF Channel Receiver Features.

- Uses single RF channel for reception of several EVA signals
- Analog-to-digital conversion is performed at IF
- AGC function is performed in the digital processor
- Signal demodulation is performed in the digital processor
- Digital processing permits detection and identification of different commands from multipath EVAs.

Table 8.3.3-2. Design Issues Pertaining to the Single Channel Receiver.

- Frequency plan (selection of IF frequency)
- Handling of several signals of different signal strength
- Signal level stabilization (AGC vs. hard limiting)
- A/D converter performance
- Digital processor architecture and complexity

9.0 SPACE STATION INFORMATION SYSTEM CODING

The initial effort on the Space Station Information System (SSIS) coding was directed toward an investigation of alternate error detection and/or error correction schemes for the transfer frame and the transfer frame header. During this investigation, Axiomatix was directed to examine the viability of a new code developed by Don Schilling and David Manela, dubbed the SM code, for use with the SSIS links.

The initial investigation analyzed the performance of a (255,223) 8 bit per symbol error correction code for the transfer frame capable of correcting 16 symbol errors. We have shown that even using the full error correction capability of the code, the probability of undetected error is less than 10^{-13}. Three codes were investigated for the transfer frame header. All three codes are (64,48) codes having 16 check bits. The error detection performance of these codes was simulated by generating a series of pseudorandom error sequences for input to each of the three types of decoders. Each decoder uses the same series of pseudorandom sequences, so that the relative performance can be directly compared. We have simulated a binary Hamming code, a binary BCH code, and a 16-ARY Reed-Solomon code. Details of the analysis and simulation are given in Appendix P of this report.

Warner Miller and Henry Chen sent us a copy of a report by Robert Deng [9.1] concerning the use of a Kasami code for the frame header. We reviewed the report and responded with a technical memo, included as Appendix Q of this report.

Axiomatix also assessed the performance of a new class of codes, the Schilling-Manela or SM codes. We reviewed the Manela thesis, which describes the various classes of SM type codes, and implemented an SM-4 and SM-8 decoder on the PC in FORTRAN. Our goal was to duplicate the results from the thesis in order to independently verify the code performance. The code performance is strongly dependent on the slopes selected for computation of the parity bits. We were not able to duplicate the code performance for either the SM-4 or SM-8 code, having tried several different combinations of parity slopes.

We contacted David Manela to obtain the slopes he used to get his results, but for proprietary reasons, he was reluctant to divulge his optimum slopes.

Our findings concerning the SM codes are discussed in Appendix R. Basically, our opinion at the time was that the SM codes are not sufficiently well understood to supplant the more well known codes being considered. This opinion was conveyed to Sid Novosad via a technical memo, included as Appendix S.

[9.1] Deng, Robert H., "An Optimum (85,64) shortened Cyclic 10-Burst-Error-Correcting Code and Its Performance Analysis," Notre Dame Department of Electrical Engineering, April 14, 1987.

10.0 WANDERER TRACKING

Axiomatix was tasked under the aegis of the Space Station program to assist in the NASA effort to develop a low-cost means of tracking and locating memory-impaired individuals, perhaps using identification tag technology proposed for the Space Station item identification. Axiomatix reviewed the various relevant documents, including the Johnson Engineering study on active ID tags [10.1], and the CORTREX progress reports. We independently submitted a technical memo, describing a locater system utilizing a normally-off transmitter to minimize battery power requirements for the wearer unit. We also derived a candidate modulation scheme to uniquely identify each wearer.

A more detailed description of our proposed system configuration is included as Appendix T.

[10.1] "Study Report for an Item Tracking System Using Active Identification Tags," Johnson Engineering under NASA contract NAS9-16415, May 10, 1987.

11.0 OPTICAL COMMUNICATION SYSTEMS ANALYSIS

Axiomatix had tasked the University of Kansas, under a subcontract to this contract, to provide a simulation model for an optical communication system. The principal investigator under this subcontract was Dr. K. Sam Shanmugan, the chief architect of the Block-Oriented Systems Simulation (BOSS) language. NASA/JSC already possesses the BOSS shell operating system for the Space Station Communications System Simulator (SCSS).

The deliverable for this subtask included a series of BOSS compatible library modules, listed below, and a subtask final report authored by Dr. Shanmugan and J.K. Townsend of the University of Kansas. The subtask final report is included in this project report as Appendix U.

The BOSS Lighwave Module library supplied to NASA contains modules which are useful for analyzing certain single mode fiber digital and analog communication links. The library features a general Single Mode Fiber module, an Avalanche Photo-detector module, a PIN Photodetector module, a Semi-Analytic Error Rate Estimator module for digital On-Off keyed (OOK) systems, and a Power Series laser module, plus various other lower-level and internal modules (listed below).

In addition, two example systems are included to demonstrate how to use the modules.

The following is a list of the modules in the Lightwave Module Library arranged according to group name:

ANALOG MODULATORS
    LASER (POWER SERIES)

BASIC BUILDING BLOCKS *TYPE/UNITS CONVERSION*
    REAL TO DMB

CALIBRATION DEVICES/METERS
    DELAY METER (REAL)
    OPTICAL AVERAGE POWER
    PRINT AVERAGE OPTICAL POWER

CHANNELS
    SINGLE MODE FIBER (LINEAR)

DIGITAL SOURCES
    OOK OPTICAL SOURCE

ESTIMATORS
    NOISE BW IMPULSE INJECT (REAL)
    OOK_ERROR RATE ESTIMATOR

ESTIMATORS *INTERNALS*
    COUNT ERRORS_& GENERATE STOP
    DELAY TX_SIG
    NOISE_BW COMPUTER (REAL)
    OOK ERROR PROB CALCULATE
    OOK PRINT
    OOK_POINT TO_DISTANCE

FILTERS
    BUTWTH FILTER (REAL)

FILTERS *INTERNALS*
    2ND ORDER IIR SECTION (REAL)
    TAPPED DELAY LINE CELL (REAL)

NOISE AND INTERFERENCE
    AVALANCHE PHOTO-DETECTOR
    AVALANCHE PHOTODIODE RAN_GEN
    PIN PHOTO-DETECTOR

The top-level modules are discussed in more detail in the appendix. Many of the modules in the lightwave database are lower-level internal modules and are not explicitly discussed in detail here. Of course, on-line documentation is available for these modules as well as all other modules in BOSS. On-line documentation for the modules discussed below is provided in the appendix.

APPENDIX A

SPACE STATION TRACKING WITH STANDARD GPS

SPACE STATION TRACKING WITH STANDARD GPS

Prepared for

Contract No. NAS9-17414
Lyndon B. Johnson Space Center
Houston, Texas 77058

Prepared by

Kai T. Woo

Axiomatix
9841 Airport Boulevard, Suite 912
Los Angeles, California 90045

Axiomatix Report No. 8510-1
October 18, 1985

Table of Contents

List of Figures

List of Tables

Summary

It is expected that some of the Space Station Tracking Requirements, including short range tracking, long range tracking and proximity tracking, can be met by using the NAVSTAR Global Positioning System (GPS) or radio navigation systems based on the reception of GPS signals. The advantages of using GPS include superior tracking accuracies, and relatively low hard-ware development costs and complexity. The latter advantage stems from the fact that GPS is a partially developed system with demonstrated hardware and excellent test results.

At least three GPS based positioning techniques will be evaluated with respect to their achievable accuracies and feasibilities for Space Station Tracking. These are:

(i) Standard GPS, using L1 , C/A or P-Code signals;

(ii) Differential GPS (DGPS) using either L1 P-code or C/A code signals;

(iii) Radiometric systems such as the SERIES-X reported in [13] , which determines range using the GPS transmitted clocks and carriers but is essentially a code-less operation.

The Standard GPS approach has the advantage of being a stand-alone, receive-only operation; whereas, the DGPS and SERIES are both differential operations which require cooperative reference stations with surveyed locations, and communication links between users and the reference station.

In this current report the achievable accuracies of the Standard GPS in the Space Station altitude are discussed in detail. The following conclusions are obtained:

(i) A 9 m positioning accuracy is achievable using the GPS L1-P-code signal in the Space Station altitude of 500 km. P-code performance using the standard GPS navigation solution is relatively insensitive to the receiver noise figure (noise fig-

ures in the range from 1 to 5 dB will be acceptable). This will meet the Space Station's short and long range tracking requirements of 100 m and 15 m positioning accuracies, respectively.

(ii) C/A code positioning accuracy will be degraded to 100 m under accuracy denial according to the current DOD Selective Availability Plan. Without accuracy denial the L1, C/A code positioning accuracy in the Space Station altitude is expected to be ≈ 12 m and 10 m, for receivers with 5 dB and 1 dB noise figures, respectively. The Selective Availability Plan is expected to be in effect in the operational GPS. Thus, it can be concluded that the C/A code users, utilizing the standard GPS navigation solution, can only meet the short range tracking requirement of the Space Station.

(iii) Lowering the receiver noise figure to 1 dB (from 5 dB) does not provide significant performance improvements for the standard GPS, using either P or C/A codes. The dominating error sources in standard GPS are errors in the GPS Space and Control Segments. They can not be eliminated unless some forms of differental GPS are used.

It is expected that either the Differential GPS or the SERIES-X types of radio positioning, both of which are capable of mitigating the effects of the denial of accuracy and the errors common to the user and the reference station, will have better achievable positioning accuracies than the Standard GPS results. The performances of DGPS and the SERIES-X types of positioning techniques will be discussed in forthcoming reports.

The estimated positioning accuracies using L1, C/A or P-code signals with Standard GPS navigation positioning algorithms are summarized in the following table for easy reference.

Summary of Positioning Accuracy*

RECEIVER NOISE FIG.	BEFORE OR AFTER FILT.	C/A CODE WITH ACCURACY DENIAL	C/A CODE WITHOUT ACCURACY DENIAL	P-CODE WITH SELECTIVE AVAILABILITY
5 DB (28 DB°K)	BEFORE FILTERING	100 M	27.4 M	13.0 M
	AFTER FILTERING	100 M	11.9 M	8.8 M
1 DB (18.76 DB°K)	BEFORE FILTERING	100 M	18.9 M	12.3 M
	AFTER FILTERING	100 M	9.9 M	8.6 M

*L1 Link with PDOP = 3.0 are assumed for all cases here.

1.0 INTRODUCTION

The Space Station System consists of unmanned space platforms, free-flying satellites, orbital transfer vehicles (OTV), and orbital maneuvering vehicles (OMV) that interact with the manned Space Station, along with the Space Transportation System (STS), in orbit. [1]. In addition, the Space Station System is aided by the TDRSS (Satellites and Whitesand Ground Terminal) and ground control stations (Network Control Center NCC and Mission Control Center MCC). Figure 1-1 illustrates the Space Station System graphically. Table 1-1 summarizes the number of vehicles and their expected ranges from the Space Station.

For efficient utilization of these vehicular elements many detached operations will be performed in parallel. This will require the Space Station to have a traffic control system to monitor and coordinate these related operations. The relative positions of the Space Station and the vehicles must be determined continuously. In other words, both the Space Station and the detached vehicles must be tracked.

In order to facilitate and standardize the Space Station tracking and traffic control operations, an "Operational Control Zone" (OCZ) concept was described in [1], which segments the Space Station's communication and tracking requirements into coverage "zones" according to functions. Figure 1-2 illustrates the Operational Control Zones as described in [1].

Considering both the vehicle range requirements and the OCZ's illustrated in Figure 1-2, the Space Station Tracking Performance Requirements are summarized in Table 1-2, which divides tracking requirements into four categories: Long Range Tracking, Short Range Tracking, Proximity Operations Tracking, and Docking Sensors [2].

One of the objectives of this study is to investigate the feasibility of using the NAVSTAR Global Positioning System (GPS) or a GPS-based system for Space Station Tracking. In particular, the short range, long range, and proximity operation tracking requirements listed in Table 1-2 are of special interest

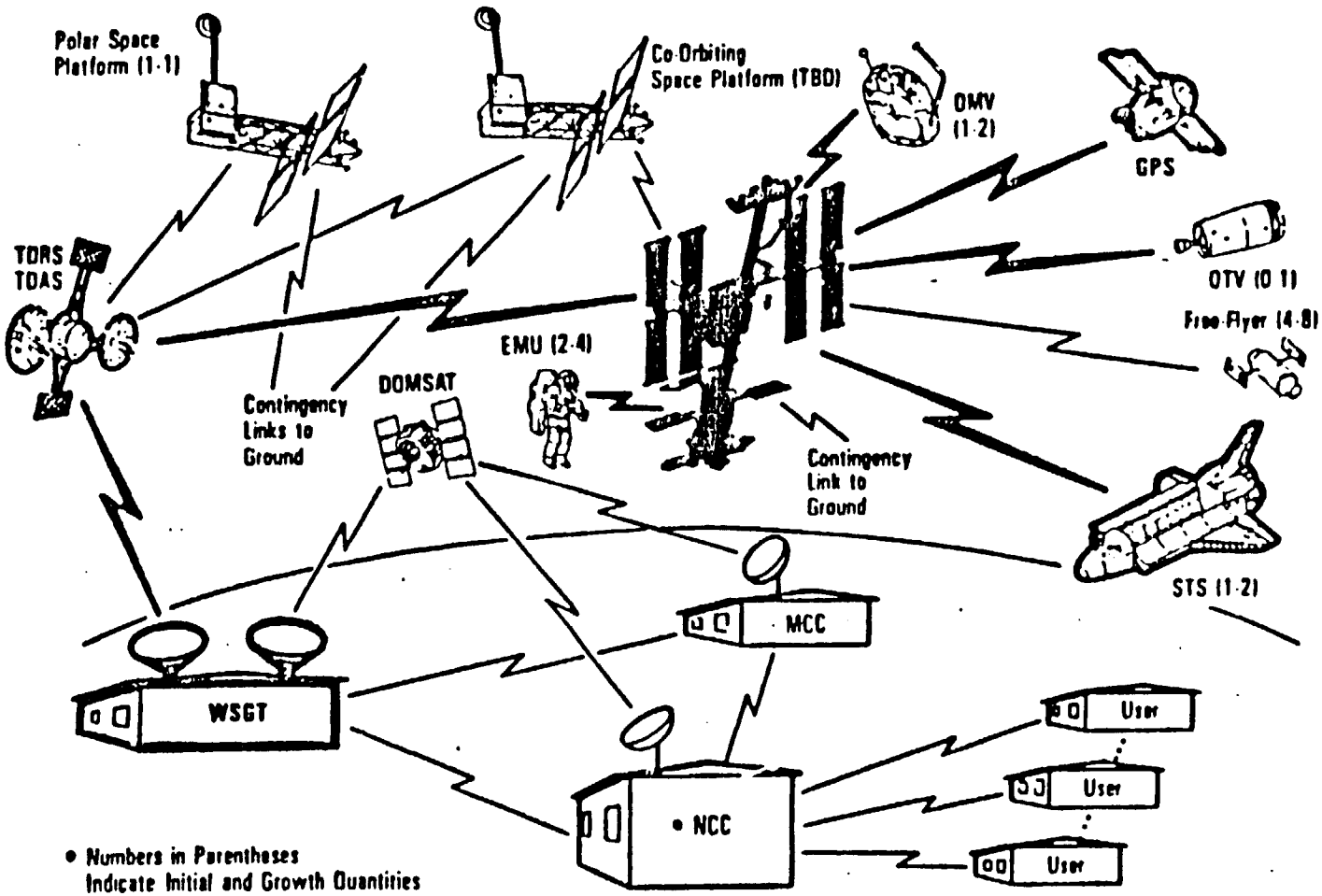

Figure 1-1 Vehicle Tracking Requirements in the Space Station System

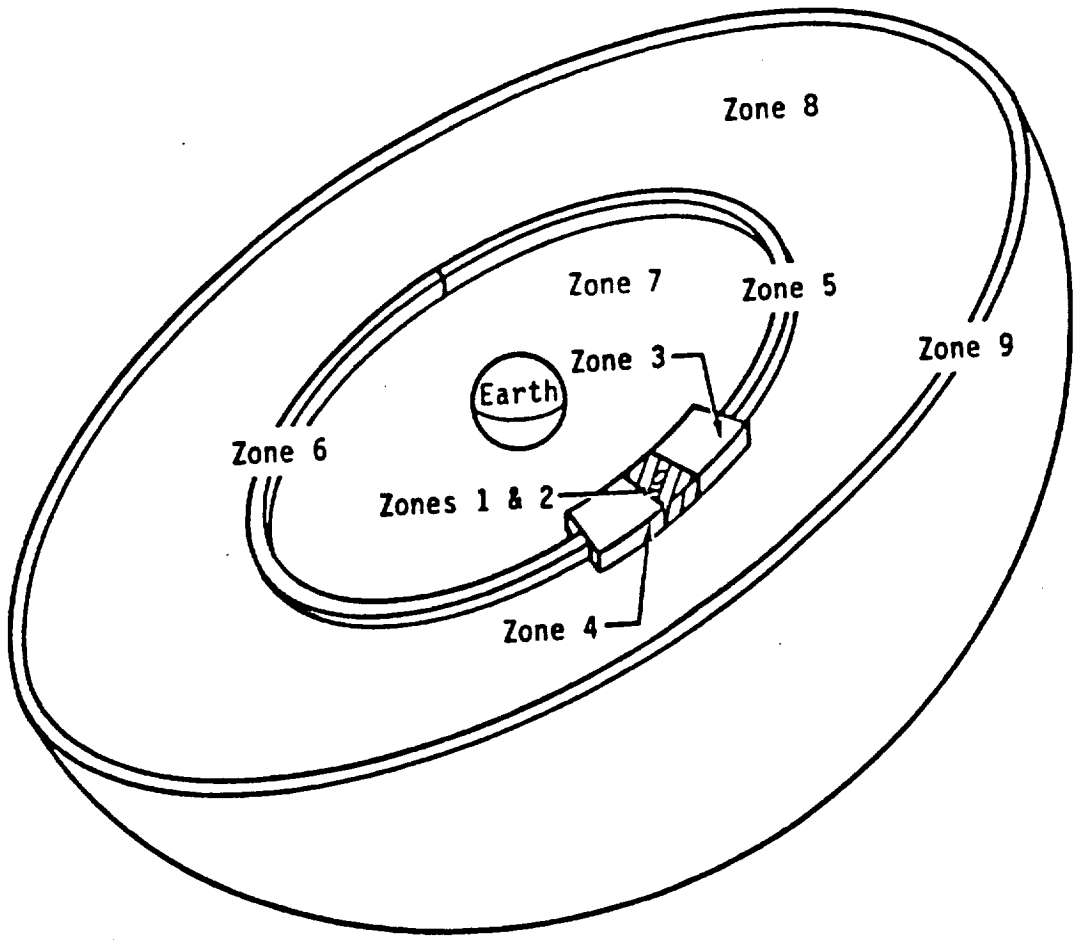

Figure 1-2 Cutaway view of operational control zones (hemispherical cutaway) for Space Station Tracking and Traffic Control (from ,, [1])

Table 1-1. Number of Vehicles and Ranges From The Space Station

Vehicle Type	Quantities	Ranges
Free Flyers	4-8	2000 Km
Space Shuttle Orbiters	1-2	37 Km
Orbital Transfer Vehicles (OTV)	1	185 Km
Orbital Maneuvering Vehicles (OMV)	1-2	185 Km
Extravehicular Mobility Units (EMU)	2-4	1 Km

Table 1-2. Summary of Space Station Tracking Requirements

FUNCTION	PERFORMANCE REQUIREMENT
Long Range Tracking	Max Range: 1080 nm Coverage: Limited to Comm data link coverage Accuracy: (GPS Position) +/- 15 m (49.2 ft)
Short Range Tracking	Max Range: 20 nm Coverage: 4 PI Steradians Accuracies: Angle: +/- 10 MRad (0.57 Deg) Range: +/- 100 m (328 ft) or 1% Velocity: .3 m/sec (1 fps) or 1%
Proximity Operations Tracking	Max Range: 1000 ft Coverage: Limited to Comm data coverage Accuracy: GPS position +/- 1m (3.3 ft)
Docking Sensors	Max Range: 1000 ft Coverage: 20 Deg cone Accuracies: Range: +/- 0.5 cm (.02 ft) Angle: +/- 2 MRad (0.1 Deg) Velocity: 1.0 cm/sec (0.03 fps) Attitude: +/- 10 MRad (0.57 deg)

m = meter

M = milli

here because the accuracy requirements of these three types of Space Station Tracking objectives are approximately within the capability of appropriately designed GPS based systems.

There are at least three known approaches in using GPS transmissions for radio-navigation and user position determination:

(i) Standard GPS using P-code or C/A code;
(ii) differential GPS using P-code or C/A code;
(iii) radio-interferometry using SERIES-X (Satellite Emission Range Inferred Earth Surveying) type of techniques which does not require the knowledge of either the P or the C/A codes. [3], [4], [13].

The Standard GPS approach has the advantage of not requiring a cooperative reference station whose location is required to be known. However, it has some drawbacks. With GPS's Selective Availability Plan (see Section 2) the accuracy of a C/A code user is degraded. The P-code user can achieve good accuracy. However, P-code is classified and its access requires Department-of-Defense permission.

Differential GPS (DGPS) and the SERIES type of approaches can offer better accuracy than the standard GPS since they are differential approaches and have the capability of cancelling error sources which are common to both the user and the reference station. This capabilty also allows them to mitigate the effect of denial of accuracy created by the GPS's Selective Availability Plan. Being differential approaches they both will, however, require cooperative reference stations whose locations are surveyed and known. Another drawback of the differential approaches is that there will be an error contribution, due both to the distance between the reference and the user and the uncertainty in the knowledge of the ephemeris of the GPS satellite. When the distance between the user and the reference station is large, this error can be significant, and may destroy the performance advantages of the differential approaches over the standard approach.

In this report only the achievable accuracies of

Standard GPS with respect to the Space Station requirements will be discussed. The accuracies with DGPS and SERIES type of arrangements will be discussed in subsequent reports that will follow this one.

In Section 2.0 the GPS error sources that affects positioning accuracy when using standard GPS will be discussed. In Sections 3.0 and 4.0 the achievable accuracies with and without accuracy denial will be discussed. In Section 5.0 we summarize the capability of standard GPS in meeting the Space Station requirements and give conclusions of this report. Detailed link budget calculations are given in Appendix A.

2.0 GPS ERROR SOURCES

A GPS user determines his own position and time by measuring the pseudo-ranges to four selected GPS satellites and solve for a set of navigation equations. The measurement of range to the satellites, made by the user with an imprecise clock, is called "pseudo-range" because it contains a bias of fixed maguitude in each range estimate due to the clock error.

The error sources can basically be divided into two main categories according to their effects. First, there are error sources that basically contribute only to the pseudo-range measurements. These include the effect of denial of accuracy (for C/A code users), the GPS Space and Control Segment error sources, error sources in the propagation link (ionospheric and tropospheric delay errors), and error sources in the user receiver. Secondly, there are factors that affect the dilution of precision parameters of the GPS measurement. These parameters will amplify the pseudo-range error to give an increased error in GPS positioning (see following discussions). Table 2-1 summarizes these error sources and their respective effects.

The geometry of the four selected GPS satellites affects the accuracy of the GPS positioning solution, in addition to pseudo-range measurement errors. The effect of geometry is expressed by the "Geometric Dilution of Precision"

(GDOP) parameter [5]. These parameters include PDOP, which reflects the dilution of precision in position in 3-dimensions; HDOP, dilution of precision in the two horizontal dimensions; VDOP, dilution of precision in the vertical dimensions, and TDOP, dilution of precision in time, i.e., in the estimate of the range equivalent of the user clock bias. Small values of GDOP parameters indicate good arrangements in the geometry of the selected satellites and correspondingly small errors in position and time fixes. Figure 2-1 illustrates two satellite geometry which gives poor and good PDOP's, respectively.

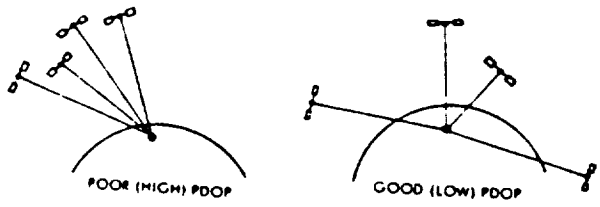

Figure 2-1 Geometries of Selected GPS Satellites Giving Rises to Poor and Good GDOP's

Let σ_x, σ_y, σ_z and σ_T be the 1-sigma errors in the GPS 3-dimensional position time fixes, respectively. Then these errors are related to the 1-sigma pseudo-range measurement error σ_{PR} through the following relationship [5]:

$$\begin{aligned}
\sqrt{\sigma_x^2 + \sigma_y^2 + \sigma_z^2 + \sigma_T^2} &= \text{GDOP} \cdot \sigma_{PR} \\
\sqrt{\sigma_x^2 + \sigma_y^2 + \sigma_z^2} &= \text{PDOP} \cdot \sigma_{PR} \\
\sqrt{\sigma_x^2 + \sigma_y^2} &= \text{HDOP} \cdot \sigma_{PR} \\
\sigma_z &= \text{VDOP} \cdot \sigma_{PR} \\
\sigma_T &= \text{TDOP} \cdot \sigma_{PR}
\end{aligned} \qquad (2\text{-}1)$$

In addition, the dilution of precision parameters are related to each other in the following manner:

$$GDOP = \sqrt{PDOP^2 + TDOP^2}$$

$$PDOP = \sqrt{HDOP^2 + VDOP^2} \qquad (2\text{-}2)$$

The dilution of precision parameters depends on the geometry of the selected satellites, and are functions of the User's location and time-of-day (which determines how many satellites are visible), the user's mask angle and his satellite selection strategy, and the User's navigation solution algorithm (e.g., standard GPS or Differential GPS). Nominal values of these parameters for a surface user can be assumed to be the following [6], [7]:

$$\begin{aligned} \text{Nominal PDOP} &= 3.0 \\ \text{Nominal HDOP} &= 1.5 \\ \text{Nominal VDOP} &= 2.5 \end{aligned} \qquad (2\text{-}3)$$

Since the Space Station and the detached vehicles are at a nominal altitude of 500 km, it is expected that their GPS dilution of precision parameters should be at least as good as the surface users (this will be discussed in a forthcoming report). Thus, the nominal values listed in equation (2-3) can also be assumed to be typical in the Space Station environment.

The GPS C/A code users' achievable positioning accuracies are significantly affected by the Department of Defense Selective Availability (SA) Plan, which is also called "Denial of Accuracy". The exact effect of SA is discussed in Section 3.0. With accuracy denial the GPS downlink signal is intentionally perturbed so that the C/A code user's achievable accuracy will be significantly degraded. P-code users, with selective availability, will not be affected however. With accuracy denial the dominating error sources will be items 1, 5, 6, 7 and 8 in Table 2-1. Denial of accuracy will be the dominating error source in the pseudo-range measurement, while

this effect is amplified by the dilution of precision parameters which are functions of user location and time, user mask angle, user satellite selection algorithm and the user navigation solution algorithm.

For P-code users (and also for C/A code users when there is no accuracy denial) the dominating errors in their pseudo-range measurements are due to error sources in the GPS Space and Control Segments, in the GPS user receiver, and in the propagation link which consists of ionospheric and tropospheric delay compensation errors. Table 2-2 summarizes the P-code user error sources and their budgets (1-sigma system responsibilities). The information on Table 2-2 is taken from the GPS system specification SS-GPS-300B [8]. The implicit assumptions made in Table 2-2 are that

(i) the user is on the earth's surfaces

(ii) standard GPS receiver's are assumed, which have an equivalent system noise temperature of 28 dB K (i.e., noise figure 5 dB for a cold sky)

(iii) the receiver will use ionospheric and tropospheric delay compensations;

(iv) the 1-sigma UERE (user equivalent range error) is the pseudo-range error prior to filtering. Filtering will reduce the random type of errors, while the bias type of errors will not be affected (which can be mitigated by differential GPS).

While the error budgets of the GPS Space and Control Segments cannot be further reduced, the user segment errors are somewhat under the user's control. For example, by improving the receiver's noise figure the random error component in the receiver can be reduced, which will also affect the ionospheric delay compensations error if the dual frequency (L1, L2) ionospheric delay compensation algorithm is used.

The Space-Station's altitude is normally at 500 km. At this altitude the tropospheric delay error is negligible after compensation. Also the multipath error of 1.2 m assumed in Table 2.2 are for surface users which may receive multipath reflections

Table 2-1. GPS Positioning Error Sources

- FACTORS THAT CONTRIBUTE TO PSEUDO-RANGE MEASUREMENT ERRORS

  1. DENIAL OF ACCURACY
  2. GPS SPACE SEGMENT ERROR SOURCES
  3. GPS CONTROL SEGMENT ERROR SOURCES
  4. USER SEGMENT ERROR SOURCES AND PROPAGATION LINK ERRORS

- FACTORS THAT AFFECT DILUTION OF PRECISION PARAMETERS

  5. USER LOCATION AND TIME-OF-DAY
  6. THE USER MASK ANGLE
  7. THE USER SATELLITE SELECTION STRATEGY
  8. THE USER NAVIGATION SOLUTION ALGORITHM

Table 2-2. P-Code User (with Selective Availability) UERE Error Budget
(From SS-GPS-300 B)

	SEGMENT SOURCE	ERROR SOURCES	SYSTEM RESPONSIBILITY (1σ), METERS	
	SPACE	CLOCK & NAV.SUB-SYSTEM STABILITY	2.7	(RANDOM)
		PREDICTABILITY OF SV PERTURBATIONS	1.0	(BIAS)
		OTHERS	0.5	(RANDOM)
	CONTROL	EPHEMERIS PREDICTION & MODEL IMPLEMENTATION	2.5	(BIAS)
		OTHERS	0.5	(RANDOM)
CAN BE SOMEWHAT CONTROLLED BY USER	USER	RECEIVER NOISE & RESOLUTION	1.5	(RANDOM)
		MULTIPATH	1.2	(RANDOM)
		IONOSPHERIC DELAY COMPENSATION	2.3	(RANDOM)
		TROPOSPHERIC DELAY COMPENSATION	2.0	(RANDOM)
		OTHERS	0.5	(RANDOM)
		1-σ UERE =	5.3	METERS

such as from the ocean's surface. The multipath effect may not be as large in the Space Station environment..

In conclusion, we see that if P-code is used the GPS positioning error (for a surface user, according to the error budget of Table 2-2) will be 16 meters if a PDOP of 3 is assumed. In Section 4 we will further investigate the expected GPS accuracy, assuming a Space Station environment, which should be somewhat better than the surface user. We first consider the C/A code user accuracy in Section 3.0.

3.0 ACHIEVABLE ACCURACIES USING C/A CODE GPS FOR SPACE STATION TRACKING

For OMV's and OTV's that may not have access to the GPS P-code, their positioning, using standard GPS, will have to rely on the C/A code.

The achievable accuracy of the C/A code depends on whether accuracy denial is placed on the GPS downlink signal. In this section the C/A code tracking accuracies with or without Selective Availability will be discussed.

Under the Department of Defense Selective Availability (SA) program access to the P-code will be strictly controlled through an appropriate encryption mechanism, and the accuracy available from the C/A code will be intentionally degraded [6], [7], [8], [9], [10]. This accuracy level, to be imposed when GPS becomes fully operational, was initially set at 200 m (CEP or 50% confidence level which equates to aproximately 500 m at 95% confidence level (i.e., 2-dimensional rms). Subsequent improvements in accuracy are expected to be instituted as national security conditions permit. In 1983 the Department of Defense announced (e.g., see [6].) that the Standard Positioning Service (SPS) using C/A code will be made available at an accuracy of 100 m (95% confidence), which is approximately 40 m CEP or 50% confidence level. The 95% level 2-dimensional rms horizontal positioning error is approximately given by [7]:

$$100 \text{ m} = 2\sqrt{\sigma^2 + \sigma^2} = 2.\text{HDOP}.\sigma_{PR} \qquad (3\text{-}1)$$

Assuming a nominal value of 1.5 for HDOP (see equation 2.3), we can solve for σ_{PR}, the equivalent pseudo-range 1-σ error for the C/A code user under accuracy denial from (3-1), giving σ_{PR} =33.33

meters, which is approximately 7 times worse than the P-code accuracy according to the error budget of Table 2-2.

Assuming nominal values of 1.5, 2.5, and 3.0 for HDOP, VDOP and PDOP, we can estimate the GPS positioning performance using C/A code, with accuracy denial in effect. The results are shown in Table 3-1.

Table 3-1. Estimated Accuracies of C/A Code Users Under Accuracy Denial

Measurements	Accuracy (1-σ)
Radial Error in User Position in the horizontal plane	50 m
Vertical Error in User Position	83.33 m
Radial Error in User Position, in 3-dimensions	100. m

It is of interest to note that the Standard GPS C/A code accuracy under denial of accuracy can only meet the Space station short range tracking requirement of 100 m. Improvement on this accuracy is feasible using differential GPS. This will be studied in another report. In the following the C/A code accuracy without accuracy will be discussed.

C/A code can be obtained from L1, which have both C/A and P code modulations in quadrature. Currently, L2 has P-code only; however, L2 can have either C/A or P according to ICD-GPS-200 [11]. The following table summarizes the expected GPS received power according to [11].

Table 3-2. GPS Received Minimum RF Signal Strength [11]

Channel \ Signal	P	C/A
L1 (1575.42 MHz)	-163.0 dBw	-160.0 dBw
L2 (1227.6 MHz)	-166.0 dBw or	-166.0 dBw

The C/A code on L1 will have a 6 dB stronger signal than that of L2. The received signal power listed are minimum power levels for surface users. Assuming the Space Station and the detached vehicles have a nominal altitude of 500 km, the distance between them and any GPS satellite (at 20,200 km altitude) can vary between 19,700 km (at zenith) to the maximum distance of 28,368 km as illustrated in Figure 3-1. Assuming L1 will be chosen, since it has a stronger GPS C/A signal, and assuming the worst case distance of 28,368 km, the received C/N_o is expected to be ≈36.55 dB-Hz for a GPS receiver with a equivalent noise temperature of 28 dB°K (noise figure ≈5 dB). (See Appendix A). The receiver is assumed to have a full-time non-coherent PN code tracking loop, whose noise jitter and steady state phase error are given respectively by

$$\left(\frac{\sigma}{T_c}\right)^2 = \frac{N_o B_L}{2P_s}\left[1 + \frac{2N_o B_I}{P_s}\right]$$

$$\frac{\phi_{ss}}{T_c} = \frac{\ddot{R}/C}{T_c\,(1.89\,B_L)^2} \qquad (3\text{-}2)$$

where σ/T_c is the normalized code loop jitter, P_s/N_o is the received signal power to noise power spectral density ratio, B_L is the loop bandwidth, B_I is the input bandwidth, T_c is the code-chip-time, ϕ_{ss}/T_c is the normalized steady state error, and $(\ddot{R}/C)/T_c$ is the acceleration induced doppler rate on the code clock.

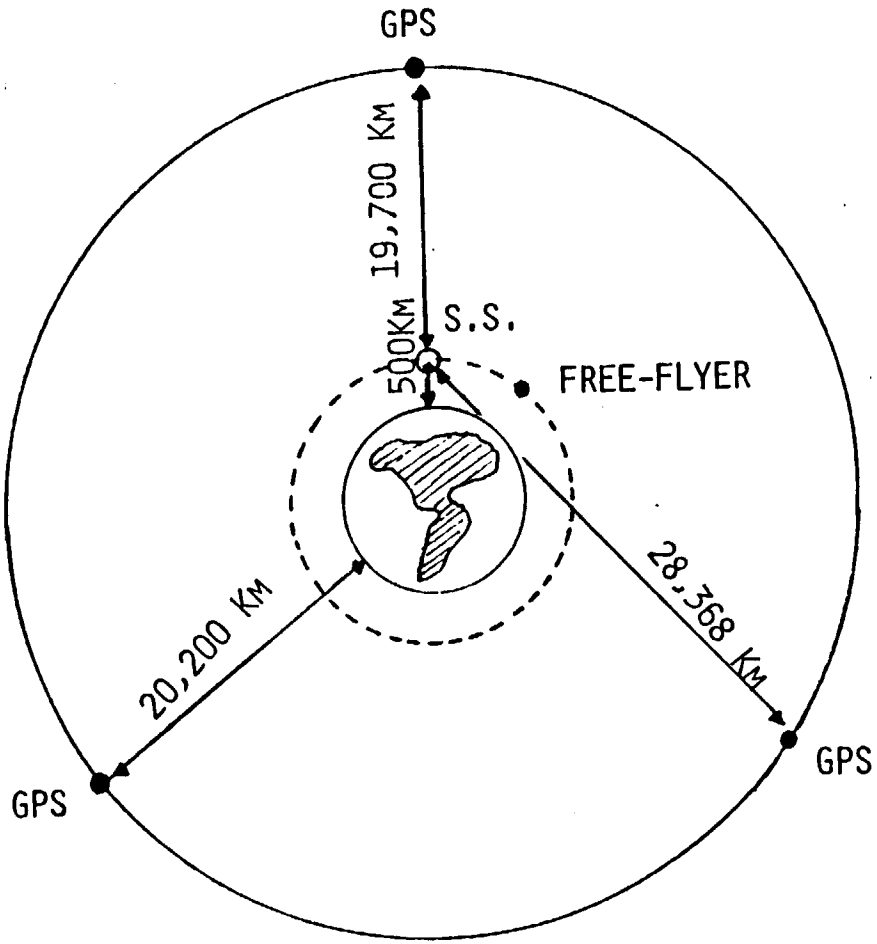

Figure 3-1. Space-Station Tracking with GPS

Assuming a loop bandwidth B_L = 0.5 Hz and and input bandwidth B_I = 100 Hz, the resulting noise jitter in range equivalent will be 2.2 meters. The steady state error for C/A code tracking is negligible even for accelerations up to 1G. Another error source in code loop jitter is NCO quantization. Assuming quantization to 1/64 of a chip, the quantization noise induced jitter is ≈ 1.3 m in range equivalent. Finite word size in Kalman filter mechanization also introduces an error source which is random in nature. It can be bounded by ≤ 1 m.

Ionospheric and tropospheric delays require corrections. Ionospheric delay depends on the vertical electron content in the propagation path and is approximately given by [12]:,

$$\Delta_{ION} = \frac{b}{4\pi^2 f^2} I_V \sqrt{\csc(E^2 + 20.3^2)} \qquad (3\text{-}3)$$

where

Δ_{ION} = ionospheric delay in meters
b = 1.6×10^3 (constant in MKS system)
f = carrier frequency
I_V = vertical electron content in electrons/m^2 ($\approx 10^{18}$)

E = elevation angle in degrees

For the worst case elevation angle of 5° the expected ionospheric delay for L1 is in the order of 46 meters. Assuming dual frequency (L1, L2) correction is used to compensate for the ionospheric delay, which estimates the "net pseudo-range" (i.e., not including Δ_{ION}) by forming the estimate [12]:

$$\hat{R} = 2.566\ \hat{R}_1 - 1.566\ \hat{R}_2 \qquad (3\text{-}4)$$

where R_1, R_2 are the pseudo-range measurements on L1 and L2, respectively. Then the error in the ionospheric delay compensation is given from (3-4) by

$$\sigma_{\Delta_{ION}} = \sqrt{(2.566)^2 + (1.566)^2}\ \sigma_{PN} = 3\sigma_{PN} \qquad (3\text{-}5)$$

where σ_{pn} is the range equivalent of the code loop noise jitter. This is estimated to be ~7.77 meters for the combined (rss) code loop noise and quantization effects of 2.88 meters. Tropospheric delay depends on the elevation angle E and the line integral of the reflectivity function of the user-to-satellite path. Assuming an altitude-dependent mathematical model is used to compensate for tropospheric delay [12], the residual tropospheric delay error is approximately given by

$$\sigma_{\Delta_{TROP}} \cong \Delta c.\exp\left[-\frac{0.034\ h}{T}\right].\csc(E) \qquad (3\text{-}6)$$

where

$\sigma_{\Delta_{TROP}}$ = residual tropospheric delay error

Δc = residual compensation magnitude ≈0.1 meters
h = vehicle atlitude in meters (500 km)
T = absolute temperature
E = elevation angle to satellite

From (3-6) we see that the residual tropospheric delay error for the Space Station altitude of 500 km is negligible, even for the worst case elevation angle (E=5°).

Multipath error can be significant for surface users (e.g., ships, with multipath signals due to reflections from the surface of the ocean), which is assumed to be 1.2 meters in Table 2-2. The Space Station and the detached vehicles will face a less severe multipath problem normally. A multipath error of

≈0.2 meters is assumed here for the Space Station tracking error budget.

Table 3-3 summarizes these effects and gives the estimate of the 1-σ User-Equivalent-Range-Error (UERE) for GPS receivers in the Space Station environment, using the L1, C/A signal. The GPS Space and Control Segment error budget are the same as those of Table 2-2. The user segment error budget is different than those shown in Table 2-2. They reflect the effect of C/A code tracking and the Space Station altitude. The resultant 1-σ UERE is ≈ 9.14 meters.

It is of interest to examine the effect of lowering the receiver noise figure to 1 dB (equivalent noise temperature ≈ 18.76 dB°k). The resultant C/No for this case is ~ 45.8 dB-Hz (see Appendix A) and the corresponding 1σ UERE is 6.3 meters (Table 3-4).

The positioning accuracy of the C/A code receiver can be obtained from these 1-σ UERE's, assuming a PDOP of 3.

The positioning accuracies will be 27.4 m and 11.9 m, respectively, before and after filtering, for the 5-dB noise figure receiver. The corresponding accuracies for the 1-dB noise figure receiver are 18.9 m and 9.9 m, respectively. It is assumed here that filtering will reduce the random errors by a factor of 3 in these calculations, which is a reasonable assumption for GPS receivers [6].

Table 3-5 summarizes the C/A code receiver performances discussed above.

Table 3-3. Estimated GPS Range Accuracy Using L1, C/A Signal*

Assume:
- Worst case distance
- Receiver noise figure = 5 dB
- Without accuracy denial

```
GPS L1  .  C/A CODE LINK UERE SUMMARY
 DISTANCE=28368.0 KM
 REC C/NO=    36.5 DB-HZ
 ACCEL.   =     1.0 G s

SPACE SEGMENT ERROR SOURCES
   CLOCK & NAV.SUBSYSTEM STABILITY    =   2.700  M
   PREDICTABILITY OF SV PERTURBATIONS=   1.000  M
   OTHERS                             =   0.500  M

CONTROL SEGMENT ERROR SOURCES
   EPHEMERIS PREDICTION ERROR         =   2.500  M
   OTHERS                             =   0.500  M

USER SEGMENT ERROR SOURCES
   RECV NOISE,RESOL.,TSS,& KALMAN ERR=   2.777  M
   MULTIPATH                          =   0.200  M
   IONOSPHERIC DELAY COMPENSATION     =   7.772  M
   TROPOSPHERIC DELAY COMPENSATION    =   0.000  M
   OTHERS                             =   0.500  M

1-SIGMA USER EQ. RANGE ERROR(UERE)=   9.135    METERS
```

*Note: See Appendix A for detailed link budget

Table 3-4. Estimated GPS Range Accuracy Using L1, C/A Signal*

Assume:
- Worst case distance
- Receiver noise figure = 1 dB
- Without accuracy denial

```
GPS L1      C/A CODE LINK UERE SUMMARY
 DISTANCE=20368.0 KM
 REC C/NO=    45.0 DB-HZ
 ACCEL.   =     1.0 G s

SPACE SEGMENT ERROR SOURCES
   CLOCK & NAV.SUBSYSTEM STABILITY    =  2.700  M
   PREDICTABILITY OF SV PERTURBATIONS=  1.000  M
   OTHERS                             =  0.500  M

CONTROL SEGMENT ERROR SOURCES
   EPHEMERIS PREDICTION ERROR         =  2.500  M
   OTHERS                             =  0.500  M

USER SEGMENT ERROR SOURCES
   RECV NOISE,RESOL.,TSS,& KALMAN ERR=  1.821  M
   MULTIPATH                          =  0.200  M
   IONOSPHERIC DELAY COMPENSATION     =  4.566  M
   TROPOSPHERIC DELAY COMPENSATION    =  0.000  M
   OTHERS                             =  0.500  M

1-SIGMA USER EQ. RANGE ERROR(UERE)=  6.285   METERS
```

*Note: See Appendix A for detailed link budget

Table 3-5 Summary of Positioning Accuracy Estimates for Space Station and Detached Vehicles using GPS L1 C/A Code

Assume:

- PDOP = 3.0
- Worst Case Satellite to Receiver Distance

Denial of Accuracy	Filter-Positioning Accuracy	Receiver with 5dB Noise Figure (28dB° K Eq. Noise Temperature)	Receiver with 1dB Noise Figure (18.8 dB° K Eq. Noise Temperature)
With Accuracy Denied	Before Filtering	100 m	100 m
	After Filtering	100 m	100 m
With No Accuracy Denial	Before Filtering	27.4 m	18.9 m
	After Filtering	11.9 m	9.9 m

4.0 ACHIEVABLE ACCURACIES USING P-Code GPS FOR SPACE STATION TRACKING

For the Space Station itself and some detached vehicles such as the free-flying satellites and the Space Shuttle Orbiter, it is practical to assume that their GPS receivers will have access to the GPS P-code, and are thus not subject to denial of accuracy under the current DOD Selective Availability Plan. For these P-code users their expected positioning accuracies will be better than the achievable C/A code accuracies tabulated in Table 3-5. Using L1 the P-signal received C/N_o's are expected to be 33.6 dB-Hz and 42.8 dB-Hz, for receivers with 5 dB and 1 dB noise figures, respectively. The corresponding C/N_o's for L2 will be 31 dB-Hz and 40.25 dB-Hz, respectively. Detailed link budgets are shown in Appendix A for L1 P-code links.

Assume L1 will be used, and assume a full-time noncoherent PN loop with a loop bandwidth of 1 Hz and an input bandwidth of 150 Hz. The resultant code loop noise jitters will be, in range equivalent, 0.46 meters and 0.152 meters, respectively, for the 5 and 1 dB noise figure receivers. Code loop NCO quantization noise will be $\simeq$0.132 meters. Steady state error will be negligible for accelerations up to 1G. Assuming a Kalman mechanization error of $\simeq$1 meter, in addition to code loop jitter, the total receiver noise, quantization, steady state error, and Kalman mechanization error will be $\simeq$1.114 meters and 1.024 meters, for the P-code receiver with 5 and 1 dB noise figures, respectively.

Ionospheric delays of approximately 45.8 meters will be experienced at L1 (assuming the worst case elevation angle of 5°). Using dual frequency correction by making pseudo-range measurements on L1 and L2 simultaneously, the ionospheric delay compensation errors, depending on the code loop noise and quantization error, are expected to be $\simeq$1.446 meters and 0.603 meters, respectively, for the receivers with 5 and 1 dB noise figures. Similar to the C/A code case, the tropospheric delay is $\simeq$2.5 meters at

the 500 km Space Station altitude and the tropospheric delay compensation error is ≈0 at this altitude.

The 1-σ UERE's of the P-code receivers in the Space Station altitude are summarized in Tables 4-1 and 4-2 for the P-code receivers with 5 and 1 dB noise figures, respectively. In these tables the multipath effect is assumed to be 0.2 meters in range equivalent, which is again based on the fact that the multipath effect in the Space Station environment should be much less than the surface users, which is assumed to be ≈1.2 meters in SS-GPS-300 B.

Assuming a PDOP of 3.0 again the Space Station tracking accuracies using the GPS P-code are summarized in Table 4-3, for GPS receivers with 5 and 1 dB noise figures.

Table 4-1. Estimated GPS Range Accuracy Using L1, P-Code Signal*

Assume: . Worst case distance

. Receiver noise figure = 5 dB

```
GPS L1        P  CODE LINK UERE SUMMARY
 DISTANCE=20363.0 KM
 REC C/NO=    33.5 DB-HZ
 ACCEL.  =     1.0 G s

SPACE SEGMENT ERROR SOURCES
   CLOCK & NAV.SUBSYSTEM STABILITY    =   2.700   M
   PREDICTABILITY OF SV PERTURBATIONS=   1.000   M
   OTHERS                             =   0.500   M

CONTROL SEGMENT ERROR SOURCES
   EPHEMERIS PREDICTION ERROR         =   2.500   M
   OTHERS                             =   0.500   M

USER SEGMENT ERROR SOURCES
   RECV NOISE,RESOL.,TSS,& KALMAN ERR=   1.114   M
   MULTIPATH                          =   0.200   M
   IONOSPHERIC DELAY COMPENSATION     =   1.446   M
   TROPOSPHERIC DELAY COMPENSATION    =   0.000   M
   OTHERS                             =   0.500   M

1-SIGMA USER EQ. RANGE ERROR(UERE)=   4.320    METERS
```

*Note: See Appendix A for detailed link budgets

Table 4-2. Estimated GPS Range Accuracy Using L1, P-Code Signal*

Assume: . Worst case distance

. Receiver noise figure = 1 dB

GPS L1 P CODE LINK UERE SUMMARY
DISTANCE=28368.0 KM
REC C/NO= 42.8 DB-HZ
ACCEL. = 1.0 G.s

SPACE SEGMENT ERROR SOURCES			
CLOCK & NAV.SUBSYSTEM STABILITY	=	2.700	M
PREDICTABILITY OF SV PERTURBATIONS	=	1.000	M
OTHERS	=	0.500	M
CONTROL SEGMENT ERROR SOURCES			
EPHEMERIS PREDICTION ERROR	=	2.500	M
OTHERS	=	0.500	M
USER SEGMENT ERROR SOURCES			
RECV NOISE,RESOL.,TSS,& KALMAN ERR	=	1.024	M
MULTIPATH	=	0.200	M
IONOSPHERIC DELAY COMPENSATION	=	0.603	M
TROPOSPHERIC DELAY COMPENSATION	=	0.000	M
OTHERS	=	0.500	M
1-SIGMA USER EQ. RANGE ERROR(UERE)	=	4.092	METERS

*Note: See Appendix A for detailed link budgets

Table 4-3. Summary of Positioning Accuracy Estimates for Space Station and Detached Vehicles Using GPS L1 P-Code

Assume: . PDOP = 3.0
. Worst case satellite to receive distance

Positioning Accuracy	Receiver with Noise Figure=5dB (Eq. Noise Temp. = 28 dB°K)	Receiver with Noise Figure=1 dB (Eq. Noise Temp. = 18.8 dB°K)
Before Filtering	13.0 meters	12.3 meters
After Filtering	8.8 meters	8.6 meters

5.0 CONCLUSIONS

Based on the C/A and P-code positioning results derived in Sections 3 and 4 the following conclusions can be made:

(i) A 9-m positioning accuracy is achievable using the GPS L1-P-code signal in the Space Station altitude of 500 km. P-code performance using the standard GPS navigation solution is relatively insensitive to the receiver noise figure (noise figures in the range from 1 to 5 dB will be acceptable). This will meet the Space Station's short and long range tracking requirements of 100 m and 15 m positioning accuracies, respectively.

(ii) C/A code positioning accuracy will be degraded to 100 m under accuracy denial according to the current DOD Selective Availability Plan. Without accuracy denial the L1, C/A code positioning accuracy in the Space Station altitude is expected to be ≈ 12 m and 10 m, for receivers with 5 dB and 1 dB noise figure respectively. The Selective Availability Plan is expected to be in effect in the operational GPS. Thus, it can be concluded that the C/A code users, utilizing the standard GPS navigation solution, can only meet the short range tracking requirement of the Space Station.

(iii) Lowering the receiver noise figure to 1 dB (from 5 dB) does not provide significant performance improvements for the standard GPS using either P or C/A codes. The dominating error sources in standard GPS are errors in the GPS Space and Control Segments. They cannot be eliminated unless some forms of differental GPS are used.

It is expected that either the Differential GPS (DGPS) or the SERIES-X types of radio positioning, both of which are capable of mitigating the effects of the denial of accuracy and

the errors common to the user and the reference station (such as GPS Space and Control Segment errors), will have better achievable positioning accuracies than the standard GPS results. However, these differential schemes will require cooperative reference stations whose locations are surveyed, and communication links between the reference station and the users. The performance of DGPS and the SERIES-X types of positioning techniques will be discussed in forthcoming reports.

The estimated positioning accuracies using L1, C/A or P-code signals with Standard GPS navigation positioning algorithms are summarized in Table 5-1 for easy reference.

Table 5-1. Summary of Positioning Accuracy*

RECEIVER NOISE FIG.	BEFORE OR AFTER FILT.	C/A CODE WITH ACCURACY DENIAL	C/A CODE WITHOUT ACCURACY DENIAL	P-CODE WITH SELECTIVE AVAILABILITY
5 DB (28 DB°K)	BEFORE FILTERING	100 M	27.4 M	13.0 M
	AFTER FILTERING	100 M	11.9 M	8.8 M
1 DB (18.76 DB°K)	BEFORE FILTERING	100 M	18.9 M	12.3 M
	AFTER FILTERING	100 M	9.9 M	8.6 M

*L1 Link with PDOP = 3.0 are assumed for all cases here.

Appendix A

The received C/N_o's discussed in this report are calculated by using the worst case distance (28,368 km) between the GPS satellite and the receivers on the Space Station or the detached vehicles. The link parameters assumed are documented in the link budgets included in this Appendix. These link budgets are evaluated for the receiver with a 5 -dB noise figure (28 dB° K equivalent noise temperature). The 1 dB noise figure case can be appropriately scaled.

Table A-1. C/A Code GPS-to-Space Station Link Budget Calculations

GPS L1 LINK DISTANCE= 28368. KM

C-CODE

GPS SAT. EIRP	=	26.80	DBW
SPACE LOSS	=	-185.45	DB
POINTING LOSS	=	-0.40	DB
POLARIZATION LOSS	=	-0.40	DB
ATMOSPHERIC LOSS	=	0.00	DB
RECV ANTENNA GAIN	=	-1.00	DB
RECV CIRCUIT LOSS	=	-2.60	DB
CORRELATION LOSS	=	-1.00	DB
EQ.NOISE TEMP.	=	28.00	DB-K
RECEIVED SIGNAL POWER	=	-164.05	DB-W
BOLTZMAN CONSTANT	=	-228.60	DBW/HZ-K
NO	=	-200.60	DBW/HZ
RECEIVED C/NO	=	36.55	DB-HZ

GPS L2 LINK DISTANCE= 28368. KM

C-CODE

GPS SAT. EIRP	=	19.10	DBW
SPACE LOSS	=	-183.29	DB
POINTING LOSS	=	-0.40	DB
POLARIZATION LOSS	=	-0.40	DB
ATMOSPHERIC LOSS	=	0.00	DB
RECV ANTENNA GAIN	=	-1.00	DB
RECV CIRCUIT LOSS	=	-2.60	DB
CORRELATION LOSS	=	-1.00	DB
EQ.NOISE TEMP.	=	28.00	DB-K
RECEIVED SIGNAL POWER	=	-169.59	DB-W
BOLTZMAN CONSTANT	=	-228.60	DBW/HZ-K
NO	=	-200.60	DBW/HZ
RECEIVED C/NO	=	31.01	DB-HZ

Table A-2. P-Code GPS-to-Space Station Link Budget Calculations

GPS L1 LINK DISTANCE= 28368. KM

P-CODE

GPS SAT. EIRP	=	23.80	DBW
SPACE LOSS	=	-185.45	DB
POINTING LOSS	=	-0.40	DB
POLARIZATION LOSS	=	-0.40	DB
ATMOSPHERIC LOSS	=	0.00	DB
RECV ANTENNA GAIN	=	-1.00	DB
RECV CIRCUIT LOSS	=	-2.60	DB
CORRELATION LOSS	=	-1.00	DB
EQ.NOISE TEMP.	=	28.00	DB-K
RECEIVED SIGNAL POWER	=	-167.05	DB-W
BOLTZMAN CONSTANT	=	-228.60	DBW/HZ-K
NO	=	-200.60	DBW/HZ
RECEIVED C/NO	=	33.55	DB-HZ

GPS L2 LINK DISTANCE= 28368. KM

P-CODE

GPS SAT. EIRP	=	19.10	DBW
SPACE LOSS	=	-183.29	DB
POINTING LOSS	=	-0.40	DB
POLARIZATION LOSS	=	-0.40	DB
ATMOSPHERIC LOSS	=	0.00	DB
RECV ANTENNA GAIN	=	-1.00	DB
RECV CIRCUIT LOSS	=	-2.60	DB
CORRELATION LOSS	=	-1.00	DB
EQ.NOISE TEMP.	=	28.00	DB-K
RECEIVED SIGNAL POWER	=	-169.59	DB-W
BOLTZMAN CONSTANT	=	-228.60	DBW/HZ-K
NO	=	-200.60	DBW/HZ
RECEIVED C/NO	=	31.01	DB-HZ

References

1. Nader, B.A., and DuPont, A.L., "Space Station Operations Operational Control Zones", Report No. 84-FM-62/JSC-20235, published by Mission Planning and Analysis Division, NASA-JSC, May, 1985.

2. Draft Statement of Work on "Space Station Tracking Requirements Feasibility Study", issued by NASA/JSC, May, 1985.

3. MacDoran, P.F., et al, "Codeless GPS Systems for Positioning of Offshore Platforms and 3D Seismic Surveys", J. of the Institute of Navigation, Vol. 31, No. 2, Summer, 1984.

4. Ondraski, V.J. and Wu, S.C., "A Simple and Economical Tracking System with Subdecimeter Earth Satellite and Ground Receiver Position Determination Capabilities", 3rd International Symposium on the Use of Artificial Satellites for Geodesy and Geodynamics, Ermioni, Greece, Sept. 20-24, 1982.

5. Milliken, R.J. and Zollen, C.J., "Principle of Operation of NAVSTAR and System Characteristics", Institute of Navigation Special Issue on GPS, Vol.1, 1980.

6. Beser, J.B., and Parkinson, B.W., "The Application of NAVSTAR Differential GPS in the Civilian Community", Institute of Navigation Special Issue on GPS, Vol. 2, 1980.

7. Kalafus, R.M., et al, "Differential Operation of NAVSTAR GPS", Institute of Navigation Special Issue on GPS, Vol. 2, 1980.

8. SS-GPS-300B, System Specification for the NAVSTAR GPS, Code IDENT 07868, 3 March 1980..

9. "Federal Radio Navigation Plan-Volume 3, Radionavigation System Characteristics", DOD-4650.4-p-III, DOT-TSC-RSPA-18-12 -III, March, 1982.

10. "Federal Radionavigation Plan-Vol. 2, Requirements",DOD-4650. 4 P-I, DOT-TSC-RSPA-81-12-1, March, 1982.

11. ICD-GPS-200, GPS Interface Control Document, CODE IDENT No. 03953, September 26, 1984.

12. Martin, E.H., "GPS User Equipement Error Models", Institute of Navigation Special Issue on GPS, Vol. 1, 1980.

13. Crow, R.B., et al., "SERIES-X Final Engineering Report", NASA JPL Report JPL-D-1476, August, 1984.

APPENDIX B

PERFORMANCE OF DIFFERENTIAL GPS FOR SPACE STATION TRACKING AND TRAFFIC CONTROL

PERFORMANCE OF DIFFERENTIAL GPS FOR SPACE STATION TRACKING AND TRAFFIC CONTROL

Prepared for

Contract No. NAS9-17414
Lyndon B. Johnson Space Center
Houston, Texas 77058

Prepared by

Dr. Kai T. Woo

Axiomatix
9841 Airport Boulevard
Suite 912
Los Angeles, California 90045

Axiomatix Report No. R8604-5
May 1, 1986

Table of Contents

SUMMARY

Numerous spacecraft with widely varying characteristics and orbits are expected in the Space Station environment. This presents a significant problem in space traffic control, which requires good sensors to determine the relative positions of the detached vehicles and the Space Station. In this area, many types of GPS based sensor systems can be utilized. The following GPS based position determination systems show significant promises for this application:

(a) Standard GPS

(b) Differential GPS (DGPS)

(c) Bent pipe GPS

The available relative positioning accuracy with DGPS is studied in this report. It is shown here that, with low noise receiver designs and special attentions given to antenna design and placements to minimize multipath effects, P-code DGPS can potentially meet both long-range, short-range, and proximity-operations tracking requirements of the Space Station.

The concept of DGPS, the various error sources in the differential pseudorange measurements, the geometric dilution of precision and Space Station's position uncertainty effect on relative positioning accuracy, and the estimated relative positioning accuracies for Space Station traffic control tracking using DGPS are discussed in some detail in this report.

List of Figures

List of Tables

1.0 INTRODUCTION

Performance of Space Station tracking with standard GPS was discussed in an earlier report [1]. It was estimated that in the Space Station environment the positioning accuracies of the Space Station and the detached vehicles using standard GPS P-code ranging can be as good as ≈9m (1-σ). This is appreciably more accurate than the commonly budgeted P-code position accuracy of 15m. There are two justifications for this expected improvement: (i) the tropospheric delay error is negligible at the Space Station's 500 km altitude; and (ii) the multipath error can be appreciably smaller than surface users by careful design and placement of the GPS antennas.

While the 9m position accuracy can meet the long range and short range tracking requirements (± 15m and ± 100m, respectively) of the Space Station, it does not meet the proximity operation requirement of ± 1m. In order to meet the accuracy requirement of proximity operations, it is necessary to apply some form of differential GPS (DGPS) measurement rather than the standard GPS method of position determination. In the DGPS process, the common error sources such as satellite clock error, satellite ephemeris prediction errors, and denial of accuracy effects, which are observed simultaneously by the Space Station and the detached vehicles, can be eliminated. This results in improved relative positioning accuracy between the Space Station and the detached vehicles. The various error sources in DGPS position determination and the achievable accuracies are discussed in this report. It should be noted here that in the proposed DGPS approach relative positions are determined rather than absolute positions. This, however, should not have any significant negative impacts on traffic control since relative positions between the Space Station and the detached vehicles are more important than their respective absolute positions for this application.

It is deemed necessary to have both standard GPS and differential GPS navigation capabilities for Space Station tracking, however, although DGPS can provide

better accuracies in relative position determination than standard GPS. The reasons for requiring standard GPS capabilities are the following:

(1) DGPS requires the Space Station and the detached vehicles to be in view of the same set of four GPS satellites. This may not be possible for some detached vehicles in certain orbital conditions (e.g., the Space Shuttle during ascent). For those situations standard GPS will be useful for relative tracking.

(2) In order to achieve high relative positioning accuracy, the pseudorange measurements made by the Space Station and the detached vehicles must be accurately time-tagged and compared. Due to high orbital velocities, time-tagging should be performed with user clocks which are properly aligned with GPS system time by the GPS Time-Transfer Approach (see Section 3.5). This requires standard GPS receivers for time-transfer operations, which can result in time-transfer errors of the order of ≤ 1 μs.

With a low-noise (1-dB noise figure) receiver design, proper antenna configuration to minimize multipath, and accurate system timing to minimize time-tagging error, this report shows that DGPS can provide relative position accuracies of $\approx$ 1.01m and 1.3m, respectively, for the Space Station proximity operations and short range tracking requirements. Long range tracking, if needed, can be provided by standard GPS which can achieve position accuracies of 9m. In both cases P-code is assumed available.

In Section 2 of this report, the concept of DGPS is reviewed. The various error sources in DGPS are quantified in Section 3. the effects of GPS satellite geometry and Space Station position uncertainty on relative positioning accuracies are discussed in Section 4. The preliminary Kalman filter consideration for DGPS navigation solution is briefly discussed in Section 5. The estimated P-code tracking accuracy with DGPS is discussed in Section 6. Conclusions of this report in given in Section 7.

2.0 CONCEPT OF DIFFERENTIAL GPS (DGPS)

The original motivation of DGPS is to enhance the positioning accuracy of the civilian GPS user community with Standard Positioning Service (SPS), whose positioning accuracy will be limited to $\approx$ 100m (1-σ) according to the 1983 DOD Selective Availability Program (see [1], [2]). The basic concept is to perform user position determination by comparing the GPS signals received at the user to those received by the reference station whose location is surveyed. The denial of accuracy effects on C/A code users observed both by the user and the reference station can be minimized by this differential approach. Availabilities of the reference station and the communication links between it and the users are, however, required for the DGPS application. In addition to improving C/A code positioning accuracy, P-code accuracy can also be improved using DGPS. In fact, it is the P-code DGPS that is of interest for the Space Station application considered here.

The exact implementation of DGPS can be divided into two categories as follows:

(I) Absolute Position Determination by DGPS

In the first approach, the users improve their own position accuracy by utilizing the correction terms sent to him by the reference station at a surveyed location, who derives these correction terms by comparing the GPS derived solution to its own surveyed location. This DGPS concept can be implemented in one of the following three forms [1]

(a) A receiver is placed in the reference station (at a known location) and the errors (Δx, Δy, Δz) in the solution derived from GPS satellites are measured. This information is then transmitted to the vehicle using its own GPS receiver. Issues here are the degradation of the validity of the correction terms as a function of the distance between the two receivers and the fact that these correction terms are only valid if both receivers use the same set of satellites. The issue of common satellite visibility is a fundamental

drawback of this concept. However, for localized applications such as proximity operations, it is unlikely that different constellations will be selected by the user and the reference station.

(b) The reference station will determine the errors in the pseudorange to all visible satellites and transmitted to the user. With this technique, there is no need for the user to use the same constellation as the reference station, since he is getting the correction terms for all the satellites.

(c) The reference station is acting as a pseudo-satellite. The biases in pseudorange for all satellites are calculated and included in the navigation data message broadcast by the pseudo-satellite. The user can collect this information as part of the regular navigation message and correct his solution accordingly. This technique is attractive in areas where four satellites are not always available.

In the above configuration the correction signals are always transmitted to the users from the reference station. It is also possible to have all the users to send their pseudorange measurements to the Reference (Space) Station for DGPS processing. This is probably a viable approach since the Space Station is sufficiently large to support all the processing requirements.

A crucial assumption made in Approach (I) is that the reference stations location is exactly known. This allows for determinations of the DGPS correction terms (Δx, Δy, Δz) for user position corrections. This may be difficult for the Space Station application since its own location is calculated from standard GPS and may have a 1-σ uncertainty of $\leq \pm 15$m (P-code accuracy). Because of this reason, it seems that the more appropriate DGPS approach for Space Station traffic control is relative position determination. This is discussed below.

(II) Relative Position Determination by DGPS

DGPS can be used to determine the absolute position of the user, as discussed in (I), when the position of the reference station is known. It can also be used to

determine the relative positions between the users and the reference station. This is more meaningful in traffic control and relative navigation, especially when the reference station's own position is not exactly surveyed. The difference in these two concepts can be explained by the following discussions. Figure 2-1 illustrates the application scenario of DGPS in the Space Station's environment.

Let ρ_{ui}, ρ_{Ri} be, respectively, the pseudoranges from the user and the reference (Space Station) to the i^{th} GPS satellite, i = 1, 2, 3, 4. Then the difference between ρ_{ui} and ρ_{Ri} can be expressed as

$$\delta_i \equiv \rho_{ui} - \rho_{Ri} = |\underline{U} - \underline{S}_i| - |\underline{R} - \underline{S}_i| + (\Delta T_u - \Delta T_R) \quad (i = 1, 2, 3, 4) \tag{2-1}$$

where

$\underline{U}$ = User's position = (x_u, y_u, z_u)

$\underline{S}_i$ = Position of Satellite i = (x_i, y_i, z_i)

$\underline{R}$ = Reference Station's assumed position = (x_R, y_R, z_R)

ΔT_u = User clock error (with respect to GPS system time)

ΔT_R = Reference's clock error (with respect to GPS system time)

and where the expression $|\underline{x}|$ denotes the length of the vector $\underline{x}$. In (2-1) we have temporarily omitted the errors in the pseudorange measurements (see Section 3) for this discussion.

If the position $\underline{R}$, $\underline{S}_i$ of the reference station and satellites are known, the only unknowns in (2-1) are the user's position $\underline{U} = (x_u, y_u, z_u)$ and clock error difference $\Delta T \equiv \Delta T_u - \Delta T_R$. These four unknowns can be solved from the differential pseudorange measurement δ_i, i = 1, 2, 3, 4, by the set of 4 simultaneous nonlinear equations (2-1). The solution $\underline{U}$ will be the absolute position of the user. It is easy to see that the error in the reference position $\underline{R}$ will definitely affect the accuracy of the user's position determination. For example, if the reference station's position uncertainty is ±15m, the uncertainty in the

Figure 2-1 DGPS Tracking for Space Station

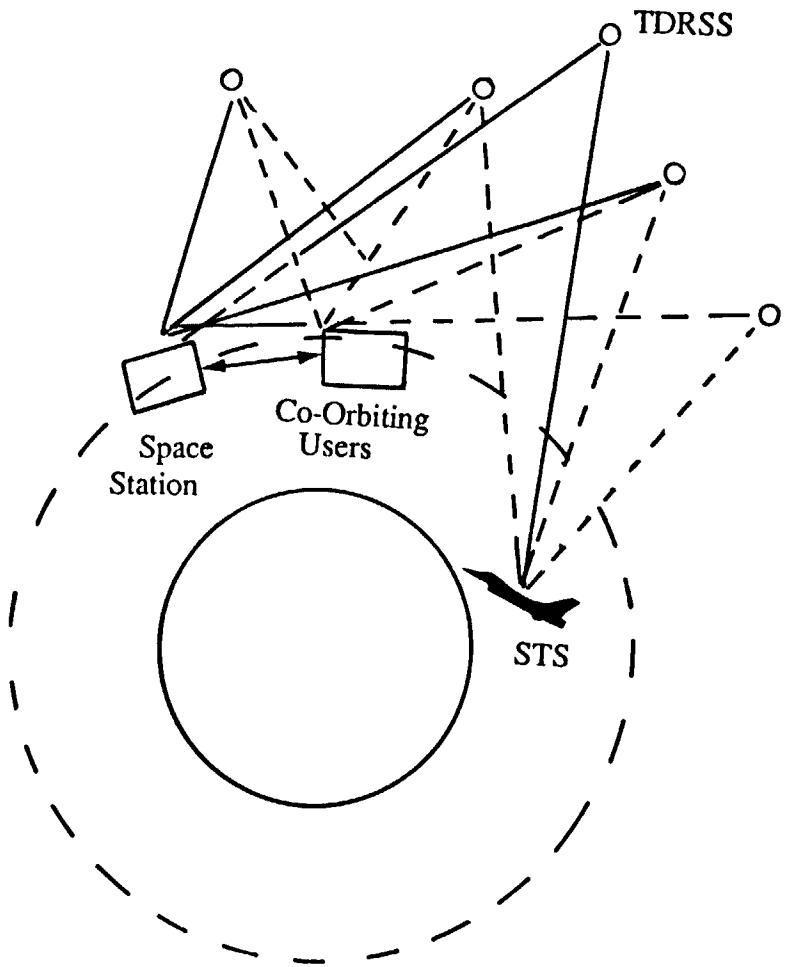

- DGPS requires the Space Station and the detached vehicles to select the same four GPS satellites for position locating.
- STS would probably have to use standard GPS until it is close to the station due to satellite visibility considerations.

solution $\underline{U}$ will be at least as large as ±15m. The following discussions will further demonstrate the differences between Approach I and II.

Let $\underline{R}_o$ be the true location of the reference station and $\underline{\Delta R}$ be the difference between the assumed location $\underline{R}$ and $\underline{R}_o$. The pseudorange ρ_{Ri} measured between the reference station and the i^{th} GPS satellite is then given by

$$\begin{aligned}\rho_{Ri} &= |\underline{R}_o - \underline{S}_i| + \Delta T_R = |R + \underline{\Delta R} - S_i| + \Delta T_R \\ &= \Delta T_R + \sqrt{(x_R + \Delta x_R - x_i)^2 + (y_R + \Delta y_R - y_i)^2 + (z_R + \Delta z_R - z_i)^2}\end{aligned} \tag{2-2}$$

Similarly, let $\underline{U}_n$ be the nominal (assumed) location of the user and let $\underline{\Delta U} \equiv \underline{U} - \underline{U}_n$ be the difference between $\underline{U}_n$ and $\underline{U}$. Then the pseudorange measured between $\underline{U}$ and $\underline{S}_i$ is given by

$$\begin{aligned}\rho_{Ui} &= |\underline{U}_n + \underline{\Delta U} - S_i| + \Delta T_U \\ &= \Delta T_U + \sqrt{(x_{un} + \Delta x_u - x_i)^2 + (y_{un} + \Delta y_u - y_i)^2 + (z_{un} + \Delta z_u - z_i)^2}\end{aligned} \tag{2.3}$$

To determine the absolute location of user location $\underline{U}$ (i.e., Approach I), we are interested in the solution of $\underline{\Delta U}$ from the differential pseudorange δ_i:

$$\delta_i \equiv \rho_{ui} - \rho_{Ri} = |\underline{U}_n + \underline{\Delta U} - S_i| - |\underline{R} + \underline{\Delta R} - S_i| + \Delta T \tag{2-4}$$

Since $|\underline{\Delta R}| << |\underline{R}|$ and $|\underline{\Delta U}| << |\underline{U}|$, the terms in (2-4) can be approximated by ignoring 2nd and higher order terms in $\underline{\Delta R}$, $\underline{\Delta U}$, as follows:

$$\begin{aligned}|\underline{U}_n + \underline{\Delta U} - S_i| &\approx |\underline{U}_n - S_i| + \alpha_{Ui}\Delta x_u + \beta_{Ui}\Delta y_u + \gamma_{Ui}\Delta z_u \\ |\underline{R} + \underline{\Delta R} - S_i| &\approx |\underline{R} - S_i| + \alpha_{Ri}\Delta x_R + \beta_{Ri}\Delta y_R + \gamma_{Ri}\Delta z_R\end{aligned} \tag{2-5}$$

where α, β, γ are the directional cosines from the user ($\underline{U}_n$) and the reference station ($\underline{R}$) to the i^{th} satellite, respectively, defined as follows:

$$\alpha_{Ri} \equiv \frac{x_R - x_i}{|\underline{R} - \underline{S}_i|} \; ; \; \beta_{Ri} \equiv \frac{y_R - y_i}{|\underline{R} - \underline{S}_i|} \; ; \; \gamma_{Ri} \equiv \frac{z_R - z_i}{|\underline{R} - \underline{S}_i|}$$

$$\alpha \equiv \frac{x_{un} - x_i}{|\underline{U}_n - \underline{S}_i|} \; ; \; \beta \equiv \frac{y_{un} - y_i}{|\underline{U}_n - \underline{S}_i|} \; ; \; \gamma \equiv \frac{z_{un} - z_i}{|\underline{U}_n - \underline{S}_i|} \tag{2-6}$$

Substituting (2-5) into (2-4), we obtain (for i = 1, 2, 3, 4)

$$\begin{aligned} \delta_i = {} & |\underline{U}_n - S_i| - |\underline{R} - S_i| + (\alpha_{Ui}\Delta x_u + \beta_{Ui}\Delta y_u + \gamma_{Ui}\Delta z_u) \\ & - (\alpha_{Ri}\Delta x_R + \beta_{Ri}\Delta y_R + \gamma_{Ri}\Delta z_R) + \Delta T \end{aligned} \tag{2-7}$$

Define δ_{in} to the nominal differential pseudorange which the user can compute from its nominal location $\underline{U}_n$ and the assumed location $\underline{R}$ of the reference station

$$\delta_{in} \equiv |\underline{U}_n - \underline{S}_i| - |\underline{R} - \underline{S}_i| \tag{2-8}$$

Then (2-7) can be written in matrix form as

$$\begin{bmatrix} \delta_1 - \delta_{1n} \\ \delta_2 - \delta_{2n} \\ \delta_3 - \delta_{3n} \\ \delta_4 - \delta_{4n} \end{bmatrix} = \begin{bmatrix} \alpha_{u1} & \beta_{u1} & \gamma_{u1} & 1 \\ \alpha_{u2} & \beta_{u2} & \gamma_{u2} & 1 \\ \alpha_{u3} & \beta_{u3} & \gamma_{u3} & 1 \\ \alpha_{u4} & \beta_{u4} & \gamma_{4u} & 1 \end{bmatrix} \begin{bmatrix} \Delta x_u \\ \Delta y_u \\ \Delta z_u \\ \Delta T \end{bmatrix} + \begin{bmatrix} \alpha_{R1} & \beta_{R1} & \gamma_{R1} & 1 \\ \alpha_{R2} & \beta_{R2} & \gamma_{R2} & 1 \\ \alpha_{R3} & \beta_{R3} & \gamma_{R3} & 1 \\ \alpha_{R4} & \beta_{R4} & \gamma_{R4} & 1 \end{bmatrix} \begin{bmatrix} \Delta x_R \\ \Delta y_R \\ \Delta z_R \\ 0 \end{bmatrix} \tag{2-9}$$

or more compactly as

$$\underline{\Delta\delta} = A_u \underline{\Delta U} + A_R \underline{\Delta R} \tag{2-10}$$

where A_u, A_R are the directional cosine matrices of the user and the reference, respectively, $\underline{\Delta U}$ is the correction to user location $\underline{U}_n$ derived from this computation, $\underline{\Delta R}$ is the reference position error, and $\underline{\Delta\delta}$ is the observed difference between nominal difference pseudorange and the observed difference pseudoranges. The solution, for Approach I, is thus given by

$$\underline{\Delta U} = A_u^{-1}\,\underline{\Delta\delta} + A_u^{-1}\,A_R\,\underline{\Delta R} \tag{2-11}$$

From (2-11), it is clear that the position error $\underline{\Delta R}$ in the reference station affects the user's position determination directly. When the user and the reference are in close proximity, for example, we have $A_u \approx A_R$ and the error $\underline{\Delta R}$ appears directly in the solution $\underline{\Delta U}$, as discussed previously. This is the drawback of absolute position determination when $\underline{\Delta R} \neq 0$.

In Approach II, the relative position between $\underline{U}$ and $\underline{R}$ is desired rather than the absolute position $\underline{U}$. For this solution, we can re-write (2-10) as follows:

$$\underline{\Delta\delta} = A_u\,(\underline{\Delta U} - \underline{\Delta R}) + (A_R - A_u)\,\underline{\Delta R} \tag{2-12}$$

The desired relative position solution $\underline{\Delta U} - \underline{\Delta R}$ can then be obtained from (2-12) to be

$$\underline{\Delta U} - \underline{\Delta R} = A_u^{-1}\,\underline{\Delta\delta} + (A_u^{-1}\,A_R - I)\,\underline{\Delta R} \tag{2-13}$$

It is easy to see from (2.2.4-13) that when $\underline{U}$ and $\underline{R}$ are in close-proximity $A_u^{-1}\,A_R \approx I$ and the effect of reference position error $\underline{\Delta R}$ on the desired solution is small.

Since the Space Station's position is determined by standard GPS, its position error ΔR is $\approx$ 15 m (1-σ). Correspondingly, it is necessary to determine the relative position between it and the detached vehicles rather than to determine their absolute locations. This is the recommended approach here and in the following sections of this report, we will assume relative position determination will be adequate for Space Station traffic control.

3.0 ERROR SOURCES ON DIFFERENTIAL PSEUDORANGE MEASUREMENTS

In addition to the reference station's position uncertainty, the measurement errors on the differential pseudoranges also contribute to DGPS position errors. These error sources are further modified by the GPS satellites's geometry with respect to the user and the reference station when they affect the DGPS relative position solutions, in ways similar to the effect of Geometric Dilution of Precision (GDOP) of standard GPS [3]. The error souces on differential pseudoranges will be quantified in this section. The GDOP effects will be further detailed in Section 4.0.

The pseudoranges measured by the reference station and the user, respectively, to the i^{th} GPS satellite can be symbolically characterized by

$$\begin{aligned} \rho_{Ri} &= |\underline{R}_o - \underline{S}_i| + \Delta T_i + \Delta T_R + \varepsilon_{iR} + N_{Ri} + L_{Ri} \\ \rho_{Ui} &= |\underline{U}_o - \underline{S}_i| + \Delta T_i + \Delta T_u + \varepsilon_{iu} + N_{Ui} + L_{Ui} \end{aligned} \tag{3-1}$$

where

ρ_{Ri}, ρ_{Ui} = measured pseudoranges from, respectively, the reference receiver and the user receiver to the i^{th} satellite

$\underline{R}_o, \underline{U}$ = true locations of the reference receiver and the user receiver

$\underline{S}_i$ = assumed locations of Satellite i

$\underline{S}_{io}$ = true location of Satellite i ($\underline{S}_{io} = \underline{S}_i + \Delta\underline{S}_i$)

$\Delta T_i, \Delta T_R, \Delta T_U$ = clock errors of the i^{th} satellite, the reference receiver, and the user receiver, respectively

ε_{iR} = error effect on ρ_{Ri} due to Satellite i ephemeris uncertainty =

$$|\underline{S}_{io} - \underline{R}| - |\underline{S}_i - \underline{R}|$$

ε_{iU} = error effect on ρ_{Ui} due to Satellite i ephemeris uncertainty =

$$|\underline{S}_{io} - \underline{U}| - |\underline{S}_i - \underline{U}|$$

N_{Ri}, N_{Ui} = receiver noise and quantization errors on ρ_{Ri}, ρ_{Ui} measurements, respectively

L_{Ri}, L_{Ui} = tropospheric and ionospheric delay compensation errors on ρ_{Ri}, ρ_{Ui} measurements, respectively.

Table 3-1 summarizes the User-Equivalent-Range-Error (UERE) budget of a typical P-Code GPS User as specified by [4]. The receiver noise effect corresponds to a P-code receiver with an equivalent noise temperature of 28.8°K (noise figure ≈ 5 dB). The multipath and tropospheric delay error effects assumed on Table 3-1 are reasonable for surface users. For the Space Station and the detached vehicles in 500km altitudes, these error assumptions are overly pessimistic.

In DGPS processing, the navigation solution is based on the differential pseudoranges, which are obtained from (3-1) to be:

$$\delta_i = \rho_{Ri} - \rho_{Ui} = |\underline{S}_i - \underline{R}_o| - |\underline{S}_i - \underline{U}| + (\varepsilon_{iR} - \varepsilon_{iU}) + (\Delta T_R - \Delta T_U) + (N_{Ri} - N_{Ui}) + (L_{Ri} - L_{Ui}) \quad (3\text{-}2)$$

By differencing the pseudoranges ρ_{Ri} and ρ_{Ui}, the satellite clock error of the i^{th} satellite, which is obeserved both by the user and the reference receiver, will be eliminated. This includes effects of satellite clock and navigation subsystem stability (≈ 2.7m), predictability of space vehicle perturbations (≈ 1.0m), and other error sources from the i^{th} satellite (≈ 0.5 m).

In summary, the errors in the differential pseudorange measurements are receiver noise, quantization, and multipath effects.

3.1 Receiver Noise, Quantization, and Multipath Effects in Both Reference and User Receivers

Both the user and reference receiver suffer receiver noise, quantization noise, and multiphath effects. Their (RSS) combined effect will affect the differential pseudorange measurements.

In standard GPS processing, the dominating error sources are errors in the GPS satellites. Thermal noise effects are, thus, not too critical. However, in DGPS

Table 3-1 P-Code User (with Selective Availability) UERE Error Budget

(From SS-GPS-300 B)

SEGMENT SOURCE	ERROR SOURCES	SYSTEM RESPONSIBILITY (1σ), METERS	
SPACE	CLOCK & NAV. SUB-SYSTEM STABILITY	2.7	(RANDOM)
	PREDICTABILITY OF SV PERTURBATIONS	1.0	(BIAS)
	OTHERS	0.5	(RANDOM)
CONTROL	EPHEMERIS PREDICTION & MODEL IMPLEMENTATION	2.5	(BIAS)
	OTHERS	0.5	(RAMDOM)
USERS	RECEIVER NOISE & RESOLUTION	1.5	(RANDOM)
	MULTIPATH	1.2	(RANDOM)
	IONOSPHERIC DELAY COMPENSATION	2.3	(RANDOM)
	TROPOSPHERIC DELAY COMPENSATION	2.0	(RANDOM)
	OTHERS	0.5	(RANDOM)
	1-σ UERE =	5.3	METERS

processing, the satellite errors are cancelled in the differential pseudorange observations. Thermal and quantization noise effects become more significant. Consequently, appreciable improvements in DGPS accuracies can be obtained by low noise receiver designs with fine code loop NCO quantization.

The L1 P-code receiver's combined noise and quantization error is ≈ 0.48m and 0.2m (see Table 3-2), for receivers with 5 dB and 1 dB noise figures, respectively. The NCO resolution is assumed to be 1/64 chip in both cases. A code loop bandwidth of ≈1.0 Hz is assumed here, which should have transient errors ≤ 0.1m for accelerations ≤1g.

Another source of receiver error is multipath. In [4] the error budget for multipath effect is assumed to be ≈1.2m. This assumption corresponds to the worst-case multipath effects such as those suffered by users on the ocean surface. Multipath effect in the Space Station environment is expected to be much smaller.

Currently, no test data on multipath error effects have been reported. It is believed that with careful antenna placement and design, and with special attention given to vehicular approach trajectory, Space Station configuration, and reflective surfaces on GPS users in close proximity, the P-code GPS receiver's multipath error should be ≤ 0.2m when operating in the Space Station environment.

3.2 Residual Errors after Ionospheric and Tropospheric Delay Compensations

Tropospheric and ionospheric delays are compensated by GPS receivers. Altitude dependent mathematical models can be used for tropospheric delay compensation. The residual tropospheric delay error is a function of user altitude and elevation angle, and is given by [5]

$$\text{Residual Tropospheric Delay Error} \cong \Delta C \cdot \exp\left(-\frac{0.034}{T} h\right) \csc(E) \qquad (3\text{-}3)$$

where ΔC≈0.1m, E is the elevation angle, h is altitude in meters, and T is the absolute temperature. For spacecraft altitudes ≥500km (for example, the Space Station), the residual tropospheric delay error is negligible.

Table 3-2 Receiver Noise and Quantization Effects

Receiver Equivalent Noise Temperature	Performance of L_1 P-Code Receiver	Performance of L_1 C/A Code Receiver
627° K (28 dB° K) Noise Figure = 5 dB	• $C/N_0 \geq 33.55$ dB-Hz • Code Loop Noise Jitter = 0.46m (B_L = 1 Hz, B_I = 150 Hz) • Transient Error ≤ 0.1m for acceleration ≤ 1g • Quantization Noise = 0.132m (1/64 chip NCO Resolution) • Combibed Noise & Quantization = 0.48m	• $C/N_0 \geq 36.55$ dB-Hz • Code Loop Noise Jitter = 2.23m (B_L = 0.5 Hz, B_I = 100 Hz) • Transient Error ≤ 0.01m for acceleration ≤ 1g • Quantization Noise = 0.14m (1/512 Chip NCO Resolution) • Comined Noise & Quantization = 2.23m
71.5° K (18.76 dB° K) Noise Figure = 1 dB	• $C/N_0 \geq 42.8$ dB-Hz • Code Loop Noise Jitter = 0.15m (B_L = 1 Hz, B_I = 150 Hz) • Transient Error ≤ 0.1m for acceleration ≤ 1g • Quantization Noise = 0.132m (1/64 Chip Quantization) • Combined Noise & Quantization = 0.2m	• $C/N_0 \geq 45.8$ dB-Hz • Code Loop Noise Jitter = 0.76m (B_L = 0.5 Hz, B_I = 100 Hz) • Transient Error ≤ 0.01m for acceleration ≤ 1g • Quantization Noise = 0.14m (1/512 Chip NCO Resolution) • Combined Noise & Quantization = 0.77m

Ionospheric delay varies with respect to location and time-of-day, over a delay range up to 50 μs. Dual frequency (L_1, L_2) measurement or polynomial fits can be used to compensate for ionospheric delays. The residual error after dual frequency correction is proportional to the code loop jitter, and is basically given by 3σ, where σ is the code loop noise error in meters. For the 1-dB noise figure P-code receiver discussed in 3.1, the code loop noise and quantization error is ≈ 0.2m. This corresponds to a residual ionospheric delay error of ≈ 0.6m. The residual error after polynomial fit correction is ≈9m [8].

The ionospheric delay compensation error effects on the differential pseudorange measurements in DGPS is also a function of the separation between the user and the reference station. For short range and proximity operations tracking, the reference station can assume that the users will suffer the same amount of ionospheric delay as the reference receiver. For these cases, the ionospheric delays will be cancelled in differencing the uncompensated pseudoranges. Thus, for short range operations, the ionopsheric delay compensation errors should be negligible. For long range tracking (e.g., ≈ 2,000km separations), this assumptions may not be valid. Ionospheric delay corrections need to be applied by the reference station and the users independently. Assume the user and the reference receivers will both use dual-frequency corrections. The resulting ionospheric delay compensation error on the differential pseudorange measurements will then be $\approx\sqrt{2}$ x 0.6 = 0.84m for the 1-dB noise figure receivers discussed.

These discussions are summarized in Table 3-3.

3.3 Geometric Decorrelation Error Effects Due to Satellite Ephemeris Uncertainty

Satellite ephemeris errors affects pseudorange and differential pseudorange measurements. This error has three components: the radial component, the along-track component, and the cross-track component. The radial component affects psuedorange measurements most significantly. For differential pseudorange measurements, however, along-track and cross-track ephemeris erros are the dominating error components. It can be

Table 3-3 Summary of Ionospheric and Tropospheric Delay Compensation Errors on Differential Pseudorange Measurements

- Estimates of Ionospheric Delay Compensation Error on Differential Pseudoranges

	P-Code Users	C/A Code Users
Long Range Tracking	• Both reference station and detached vehicles apply dual frequency correction independently. • Ionospheric delay error = 0.84m	• Reference station applies dual frequency correction. Detached vehicle applies polynomial fit correction. • Ionospheric delay error = 9.02m
Short Range and Proximity Operations Tracking	• Assume same delays on reference station and detached vehicles. • Ionospheric delay error ≈ 0	• Assume same delays on reference station and detached vehicles. • Ionospheric delay error ≈ 0

- Estimates of Tropospheric Delay Compensation Error
  - Use altitude dependent mathematical model for delay compensation.
  - Residual error ≈ $\Delta C \exp(-0.034\, h/T) \csc(E) \approx 0$ for h ≈ 500km

    $\Delta C \cong 0.1$m, h = altitude in meters, T = absolute temperature, E = elevation angle

shown that the 1-σ contribution to differential pseudorange error by satellite ephemeris uncertainties can be expressed as:

1-σ satellite ephemeris uncertainty contribution on differential pseudorange error

$$\leq \frac{\delta}{\rho} \quad \sigma^2_{\text{along track}} + \sigma^2_{\text{cross track}} \tag{3-4}$$

where $\sigma_{\text{along track}}$ and $\sigma_{\text{cross track}}$ are the along track and cross track satellite ephemeris errors and where

δ = distance from reference station to the user receiver

ρ = distance from reference station to the GPS satellite

As illustrated in Figure 2-1, GPS satellites have altitudes of 20,200km. The Space Station's nominal altitude is ≈500km. This results in $\rho \geq$ 19,700km. The distance δ between the reference and the user varies. Typical values are δ = 1,975km for long range tracking, δ = 37km for short range tracking, and $\delta \approx$ 300m for proximity operations tracking.

The ephemeris data transmitted by the GPS satellites are calculated by curve-fitting. In the first 24 hours after an upload from the master control station, they are calculated based on curve fits over 4 hours intervals ([7], pp. 72-79). For data sets transmitted during the 2nd through 14th day after an upload, the curve fits shall be over 6 hour intervals. The ephemeris errors in the transmitted data set were measured at YUMA (1978) and the results were reported in [6]. Table 3-3 summarizes the measured accuracy of the broadcasted ephemeris reported by [6]. In the following analyses, the YUMA test results for 24 hours after upload will be used as the ephemeris error model. With this ephemeris error model, the expected geometric decorrelation error for DGPS processing between the Space Station and the detached vehicles for long range, short range, and proximity operations tracking scenarios can be computed (with equation 3-4). The results are summarized in Table 3-4.

As shown in Table 3-4, the geometric decorrelation error effects on differential pseudorange measurement increases with the detached vehicle to Space Station separation. For proximity operation and short range trackings, this error contribution is not significant. It becomes appreciable for long range tracking scenarios (1.53m). Nevertheless, it is not of significant concern here since the positioning accuracy requirement for long range tracking is ±15m.

There are two additional points in the above discussions that are of interest to be noted. They are discussed below.

(i) The YUMA test data on broadcast GPS ephemeris accuracy is consistent with the budgetted pseudorange error due to satellite ephemeris effects (2.5m) given in Table 3-1. This effect depends on the angle α between the GPS to user and the GPS to earth center lines (see Figure 3-1). Using the 24 hours after upload ephemeris error model of Table 3-3, the pseudorange error measurement error due to this effect is computed to be between 1.7m to 4.3m, for $0° \leq \alpha \leq 15°$, which is the case for near-earth users. This is consistent with the 2.5m error budgetted in [4].

(ii) The received GPS ephemeris on the C/A code channel is degraded during denial-of-accuracy. The degraded ephemeris accuracy is ± 1km [1]. This is not of any concern, however, for the Space Station application since: (i) the Space Station has access to P-code, and (ii) the detached vehicles are likely to have access to P-code also. Even if the detached vehicles do not have access to P-code, this denial-of-accuracy effect will not affect the proposed Space Station DGPS processing since all the DGPS processing are performed on the Space Station, which will have accurate ephemeris data of the GPS satellites.

Figure 3-1 Satellite Ephemeris Error Effects on Pseudorange and Differential Pseudorange Measurements

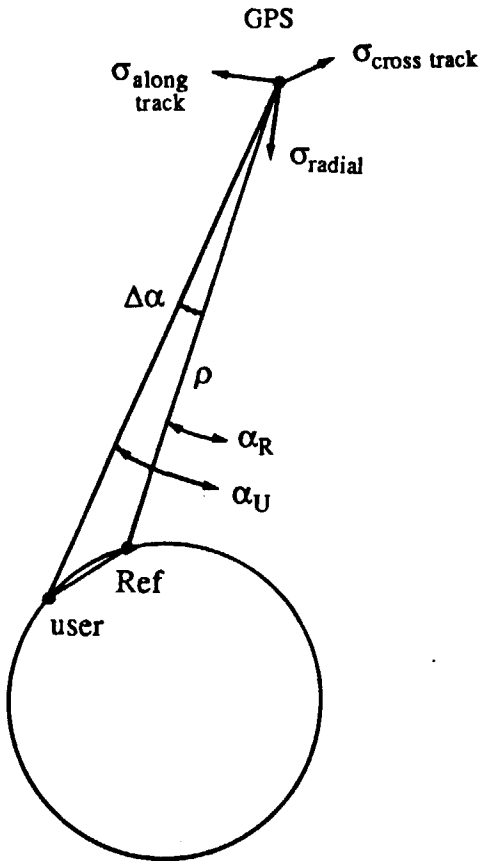

$|\alpha_U| \leq 15°$

- Effects on User Pseudorange Measurement

$$1\text{-}\sigma \text{ contribution} = \sqrt{\cos^2\alpha_u \cdot \sigma^2_{\text{radial}} + \sin^2\alpha_u \, (\sigma^2_{\text{cross track}} + \sigma^2_{\text{along track}})}$$

$$\approx \sigma_{\text{radial}}$$

- Effects on Differential Pseudorange Measurement

$$1\text{-}\sigma \text{ contribution} \leq \frac{\delta}{\rho} \sqrt{\sigma^2_{\text{along track}} + \sigma^2_{\text{cross track}}}$$

δ = distance from reference station to user

ρ = distance from reference station to GPS satellite

Table 3-4 YUMA (1978) Test Results on GPS Broadcast Satellite Ephemeris Error (From [6])

Errors in Transmitted GPS Ephemeris Data	Time Period after Uploads from Master Control Station	
	2 Hours	24 Hours
Radial Error Component	0.818m	1.69m
Along Track error Component	6.31m	15.0m
Cross Track Error Component	3.01m	2.8m

Table 3-4 Geometric Decorrelation Error Effects on DGPS Differential Pseudorange Measurement for Space Station Tracking

Tracking	Separation between Space Station and Detached Vehicles	Geometric Decorrelation Error Effects on Differential Pseudorange Measurement
Long Range	1975 km (1080 nm)	1.53 m
Short Range	37 km (20 nm)	0.28 m
Proximity Operations	305 m (1000 ft)	0.02 m

3.4 Time Tagging Error Effects on Differential Psuedo-range measurements

In evaluating the various error components in the differential pseudorange measurement (of Equation 3-1), it was assumed that the effect of GPS satellite errors such as satellite clock error, space vehicle perturbations, and denial-of-accuracy (for C/A code users only) effects are completely eliminated in the differential pseudorange computations. This assumption is valid only when the associated pseudorange measurements of the reference station and the detached vehicle are made at the same (or nearly the same) instant of time. Otherwise, these effects on the reference receiver's and the user receiver's pseudorange measurements may not cancel each other completely because they are time-varying processes.

Figure 3-2 illustrates the functional block diagram of a non-coherent full-time PN tracking loop. Pseudorange measurement is made by comparing the phases of the receiver's own free-running PN code generator with the received PN code, which is tracked by PN loop's PN code generator. Thus, there are two alternatives for time tagging:

(i) Time tagging with the received PN code phase;

or (ii) Time tagging with the receiver's own free-running PN code phase.

These alternatives correspond to time tagging with the satellite's timing and with the receiver's timing, respectively. Their tradeoffs are discussed in the following sub-sections.

(i) Time tagging with the received PN code phase

With this approach the pseudoranges having the same time-tags correspond to pseudoranges measured with respect to satellite signals transmitted at the same time. The distinct advantage of this approach is that the satellite's clock error and denial-of-accuracy effects (if present, for C/A code users) will be completely eliminated in the differential pseudorange measurement when the pseudoranges are subtracted from each other.

However, due to range difference, the satellite signals (originated at the same instant of time) will be received by the reference and user receivers at different instants of time. This situation is illustrated in Figure 3-3. Let T_1 be the time at which the

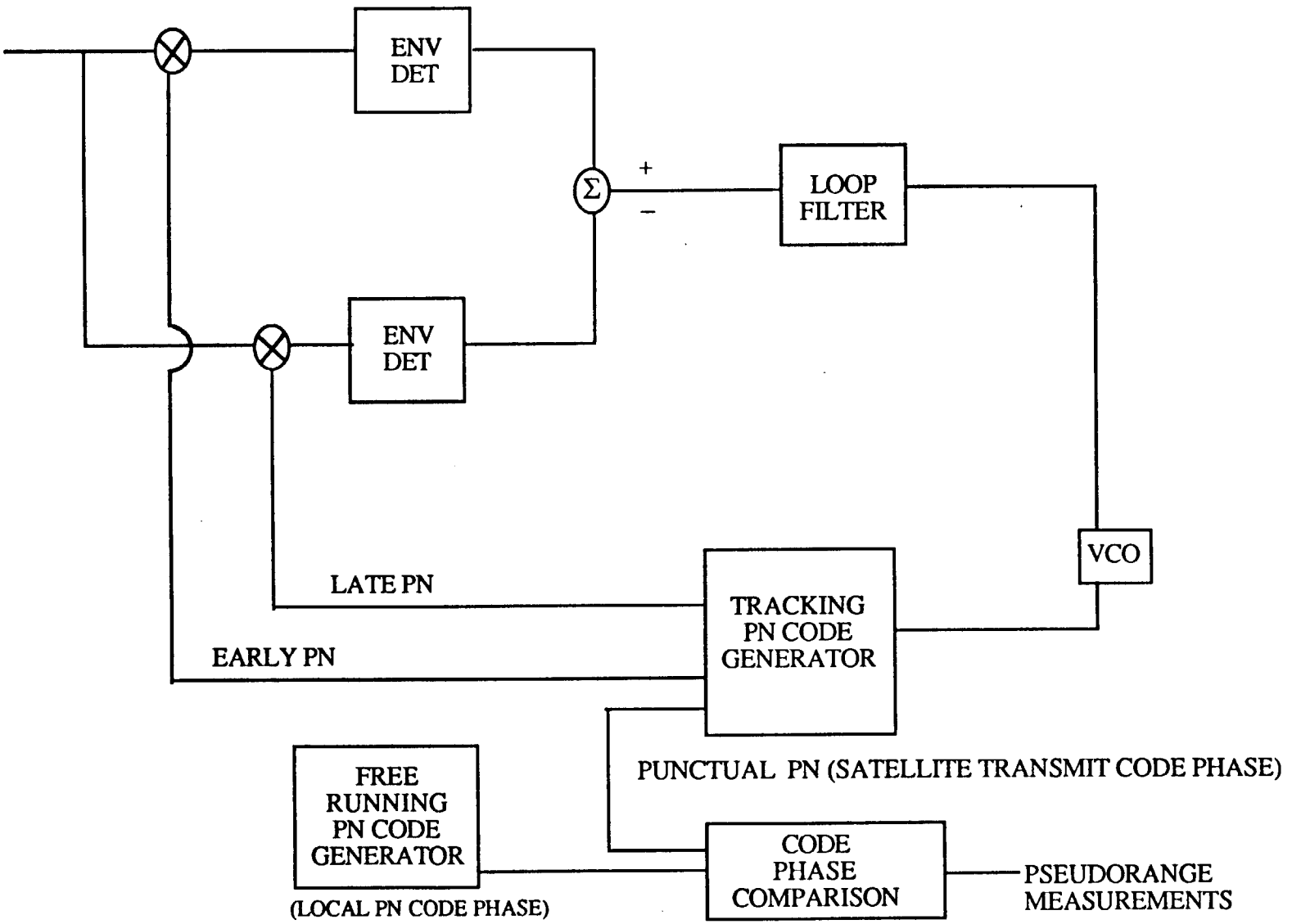

Figure 3-2 Pseudorange Measurement and Time Tagging

T_1 = Time at which GPS signal is transmitted

T_2 = Time at which the reference station detects the GPS signal transmitted at T_1

T_3 = Time at which the detached vehicle detects the GPS signal transmitted at T_1

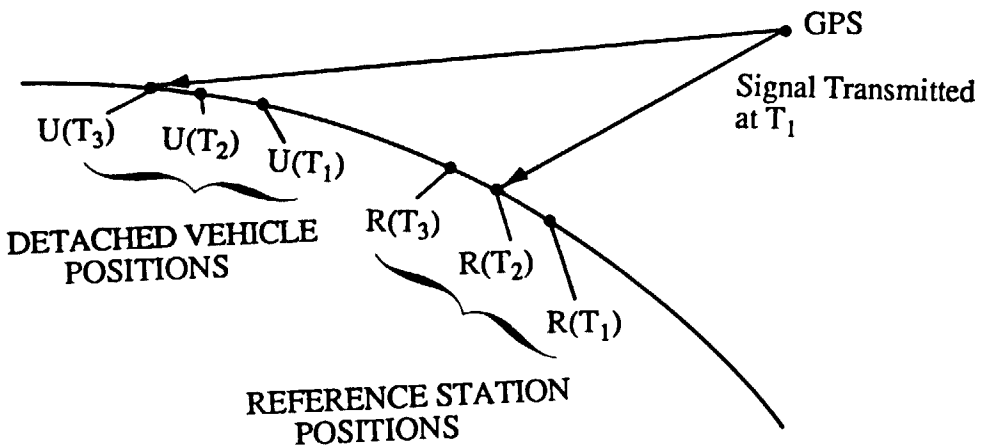

- For Long Range Tracking $T_3 - T_2 \simeq \dfrac{2000\text{ km}}{C} = 6.7$ ms

- Space Station/Detached Vehicle Orbital Speed

$$= \frac{2\pi \times 6870\text{ km}}{1.5\text{ Hr}} = 8\text{ km/sec}$$

- $|U(T_2) - U(T_3)| \simeq 53.6$ meters

- Tracking error too large to be acceptable

Figure 3-3 Time tagging Approach I: Tracking Error Due to Orbital Motions

GPS signal is originated. Let T_2 be the time at which this GPS signal is received at the reference receiver. Let T_3 be the time at which this GPS signal is received by the detached vehicle. Further, let $\underline{R}(T_1)$, $\underline{R}(T_2)$, $\underline{R}(T_3)$; $\underline{U}(T_1)$, $\underline{U}(T_2)$, $\underline{U}(T_3)$ be, respectively, the locations of the reference and user receivers at these instants of time. The pseudorange measured by the reference station (with T_1 time tag) corresponds to the range between the GPS satellite (at time T_1) and $\underline{R}(T_2)$. Similarly, the pseudorange measured by the detached vehicle (with T_1 time-tag) corresponds to the range between the GPS satellite at T_1 and $\underline{U}(T_3)$. The relative position solution obtained from these pseudoranges thus correspond to $\underline{R}(T_2) - \underline{U}(T_3)$, instead of $\underline{R}(T_2) - \underline{U}(T_2)$. Since the separation between the Space Station and the detached vehicle can be as large as 2,000km (long range tracking), the time difference $T_3 - T_2$ can be as large as $\approx$ 6.7ms. The orbital velocity of the Space Station (assuming a 90 minutes orbit) is $\approx$ 8km/sec. In the period of 6.7ms, the detached vehicle would have moved a distance of 53.6m. This indicates a relative positioning error of up to 53.6 meters, which is too large to be acceptable.

(ii) Time Tagging with the Receiver's Own PN Code Phase

The alternative approach is to time-tag the pseudorange measurement with the receiver's own PN code generator. This corresponds to time-tagging with user's signal reception times. This approach requires the detached vehicles to align their PN code timing with the Space Station. Standard GPS Time-Transfer [9] can be used to align the Space Station's and detached vehicle's timing with respect to the GPS satellite to within 1μs accuracy. Thus, the pseudorange will be time-tagged by almost identical reception times. They do, however, correspond to GPS signals originated at different times. The situation is illustrated in Figure 3-4. This implies that the satellite clock error and denial-of-accuracy effects may not be completely cancelled in calculating the differential pseudoranges since the received GPS signals at the reference and user receivers may originate at times differing by upto 6.67ms (for user and reference station separated by up to 2000km).

Figure 3-4 Time Tagging Approach II: Incomplete Cancellation of Satellite Clock Error and Denial of Accuracy Effects

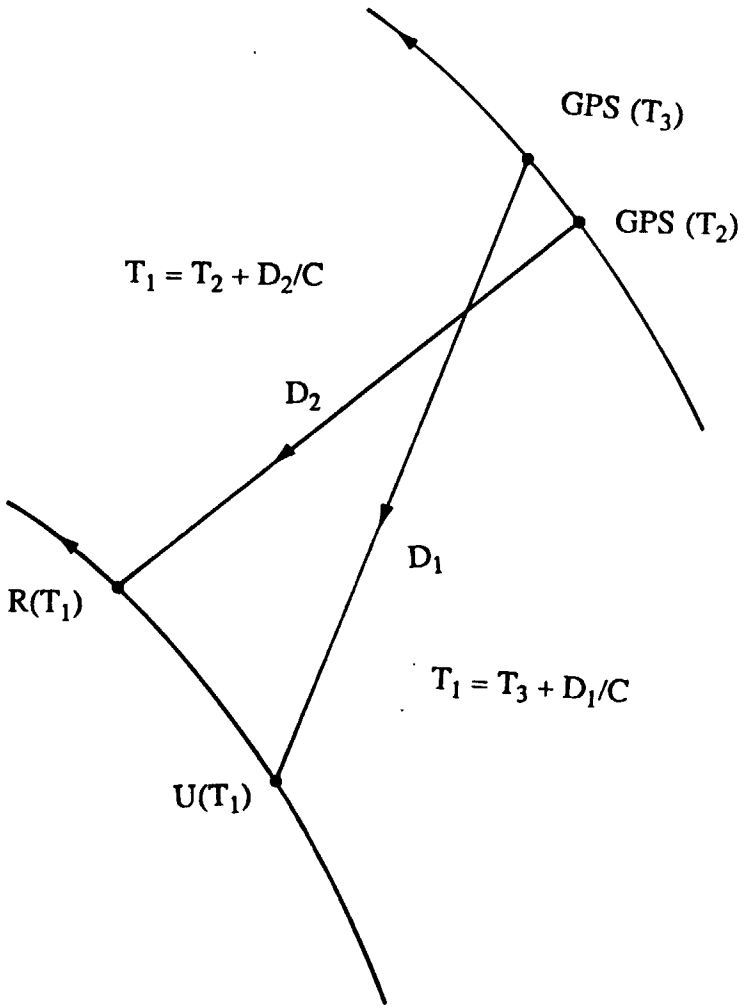

T_1 = Pseudorange Measurement Times at Reference and User

T_2 = T_1 - Apparent Range Delay from Satellite to Reference

T_3 = T_1 - Apparent Range Delay from Satellite to User

Since $T_2 \neq T_3$ there will be incomplete cancellation of satellite clock error and denial of accuracy effects.

The satellite clock error is a slow-varying process. The 1-sec Allan Variances for Cesium and Rubidium sources are 5×10^{-11} and 2×10^{-11}. This indicates time changes in 1 second will be , in equivalent range, ≤ 15mm and 6mm, respectively. The time errors in 6.67ms will be, in range equivalent, ≤ 0.1mm and 0.04mm, respectively. The accumulated errors in satellite clock drifts due to time-tagging discrepancies are, thus, negligible.

Another concern is denial-of-accuracy for C/A code users. Figure 3-5 shows the selective availability probability distribution and its rate distribution [2]. It shows that the maximum rate of change of delay error due to denial-of-accuracy is ≤±1.25m/sec, and the standard deviation of this rate of change of delay error is approximately equal to 0.43m/sec (or 0.129m/sec). This change in range error implies a rate of change in positional error of ≈0.4m/sec for a PDOP of 3. For the ≤6.67ms GPS signal originating time difference suffered by the pseudoranges measured by the Space Station and the detached vehicles using this time-tagging approach, the corresponding range error due to denial-of-accuracy effect is, thus, ≤ 0.129m/sec x 6.67ms = 0.9mm. The 1-σ position error due to this effect is, thus, ≤ 2.7mm assuming a PDOP of 3. Thus, the residual error due to imcomplete cancellation of denial-of-accuracy effects using this approach of time tagging (with aligned receiver clocks) is basically negligible.

From the above considerations, Approach II for time-tagging is recommended. The associated positional error due to time-tagging should be negligible.

3.5 Differential Pseudorange Error Budget Summary

The effects of the various error sources on measured differential pseudorange error are summarized in Tables 3-5 and 3-6. Table 3-5 summarizes the error budget for differential pseudorange measurements when C/A codes are used (for both the Space Station and the detached vehicle). Table 3-6 summarizes the error budget for the P-code case. In either cases, the expected errors for long range, short range, and proximity operation tracking are tabulated. It should be noted here that the differential P-code

Figure 3-5 Denial of Accuracy Delay and Rate of Change Distributions

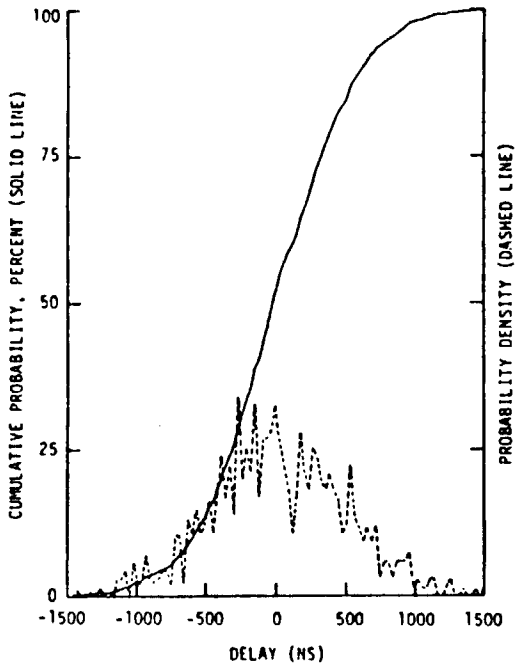

SELECTIVE AVAILABILITY PROBABILITY DISTRIBUTION

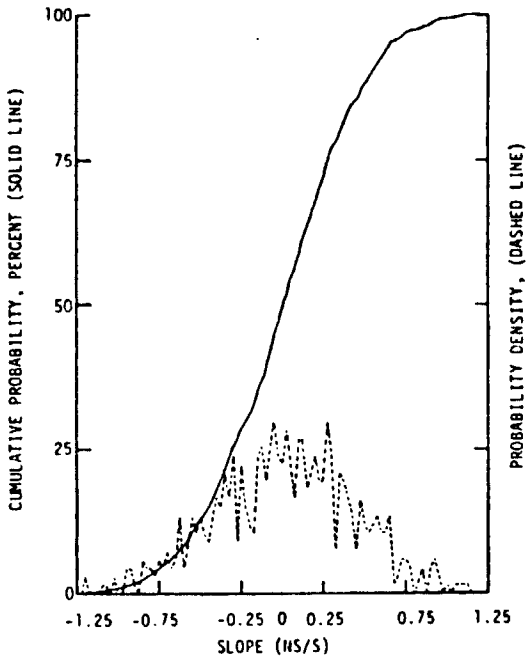

SELECTIVE AVAILABILITY RATE DISTRIBUTION

From Kalafus, R. M. Et Al, "Differential Operation of NAVSTAR GPS, the Institute of Navigation Special Issue on GPS, Volume 2, pp 197-214, 1984

Table 3-5 C/A Code DGPS Error Budgets for Space Station Tracking

Error Sources	Long Range Tracking	Short Range Tracking	Proximity Operations
Geometric Decorrelation Error (Bias)	1.53 m	0.28 m	0.02 cm
Receiver Noise & Quantization (Random)	1.90 m	1.09 m	1.09 m
Multipath (Random)	0.71 m	0.71 m	0.71 m
Ionospheric Delay Compensation Error (Random)	9.02 m	0.00 m	0.00 m
Tropospheric Delay Compensation Error (Random)	0.00 m	0.00 m	0.00 m
Others in Receiver Mechanization (Random)	0.71 m	0.71 m	0.71 m
Time Tagging Error	Negligible	Negligible	Negligible
Estimated 1-σ Equivalent Range Error (Before Kalman Filtering)	9.27 m	1.51 m	1.48 m

Table 3-6 P-Code DGPS Error Budgets for Space Station Tracking

Error Sources	Long Range Tracking	Short Range Tracking	Proximity Operations
Geometric Decorrelation Error (Bias)	1.53 m	0.28 m	0.02 cm
Receiver Noise & Quantization (Random)	0.28 m	0.28 m	0.28 m
Multipath (Random)	0.28 m	0.28 m	0.28 m
Ionospheric Delay Compensation Error (Random)	0.85 m	0.00 m	0.00 m
Tropospheric Delay Compensation Error (Random)	0.00 m	0.00 m	0.00 m
Others in Receiver Mechanization (Random)	0.71 m	0.71 m	0.71 m
Time Tagging Error	Negligible	Negligible	Negligible
Estimated 1-σ Equivalent Range Error (Before Kalman Filtering)	1.93 m	0.86 m	0.81 m

differential pseudorange accuracy is significantly better than that of pure pseudorange measurements (compare Tables 3-6 and 3-1). While P-code pseudorange accuracy cannt be better than ≈ 4m (even with low noise receiver and fine NCO quantization), the corresponding differential pseudorange accuracy can be ≈0.81 to 0.86m for proximity operation and short range trackings and ≤ 2m for long range tracking, which is appreciably more accurate.

4.0 GEOMETRIC DILUTION OF PRECISION AND REFERENCE STATION POSITION UNCERTAINTY EFFECTS ON RELATIVE POSITIONING ACCURACIES

Relative positioning accuracy in the DGPS solution will be affected by the geometry of the selected satellites, in a way identical to the geometric dilution of precision (GDOP) effect encountered in standard GPS positioning solutions. This GDOP factor and its effect in conjunction with measurement errors in differential pseudorange measurements on DGPS positioning accuracy, as well as the reference station's own position uncertainty effects in conjunction with the associated DGOP due to reference position uncertainty, are computed in this section.

When differential pseudorange measurement errors are present, Equation (2-13), which relates $\Delta\delta$, the observed differential pseudorange deviation from the nominal (last step) differential pseudorange, to the derived relative position update (from the last solution and assumed reference location) $\underline{\Delta U} - \underline{\Delta R}$, is given by (cf 2-13):

$$\underline{\Delta U} - \underline{\Delta R} = A_u^{-1}\,\underline{\Delta\delta} + (A_u^{-1} A_R - I)\,\underline{\Delta R} + A_u^{-1}\,\underline{E_{dr}} \tag{4-1}$$

Where $\underline{E_{dr}}$ is the differential pseudorange measurement error vector

$$\underline{E_{dr}} = \begin{bmatrix} e_1 \\ e_2 \\ e_3 \\ e_4 \end{bmatrix} \tag{4-2}$$

with e_1, e_2, e_3, e_4 being the measurement errors on the four differential pseudoranges to the four selected satellites. The error vectors $\underline{\Delta R}$ and $\underline{E_{dr}}$ are uncorrelated. Thus, mean square error of the estimate $\underline{\Delta U} - \underline{\Delta R}$ is given by:

$$\begin{aligned}&\text{Mean square error in relative position} = \text{Trace}\,[(\underline{\Delta U} - \underline{\Delta R})\,(\underline{\Delta U} - \underline{\Delta R})] \\ &= \text{TR}\left\{ A_u^{-1}\,[\,\underline{E_{dr}} \cdot \underline{E_{dr}}^T]\,A_u^{-T} + (A_u^{-1} A_R - I)\,[\underline{\Delta R} \cdot \underline{\Delta R}^T]\,(A_u^{-1} A_R - I)^T\right\}\end{aligned} \tag{4-3}$$

where in (4-3) the overbar denotes the expectation operation, and super-script T denotes the transpose of. Assume the error components in x, y, z dimensions are independent, identically distributed with zero mean and variances σ_e^2 and $\sigma_{\Delta R}^2$, respectively, for the error vector $\underline{E}_{dr}$ and $\underline{\Delta R}$. Then, the covariance matrices in (4-3) can be written as

$$\underline{E}_{dr} \cdot \underline{E}_{dr}^T = \sigma_e^2 I \tag{4-4}$$

$$\underline{\Delta U} \cdot \underline{\Delta R}^T = \sigma_{\Delta R}^2 I \tag{4-5}$$

where I is 4 x 4 identity matrix. With this assumption, the mean square error in the relative position solution is, thus, given by:

$$\text{Mean square error in and relative position clock error solution} = \sigma_c^2 \; TR[(A_u^T A_u)^{-1}] + \sigma_{\Delta R}^2 TR[(A_u^{-1}A_R - I)(A_u^{-1}A_R - I)^T] \tag{4-5}$$

The term $TR[(A_u^T A_u)^{-1}]$ in (4-5) is identical to the conventional GDOP term in standard GPS, which is only a function of the directional cosines of the user (detached vehicle) to the four GPS satellites. The second term in (4-5) relates to the reference receiver's position uncertainty, and is modified by a modified GDOP term defined by

$$RGDOP = TR\,[(A_u^{-1} A_R - I)(A_u^{-1} A_R - I)^T] \tag{4-6}$$

4.1 GDOP and RGDOP Calculations for Space Station and Detached Vehicles

A simulation program has been completed which calculates the 18 GPS satellites' positions as functions of time. From these positions relative to the Space Station's (or detached vehicles's) position, the satellite visibility can be checked, and the GDOP and RGDOP factors can be computed. Figures 4-1 and 4-2 plot examples of the GDOP and RGDOP for the Space Station and detached vehicle at 500km altitudes. A separation of 300m (proximity operations) is assumed between the reference station and the detached vehicle for the illustrated RGDOP computation of Figure 4-2. The GDOP's

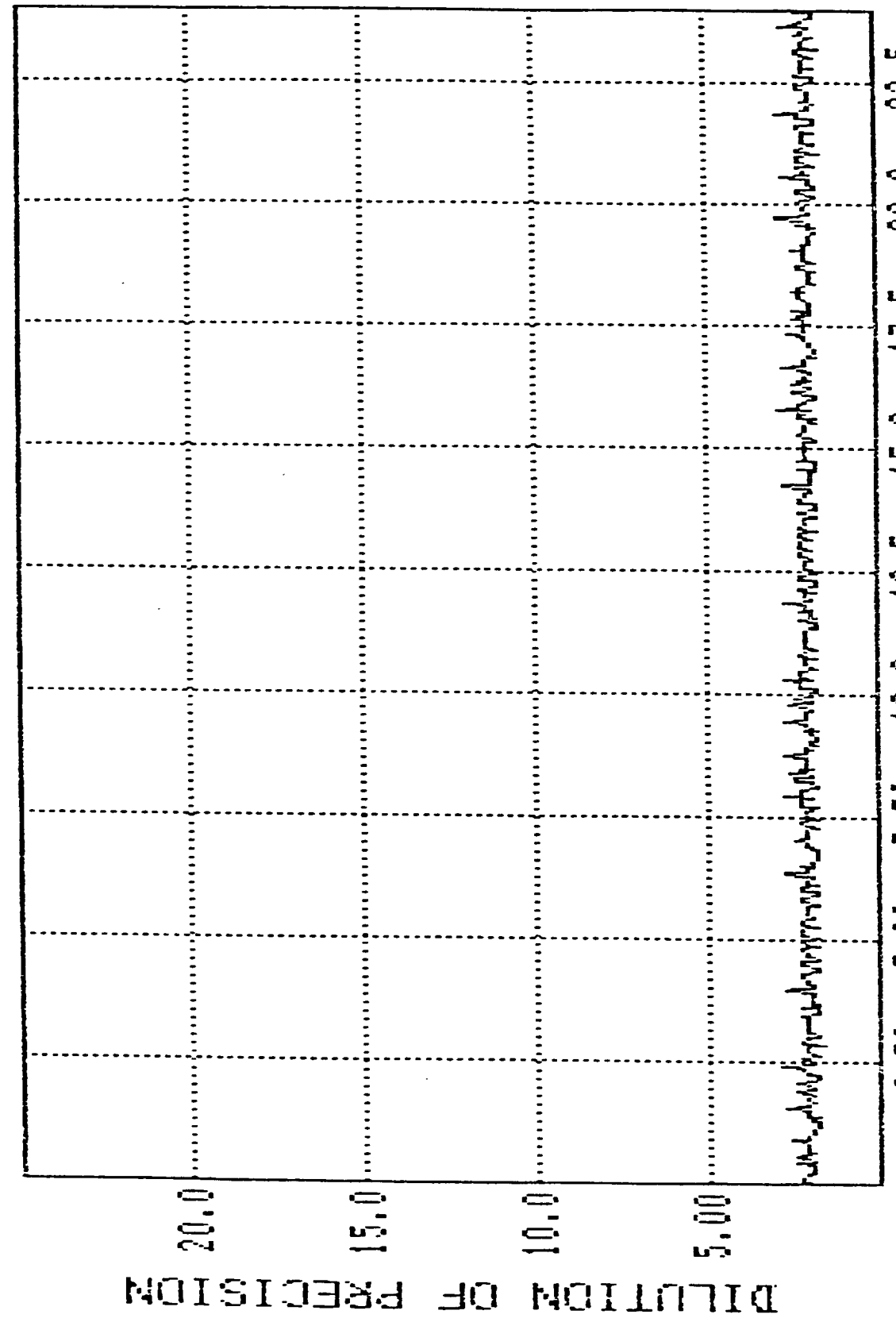

Figure 4-1 GDOP for Space Station Orbit

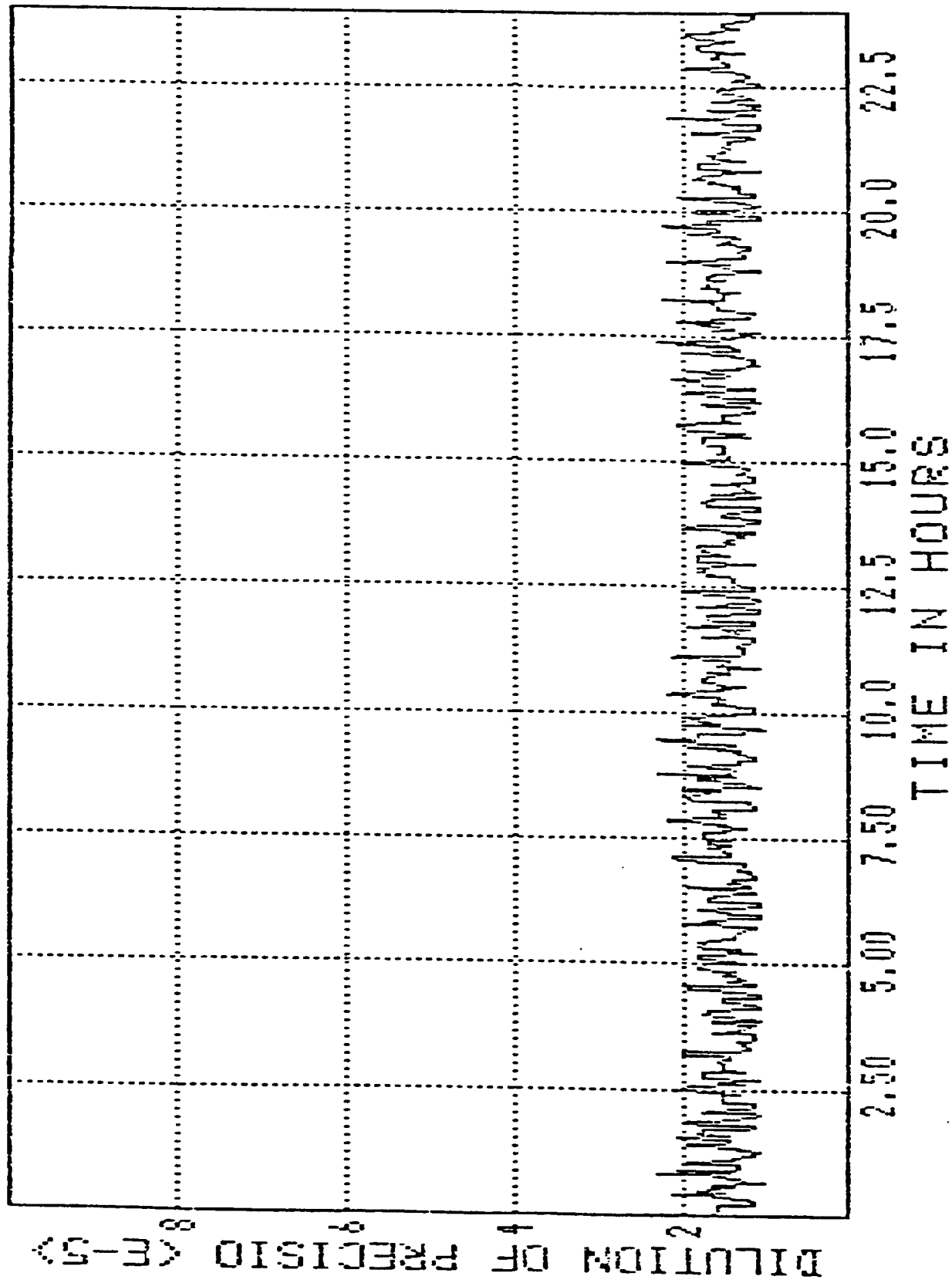

Figure 4-2 GDOP for Space Station Orbit
(Reference Station to User Separation = 300m)

plotted in these figures correspond to the minimum achievable GDOP provided by the best set of four satellites selectable as a function of time.

Table 4-1 summarizes the average GDOP and RGDOP results for receivers at Space Station's (500km) altitude and on the earth surface, respectively. Two entries are given for DGPS considerations, corresponding to GDOP and RGDOP, respectively.

Two observations can be made with respect to Table 4-1:

(1) As expected, the average GDOP for users in the 500km altitude is better than that of earth surface users in identical latitudes and longitudes, due to improved satellite visibilities. Table 4-1 shows the average GDOP for a user at 0° longitude, 0° latitude,and at 500km altitude has an average GDOP of 2.09, which is compared to the GDOP of 2.68 for the surface user at the same latitude and longitude.

(2) RGDOP's values are relatively small for proximity operations and short range tracking. This indicates that if the detached vehicle is not too far away from the Space Station (e.g., $\leq$ 185km), the reference receiver's position uncertainty effect is small (RGDOP $\leq 10^{-2}$). For example, if the reference receiver's position uncertainty is $\pm$15m, the resultant error due to this uncertainty is $\pm$0.15m, for the RGDOP value of 10^{-2}. This shows that relative positioning in DGPS processing is indeed the appropriate positioning algorithm in this application, since the Space Station's position uncertainty will be of the order of $\pm$15m if standard GPS is used for its own position determination.

Table 4-1 Summary of GDOP Computations *

Altitude	Space Station	Ground
Standard GPS	2.901	2.681
Differential GPS	2.901	2.681
0.3 km	1.498×10^{-5}	1.862×10^{-5}
Differential GPS	2.094	2.687
37 km	1.875×10^{-3}	1.066×10^{-3}
Differential GPS	2.109	2.753
185 km	9.03×10^{-3}	1.037×10^{-2}
Differential GPS	2.299	3.187
2000 km	9.633×10^{-2}	0.1169

* The data for the ground user is computed at latitude 0° and longitude 0°.

5.0 ESTIMATED RELATIVE POSITIONING ACCURACY WITH DGPS

Kalman filtering is a commonly used technique to obtain GPS position determination from pseudorange measurements through a set of four simultaneous nonlinear equations. While providing an iterative solution, Kalman filtering also reduces the error variances to arrive at a more accurate solution. The limit to which noise effects can be reduced will depend on the accuracy in modelling the physical system in the state equation.

Two Kalman filter algorithms can be considered for Space Station application: the PVA (position, velocity and acceleration) model and the orbital mechanic model. The PVA model is more suitable for detached vehicles undergoing dynamic maneuvers (such as the EVA) while the orbital mechanic model is more suitable for vehicles in orbital motion (such as the free-flyers or the Space Station).

For DGPS tracking, the observations are differential pseudorange. Correspondingly, the standard GPS Kalman filter algorithm must be modified to take into consideration differential processing and relative position determination.

In this current report, the details of the Kalman filter algorithm will not be discussed. It will be addressed in another Axiomatix report [10]. In this report, the main objective is to investigate the achievable accuracy of DGPS processing for Space Station traffic control tracking. The assumption made here regarding Kalman filtering performance is that it will reduce the standard deviation of each random error contribution by a factor of 3; this is a fairly conservative assumption and is achievable with reasonably well-designed Kalman filter algorithms (the same assumption was used in [1] for GPS accuracy evaluations). With this assumption, and assuming a GDOP of 3, which is also somewhat conservative (see Table 4-1), and with the differential pseudorange error budgets of Table 3-5 and 3-6, the achievable accuracies with C/A or P-codes for relative positioning between the Space Station (which acts as the reference station) and the detached vehicle are computed. The results are summarized in Table 5-1. It shows that with low-noise receiver

Table 5-1 Three-Dimensional Positioning Error Summary --DGPS Relative Positioning between Space Station and Detached Vehicles for Traffic Control

Assumptions:

- PDOP = 3.0
- Kalman filtering can reduce random error to 1/3
- Kalman mechanization error ≤ 0.2 m
- Time tagged error on PR measurements are negligible
- Relative position determination

DGPS Relative Positioning Errors after Filtering--Estimates

	Long Range Tracking	Short Range Tracking	Proximity Tracking
DGPS--C/A Code	10.25 m	1.81 m	1.60 m
DGPS--P-code	4.78 m	1.31 m	1.01 m

designs, P-code DGPS can meet the traffic control tracking requirements of the Space Station. The main conclusions here is that P-code DGPS can achieve 1.31m and 1.01m relative positioning accuracies for short range (≤ 37km) and proximity operations trackings, respectively. A 5m accuracy can be expected for long range tracking up to 2000km.

6.0 CONCLUSIONS

Two main conclusions come as a result of this study:

(1) With careful receiver designs and enviromental control for multipath, it is expected that P-code DGPS can meet the relative positioning accuracy requiremetns for space station traffic control. C/A code DGPS will meet the long and short range tracking requirements; however, it falls short of meeting the proximity operation requirement (accuracy = 1.6m instead of 1.0m). The design constraints can be summarized as follows:

- Low noise receiver design (NF = 1dB)
- Narrow code loop bandwidth (0.5 to 1 Hz)
- Fine code loop NCO resolution (1/64 for P, 1/512 for C/A)
- Careful placement and design of GPS antennas (0.2m for P-code, 0.5m for C/A code).
- Small Kalman filter mechanization error ($\leq$ 0.2m)
- Minimum time tagging errors in differential ranges
- Position locations are relative to reference station (i.e., not absolute location determination).

(2) Both DGPS and standard GPS should be valid sensors for Space Station traffic control tracking. DGPS will be needed for short range and proximity operations tracking because of accuracy requirements for close range applications. Standard GPS will be required for time transfer to allow clock alignments for the purpose of time-tagging. It will also be needed for some long range tracking operations where the detached vehicle and the Space Station cannot both see the same set of four GPS satellites. Table 6-1 summarize these conclusions.

BOTH STANDARD GPS AND DGPS SHOULD BE VALID SENSORS FOR SPACE STATION TRACKING , WITH OVERLAPPING REGIONS OF COVERAGE.

TECHNIQUE	APPLICATIONS	ESTIMATED PERFORMANCE
STANDARD GPS	LONG RANGE AND SHORT RANGE TRACKING, ESPECIALLY WHEN THE SPACE STATION AND THE DETACHED VEHICLE CANNOT SEE THE SAME 4 GPS SATELLITES	$1-\sigma$ POSITION ERRORS (PDOP =3): P-CODE = 8.6 - 8.8 m C/A CODE WITHOUT ACCURACY DENIAL =12.5 -18 m C/A CODE WITH ACCURACY DENIAL = 100 m
DGPS	SHORT RANGE AND PROXIMITY OPERATION TRACKING (AND POSSIBLY LONG RANGE TRACKING), WHEN SPACE STATION AND DETACHED VEHICLE CAN SEE THE SAME 4 GPS SATELLITES, ALSO WHEN HIGH TRACKING ACCURACIES ARE REQUIRED.	$1-\sigma$ RELATIVE POSITION ERRORS (PDOP =3): P-CODE = 1.01 m (PROXIMITY) 1.31 m (SHORT RANGE) C/A CODE: 1.60 m (PROXIMITY) 1.81 m (SHORT RANGE)

Table 6-1 PRELIMINARY CONCLUSIONS

References

[1] Beser, J. and Parkinson, B. W., "The Application of NAVSTAR Differential GPS in the Civilian Community," Institute of Navigation Special Issue on GPS, Volume II, 1984.

[2] Kalafus, R. M.; Vilcans, J.; and Knable, N.; "Differential Operation of NAVSTAR GPS," Institute of Navigation special issue on GPS, Volume II, 1984

[3] Woo, K. T., "Space Station Tracking with Standard GPS," Axiomatix Report No. 8510-1, submitted to Johnson Space Center under Contract No. NAS9-17414, October 18, 1985.

[4] SS-GPS-300B, "System Specification for the NAVSTAR GPS," Code Ident. 07868, March 3, 1980.

[5] Martin, E. H., "GPS User Equipment Error Models," Institute of Navigation Special Issue on GPS, Volume I, 1980

[6] Russell, S. S.and Schaibly, J. H., "Control Segment and User Performance," Institute of Navigation Special Issue on GPS, 1983.

[7] ICD-GPS-200, "Navstar GPS Space Segment/Navigation User Interfaces," Code Ident. No. 03953, September 26, 1984.

[8] Klobuchar, J. A., "A First Order, Worldwide, Ionospheric Time-Delay Algorithm," AFCRL-TR-75-0502.

[9] Van Dierendonck, A. J. and Melton, W. C., "Application of Time Transfer Using NAVSTAR GPS," Institute of Navigation Special Issue on GPS, Volume II, 1984.

[10] U. C. Cheng, "Kalman Filter Consideration for Space Station Tracking with DGPS," Axiomatix Report No. R8605-1, May 1986.

APPENDIX C

AN ANALYSIS OF CODELESS DOPPLER NAVIGATION USING GPS SATELLITE SIGNALS

An Analysis of Codeless Doppler Navigation Using GPS Satellite Signals

Contract No. NAS9-17414

Prepared for
NASA Lyndon B. Johnson Space Center
Houston, Texas 77058

Prepared by
R. Scholtz

Axiomatix
9841 Airport Boulevard
Suite 912
Los Angeles, California 90045

Axiomatix Report No. R8601-3
May 5, 1986

Table of Contents

An Analysis of Codeless Doppler Navigation Using GPS Satellite Signals

Abstract

This report describes a study of a method for spacecraft position location based on observations of the Global Positioning System (GPS) satellites' signals. In the "codeless technique" described here, the user does not require access to the P-code information used in standard GPS receivers to demodulate the wideband GPS signal with a correlation detector. Instead, the user develops a set of Doppler-shifted tones from each satellite's wideband signal, and derives its location via Doppler navigation and tone-ranging techniques.

The study was terminated when it was determined that P-code assess would be granted to Space Station users.

An Analysis of Codeless Doppler Navigation Using GPS Satellite Signals

1. Background

Certain Earth-surveying systems, developed originally at JPL, determine location using the signals from the Global Positioning System (GPS) in an unusual manner. The wideband signals, carrying considerable useful information, are compressed to pure tones via a delay, self-multiply, and filter circuit, without extraction of modulated information or use of the spread-spectrum (SS) codes which structure the signal. In effect, the GPS satellites are viewed as orbiting oscillators, employing very stable clocks, producing tones at the C/A, P, $2L_1$ and $2\ L_2$ frequencies. This viewpoint bypasses any need to know the GPS-SS codes, but requires that GPS satellite orbit information be supplied from some source to the system.

The only information remaining for a receiver to use in the navigation process is the Doppler-shift signatures of the signals coming from the GPS satellites. In the case of the JPL system, this is sufficient to

(a) identify the satellite producing each observed tone,

(b) locate the receiver with an error of less than 150 meters via Doppler navigation techniques, and then

(c) use tone ranging on signals from each satellite to further reduce location errors to sub-meter levels.

The issue here is a receiver's ability to do the same kinds of processing in the more dynamic orbiting vehicle environment that stationary surveying systems on the earth have accomplished. JPL is attempting to move their system into space on the TOPEX satellite, but their scenario involves non-real time processing of recorded signals over a period of weeks, months, or longer.

The open literature references to the codeless use of GPS-signals [1]-[5] contain little detailed analysis of performance. Hence, in the sections to follow we will for the most part work without the benefit of knowledge of previous analyses.

2. Simple Orbit Models

To a first approximation, the orbits of artificial earth satellites are ellipses with the earth at one of the ellipse's foci. It is possible to derive the unperturbed orbit of the artificial satellite directly from Kepler's laws [6], [7], and in our feasibility studies we will limit our orbit models to ellipses.

Six parameters are required to specify an elliptic orbit. Two of these are ellipse shape parameters, namely:

(1) a = length of the semi-major axis of the ellipse,

(2) e = eccentricity of the ellipse

= (distance from earth center at focus to ellipse center)/a.

The location of the satellite within the elliptic orbit can be determined from a third parameter:

(3) τ = time of perigee passage.

The perigee is the location on the orbital path, which is closest to the earth center focus (the perigee is on the semi-major axis of the ellipse at a distance of a (1-e) from earth center).

The three remaining parameters orient the elliptic orbit in space. Directions are related to the vernal equinox (first point of Ares), i.e., the direction of a line through the centers of the earth and sun on the first day of spring, which is nominally the intersection of the earth's orbital plane and the earth's equatorial plane. The line of nodes is the intersection of the satellite's orbital plane with the earths equatorial plane. The remaining orbit parameters are:

(4) i = inclination angle

= angle between the satellite orbital plane and the equatorial plane.

(5) Ω = Longitude of the ascending node

= angle between the vernal equinox and the line of nodes (measured in the direction of earth rotation in the equatorial plane)

(6) ω = argument of perigee

= angle between the line of nodes and the semi-major axis of the ellipse (measured on the perigee side)

In an ideal model, unperturbed by a variety of secondary effects, all of the above six parameters would be constants.

Location within an orbit at time t is computed via Kepler's equation,

$$\mu^{1/2} (t-\tau) = a^{3/2} (E - e \sin E), \quad (1)$$

where $\mu = 3.986032 \times 10^{14}$ m^3/s^2 [6]. This permits calculation of the eccentric anomaly E (in radians) from the time $(t-\tau)$ past perigee. Note that the period T of the orbit, given by

$$T = 2\pi a^{3/2} / \mu^{1/2}, \quad (2)$$

was used in developing (1). The eccentric anomaly E is the one angle in this orbital geometry which is not measured between lines passing through the earth's center, but instead is measured between lines passing through the ellipse's center (the interpretation of this angle is not important here). Given the eccentric anomaly E for a given time t (i.e., $t-\tau$ past perigee), we can compute the location of the satellite in polar coordinates (r,f) in the orbital plane with the earth at (0,-) and perigee at (a(1-e),0),

$$r = a(1-e \cos E) \quad (3)$$

$$\tan\left(\frac{f}{2}\right) = \left(\frac{1+e}{1-e}\right)^{1/2} \tan\left(\frac{E}{2}\right) \quad (4)$$

and this calculation can be checked by the equation

$$r = \frac{a(1-e^2)}{1+e\cos f} \quad (5)$$

The quantity f is called the true anomaly of the satellite (at time t). Hence, either E or f or t can in principle be used to specify a location in orbit, given a, e, and τ.

A sequence of transformations involving i, Ω and ω is necessary to orient the orbit in space. Specifically, consider the earth-centered inertial coordinate system in which the x axis is the vernal equinox, the y axis is also in the equatorial plane at an equinox, the y axis is also in the equatorial plane at an angle 90° to the x axis in the direction of earth rotation, and the z axis is directed through the north pole. Then as f and r vary according to (5),

$$\begin{bmatrix} x \\ y \\ z \end{bmatrix} = \begin{bmatrix} r\cos(f) \\ r\sin(f) \\ 0 \end{bmatrix} = \underline{y}$$

describes an ellipse in the equatorial plane with with perigee on the positive x axis.

Let's now define the following rotational transformation matrices:

$$W = \begin{bmatrix} \cos\omega & -\sin\omega & 0 \\ \sin\omega & \cos\omega & 0 \\ 0 & 0 & 1 \end{bmatrix}$$

$$I = \begin{bmatrix} 1 & 0 & 0 \\ 0 & \cos i & -\sin i \\ 0 & \sin i & \cos i \end{bmatrix}$$

$$\Theta = \begin{bmatrix} \cos\Omega & -\sin\Omega & 0 \\ \sin\Omega & \cos\Omega & 0 \\ 0 & 0 & 1 \end{bmatrix}$$

Then $W\underline{v}$ represents an elliptic orbit in the equatorial plane of the earth, with the perigee located at an angle ω from the vernal equinox direction. An inclined orbit with the line of nodes in the direction of the vernal equinox is represented by $IW\underline{v}$. Rotating the line of nodes in the equatiorial plane to the longitude of the ascending node gives the complete orbit representation:

$$\begin{bmatrix} x \\ y \\ z \end{bmatrix} = \Theta I W \underline{v}$$

$$= r \begin{bmatrix} \cos\Omega\cos(\omega+f)-\sin\Omega\cos i\sin(\omega+f) \\ \sin\Omega\cos(\omega+f)+\cos\Omega\cos i\sin(\omega+f) \\ \sin i\sin(\omega+f) \end{bmatrix}$$

When orbit eccentricity e is zero, then the argument of perigee is not defined, so we assume in this case that the perigee point is associated with the ascending node so that the time τ of perigee passage is replaced by the time of ascending node passage. A similar reduction in parameters occurs when the inclination angle is zero and, hence, the line of nodes and angle of the ascending node are not well defined, but we will not run into this problem in the applications discussed in this report.

We assume that the NAVSTAR-GPS satellites are in their nominal 18 satellite configuration (see [8] or [9] p 2-3,4) and neglect spares in the work to follow. With three satellites in each of six orbital planes, it is a simple matter to identify satellite #n by its orbital plane number k(n) and its number within the orbital plane j(n).

$$k(n) = \lceil n/3 \rceil \qquad , j(n) = n-3\,(k(n)-1)$$

Here $\lceil x \rceil$ denotes the smallest integer that is greater than or equal to x, and hence satellite number 1 is the first satellite in orbit plane 1. Similarly satellite 14 is the second satellite (j(14)=2) in orbit plane 5 (k(14)=5).

The orbit parameters which we assume for the GPS satellites are as follows:

$e = 0, (\omega=0)$

$$i = 55^\circ$$

$$a = 26{,}610.284 \text{ km } (T = 12 \text{ hr})$$

are the same for all satellites, while

$$\Omega = k(n) \cdot 60^\circ - 30^\circ$$

$$\tau = (j(n)-1) \cdot 120^\circ + (k(n)-1) \cdot 40^\circ] \left(\frac{-12}{360^\circ}\right) \text{ hr.}$$

vary with orbit plane and satellite number.

The GPS constellation, just described mathematically, can be described graphically by plotting time past ascension versus the ascending node angle, at the time when GPS #1 passes its ascending node.

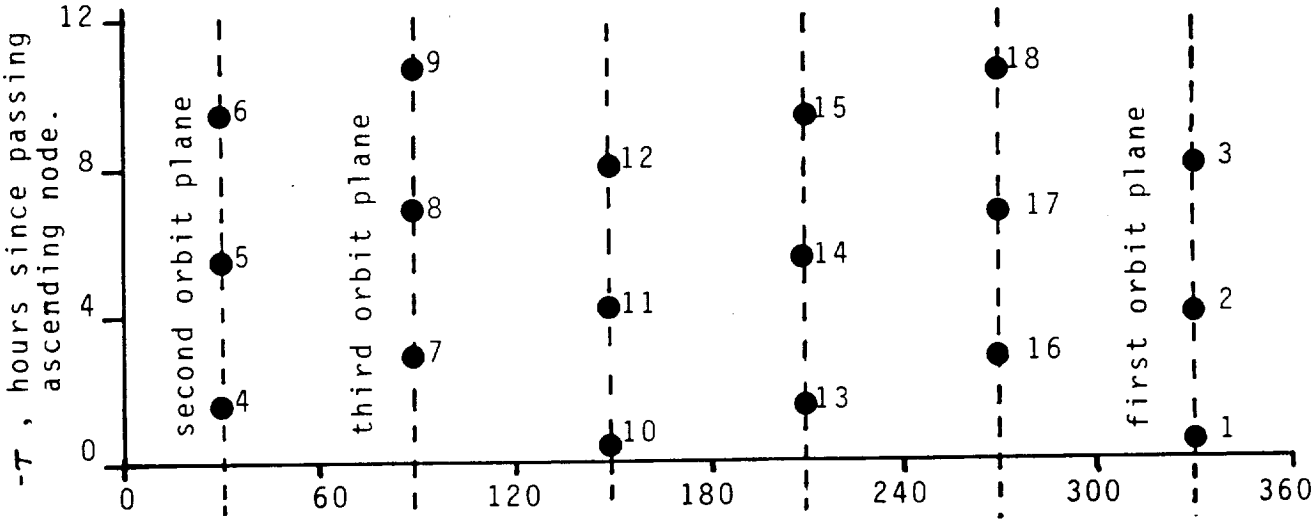

Figure 1. Graphical display of the GPS constellation with satellite numbers displayed

Note, that this constellation is quite symmetric, e.g., the same constellation is achieved by changing the horizontal scale (ascending node) by 180°. In fact, since the GPS orbits are twelve hours, the vertical axis in Figure 1 can be viewed modulo 12 hours, and the horizontal axis must be viewed modulo 360°. Hence, there exists some time change and latitude change which preserves relative locations. This suggests that codeless navigation

schemes using an exact clock will have a 180° latitude ambiguity, while schemes using relative time only will have a 60° ambiguity in latitude.

3. GPS Visibility in Space Station Orbit.

We simulated GPS and space station orbits over a twelve hour period to determine the percentage of time that at least n GPS satellites would be simultaneously visible at the Space Station (SS). The orbits of the GPS satellites were as specified in the previous section and the assumed Space Station orbit parameters were

$e = 0 \quad (\omega=0)$

$i = 28°$

$a = 6870$ km $\quad (T = 94.4$ min)

$\Omega = 0°$

$\tau = 0$ sec

The results of this simulation are shown in Table 1 below. Note that we have also

n	% of time at least n GPS satellites visible to SS	% of time at least n GPS satellites visible to SS and FF simultaneously
4	1.00000	1.00000
5	1.00000	1.00000
6	1.00000	1.00000
7	0.995833	0.963426
8	0.947917	0.851852
9	0.906018	0.799306
10	0.715741	0.477083
11	0.515972	0.366204
12	0.385417	0.239120
13	0.650463E-01	0.000000
14	0.000000	0.000000

Table 1. GPS visibility data for (a) the space station (SS) and (b) the space station and a free flyer (FF) at 2000 km arc-length separation in the SS orbit.

determined the percent of that a common set of at least n GPS satellites is visible simultaneously to both the Space Station and a free flyer trailing the Space Station in orbit by an arc length of 2000 km. This latter data may be useful when considering the use of differential navigation techniques. Attached to this report are curves indicating the normalized Doppler frequency received from different GPS satellites by a receiver in the previously specified Space Station orbit. Similar curves of the normalized rate of Doppler frequency change are also attached. All curves show a supperimposed sinusiod of approximately one cycle which denotes the latitude of the GPS satellite as a function of time. Flat segments of the Doppler and Doppler rate curves indicate times when the Space Station cannot see the GPS satellite.

4. Location Estimation from GPS Doppler

Suppose that it is possible to create a codeless electronic system for a spacecraft which at any given time t will produce a set D_t of observed GPS Doppler frequecies. That is,

$$D_t = \{x_j(t), j=1,2,...,J\},$$

where $x_j(t)$ is the j^{th} in a list of J observed Doppler signals. The observed Doppler $x_j(t)$ is of the form

$$x_j(t) = f_{n(j)}(\underline{p},t) + e_j(t),$$

where $f_n(\underline{p}, t)$ is the true Doppler observed from GPS satellite n at time t, when the true value of all unknown parameters (e.g., orbit parameters, clock errors, etc.) is $\underline{p}$. The quantity $e_j(t)$ is a measurement error caused by receiver noise, quantization, etc., and is assumed to be a mean zero, variance σ^2, random variable, independent for different values of j. It is assumed initially that not only is $\underline{p}$ unknown, but also the mapping n(j) from Doppler list location to satellite number is unknown.

In this situation, given D_t, the obvious estimation technique is to determine the values $\underline{p}$ and n(j) of $\underline{p}$ and n(j) which minimize the squared error ε,

$$\varepsilon = \sum_{j=1}^{J} \left| x_j(t) - f_{\hat{n}(j)} (\hat{\underline{p}}, t) \right|^2$$

This is actually a two step process: (a) Determine viable candidates for n(j) and (b) determine the optimum parameter vector $\underline{p}$ corresponding to each candidate. The decision then is made by final evaluation of ε.

This first problem of determining n(j) probably will require side information to reduce the complexity of signal processing. We assume for now that n(j) has been accurately determined, i.e., $\hat{n}(j) = n(j)$.

Determination of $\underline{p}$, given n(j), by analytical means is quite difficult due to the nonlinear relationship between $\underline{p}$ and f_n. However, it appears feasible to determine $\underline{p}$ by steepest descent methods on the function ε. This is an iterative technique in which the $i+1^{st}$ approximation $\underline{p}^{(i+1)}$ to $\underline{p}$ is determined from the i^{th} approximation $\underline{p}^{(i)}$ by a "downhill" adjustment; i.e.,

$$p^{(i+1)} = \underline{p}^{(i)} - c\underline{\Delta\varepsilon} (\underline{p}^{(i)})$$

where c is a positive constant and

$$\underline{\Delta\varepsilon}(\underline{p}^{(i)}) = \sum_k \underline{j}_k \left. \frac{\partial \varepsilon}{\partial p_k} \right|_{\underline{p} = \underline{p}^{(i)}}$$

is the gradient of ε, viewed as a function of $\underline{p}$, and $\underline{j}_k$ is a unit vector in the k^{th} coordinate direction. Hence

$$\underline{p}^{(i+1)} = \underline{p}^{(i)} - c \sum_k \underline{j}_k \cdot 2 \cdot \sum_{n=1}^{J} \left[x_n(t) - f_n (\underline{p}^{(i)}, t) \right] \left. \frac{\partial f_n (\underline{p}, t)}{\partial p_k} \right|_{\underline{p} = \underline{p}^{(i)}}$$

where J indicates the number of satellites in view (number of Doppler measurements). The choice of the constant c affects the rate of convergence and final accuracy.

5. Calculation of Doppler Frequency

To proceed with this approach we must determine the Doppler frequency function $f_n(\underline{p},t)$. Let $\underline{r}$ denote the time receiver location at exact time t and let $\underline{r}_n$ denote the time location of GPS Satellite n at exact time t. Then

$$f_n(\underline{p},t) = -\frac{1}{\lambda}\frac{d}{dt}|\underline{r} - \underline{r}_n|$$

where λ is the wavelength of the transmitted signal. The vector $\underline{r}$ was shown in Section 2 to be of the form.

$$\underline{r} = \begin{bmatrix} x \\ y \\ z \end{bmatrix} = \Theta I W \underline{v} \quad , \quad \underline{v} \triangleq \begin{bmatrix} r\cos f \\ r\sin f \\ 0 \end{bmatrix}$$

where (r,f) is the polar coordinate location of the vehicle in an appropriately chosen coordinate system. Note, that r and f both vary with time. We will maintain this notation $\underline{r}$ for the location of the navigating receiver, and will use the same notation subscripted with an "n" to indicate the location of the n^{th} GPS satellite.

Now the range rate function can be written as

$$\frac{d}{dt}|\underline{r} - \underline{r}_n| = \frac{d}{dt}\left[(\underline{r} - \underline{r}_n)^t(\underline{r} - \underline{r}_n)\right]^{1/2}$$

$$= \frac{(\underline{r} - \underline{r}_n)^t}{|\underline{r} - \underline{r}_n|}\frac{d}{dt}(\underline{r} - \underline{r}_n)$$

Evaluation of $\frac{d}{dt}(\underline{r}-\underline{r}_n)$ requires calculation of $\frac{d\underline{v}}{dt}$ and $\frac{d\underline{v}_n}{dt}$ as functions of time; other matrix parameters in the equation for $\underline{r}$ (and $\underline{r}_n$) are independent of time. Hence

$$\frac{d\underline{r}}{dt} = \Theta I W \frac{d\underline{v}}{dt}$$

$$= \Theta I W \left(\dot{r} \begin{bmatrix} \cos f \\ \sin f \\ 0 \end{bmatrix} + r\dot{f} \begin{bmatrix} -\sin f \\ \cos f \\ 0 \end{bmatrix} \right)$$

The quantities $\dot{r}$ and $r\dot{f}$ are given in [6] (equations (4.33) and (4.34)) as

$$\dot{r} = \frac{h}{p} e \sin f \quad , \quad r\dot{f} = \frac{h}{p} (1 + e \cos f)$$

and therefore

$$\frac{d\underline{r}}{dt} = \frac{h}{p} \Theta I W \left(\begin{bmatrix} -\sin f \\ \cos f \\ 0 \end{bmatrix} + \begin{bmatrix} 0 \\ e \\ 0 \end{bmatrix} \right)$$

The constant $\frac{h}{p}$ can be rewritten from [6] in more familiar terms as

$$\frac{h}{p} = \frac{\mu}{h} = \frac{\mu T}{2\pi a^2 (1-e^2)^{1/2}} = \left(\frac{\mu}{a(1-e^2)} \right)^{1/2}$$

Using this result, we can reduce the Doppler frequency calculation to

$$f_n(\underline{p}, t) = -\frac{1}{\lambda} \frac{(\underline{r}-\underline{r}_n)^t}{|\underline{r}-\underline{r}_n|} \left\{ \left(\frac{h}{p} \right) \Theta I W \left(\begin{bmatrix} -\sin f \\ \cos f \\ 0 \end{bmatrix} + \begin{bmatrix} 0 \\ e \\ 0 \end{bmatrix} \right) \right.$$

$$\left. - \left(\frac{h}{p} \right)_n \Theta_n I_n W_n \left(\begin{bmatrix} -\sin f_n \\ \cos f_n \\ 0 \end{bmatrix} + \begin{bmatrix} 0 \\ e_n \\ 0 \end{bmatrix} \right) \right\}$$

(Don't confuse the true anomaly f_n of the GPS #n with the Doppler function $f_n(\underline{p},t)$.) Substituting for $\underline{r}$ and $\underline{r}_n$ in the numerator of the above expression gives

$$f_n(\underline{p},t) = \frac{1}{\lambda|\underline{r}-\underline{r}_n|}\left\{\left(\frac{h}{p}\right) e\, r \sin f + \left(\frac{h}{p}\right)_n e_n r_n \sin f_n \right.$$

$$- r\left(\frac{h}{p}\right)_n \begin{bmatrix}\cos f\\ \sin f\\ 0\end{bmatrix}^t W^t I^t \Theta^t \Theta_n I_n W_n \left(\begin{bmatrix}-\sin f_n\\ \cos f_n\\ 0\end{bmatrix} + \begin{bmatrix}0\\ e_n\\ 0\end{bmatrix}\right)$$

$$\left. - r_n\left(\frac{h}{p}\right) \begin{bmatrix}\cos f_n\\ \sin f_n\\ 0\end{bmatrix} W_n^t I_n^t \Theta_n^t \Theta\, I\, W \left(\begin{bmatrix}-\sin f\\ \cos f\\ 0\end{bmatrix} + \begin{bmatrix}0\\ e\\ 0\end{bmatrix}\right)\right\}$$

The parameter vector $\underline{p}$ in this problem may include orbit elements i, Ω, ω, a, e, τ and clock errors. While I, ω, and Ω are explicitly included in the definitions of the rotational matrices I, Ω, and W, respectively, the parameters a, e, and τ are hidden in the polar coordinate variables r and f. Furthermore, the dependence of r and f on orbit parameters is not given analytically, but requires evaluation via solution of Kepler's equation for the eccentric anomaly variable E. Hence, it is difficult to further pursue the evaluation of the gradient expression of Section 4 analytically, and it appears that the required derivatives must be evaluation by a synthetic differentiation of some sort on a computer.

6. Performance of the Doppler Navigation Approach

Assuming that the steepest-descent solution for the parameter vector $\hat{\underline{p}}$ converges to the true vector $\underline{p}$, it is possible to estimate the effect of measurement noise on estimation

error as follows. We can make a Taylor's series approximation of the Doppler frequency function about the true parameter point $\underline{p}$, saving only first order terms. Thus,

$$f_n(\hat{\underline{p}}, t) \doteq f(\underline{p}, t) + \sum_k \Delta p_k \, a_{n\,k}(t)$$

where

$$\Delta p_k = \hat{p}_k - p_k$$

$$a_{nk}(t) = \frac{\partial}{\partial \hat{p}_k} f_n(\hat{\underline{p}}, t) \Bigg|_{\hat{\underline{p}} = \underline{p}}$$

Using the above approximation in the expression for squared error ε, it can be shown that

$$\varepsilon \doteq \sum_{j=1}^{J} \left| e_j(t) - \sum_k \Delta p_k \, a_{n(j)k}(t) \right|^2$$

Note, that we have shown the parameter vector $\underline{p}$ to be independent of time, as one might expect for Keplerian orbit parameters. Of course, if one instead uses cartesian coordinate location and velocity as the parameters to be estimated, $\underline{p}$ will be time-dependent, even in the short term. (It's not clear which parameter set representation is the most useful for navigation algorithm mechanization.)

The squared error expression can be restated in vector terms as

$$\varepsilon \doteq \left| \underline{e}(t) - A(t)\Delta\underline{p} \right|^2$$

where

$$\underline{e}(t) = \begin{bmatrix} e_j(2) \\ e_j(1) \\ \vdots \\ e_{j(J)} \end{bmatrix} \quad , \quad \Delta\underline{p} = \begin{bmatrix} \Delta p_1 \\ \Delta p_2 \\ \vdots \\ \Delta p_k \end{bmatrix}$$

$$A(t) = \begin{bmatrix} a_{nk} \end{bmatrix} \quad \begin{matrix} n = 1, \ldots, J \\ k = 1, \ldots, K \end{matrix}$$

Here j(n) indicates the list location of the Doppler frequency from GPS satellite #n (i.e., j(n) is the inverse of n(j)), J indicates the number of satellites in view, and K is the number of parameters to be estimated.

Assuming that ε is minimized by the steepest-descent solution and that the errors are small, the resulting parameter errors $\underline{\Delta p}$ produced by measurement errors $\underline{e}(t)$ are those which minimize the quadratic form ε in $\underline{\Delta p}$.

$$\varepsilon = |\underline{e}(t)|^2 - 2\underline{e}^t(t)\, A\,(t)\underline{\Delta p} + \underline{\Delta p}^t\, A^t\,(t)\, A\,(t)\,\underline{\Delta p}$$

Locating the minimum by differentiation with respect to each of the elements of $\underline{\Delta p}$ gives the vector equation

$$A^t\,(t)\, A\,(t)\underline{\Delta p} = A^t\,(t)\,\underline{e}(t)$$

and hence

$$\underline{\Delta p} = [\, A^t\,(t)\, A\,(t)\,]^{-1} A^t\,(t)\,\underline{e}(t)$$

This equation gives an explicit relationship between measurement noise e(t) and parameter estimation error $\underline{\Delta p}$, which should be reasonably accurate at small error levels.

When the covariance matrix of the measurement error is known, then the covariance matrix $R_{\underline{\Delta p}}$ of the corresponding parameters is easily calculated. For example, suppose that the measurement errors are uncorrelated, mean zero, variance σ^2 random variables. Then the covariance of the measurement error is $\sigma^2 I$, where I is the identity matrix, and

$$R_{\underline{\Delta p}} = \sigma^2 [\, A\,(t)\, A\,(t)]^{-1}$$

If the parameter vector being estimated was velocity and location in Cartesian coordinates, then the diagonal entries of $[A^t A]^{-1}$ are scale factors (similar to GDOP, PDOP, etc.) which relate measurement standard deviation σ to location and velocity standard deviations (diagonal entries in $R_{\Delta P}$).

Closing Comments

The prior sections of this report document the beginning of an analytical study of codeless navigation with GPS signals. On January 27, 1986, we terminated efforts on this study. But, it is worthwhile sketching the remaining research effort.

Determination of an algorithm for construction of the satellite identification function n(j) is a messy problem which must be considered. However, assuming the available of minimum a-priori information regarding location and time, there are no obvious reasons which would preclude mechanization of an algorithm for determining n(j).

As indicated in the earlier sections, analytical measures of Doppler navigation performance are difficult to obtain. A program must be written to determine the matrix A(t), which is the key to analytical estimates of the measurement error/parameter error relation. This must be calculated over several periods of the receiving spacecraft's orbit to determine how geometry affects the navigation computation. The concepts here are analogous to determining fluctuations in scale factors like GDOP, PDOP, HDOP, VDOP, and TDOP in time-delay navigation systems. This analysis should provide information concerning the necessary level of Doppler measurement accuracy, and, hence, should lead to the specification of acceptable measurement times, signal-to-noise ratios, frequency quantizations, etc.

The objective of the Doppler navigation scheme is to acquire signals, identify their sources by Doppler signature, and reduce location errors to the point where ranging errors to each of the GPS satellites in view is under 150 meters. This provides unambiguous initialization of a tone-ranging scheme to further reduce navigation error.

Tone-ranging is a well known technique [10], [11] and it appears possible to determine the necessary measurement times, signal-to-noise ratios, filtering, etc., by analytic means. Comparison of single and double differencing [1] navigation schemes should be made to determine achievable accuracy; but since these techniques are independent of the method of obtaining range information, prior analytical efforts may be useful. We expect that a Kalman filter will be necessary to meet high accuracy navigation specs.

Once the signal-to-noise ratio requirements for meeting the objectives of both the Doppler and tone-ranging schemes are known, we can determine the receiver characteristics necessary to meet system specifications. The tone extraction procedure for a spread spectrum signal (without code knowledge) employs a delay and multiply operation, as described in [1]. This processing, inherently, produces more noise than the normal GPS receiver which uses a noise-free reference signal in the despreading process. A careful receiver performance analysis will be necessary to determine the receiver noise temperature requirements necessary to meet the signal-to-noise ratio specifications for both Doppler navigation and tone-ranging.

References:

[1] T.P. Yunck, "An Introduction to SERIES-X," JPL Notes, 1982.

[2] R.B. Crow, et al., "SERIES-X Final Engineering Report," Jet Propulsion Laboratory Document No. JPL D1476, August 1984.

[3] P.F. MacDoran, et al., "Codeless GPS Positioning Offers Sub-Meter Accuracy," Sea Technology, October 1984.

[4] P.F. MacDoran, et al., "Codeless GPS Systems for Positioning of Offshore Platforms and 3-D Seismic Surveys," Journal of the Institute of Navigation, Summer 1984.

[5] P.F. MacDoran, et. al., "Codeless Systems for Positioning with NAVSTAR-GPS," presented at First International Symposium on Precise Positioning with the Global Positioning System, Rockville, MD, 15-19 April, 1985.

[6] A.E. Roy, Orbital Motion. Bristol, GB: Adam Hilger, Ltd., 1982.

[7] R.R. Bate, D.D. Mueller, and J.E. White, Fundamentals of Astrodynamics, Dover Publications, 1971.

[8] P.Kruh, "Coverage and Buildup of the NAVSTAR Constellation," Proc. GPS Symp., April 21-22, 1983 (Sponsored by the Electronic Industries Assoc.)

[9] J.K. Holmes, K.T. Woo, G.K. Huth, L. Yen, "User's Handbook for NAVSTAR GPS," Axiomatix Report No. 8509-4, September 30, 1985

[10] W.C. Lindsey and M.K. Simon, Telecommunication Systems Engineering, Chapter 4. Englewood Cliffs, NJ: Prentice-Hall, 1973.

[11] W.G. Melbourne, "On Recovering Carrier Range in GPS-Based Geodetic Systems," JPL Geodesy and Geophysic Preprint No. 140, October 1985.

APPENDIX D

BACKGROUND AND PROCEDURE FOR SPACE STATION GPS NAVIGATION SIMULATION

BACKGROUND AND PROCEDURE FOR SPACE STATION GPS NAVIGATION SIMULATION

Contract No. NA9-17414

Technical Report

Prepared for

NASA Lyndon B. Johnson Space Center
Houston, Texas 77058

Technical Monitor: Dean Bratton

Prepared by

Dr. Unjeng Cheng

Axiomatix
9841 Airport Blvd., Suite 912
Los Angeles, CA 90045

Axiomatix Report No. R8605-1
August 27, 1986

Table of Contents

List of Figures

INTRODUCTION

The material presented in this report constitutes theoretical background information used for simulation of GPS navigation by the Space Station. Section 1 deals with the computation of the satellite position in its respective orbit. Section 2 addresses an important issue of GPS satellite visibility by a user. In Section 3 the concepts GDOP and PDOP are defined analytically. Kalman filtering for pseudorange and delta pseudorange is summarized mathematically in Section 4. Finally, in Section 5 the steps involved in simulation of GPS navigation are summarized.

1.0 SATELLITE ORBITS

The first step in GPS navigation simulation is to derive the satellite position in its respective orbit. A typical orbital plane is delineated in Figure 1. A minimum of five elements is necessary to define an orbit, namely,

a – semi-major axis

e – eccentric

Ω – longitude of ascending node

i – angle of inclination

ω – argument of perigee.

The position of a satellite in the Earth-Centered Inertial (ECI) coordinate system is then given by its true anomaly and radius, denoted by f and r, respectively:

$$\begin{cases} x = r\left[\cos\Omega\cos(\omega+f) - \sin\Omega\cos i\ \sin(\omega+f)\right] \\ y = r\left[\cos\Omega\cos(\omega+f) + \cos\Omega\cos i\ \sin(\omega+f)\right] \\ z = r\ \sin i\ \sin(\omega+f) \end{cases} \tag{1}$$

The true anomaly and radius could be computed from eccentric anomaly, denoted by E:

$$f = 2\tan^{-1}\left[\left(\frac{1+e}{1-e}\right)^{1/2}\tan\left(\frac{E}{2}\right)\right] \tag{2}$$

$$r = a(1 - e\ \cos E) \tag{3}$$

Finally, the eccentric anomaly is computed from mean anomaly, denoted by M:

$$M = E - e\sin E \tag{4}$$

$$M = M_0 + n_0 t \tag{5}$$

$$n_0 = \left(\frac{\mu}{a^3}\right)^{1/2} \tag{6}$$

$$\mu = 3.986008 \times 10^{14}\ m/s^2 \tag{7}$$

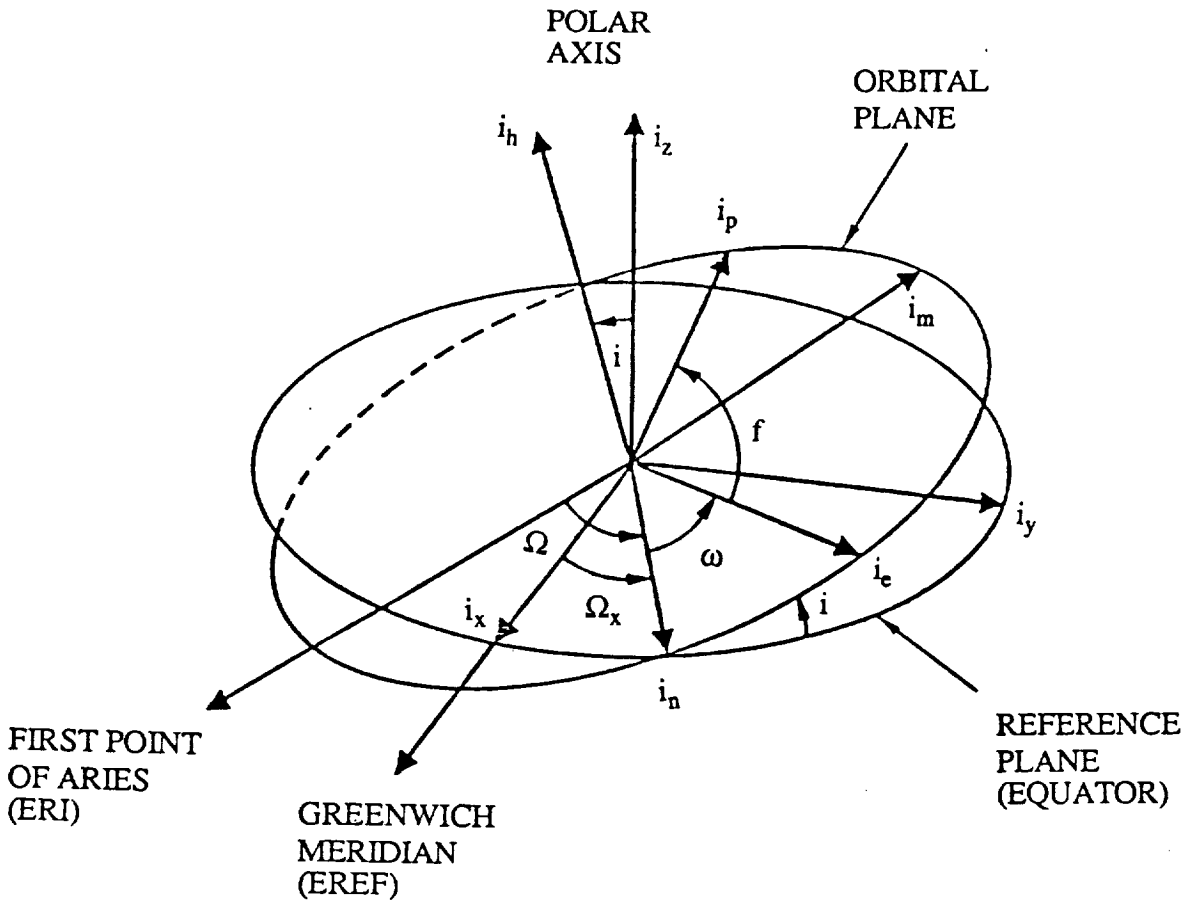

- Earth at focus of ellipse
- Perigee -- point where satellite closest to Earth
- Apogee -- point where satellite most remote from Earth

Ω Longitude of ascending node relative to first point of Aries (~constant)

Ω_x Longitude of ascending node relative to Earth $\Omega_x = \Omega - \dot{\Omega}_e (t - t_0)$

i Angle of inclination

ω Argument of perigee

$\phi = \omega + f$ Argument of latitude

Figure 1 Definition of Orbital Plane

The Newton-Ralphson method could be applied to solve (3) for E. The initial guess of E could be

$$M + \frac{e \sin M}{1 - \sin (M + e) + \sin M} \tag{8}$$

Note that for a circular obit, this initial guess is a correct answer. Typically, three or four iterations are enough to obtain very accurate result.

The period of a satellite is given by

$$T = 2\pi\left(\frac{a^3}{\mu}\right)^{1/2} \tag{9}$$

A second harmonic perturbations could be introduced to make the model more accurate. Note that Equations (1) through (5) could still be used with n, f, r, and i being replaced by

$$\begin{cases} n = n_0 + \Delta n & (10) \\ i = i_0 + \Delta i & (11) \\ f = \tilde{f} + \Delta f & (12) \\ r = \tilde{r} + \Delta r & (13) \end{cases}$$

$$\begin{cases} \Delta f = C_{fc} \cos 2(\omega + \tilde{f}) + C_{fs} \sin 2(\omega + \tilde{f}) & (14) \\ \Delta r = C_{rc} \cos 2(\omega + \tilde{f}) + C_{rs} \sin 2(\omega + \tilde{f}) & (15) \\ \Delta i = C_{ic} \cos 2(\omega + \tilde{f}) + C_{is} \sin 2(\omega + \tilde{f}) & (16) \end{cases}$$

In the Equation (11), i_0 is the designed angle of inclination. $\tilde{f}$ and $\tilde{r}$ are computed from Equations (2) and (3), respectively, by using n instead of n_0 in (5).

In order to compute the satellite position at any given time, we must know M_0 in (5). It could be computed from the given mean anomaly at a specific Greenwich time.

If Earth-Centered Earth-Fixed (ECEF) coordinate system is used, the

longitude of ascending node is a function of Greenwich time, namely,

$$\Omega_x = \Omega - \dot{\Omega}_e (t - t_0) \tag{17}$$

Clearly, t_0 could be obtained from the given Ω_x at a specific Greenwich time. Equation (1) is still valid in ECEF except Ω should be replaced by Ω_x. In Figure 2, we show a typical example of GPS satellite ephemeris data. As an example, let us compute the ephemeris data for the satellite No. 1 as follows:

$$i_0 = 63.1963 \text{ deg}$$

$$\omega = 194.6223 \text{ deg}$$

$$e = 0.00705$$

$$a = \left(\frac{\mu^{1/2} T}{2\pi}\right)^{2/3}$$

$$= \left(\frac{(3.986008 \times 10^{14})^{1/2} \times 717.9509 \times 60}{2\pi}\right)^{2/3}$$

$$= 26559719 \text{ m}$$

$$n_0 = \left(\frac{\mu}{a^3}\right)^{1/2} = \left(\frac{3.986008 \times 10^{14}}{(26559719)^3}\right)^{1/2}$$

$$= 1.4585921 \times 10^{-4} \text{ radian/sec}$$

$$M_0 = 105.6690 \text{ deg}$$

$$\Omega + \dot{\Omega}_e t_0 = \Omega_x + \dot{\Omega}_e t = 140.6544 \text{ deg}$$

Clearly, Figure 2 provides complete ephemeris information in ECEF. However, we must note that the inclination angle in ECI, namely, Ω, is not known yet.

Ephemeris = Test configuration

Epoch Date = December 6, 1985

Orbit Period = 717.9509 * Min

No	GM Time (1)	LN Node (2)	Inclin (3)	Ecentr (4)	Arg Per (5)	MN Anom (6)
1	0.000	140.6544	63.1963	0.00705000	194.6223	105.6690
2	0.000	21.3261	64.4566	0.01145000	400.7970	298.3546
3	0.000	183.4078	64.0788	0.00376000	120.9178	344.3288
4	0.000	140.6560	63.1941	0.00431000	336.7610	78.7621
5	0.000	182.9436	63.8853	0.01118000	69.6456	354.2511
6	0.000	139.8061	62.8059	0.01083000	201.0770	171.9212
7	0.000	139.4507	62.5210	0.00440000	349.5790	328.9802
8	0.000	18.7341	63.3874	0.00849000	295.6230	86.8023
9	0.000	138.9850	63.3304	0.01339000	154.5398	305.1621

Figure 2 An Example of GPS Satellite Ephemeris Data in ECEF

2.0 SATELLITE VISIBILITY

An important issue in GPS navigation simulation is to determine the visibility of GPS satellites by a user. This problem could be divided into two subproblems, namely, ground users and satellite users.

For a ground user, three things have to be considered, i.e.,

(1) compute the user location,

(2) modelling of Earth's oblateness,

(3) mask angle due to atmospheric absorption.

A simple observation is delineated in Figure 3. Clearly, a GPS satellite could be visible by a ground user if it is above the tangent plane by a degree greater than the mask angle. Therefore, the inequality which defines the visibility of GPS satellites is

$$\sin^{-1}\left[\frac{x_i n_x + y_i n_y + z_i n_z - h}{\sqrt{(x_n - x_i)^2 + (y_n - y_i)^2 + (z_n - z_i)^2}}\right] > \text{mask angle} \qquad (18)$$

where $\underline{N} = (n_x, n_y, n_z)$ is the norm of the tangent plane and h is the height of user. The way to compute $\underline{N}$ will be given in the subsequent discussion.

The surface of Earth is defined by the equation

$$x^2 + y^2 + \frac{z^2}{(1 - F)^2} = R_\oplus^2 \qquad (19)$$

where

$$F = \frac{R_\oplus - R_p}{R_\oplus} \approx \frac{1}{298.257} \qquad (20)$$

$R_\oplus$ = Earth's equatorial radius = 6378135 meters (21)

R_p = Earth's polar radius (22)

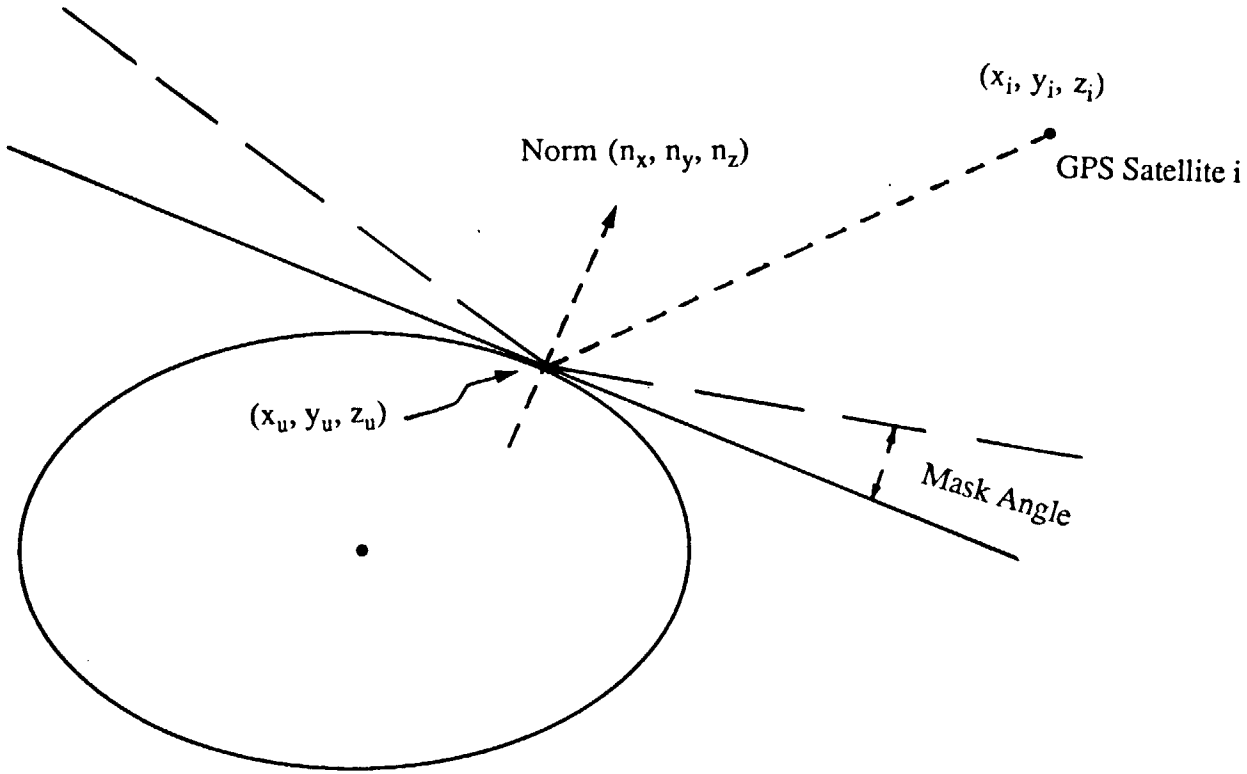

Figure 3 Visibility Model for Ground Users

The coordinate of a user in ECEF at longitude lg, latitude lt, and altitude h is given by

$$\begin{cases} x_u = (R_N + h)\cos(lt)\cos(lg) \\ y_u = (R_N + h)\cos(lt)\cos(lg) \\ z_u = (R_N(1-\varepsilon^2) + h)\sin(lt) \end{cases} \tag{23}$$

where

$$R_N = \frac{R_\oplus}{(1-e^2\sin^2(lt))^{1/2}} \tag{24}$$

$$\varepsilon^2 = 1 - (1-F)^2 \tag{25}$$

Finally, the norm $\underline{N}$ of the tangent plane passing through (x_u, y_u, z_u) is given by

$$\underline{N} = (\cos(lt)\cos(lg), \cos(lt)\sin(lg), \sin(lt)) \tag{26}$$

For a satellite user, we could use a model shown in Figure 4. We assume the atmosphere has a thickness Q meters. A GPS satellite will be visible by the user if

$$\begin{cases} \Theta > 90° \\ \text{or} \quad A > R_\oplus + Q \qquad \text{if } \Theta < 90° \end{cases} \tag{27}$$

It is easy to see that the above condition is equivalent to

$$\begin{cases} (\mathbf{r}_i - \mathbf{r}_u)\cdot\mathbf{r}_u > 0 \\ \text{or} \quad \sqrt{|\mathbf{r}_u|^2 - \dfrac{(\mathbf{r}_u\cdot(\mathbf{r}_u - \mathbf{r}_i))^2}{|\mathbf{r}_u - \mathbf{r}_i|^2}} > R_\oplus + Q \\ \text{if } (\mathbf{r}_i - \mathbf{r}_u)\cdot\mathbf{r}_u \le 0 \end{cases} \tag{28}$$

Note that Equations (27) and (28) are derived based on the worst case assumption, i.e., the Earth is a sphere with radius $R_\oplus$.

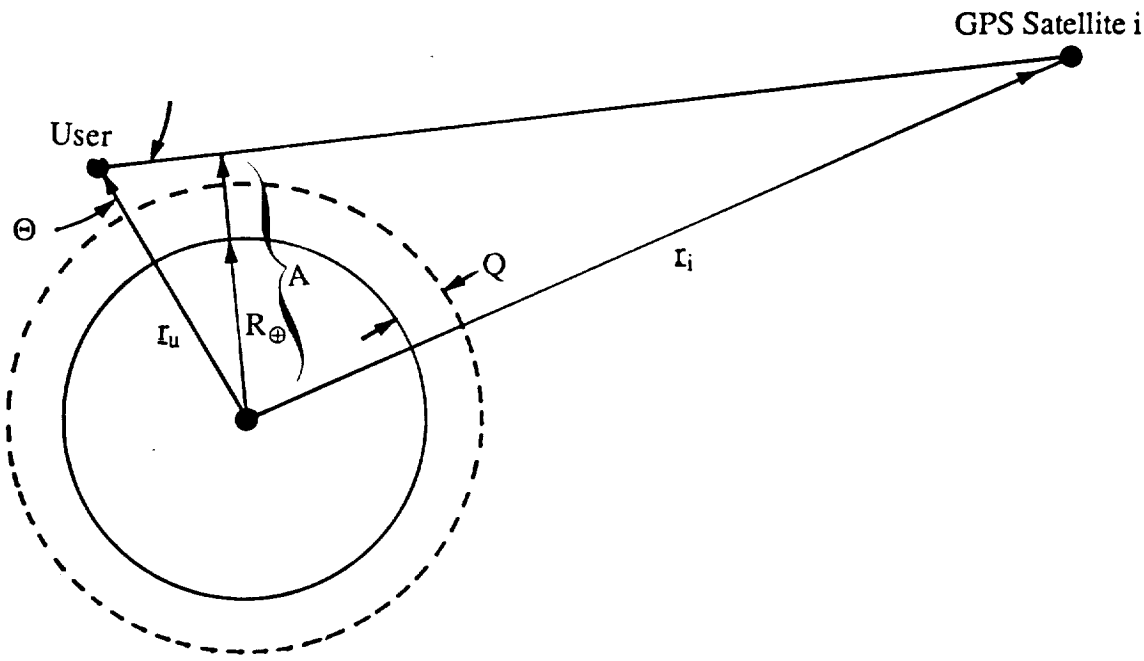

(a) The Case with $(r_i - r_u) \cdot r_u \leq 0$

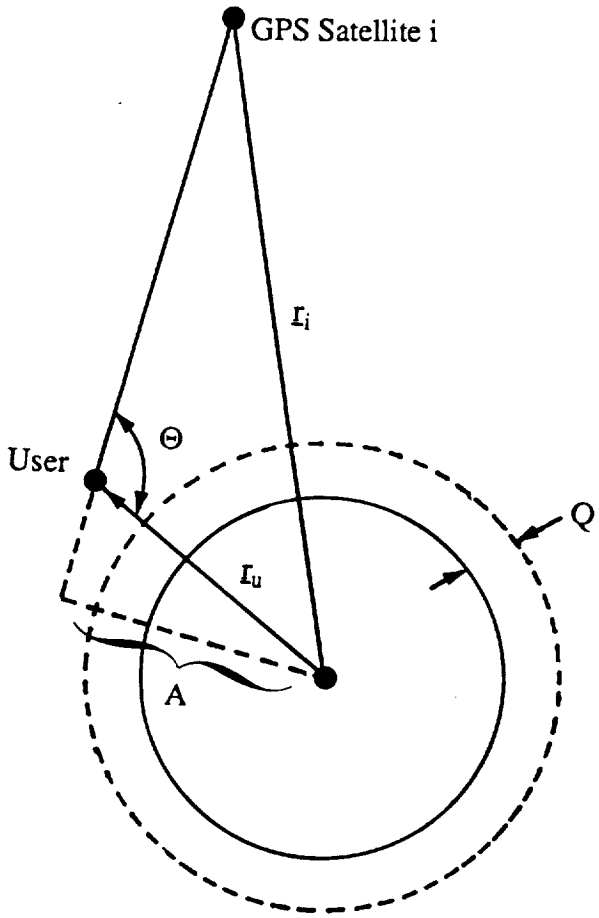

(b) The Case with $(r_i - r_u) \cdot r_u > 0$

Figure 4. Visibility Model for Satellite Users

3.0 GDOP/PDOP

In the standard GPS, the basic equations with four GPS satellites are

$$\sqrt{(x-x_i)^2+(y-y_i)^2+(z-z_i)^2}+b=R_i \tag{29}$$

where x_i, y_i, z_i are the coordinates of the ith GPS satellite and R_i is the pseudorange to it. Let x_0, y_0, z_0, b_0, and R_{0i} be the nominal values of x, y, z, b and R_i, respectively. We define

$$\begin{cases} \Delta x = x - x_0 \\ \Delta y = y - y_0 \\ \Delta z = z - z_0 \\ \Delta b = b - b_0 \\ \Delta R_i = R_i - R_{0i} \end{cases} \tag{30}$$

Equation (29) could be expanded and only the first-order terms are considered. We got

$$A\begin{bmatrix} \Delta x \\ \Delta y \\ \Delta z \\ \Delta b \end{bmatrix} = \begin{bmatrix} \Delta R_1 \\ \Delta R_2 \\ \Delta R_3 \\ \Delta R_4 \end{bmatrix} \tag{31}$$

$$A = \begin{bmatrix} \alpha_{11} & \alpha_{12} & \alpha_{13} & 1 \\ \alpha_{21} & \alpha_{22} & \alpha_{23} & 1 \\ \alpha_{31} & \alpha_{32} & \alpha_{33} & 1 \\ \alpha_{41} & \alpha_{42} & \alpha_{43} & 1 \end{bmatrix} \tag{32}$$

where

$$\alpha_{i1} = \frac{x_n - x_i}{\sqrt{(x_n-x_i)^2+(y_n-y_i)^2+(z_n-z_i)^2}}$$

$$\alpha_{i2} = \frac{y_n - y_i}{\sqrt{(x_n - x_i)^2 + (y_n - y_i)^2 + (z_n - z_i)^2}} \tag{33}$$

$$\alpha_{i3} = \frac{z_n - z_i}{\sqrt{(x_n - x_i)^2 + (y_n - y_i)^2 + (z_n - z_i)^2}}$$

GDOP is defined as

$$\begin{aligned} \text{GDOP} &\triangleq \sqrt{\text{Trace}\left[(A^T A)^{-1}\right]} \\ &\triangleq \sqrt{V_x^2 + V_y^2 + V_z^2 + V_T^2} \end{aligned} \tag{34}$$

PDOP is then defined by

$$\text{PDOP} \triangleq \sqrt{V_x^2 + V_y^2 + V_z^2} \tag{35}$$

In the differential GPS, the basic equations with four GPs satellites are

$$\sqrt{(x_u - x_i)^2 + (y_u - y_i)^2 + (z_u - z_i)^2} - \sqrt{(x_R - x_i)^2 + (y_R - y_i)^2 + (z_R - z_i)^2}$$

$$+ (b_u - b_R) = R_{ui} - R_{Ri} \tag{36}$$

where the subscript R denotes the entities pertaining to the reference station and the subscript u denotes the entities pertaining to the user. If x_R, y_R, z_R, and b_R are known exactly, Equation (36) is reduced to (29) and all results given above are also valid. However, if x_R, y_R, z_R, and b_R themself are estimated, (36) can be rewritten as

$$A_u \begin{bmatrix} \Delta x_u \\ \Delta y_u \\ \Delta z_u \\ \Delta b_u \end{bmatrix} - A_R \begin{bmatrix} \Delta x_R \\ \Delta y_R \\ \Delta z_R \\ \Delta b_R \end{bmatrix} = \begin{bmatrix} \Delta R_{u1} - \Delta R_{R1} \\ \Delta R_{u2} - \Delta R_{R2} \\ \Delta R_{u3} - \Delta R_{R3} \\ \Delta R_{u4} - \Delta R_{R4} \end{bmatrix} \tag{37}$$

Equation (37) could be interpreted in two ways, namely, Δx_u or $\Delta x_u - \Delta x_R$ is concerned.

If we intend to track the absolute position of user, (37) could be rewritten as

$$A_u \begin{bmatrix} \Delta x_u \\ \Delta y_u \\ \Delta z_u \\ \Delta b_u \end{bmatrix} = \begin{bmatrix} \Delta R_{u1} - \Delta R_{R1} \\ \Delta R_{u2} - \Delta R_{R2} \\ \Delta R_{u3} - \Delta R_{R3} \\ \Delta R_{u4} - \Delta R_{R4} \end{bmatrix} + A_R \begin{bmatrix} \Delta x_R \\ \Delta y_R \\ \Delta z_R \\ \Delta b_R \end{bmatrix} \qquad (38)$$

Therefore, the reference station position uncertainty appears as an additional noise to the estimated user position. If $A_u \approx A_R$, it is easy to see that the accuracy of the estimated user position cannot exceed the accuracy of the estimated reference station position. In certain applications, such as Space Station, we might be interested in tracking $\Delta x_u - \Delta x_R$, which is the relative position to the reference station. In this case, Equation (37) could be rewritten as

$$A_u \begin{bmatrix} \Delta x_u - \Delta x_R \\ \Delta y_u - \Delta y_R \\ \Delta z_u - \Delta z_R \\ \Delta b_u - \Delta b_R \end{bmatrix} = \begin{bmatrix} \Delta R_{u1} - \Delta R_{R1} \\ \Delta R_{u2} - \Delta R_{R2} \\ \Delta R_{u3} - \Delta R_{R3} \\ \Delta R_{u4} - \Delta R_{R4} \end{bmatrix} + (A_R + A_u) \begin{bmatrix} \Delta x_R \\ \Delta y_R \\ \Delta z_R \\ \Delta b_R \end{bmatrix} \qquad (39)$$

In Equation (39), the reference station position uncertainty still appears as an additional noise to the estimated relative user position. However, if $A_u \approx A_R$, its effects will be nearly zero. The effect of reference station position uncertainty could be manifested by

$$\text{REFPU} = \sqrt{\text{Trace}\left[A_u^{-1}\,(A_R - A_u)\,(A_R - A_u)^T\,(A_u^{-1})^T\right]} \qquad (40)$$

As we know, there could be more than four GPS satellites visible by a user. The selection of the best four could be by minimizing GDOP or PDOP.

In Figure 5, we show the average GDOP and average REFPU (see Equation (40)) for two cases, namely, the Space Station orbit user and the ground user. In general, the Space Station orbit user has slightly better GDOP. For the differential GPS case, GDOP increases with the separation between the Space Station and the user.

Altitude		Space Station Orbit	Ground
Standard GPS	GDOP	2.901	2.681
Differential GPS 0.3 km	GDOP	2.901	2.681
	REFPU	1.498×10^{-5}	1.862×10^{-5}
Differential GPS 37 km	GDOP	2.094	2.687
	REFPU	1.875×10^{-3}	1.066×10^{-3}
Differential GPS 185 km	GDOP	2.109	2.753
	REFPU	9.03×10^{-3}	1.037×10^{-2}
Differential GPS 2000 km	GDOP	2.299	3.187
	REFPU	9.633×10^{-2}	0.1169

The Space Station Orbit Parameters:

$a = 6878140$ m , $i_o = 28$ deg

$\alpha = 0$ deg , $\omega = 0$ deg

$e = 0$, $M_o = 0$

$Q = 400000$ m (see Figure 4)

The ground user is computed at latitude 0° and longitude 0°.

The mask angle is selected as 5°.

Figure 5 Typical Average GDOP and average REFPU

In Figure 6, we show the GDOP seen on the Space Station orbit for the standard GPS case. In Figure 7 through Figure 10, we show the GDOP seen on the Space Station orbit for the differential GPS case. Note that there is no blow-up in all cases. In Figure 11, we show the GDOP seen by the ground user located at longitude 5° and latitude 35°. We see two blow-ups within one day.

Another interesting entity is the density function of GDOP within a day, which provides a measure of the percentage of time, at which GDOP takes a specific value. In Figure 12, we show a probability density function for the standard GPS on the Space Station orbit.

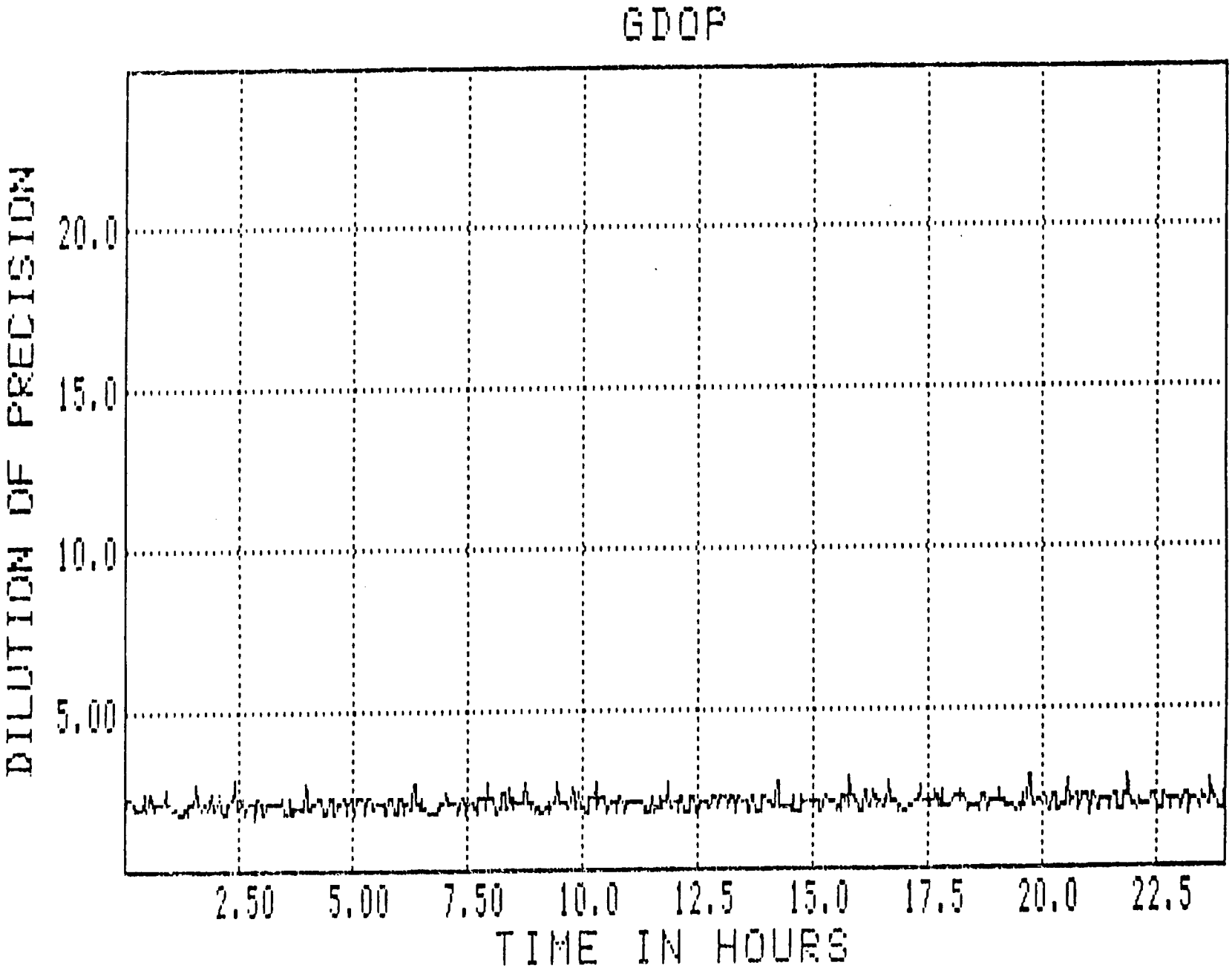

Figure 6 GDOP for the Standard GPS Seen on the Space Station Orbit

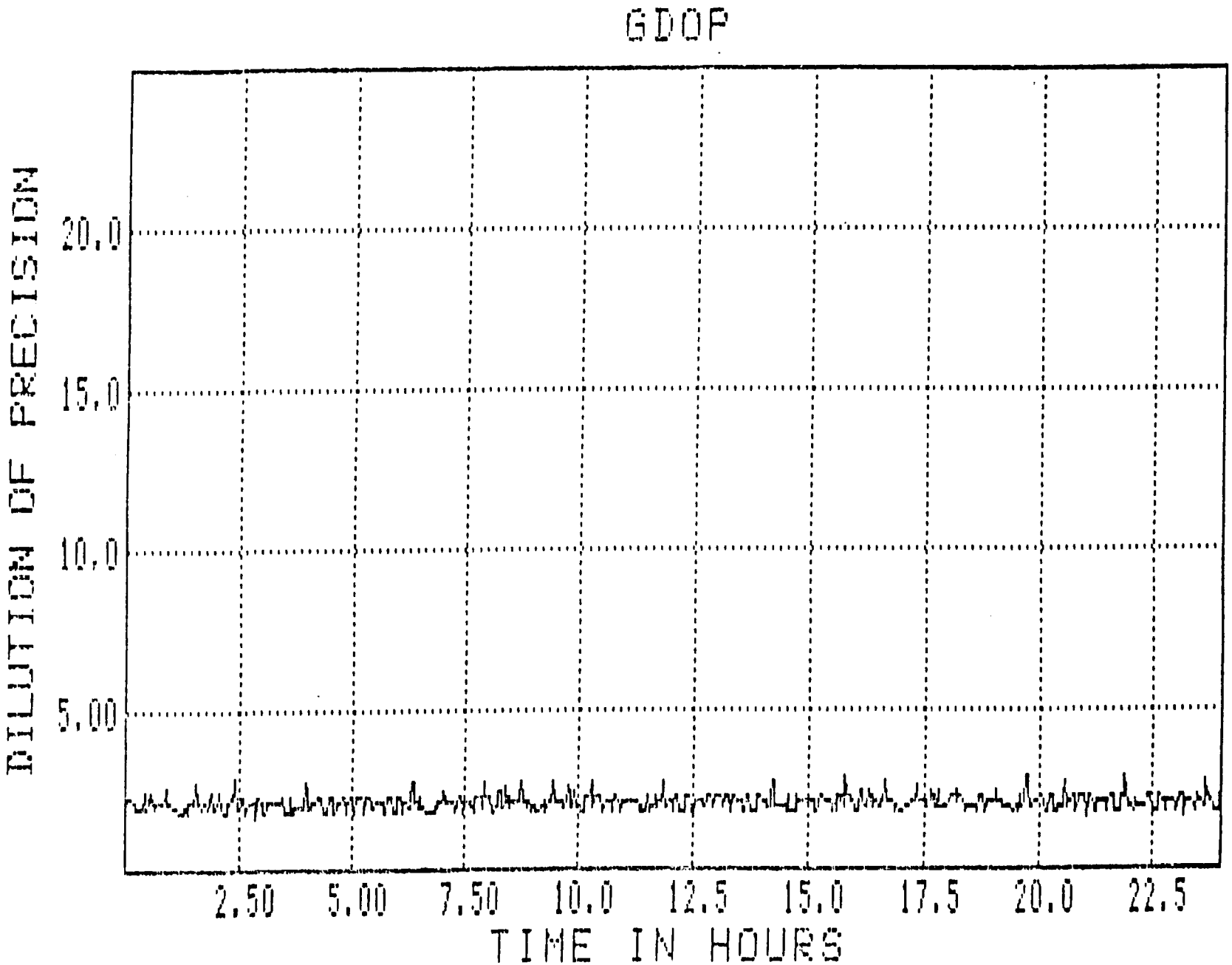

Figure 7 GDOP for the Differential GPS Seen on the Space Station Orbit, Separation by 300 m

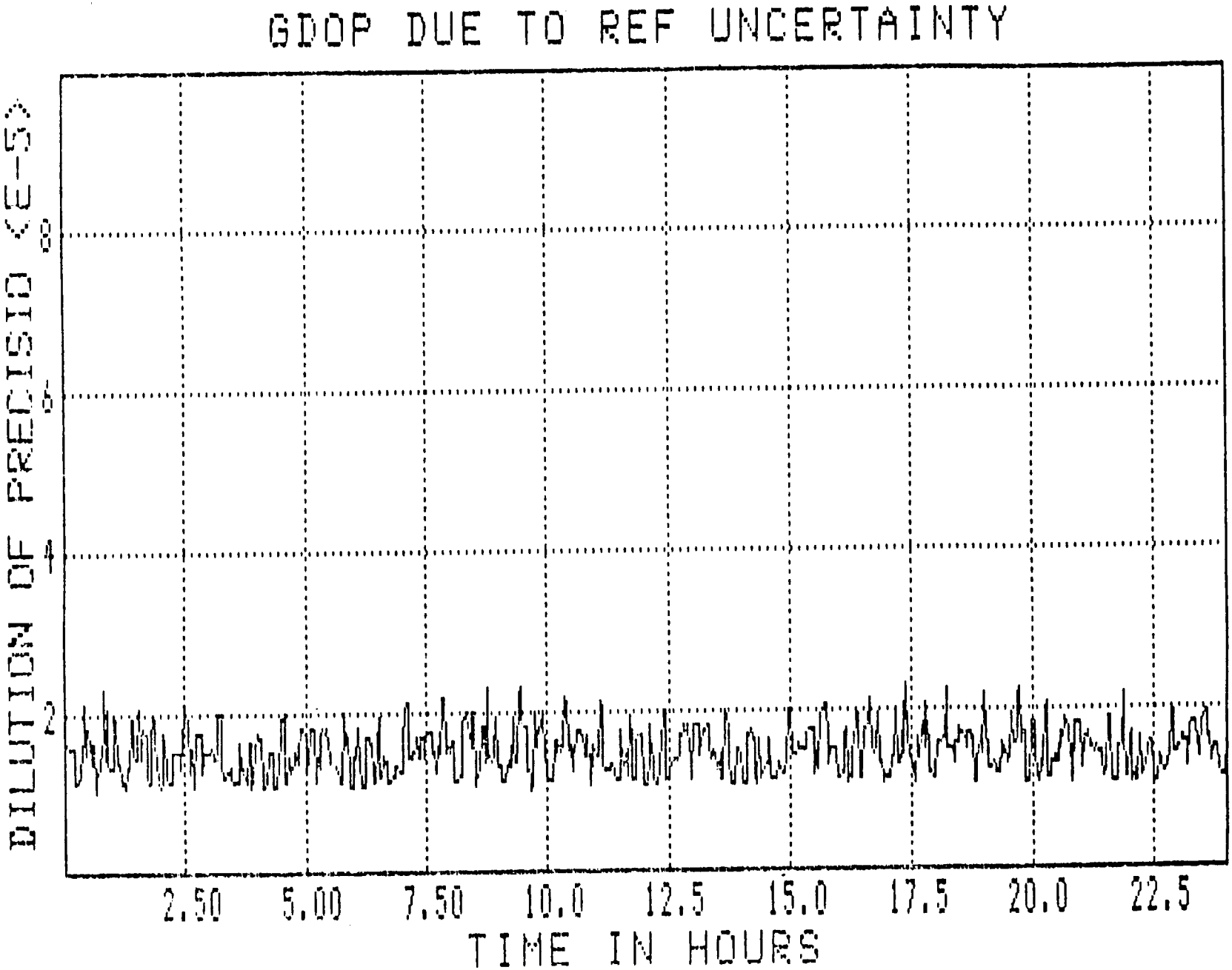

Figure 8 REFPU for the Differential GPS Seen on the Space Station Orbit, Separation by 300 m

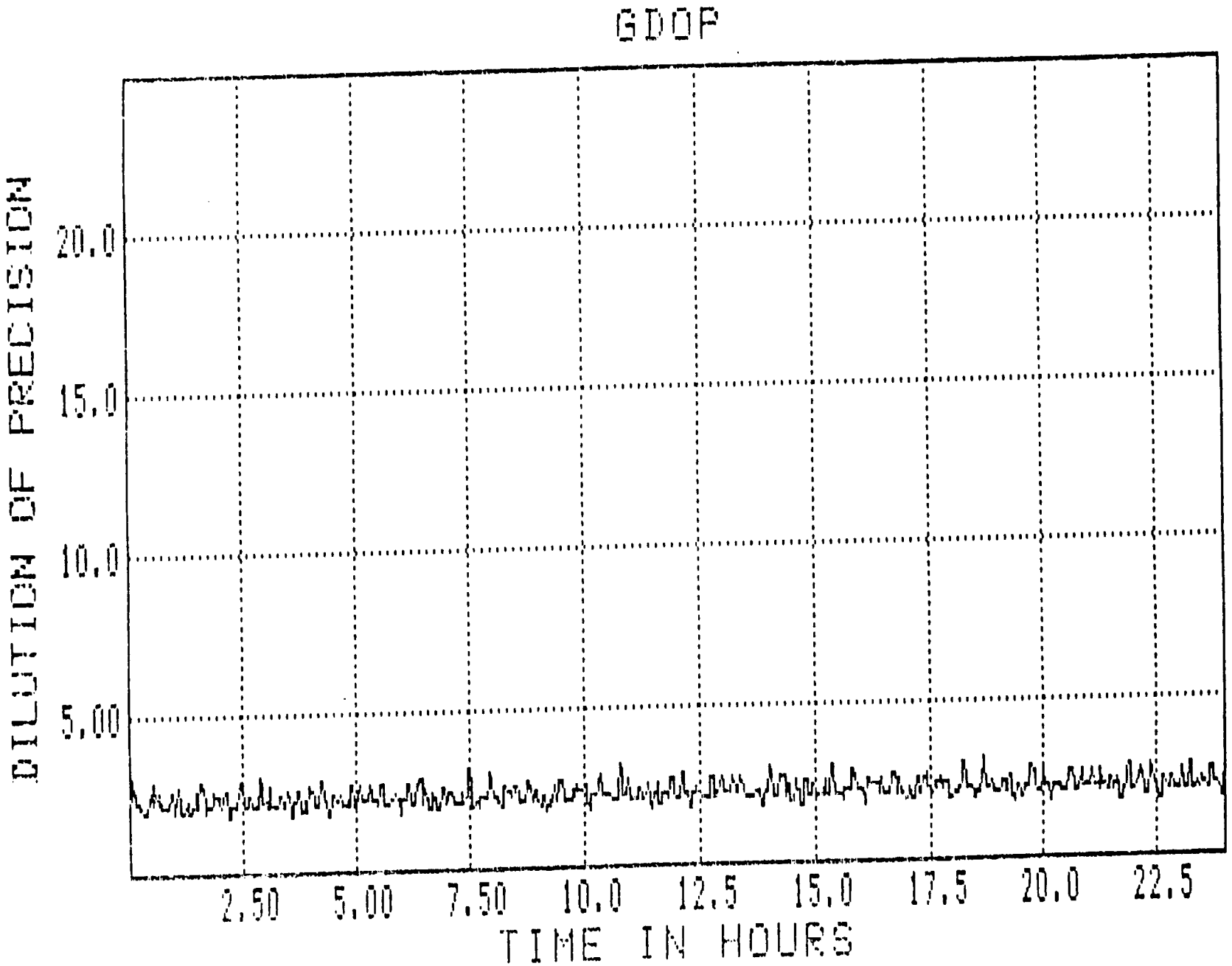

Figure 9 GDOP for the Differential GPS Seen on the Space Station Orbit, Separation by 2000 km

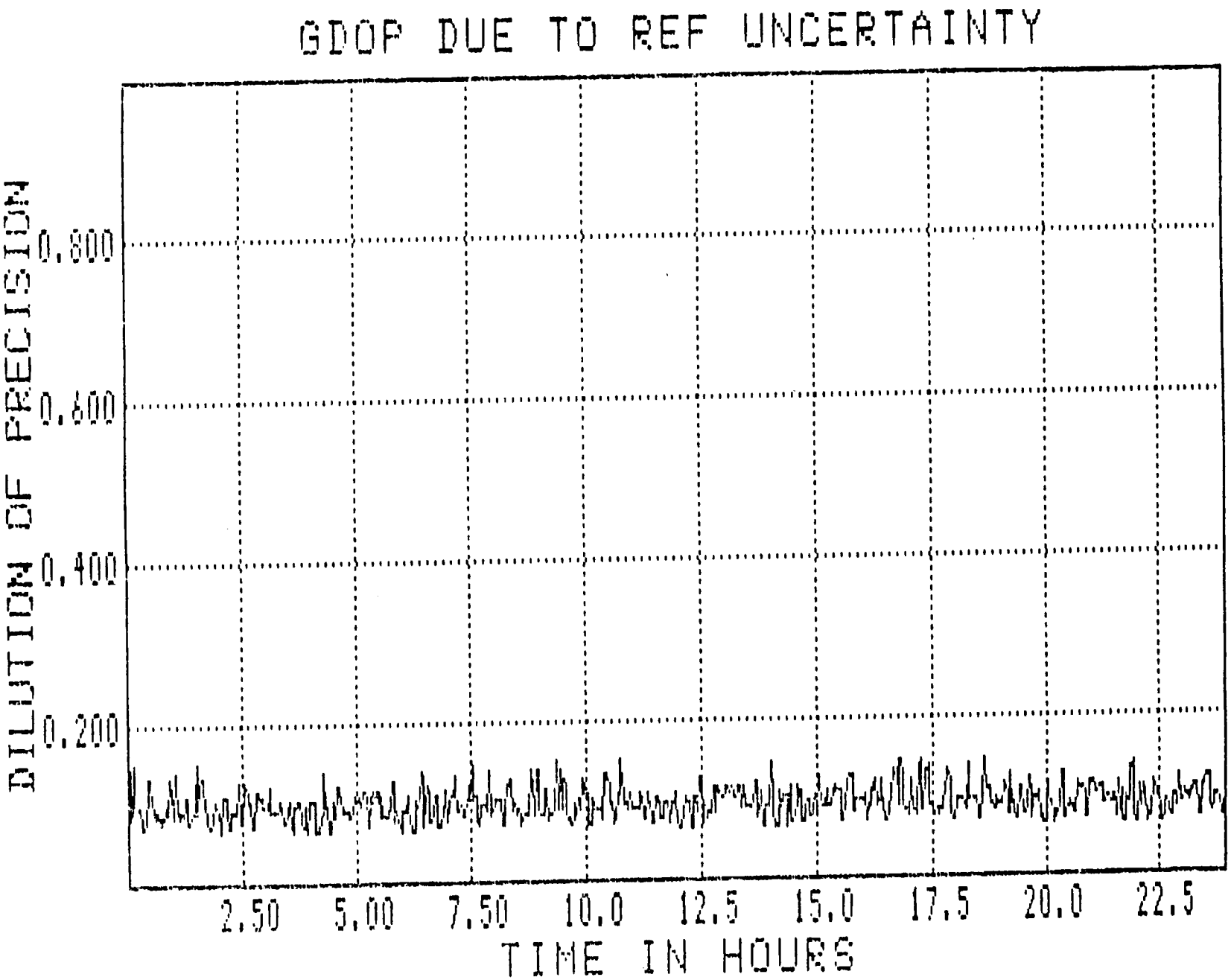

Figure 10 REFPU for the Differential GPS Seen on the Space Station Orbit, Separation by 2000 km

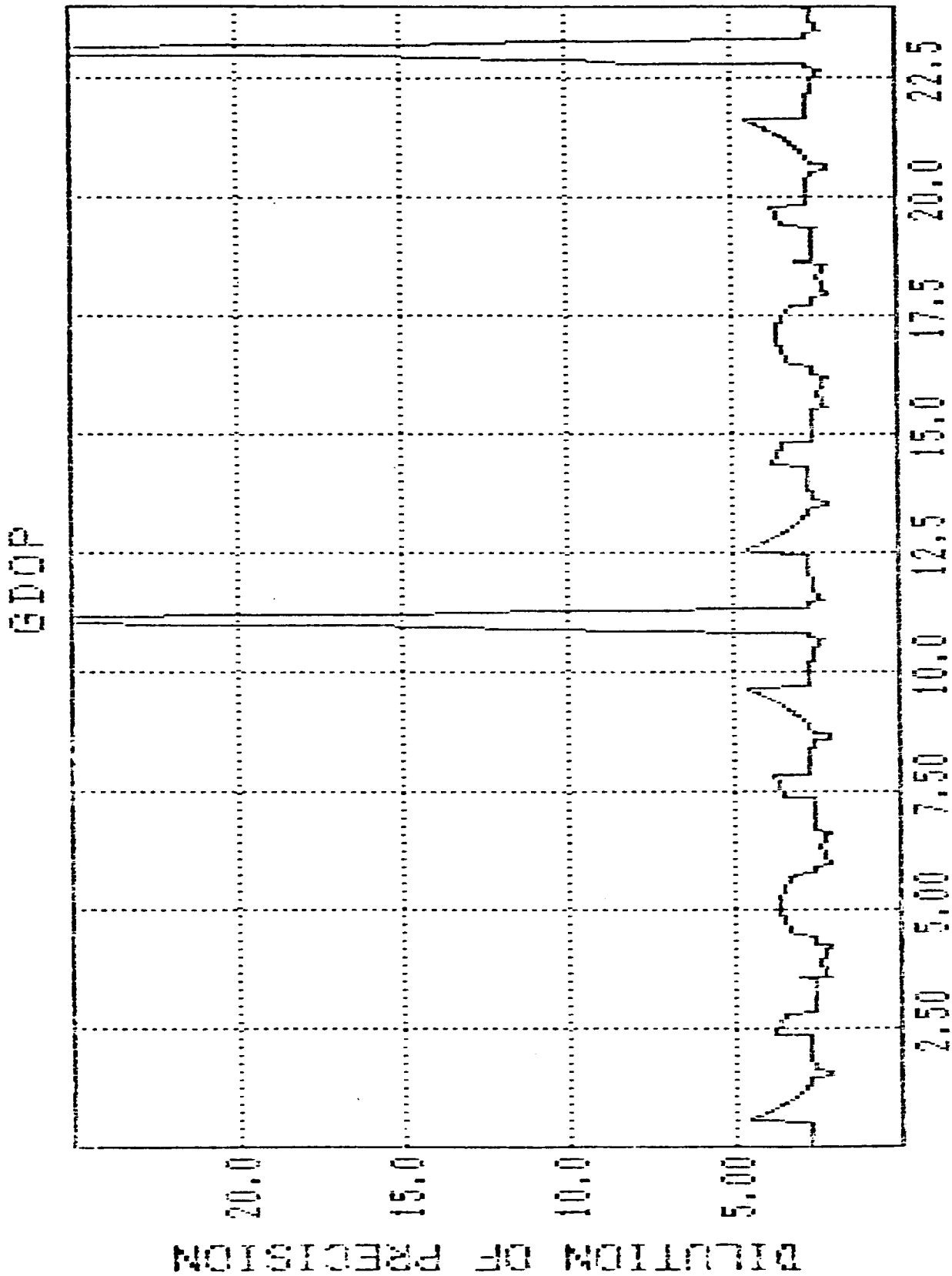

Figure 11 GDOP for the Standard GPS Seen by a Ground User Located at Longitude 5° and Latitude 35°

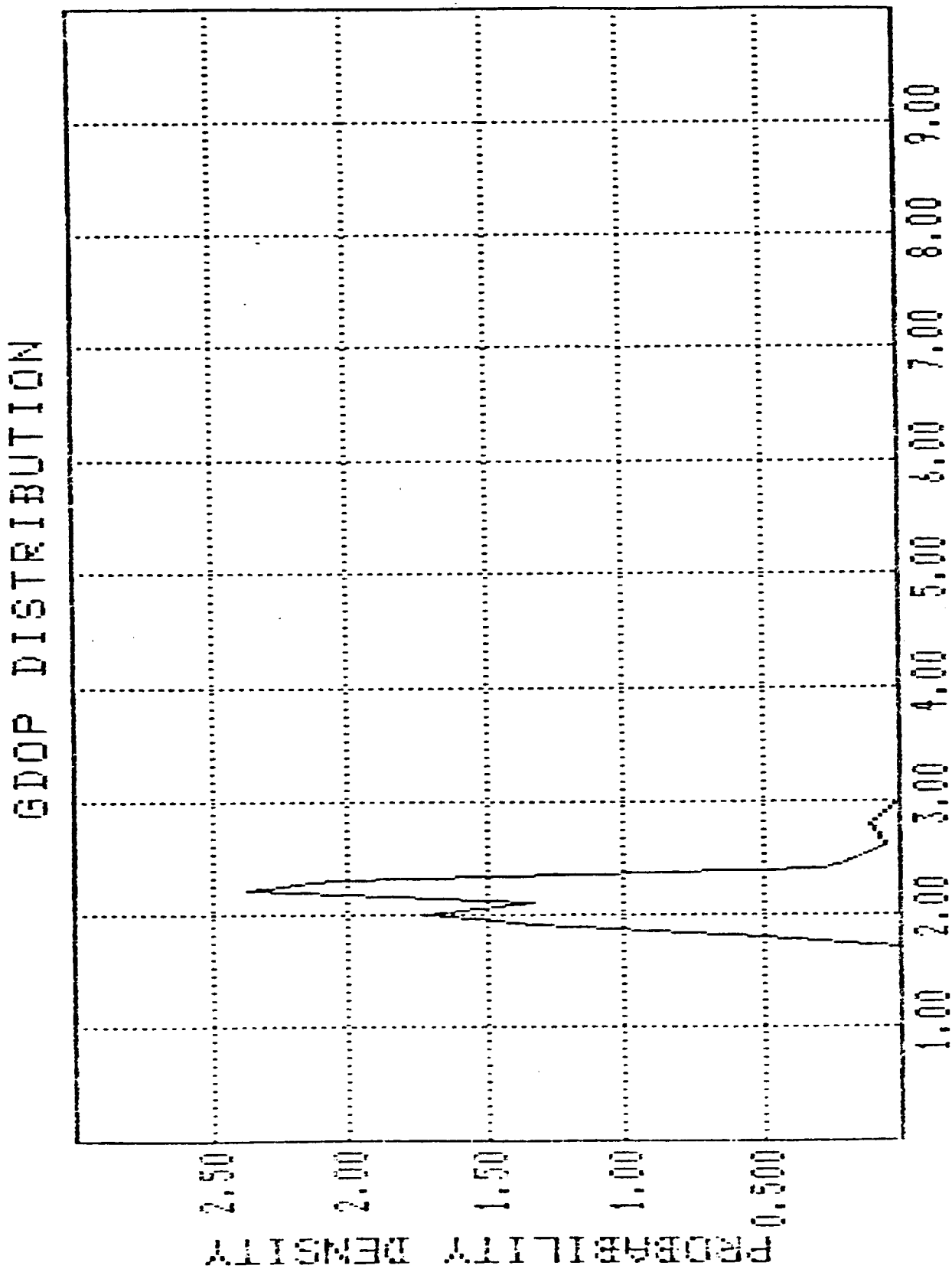

Figure 12 Probability Density for GDOP Distribution within a Day, Standard GPS on Space Station Orbit

4.0 KALMAN FILTER

Two kinds of measurements are available for the GPS navigation Kalman filters, namely, pseudorange and delta pseudorange measurements in the standard GPS and differential pseudorange and differential delta pseudorange measurements in the differential GPS.

Pseudorange from a user to the ith satellite is given

$$R_i = \sqrt{(x - x_i)^2 + (y - y_i)^2 + (z - z_i)^2} + b \tag{41}$$

Delta pseudorange measurement at the time t is given by

$$\Delta R_i = R_i(t) - R_i(t - \Delta t) \tag{42}$$

where Δt is a fixed time interval. Note that R_i is a simple function of (x_u, y_u, z_u, b_u). Hence its application is straightforward. On the other hand, $\Delta R_i(t)$ is not as simple as R_i. More detail exploration is necessary. We first note that it is not good to assume

$$R_i(t) - R_i(t - \Delta t) \approx \left(\frac{dR_i(t)}{dt} + \frac{db}{dt} \right) \Delta t$$

in a dynamic environment. However, the following assumption might be reasonable

$$\begin{aligned} \Delta R_i(t) - \Delta \hat{R}_i(t) &\approx \left(R_i(t) - R_i(t - \Delta t)\right) - \left(\hat{R}_i(t) - \hat{R}_i(t - \Delta t)\right) \\ &= \frac{d}{dt} \left((R_i - \hat{R}_i) + (b - \hat{b}) \right) \Delta t \end{aligned} \tag{43}$$

$\Delta \hat{R}_i(t)$ is the estimated delta pseudorange at the time t. In other words, Equation (43) assumes that the difference between the true and estimated pseudorange rates are almost constant over the time interval Δt. The measurement vector in the standard GPS is then

$$\underline{M} = (R_1, R_2, R_3, R_4, \Delta R_1, \Delta R_2, \Delta R_3, \Delta R_4) \tag{44}$$

In the Kalman filter solution algorithm, we need the matrix

$$H = \left.\frac{\partial \underline{M}}{\partial \underline{S}}\right|_{\underline{S} = \hat{\underline{S}}}$$

where $\underline{S}$ is the state vector in the Kalman filter. It could consist of 3 positions, 3 velocities, 3 accelerations, clock bias and frequency bias. Clearly,

$$\frac{\partial R_i}{\partial x} = \frac{x - x_i}{\sqrt{(x - x_i)^2 + (y - y_i)^2 + (z - z_i)^2}} \tag{46}$$

$$\frac{\partial R_i}{\partial y} = \frac{y - y_i}{\sqrt{(x - x_i)^2 + (y - y_i)^2 + (z - z_i)^2}} \tag{47}$$

$$\frac{\partial R_i}{\partial z} = \frac{z - z_i}{\sqrt{(x - x_i)^2 + (y - y_i)^2 + (z - z_i)^2}} \tag{48}$$

$$\frac{\partial R_i}{\partial b} = 1 \tag{49}$$

The term in (45) involving $\frac{dR_i}{dt}$ (see Equation (43)) could be computed as follows:

$$\frac{\partial}{\partial x}\left(\frac{dR_i}{dt}\right)$$

$$= \frac{\partial}{\partial x}\left(\frac{(x - x_i)(\dot{x} - \dot{x}_i) + (y - y_i)(\dot{y} - \dot{y}_i) + (z - z_i)(\dot{z} - \dot{z}_i)}{\sqrt{(x - x_i)^2 + (y - y_i)^2 + (z - z_i)^2}}\right)$$

$$= \frac{(\dot{x} - \dot{x}_i)\left[(y - y_i)^2 + (z - z_i)^2\right]}{\left((x - x_i)^2 + (y - y_i)^2 + (z - z_i)^2\right)^{3/2}} \tag{50}$$

$$\frac{\partial}{\partial y}\left(\frac{dR_i}{dt}\right) = \frac{(\dot{y} - \dot{y}_i)\left[(x - x_i)^2 + (z - z_i)^2\right]}{\left((x - x_i)^2 + (y - y_i)^2 + (z - z_i)^2\right)^{3/2}} \tag{51}$$

$$\frac{\partial}{\partial z}\left(\frac{dR_i}{dt}\right) = \frac{(\dot{z}-\dot{z}_i)\ \left[(x-x_i)^2 + (y-y_i)^2\right]}{\left((x-x_i)^2 + (y-y_i)^2 + (z-z_i)^2\right)^{3/2}} \tag{52}$$

and

$$\frac{\partial}{\partial \dot{x}}\left(\frac{dR_i}{dt}\right) = \frac{x-x_i}{\sqrt{(x-x_i)^2+(y-y_i)^2+(z-z_i)^2}} \tag{53}$$

$$\frac{\partial}{\partial \dot{y}}\left(\frac{dR_i}{dt}\right) = \frac{y-y_i}{\sqrt{(x-x_i)^2+(y-y_i)^2+(z-z_i)^2}} \tag{54}$$

$$\frac{\partial}{\partial \dot{z}}\left(\frac{dR_i}{dt}\right) = \frac{z-z_i}{\sqrt{(x-x_i)^2+(y-y_i)^2+(z-z_i)^2}} \tag{55}$$

$$\frac{\partial}{\partial \dot{b}}\left(\frac{dR_i}{dt}\right) = 1 \tag{56}$$

The measurement vector in the differential GPS is given by

$$\underline{M} = (DR_1, DR_2, DR_3, DR_4, D\Delta R_1, D\Delta R_2, D\Delta R_3, D\Delta R_4) \tag{57}$$

where

$$DR_i = R_{ui} - R_{Ri} \tag{58}$$

$$R_{ui} = \sqrt{(x_u-x_i)^2+(y_u-y_i)^2+(z_u-z_i)^2} + b_u \tag{59}$$

$$R_{Ri} = \sqrt{(x_R-x_i)^2+(y_R-y_i)^2+(z_R-z_i)^2} + b_R \tag{60}$$

$$\begin{aligned} D\Delta R_i(t) &= \Delta R_{ui}(t) - \Delta R_i(t) \\ &= \frac{d}{dt}\left((R_{ui}-\hat{R}_{ui}) + (b_u-\hat{b}_u)\right)\Delta t \\ &\quad - \frac{d}{dt}\left((R_{Ri}-\hat{R}_{Ri}) + (b_R-\hat{b}_R)\right)\Delta t + \hat{\Delta R}_{ui}(t) - \hat{\Delta R}_{Ri}(t) \end{aligned} \tag{61}$$

It is easy to see that $\frac{\partial DR_i}{\partial x_u}$, $\frac{\partial DR_i}{\partial y_u}$, $\frac{\partial DR_i}{\partial z_u}$, $\frac{\partial DR_i}{\partial b_u}$, $\frac{\partial}{\partial x_u}\frac{dDR_i}{dt}$, $\frac{\partial}{\partial y_u}\frac{dDR_i}{dt}$, $\frac{\partial}{\partial z_u}\frac{dDR_i}{dt}$, $\frac{\partial}{\partial x_u}\frac{dDR_i}{dt}$, $\frac{\partial}{\partial y_u}\frac{dDR_i}{dt}$, $\frac{\partial}{\partial z_u}\frac{dDR_i}{dt}$, and $\frac{\partial}{\partial b_u}\frac{dDR_i}{dt}$ are given by equations (46) through (56), respectively, with x, y, z, and b being replaced by x_u, y_u, z_u, and b_u. Therefore, the standard GPS and the differential GPS have the same H matrix (see Equation (45)). As mentioned before, in certain applications, such as the Space Station System, the relative position between the user and reference station is the entity we are interested in. In this case, $x_u = x_R + x_{u-R}$, $y_u = y_R + y_{u-R}$, $z_u = z_R + {}_{u-R}$, $b_u = b_R + b_{u-R}$. Therefore, Equations (46) through (56) are still valid with x, y, z, b being replaced by x_{u-R}, y_{u-R}, z_{u-R}, b_{u-R}.

Many Kalman filter models are available for the navigation application. The simpliest one is the position-velocity-acceleration-time (PVAT) model, which does not take into account the orbital mechanics. A more complex one is based on the equation of vehicle motion. We will discuss both in this report. The best choice of state vector in the Kalman filter has eleven components, namely, 3 positions, 3 velocities, 3 accelerations, clock bias, and frequency bias. The acceleration components are required in a dynamic environment. Note that reducing the number of states reduces the computational load. Therefore, in a less dynamic environment, one could use a model with 8-component state vector, which does not include 3 accelerations. If computational load has to be further reduced, we may split the 8-component state vector into two 4-component state vectors, each is processed by its respective Kalman filter.

The PVAT model of Kalman filter could be described by the following equations:

$$\begin{cases} \underline{S}(t+1) = \phi(\Delta t, \underline{\alpha}, \zeta)\,\underline{S}(t) + \underline{\omega}(t) \\ \underline{A}(t) = \underline{h}(\underline{S}(t)) + \underline{\upsilon}(t) \end{cases} \tag{62}$$

where

t – normalized discrete time

Δt – sampling time interval

$\underline{S}(t) - (x, y, z, \dot{x}, \dot{y}, \dot{z}, \ddot{x}, \ddot{y}, \ddot{z}, b, \dot{b})$

b – clock bias

$\dot{b}$ – frequency bias

$$\phi(\Delta t, \underline{a}, \zeta) = \begin{bmatrix} I_3 & (\Delta t)\, I_3 & 1/2(\Delta t)^2\, I_3 & 0 & 0 \\ 0 & I_3 & (\Delta t)\, I_3 & 0 & 0 \\ 0 & 0 & \underline{a}\, I_3 & 0 & 0 \\ 0 & 0 & 0 & 1 & \Delta t \\ 0 & 0 & 0 & 0 & \zeta \end{bmatrix} \tag{63}$$

I_3 – 3 x 3 identity matrix

$\underline{a}$ – $(a_1, a_2, a_3)^T$ is the first-order Markov parameters of stochastic acceleration models in x, y, z axes.

ζ – the first-order Markov parameter of frequency bias.

$\underline{h}(\underline{S}(t))$ – the transformation from $\underline{S}(t)$ to the pseudorange and delta pseudorange.

$\underline{A}(t)$ – pseudorange and delta pseudorange measurements.

$\underline{\omega}(t)$ – state noise with $E\{\underline{\omega}(t)\, \underline{\omega}^T(\tau)\} = R_1(t)\, \delta_{t\tau}$

$\underline{\upsilon}(t)$ – measurement noise with $E\{\underline{\upsilon}(t)\, \underline{\upsilon}^T(\tau)\} = R_2(t)\, \delta_{t\tau}$

The solution algorithm for the Kalman filter (62) is given by

$$\hat{\underline{S}}(t+1) = \phi\, \hat{\underline{S}}(t) + K(t) \left\{ \underline{A}(t+1) - \underline{h}(\phi\, \hat{\underline{S}}(t)) \right\} \tag{64}$$

$$K(t) = P(t|t)\, H^T\, R_2^{-1}(t) \tag{65}$$

$$P(t+1|t) = \phi\, P(t|t)\, \phi^T + R_1(t) \tag{66}$$

$$P(t+1|t+1) = (I - K(t)\, H)\, P(t+1|t) \tag{67}$$

The H matrix in (65) and (67) is defined by (45). It is worth mentioning that the Kalman filter model described by Equations (62) through (67) is valid for many cases, namely,

(1) standard GPS;

(2) differential GPS, absolute user position tracking;

(3) differential GPS, relative user position tracking (relative to reference station).

For the case of differential GPS, $\underline{A}(t)$ is derived from the actual location of reference station and $\underline{h}(\hat{\underline{S}}(t))$ is computed based on the estimated reference station location. Therefore, the effect of reference station location uncertainty could be envisioned as an additional observation noise included in $\underline{v}(t)$.

The orbital mechanics Kalman filter model is based on the equation of vehicle motion, namely, in ECEF

$$\ddot{\underline{r}} = \underline{a}_G + \underline{a}_D - 2\underline{\Omega} \times \dot{\underline{r}} - \underline{\Omega} \times \underline{\Omega} \times \underline{r} \tag{68}$$

where

$\underline{r}$ – position vector of vehicle

$\underline{a}_G$ – gravitational acceleration

$\underline{a}_D$ – drag acceleration

$\underline{\Omega}$ – angular velocity of Earth's self-revolution

In order to derive a discrete extended Kalman filter, Equation (68) must be linearized. Let $\underline{S}$ denote the state vector, namely, $\underline{S} = (x, y, z, b, \dot{x}, \dot{y}, \dot{z}, \dot{b}, d)$. The error state vector $\delta\underline{S}$ is defined as

$$\begin{aligned} \delta\underline{S} &= \underline{S} - \underline{S}^* \\ &= (\delta x, \delta y, \delta z, \delta b, \delta\dot{x}, \delta\dot{y}, \delta\dot{z}, \delta\dot{b}, \delta d) \end{aligned}$$

In Equation (69), d is the drag factor. $\underline{S}^*$ denotes the nominal state vector, which could be

derived from the last estimate of $\underline{S}$. Note that (68) could be rewritten as

$$\begin{aligned}\ddot{\underline{r}} &= \ddot{\underline{r}}^* + \delta\ddot{\underline{r}} \\ &= -\frac{\mu(\underline{r}^* + \underline{r}\delta)}{|\underline{r}^* + \underline{r}\delta|^3} - (d^* + \delta d)\rho\,|\underline{v}^* + \delta\underline{v}|\,(\underline{v}^* + \delta\underline{v}) \\ &\quad - 2\underline{\Omega} \times (\underline{v}^* + \delta\underline{v}) - \underline{\Omega} \times (\underline{\Omega} \times (\underline{r}^* + \delta\underline{r}))\end{aligned} \tag{70}$$

where μ is the gravitational constant and ρ is the atmospheric density. The first term on the right-hand side of the last equality of Equation (70) has

$$\begin{aligned}\frac{\mu(\underline{r}^* + \delta\underline{r})}{|\underline{r}^* + \delta\underline{r}|^3} &\approx \frac{\mu(\underline{r}^* + \delta\underline{r})}{|\underline{r}^*|^3\left(1 + \frac{3\underline{r}^* \cdot \delta\underline{r}}{|\underline{r}^*|^2}\right)} \\ &\approx \frac{\mu\underline{r}^*}{|\underline{r}^*|^3} + \frac{\mu\delta\underline{r}}{|\underline{r}^*|^3} - \frac{3\mu(\underline{r}^* \cdot \delta\underline{r})\underline{r}^*}{|\underline{r}^*|^5}\end{aligned} \tag{71}$$

The second term has

$$\begin{aligned}&(d^* + \delta d)\,\rho|\underline{v}^* + \delta\underline{v}|\,(\underline{v}^* + \delta\underline{v}) \\ &\approx (d^* + \delta d)\,\rho\left[|\underline{v}^*|\,\underline{v}^* + |\underline{v}^*|\,\delta\underline{v} + \frac{(\underline{v}^* \cdot \delta\underline{v})\underline{v}^*}{|\underline{v}^*|}\right] \\ &\approx d^*\rho\,|\underline{v}^*|\underline{v}^* + \delta d\rho\,|\underline{v}^*|\underline{v} + d^*\rho\left[|\underline{v}^*|\delta\underline{v} + \frac{(\underline{v}^* \cdot \delta\underline{v})\underline{v}^*}{|\underline{v}^*|}\right]\end{aligned} \tag{72}$$

Finally, one has

$$\begin{aligned}\delta\ddot{\underline{r}} &= -\frac{u\delta\underline{r}}{|\underline{r}^*|^3} + \frac{3u(\underline{r}^* \cdot \delta\underline{r})\underline{r}^*}{|\underline{r}^*|^5} - \delta d\rho\,|\underline{v}^*|\,\underline{v}^* \\ &\quad - d^*\rho\left[|\underline{v}^*|\,\delta\underline{v} + \frac{(\underline{v}^* \cdot \delta\underline{v})\underline{v}^*}{|\underline{v}^*|}\right] \\ &\quad - 2\,\underline{\Omega} \times \delta\underline{v} - \underline{\Omega} \times (\underline{\Omega} \times \delta\underline{r})\end{aligned} \tag{73}$$

From (73), we have

$$\delta \dot{\underline{S}} = F(\underline{S} + \dot{\underline{S}}^*)\, \delta \underline{S} \tag{74}$$

where

$$F(\underline{S}, \dot{\underline{S}}) = \begin{bmatrix} 0_3 & \underline{0} & I_3 & \underline{0} & \underline{0} \\ \underline{0}^T & 0 & \underline{0}^T & 1 & 0 \\ F_{3,1} & \underline{0} & F_{3,3} & \underline{0} & F_{3,5} \\ \underline{0}^T & 0 & \underline{0}^T & -1/\tau_F & 0 \\ \underline{0}^T & 0 & \underline{0}^T & 0 & -1/\tau_F \end{bmatrix} \tag{75}$$

$$F_{3,1} = -\frac{\mu}{|\underline{r}^*|^3}\left[I_3 - \frac{3}{|\underline{r}^*|^2}(\underline{r}^* \underline{r}^{*T}) - \underline{\Omega} \times (\underline{\Omega} \times)\right]$$

$$F_{3,3} = -\frac{d^*\rho}{|\underline{v}^*|^3}\left(|\underline{v}^*|^2 I_3 + \underline{r}^* \underline{r}^{*T}\right) - 2(\underline{\Omega} \times)$$

$$F_{3,5} = -\rho\, |\underline{v}^*|\, \underline{v}^*$$

Finally, the discrete linearized error state equation is

$$\begin{cases} \delta \underline{S}(k+1) = \Phi(k, k+1)\, \delta \underline{S}(k) + \underline{\omega}(k) \\ \underline{A}(k) = \underline{h}(\underline{S}(k)) + \underline{\upsilon}(k) \end{cases} \tag{76}$$

where

$$\Phi(k, k+1) = \mathrm{Exp}\left\{\int_{t_k}^{t_{k+1}} F(\underline{S}^*, \dot{\underline{S}}^*)\, dt\right\} \tag{77}$$

$\underline{\omega}(k)$ – state noise with $E\{\underline{\omega}(k)\, \underline{\omega}(l)^T\} = R_1(k)\, \delta_{kl}$

$\underline{\upsilon}(k)$ – measurement noise with $E\{\underline{\upsilon}(k)\, \underline{\upsilon}(l)^T\} = R_2(k)\, \delta_{kl}$

In certain applications of differential GPS, such as the Space Station System, the reference station itself is tracked by the standard GPS. The complete state vector then consists of $\underline{S}_R$, the state vector of reference station, and $\underline{S}_u$, the state vector of user. If both the reference station and user are using the standard GPS, $\underline{S}_R$ and $\underline{S}_u$ are clearly uncoupled. However, if the reference station uses the standard GPS and the user uses the differential GPS, then two Kalman filters could be coupled by the H matrix; this is because the differential pseudorange and differential delta pseudorange are function of $\underline{S}_R$. Therefore, our confidence on the current estimate of $\underline{S}_R$ will determine our confidence on the current differential pseudorange and differential delta pseudorange measurements.

If we are interested in tracking $\underline{S}_{u-R} = \underline{S}_u - \underline{S}_R$, Equation (74) must be modified appropriately. We first observe that

$$\begin{cases} \delta\dot{\underline{S}}_R = F_R\,(\underline{S}_R^*, \dot{\underline{S}}_R^*)\,\delta\underline{S}_R \\ \delta\dot{\underline{S}}_u = F_u\,(\underline{S}_u^*, \dot{\underline{S}}_u^*)\,\delta\underline{S}_u \end{cases}$$

Hence

$$\begin{aligned} \delta\dot{\underline{S}}_u &= \delta\dot{\underline{S}}_R + \delta\dot{\underline{S}}_{u-R} \\ &= F_R\,(\underline{S}_R^*, \dot{\underline{S}}_R^*)\,\delta\underline{S}_R + \delta\dot{\underline{S}}_{u-R} \\ &= F_u\,(\underline{S}_u^*, \dot{\underline{S}}_u^*)\,(\delta\underline{S}_R + \delta\underline{S}_{u-R}) \end{aligned}$$

We end up with

$$\delta\dot{\underline{S}}_{u-R} = F_u\,(\underline{S}_u^*, \dot{\underline{S}}_u^*)\,\delta\underline{S}_{u-R} + F_u\,(\underline{S}_u^*, \dot{\underline{S}}_u^*) - F_R\,(\underline{S}_R^*, \dot{\underline{S}}_R^*)\,\delta\underline{S}_R \qquad (78)$$

Equation (78) says:

(1) If $F_u\,(\underline{S}_u^*, \dot{\underline{S}}_u^*) \approx F_R\,(\underline{S}_R^*, \dot{\underline{S}}_R^*)$, $\underline{S}_R$ and $\underline{S}_{u-R}$ are coupled by the by the H matrix only.

(2) If $F_u(\underline{S}_u^*, \dot{\underline{S}}_u^*) \neq F_R(\underline{S}_R^*, \dot{\underline{S}}_R^*)$, $\underline{S}_R$ and $\underline{S}_{u-R}$ are also coupled by the state equation (78).

Note that $F_u(\underline{S}_u^*, \dot{\underline{S}}_u^*)$ can be different $F_R(\underline{S}_R^*, \dot{\underline{S}}_R^*)$ because of the following reasons:

- The user and reference station could have different altitude.
- The gravitational accelerations experienced by user and reference station could have different directions.
- The drag accelerations experienced by user and reference station could have different directions.
- The user and reference station could have different drag coefficients.
- In ECEF, the user and reference station could experience different coriolis and centrifugal forces.

$$\hat{\underline{S}}(k+1|k+1) = \hat{\underline{S}}(k+1|k) + K(k)\{\underline{A}(k+1) - \underline{h}(\hat{\underline{S}}(k+1|k)\} \quad (79)$$

$$K(k) = P(k|k)\, H(k)^T R_2(k)^{-1} \quad (80)$$

$$P(k+1|k+1) = (I - K(k)\, H(k))\, P(k+1|k) \quad (81)$$

$$P(k+1|k) = \Phi(k, k+1)\, P(k|k)\, \Phi(k, K+1)^T + R_1(k) \quad (82)$$

$\hat{\underline{S}}(k+1|k)$ means the propagated state vector from $\hat{\underline{S}}(k+1|k)$. This propagation could be done by applying the Runge-Kutta-Heun method to the equation of vehicle motion.

In the practical implementation, the measurements from four GPS satellites could be performed in a sequential manner. In such a case, the H matrix defined by (45) has a smaller dimension.

5.0 SIMULATION SOFTWARE

The block diagram of simulation software is depicted in Figure 13. Basically speaking, the program defined by the diagram has to do the following things:

- Compute the positions of user, reference station, and GPS satellites. For a ground user or reference station, we could use (23). for a satellite user, we must use Equations (1) through (9).
- The pseudorange and delta pseudorange measurements are then computed. A receiver noise is added. This noise is generated by a Gaussian random number generator.
- The visibility of GPS satellites is checked based on the actual user and GPS satellite positions.
- The best four GPS satellites are selected by computing the GDOP at the estimated user position. The positions of GPS satellites used in this calculation are computed based on the user clock.
- The solution algorithm could be implemented in many ways. Typically, for the algorithm testing purpose, matrix addition and multiplication routines are used for their generality. However, for the real-time applications, dedicated routines are designed to optimize the speed. The H matrix is computed by using equations (45) through (56).

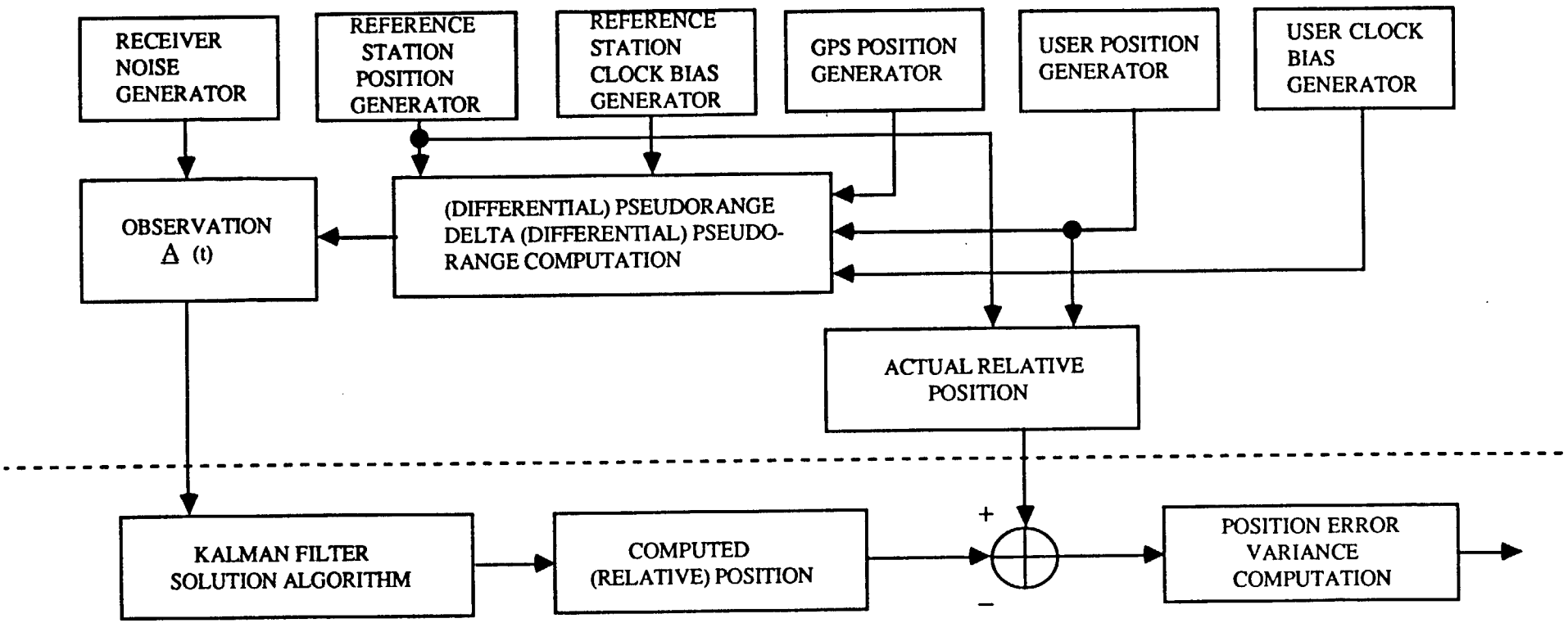

Figure 13. The Block Diagram of Simulation Softwares

APPENDIX E

FEASIBILITY CONSIDERATIONS FOR LONG RANGE TRACKING RADAR FOR SPACE STATION

FEASIBILITY CONSIDERATIONS FOR LONG RANGE TRACKING RADAR FOR SPACE STATION

Prepared

for

Contract No. NAS9-17414
Lyndon B. Johnson Space Center
Houston, Texas 77058

Prepared
by

Sergei Udalov

Axiomatix
9841 Airport Blvd., Ste. 912
Los Angeles, California 90045

Axiomatix Report No.8510-2
October 17, 1985

Table of Contents

List of Figures

List of Tables

1.0 INTROUDCTION AND SUMMARY

In this interim report we consider some key issues which are involved in regards to the feasibility of having a radar operation up to the extreme tracking range of 2000 km.

Although formally there is no radar coverage requirement for the coorbiting satellite zones 5 (leading) and 6 (trailing), several advantages of providing radar coverage within these zones should be considered. In determining any potential advantages and the associated trade-offs, one should consider following factors:

1) Function/Application
2) Coverage Requirements
3) Accuracy Requirements and Trade-Offs

and 4) Design Implementations

In addition to these general factors, such specific issues as passive (reflector) versus active (transponder-aided) radar operation must be addressed.

Although not all of the issues have been resolved to date, particularly that of coverage and accuracy requirements, the following conclusions can be reached based on range equation for radar target detection at 2000 km:

1) Detection of a skin return from a 1 m^2 target requires megawatts of peak power and tens of kilowatts of average power.

2) Equipping the target with a passive reflector such as a corner reflector (1 meter on a side) reduces the peak power requirement to tens of kilowatts and the average power to much less than one kilowatt.

3) Use of FM/CW radar with a corner reflector although requiring transmitter signal leakage

cancellation, can reduce both the peak and CW power (they are same) requirements to 50 watts. This value of power represents the capability of the Ku-band radar/communication system presently used on the Shuttle Orbiter.

4) Use of a cooperative active transponder on the target also reduces peak power requirement to about 50 watts, thus providing for a potential utilization of the Ku-band system presently used onboard Shuttle Orbiter.

At this point, consequently, the main issues center on the following:

a) Passive reflector vs. beacon (transponder) radar system.

b) Implementation trade-offs for systems listed in a) above

and c) Accuracy required and achievable with either a passive or an active (beacon) systems.

The considerations above pertain to the operation in the 185 km to 2000 km range, with particular emphasis on acquisition at 2000 km.

In the material that follows we present those considerations which we have been addressing so far.

2.0 FUNCTIONS AND APPLICATIONS

The justification for a long range radar capability for the Space Station is predicated upon the existence of several applications where the long range radar can either perform certain unique function or can significantly augment the operation of another type of tracking service such as can be provided either by GPS or, at least in part, by a communications transponder. Among the areas where the long range radar can be utilized, the following functions and/or application have been identified so far for the 185 km to 2000 km range:

1) Augmenting the tracking service provided by relaying of GPS positional data to Space Station (SS).

2) Providing tracking data to the space traffic control system.

3) Serving as a part of orbital control in the range of 185 km to 2000 km.

4) Aiding in detecting users at maximum range of 2000 km and providing angular information for pointing high gain SS comm link antennas.

5) Provide tracking information for hand-over from co-orbiting (zones 5 and 6) to rendezvous zones 3 and 4, the latter having their outer limits at 185 km.

Additional arguments supporting these potential applications are presented below.

The use of GPS receiver on co-orbiting vehicles and the telemetering of the GPS positional data to SS via a communication link has been baselined as a primary mode of long range tracking [Ref #1]. However, this baseline raises an issue of requiring a GPS receiver on all free flyers. There also exists an argument that a secondary source of tracking/navigation information can be supplied by communication system auto-tracking.

Regardless of the validity of either of the arguments, the fact remains that both of the methods require the communication link and thus are not autonomous. Beacon-aided radar/tracking, therefore, can provide for a true back-up capability for long range navigation and tracking.

Autonomous radar-based system can provide the Space Station with capability of tracking free flyers and other vehicles without dependence on the comm link or any other means such as ground track. This autonomy may be of great value to space traffic control and to the orbital control functions.

Another function which long range tracking can provide is to supply angular information for pointing high directivity antennas of the SS for establishing a high rate comm link at long ranges. This function, however, is predicated on the existence of the requirement for such high rate comm links up to 2000 km and it should thus not be the primary reason for long range radar.

3.0 COVERAGE REQUIREMENT

The considerations referring to range and angular coverage requirement for long range operation state simply the following:

Range: 185 km to 2000 km

Angle: 28 cone fore and aft of space station

The range coverage requirement stems from the definition of the co-orbital zones 5 and 6. Thus, we have taken a closer look at the linear dimensions of various zones comprising a flight path along the orbit from the end of 2000 km range to the command and control zone starting at 37 km from the space station. Figure 3-1 shows the actual angular coverage requirements as determined by linear dimensions of the various zones.

From Figure 3-1 it is evident that at the range of 185 km the vertical coverage requirement is 22.6° . This value is within to the 28 requirement. But, considerations at long range of the co-orbiting satellite trajectory indicate that at 2000 km only about 8.3 degrees vertical coverage is required to cover the free-fliers on the co-orbiting path. Thus, to provide for optimum detection and tracking of target within the coorbiting zones, a pattern optimization of detection time can be performed by increasing the dwell time for the "lower" beams which correspond to the coverage of the co-orbiting zones. As shown in Figure 3-2 the antenna beamwidth is 1° x 1° which corresponds to a pencil beam antenna used in our baseline range equation calculations for various radar implementations.

What is said above <u>should not</u> be construed as a recommendation to stay only within the 1° x 9° pattern of Figure 3-2. The point being made here, however, is that special emphasis should be placed on searching out the approximate 1° x 9° volume which encompasses the flight path of the co-orbiting satellite zones. One way to accomplish this is to perform a mini-scan over this area and to include this mini-scan pattern within a larger pattern covering the 28° cone.

One such possible approach is shown in Figure 3-3. There, the 1° x 9° area where the co-orbital targets are scanned

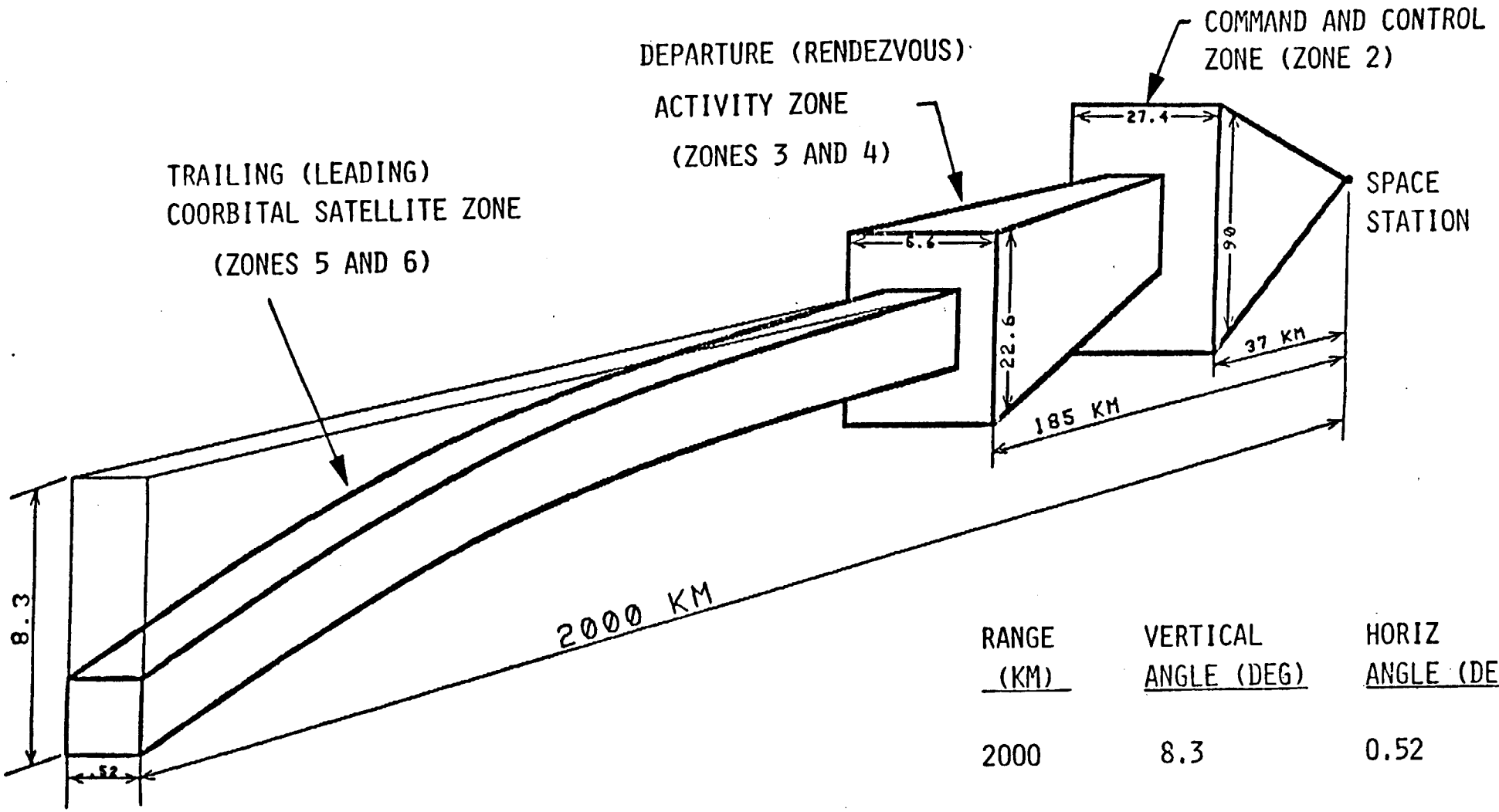

RANGE (KM)	VERTICAL ANGLE (DEG)	HORIZ ANGLE (DEG)
2000	8.3	0.52
185	22.6	5.6
37	90	27.4

NOTE: DIMENSIONS OTHER THAN KM ARE IN DEGREES.

FIGURE 3-1. ANGULAR COVERAGE REQUIREMENTS VS. RANGE

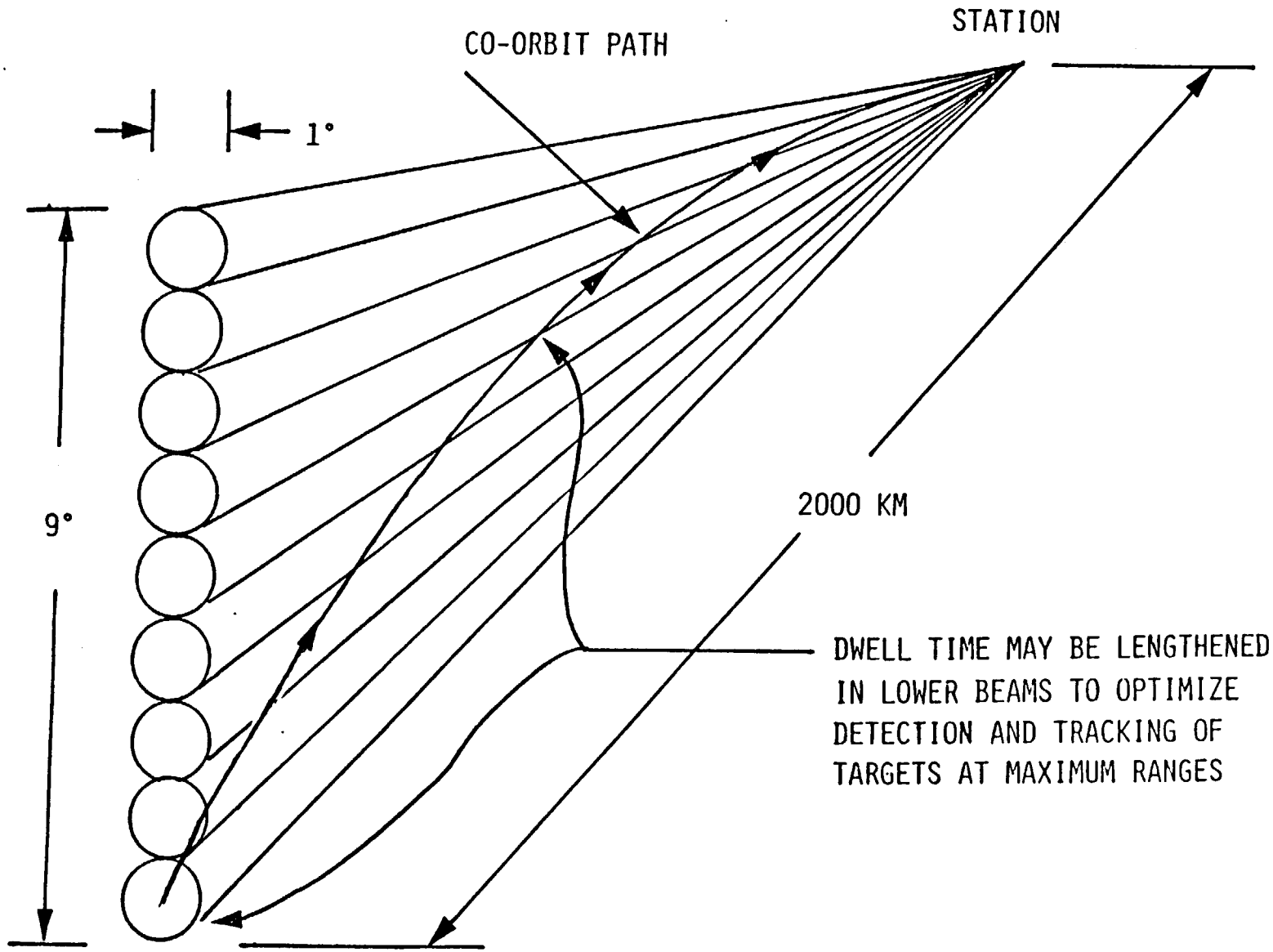

FIGURE 3-2. ANGULAR SEARCH PATTERN OPTIMIZED FOR MAX RANGE OF 2000 KM

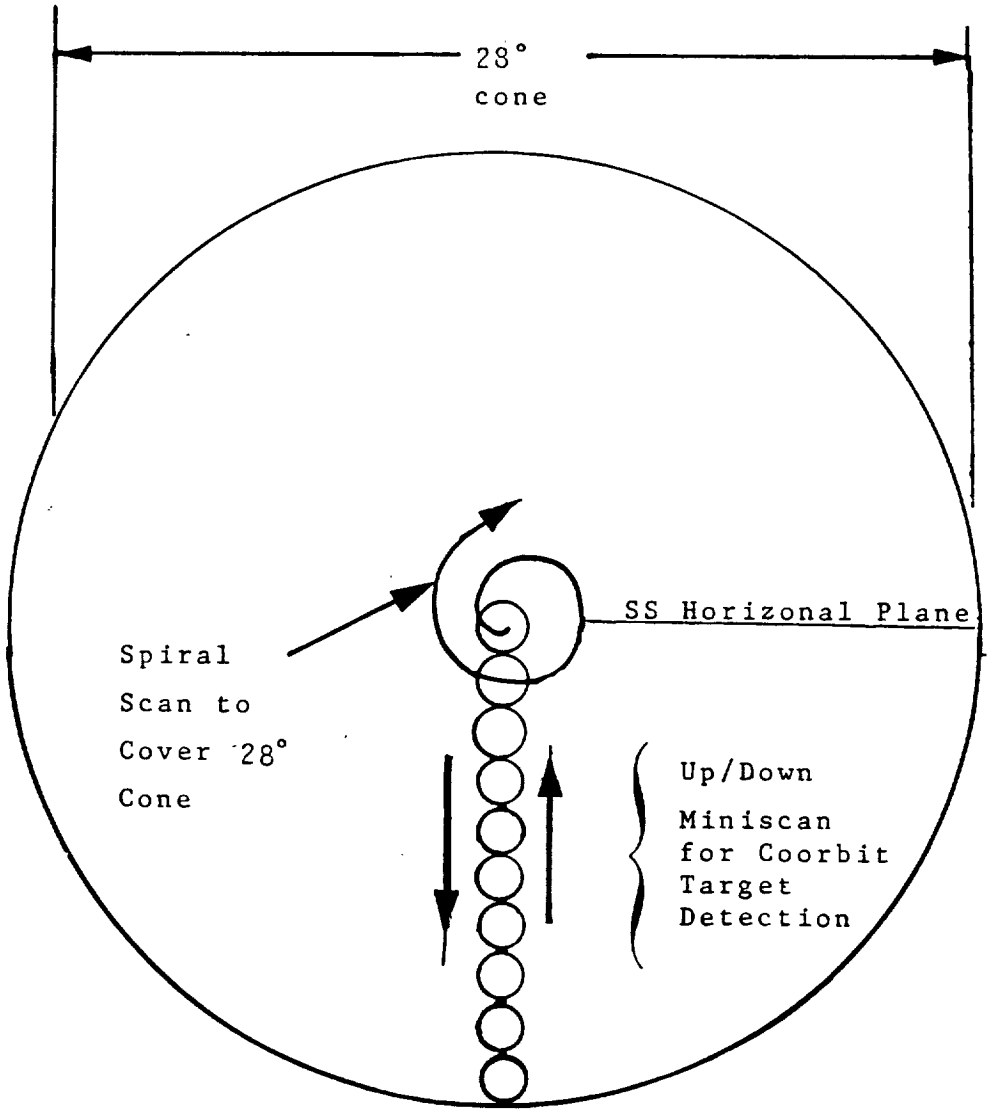

View is towards Space Station

Figure 3-3. Radar Scan of Co-orbit Path can be a Miniscan within Scan to Cover 28° Cone

by up and down mini-scan of programmed dwell time. After covering this area the antenna takes off on a spiral scan which may have different dwell times within the 28° cone. Figure 3-4 shows another variation of this approach.

The details of working out scan patterns and scan strategies must be relegated to the time when the radar system is better defined quantitatively.

4.0 ACCURACY REQUIREMENTS

So far the only accuracy requirement which is specified for long range co-orbital operation is that of ±15 meters with a GPS system [Ref. 1]. To baseline a radar system, however, one must have some idea of the following four (4) accuracies:

1. Range
2. Range Rate (velocity)
3. Angle
4. Angle Rate

Consequently, we have proceeded to establish some tentative values which could be used for baselining a radar system for the 185 km to 2000 km range. Table 1 summarizes these values. From the table it is evident that not all of the accuracy values could be established at this time and also that some may be modified in the future. Nevertheless Table 4-1 provides a starting point for the development of radar-oriented accuracy specifications. Presented below is the reasoning used for arriving at the values for Table 4-1.

Range Accuracy

As the first cut we have adapted the criterion used for the present Ku-Band radar, namely 0.01 (i.e., 1%) of the range; However, if one considers the fact that 1% of 2000 km is 20 km, the discrepancy with GPS is enormous. But, if we consider the range accuracy in term of a hypothetical radar performance, the

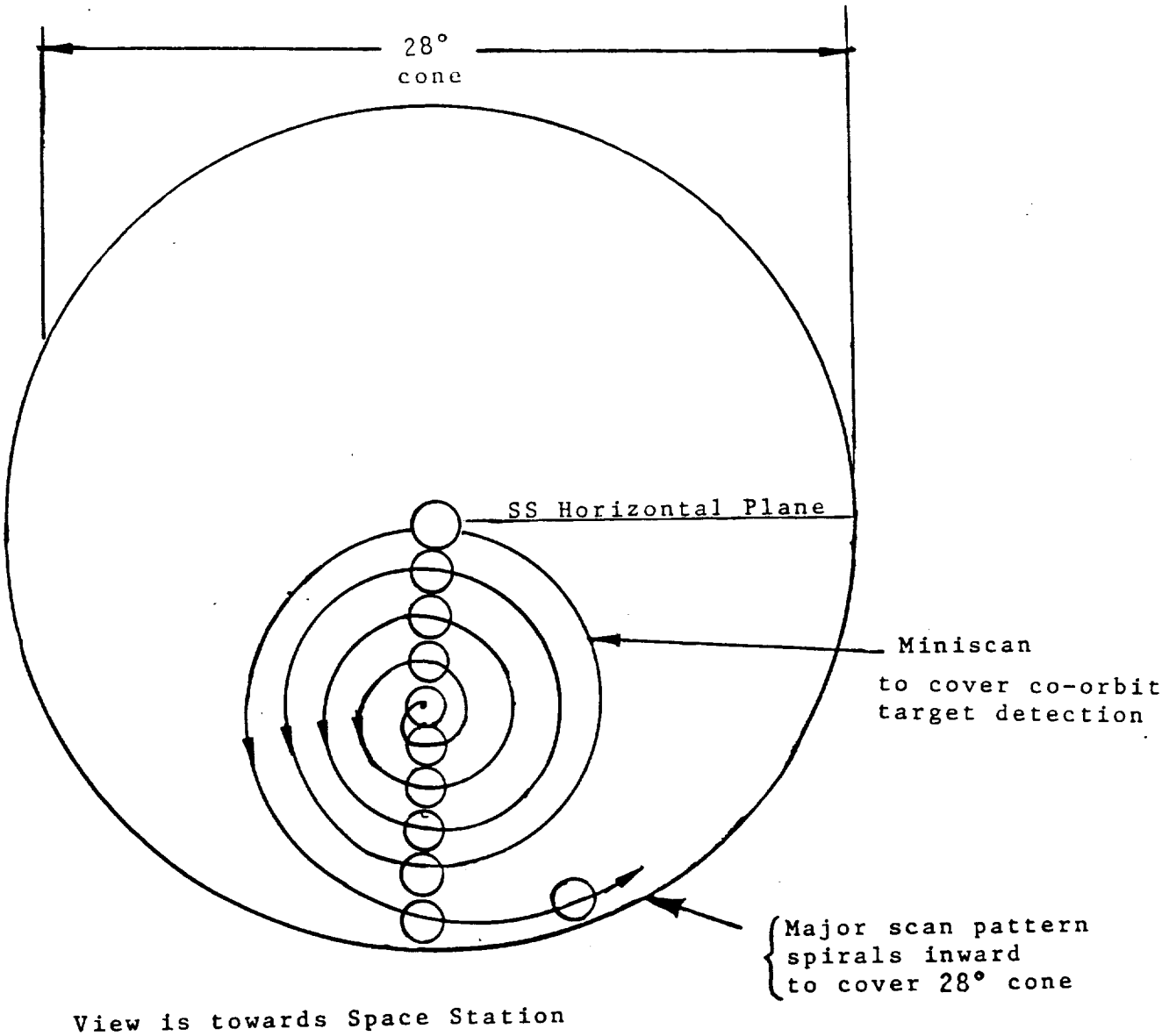

Figure 3-4. Another Possibility of a Mini-scan Within the 28° Cone Coverage

TABLE 4-1. LONG RANGE RADAR TRACKING ACCURACY REQUIREMENTS (3σ VALUES):

1. RANGE: NO REQUIREMENT FOR RADAR SET YET (TBD)

(GPS REQUIREMENT IS ±15 METERS, 1σ VALUE)

AXIOMATIX BASELINE IS 0.01 (1%) OF RANGE

(THIS VALUE MAY IMPROVE AS RESULT OF FURTHER STUDY)

2. VELOCITY: NO REQUIREMENT FOR RADAR SET YET (TBD)

AXIOMATIX BASELINE : ±3 M/SEC TO PROVIDE ORBITAL VELOCITY DIFFERENTIAL RESOLUTION OF 1%

(THIS VALUE MAY CHANGE AS RESULT OF FURTHER STUDY)

3. ANGLE: NO REQUIREMENT FOR RADAR SET YET (TBD)

AXIOMATIX BASELINE : ±0.5° COMMENSURATE WITH 1° RESOLUTION OF RADAR ANTENNA BEAM

(THIS VALUE MAY CHANGE AS RESULT OF FURTHER STUDY)

4. ANGLE RATE: TBD - RADAR TRACKING IN ANGLE IS DERIVED INDIRECTLY FROM ANGLE, RANGE, AND RANGE RATE (TRACK-WHILE-SCAN).

value may be compatible in term of GPS performance. For example, for a pulse radar we have

$$\sigma_{range} = (150 \text{ m/ sec}) \frac{\tau(\mu\text{sec})}{\sqrt{(S/N)n}} \qquad (4\text{-}1)$$

where

τ = radar pulse width
(S/N) = signal-to-noise ratio per pulse
n = number of pulses integrated

Thus, assuming a hypothetical radar which provides at 2000 km the following:

τ = 10 sec
(S/N) = 13 dB (value of 20)
n = 100

we obtain:

$$\sigma_{range} = (150 \text{ m}/\mu\text{sec}) \frac{10\mu\text{sec}}{\sqrt{(20)(100)}} = \frac{150}{4.47} = 33.5 \text{ meters} \qquad (4\text{-}2)$$

This value is the same order or magnitude as the GPS system accuracy. At this point of our investigation we can not guarantee that values in Equation 4-2 do indeed represent a real system at 2000 km. As indicated by link budgets for various radars (see sections 5.1 and 5.2) obtaining SNR's of 10 to 15 dB at 2000 km is not easy. Thus, the final values of range accuracy have to be refined as the result of the study.

Velocity

The value for velocity accuracy was arrived at by taking the 1% value of the difference between the orbital velocities of the lowest orbit of 185 km (Zone 7) and the highest orbit at 889 km (Zone 9). Our estimates indicate that these velocities relative to the Space Station in the 500 km orbit are:

For 185 km orbit: +183 m/sec
For 889 km orbit: -204 m/sec

Thus, the total difference is 387 m/sec and 1% of this value is thus approximately 3.9 meters. We have arbitrarily reduced this

number to 3 m/sec as the baseline to be modified as result of future considerations.

Angle

For long range radar we have baselined a pencil beam antenna pattern of 1° x 1° degree. Based on this beamwidth one can make a conservative assumption of 3σ angle error of 0.5 degree. This is because for SNR's of 10 dB or more the RMS error of a monopulse angle estimator is approximatly

$$\sigma_\theta \cong \frac{\theta_B}{SNR}$$

where θ_B is the 3 dB beamwidth of the antenna pattern and SNR is the signal-to-noise ratio per pulse. Thus, for SNR = 10 dB and θ_B = 1 one obtains:

$$\sigma_\theta \cong \frac{1^\circ}{10} = 0.1^\circ \text{ or } 3 = 0.3^\circ$$

Because of other factors which can not be quantified at this time, such as pointing accuracy, antenna alignment, etc., we are suggesting, conservatively, the value of 0.5°. This value must undergo further scrutiny in the future when a more definitive concept of the long range radar is established.

For example, the question of angular resolution requirement may have to be addressed in view of the relatively narrow angle ($\simeq 0.5^\circ$) subtended by the co-orbital path at distances of the order of 2000 km (see Figure 3-1). With a beamwidth of 1 x 1 degree it may be difficult to resolve targets within the co-orbital corridor if these are targets within the same range gate. However, no such requirement exists formally and thus baselining antenna beamwidths narrower than 1° x 1° may be dictated by considerations other than resolution.

Angle Rate

Because the long range radar baselined here is a track-while-scan radar, the angle rate accuracy requirement, if any,

can not be ascertained at this point. Both the target path geometries and the intrinsic radar capabilites have to be considered to provide some meaningful and realizable value for angle track accuracy. Thus, additional data is required in this area to come up with realistic and realizable requirement.

5.0 POTENTIAL CANDIDATES FOR LONG RANGE RADAR

5.1 Passive Target Radar

In this section the feasibility of radar operation with a passive target is considered from the standpoint of transmitter power requirements to achieve reliable signal detection at the maximum range of 2000 km. Two types of passive targets are considered: 1) skin return and 2) corner reflector. As the subsequent link budgets indicate pulsed, low duty cycle radar operation is difficult to achieve at the maximum range of 2000 km. Thus some assumptions have been made to make the problem at least boundable. These assumptions are:

1) Passive target (skin return): Target cros-section is 10 meters^2 and frequency diversity is used to eliminate target fluctuation (scintillation)

2) Passive target (corner reflector): Target is a corner reflector of 1 meter on a side and thus the radar return is at least 30 dB above 1 m^2 target and frequency diversity is not required.

5.1.1. Skin Return Link Budget for Pulsed Radar

Figure 5-1 shows the link budget for a noncoherent pulsed radar operating on a skin basis return only. The link budget is solved for the peak transmitted power required to

produce a reliable return (P_D=0.9, P_{fa}=10^{-8}) on a single pulse. As stated earlier, it is assumed that frequency diversity is used to provide a non-fluctuating return of 10 m^2 magnitude. Also X-band operation is assumed which helps somewhat with the λ^2-term. The peak power required is about 200 Megawatts. The average power is based on 13.3 msec round-trip time to a target at 2000 km:

$$P_{ave} = (200\ MW) \times \frac{10\ Sec}{13{,}300\ Sec} = (200\ MW)(0.00075)$$
$$= 0.150\ MW$$
$$= 150\ KW$$

These numbers are totally unreasonable for the task on hand. If we considered integrating* up to 1000 pulses, which would require a dwell time of 13.3 seconds for each target, the power requirement reduction would be:

$$P_p\ (1000) = \frac{200\ MW}{1000} = 0.2\ MW = 200\ Kilowatts$$

and

$$P_{ave}\ (1000) = \frac{150\ MW}{1000} = 150\ watts$$

This is somewhat reasonable and is within a realm of being "doable" with conventional pulse radar. However, there is no margin allowance and any additional losses will bring the peak power requirement back up to megawatts and the average power requirement into the killowatt region. Consequently, we have to consider such aids as the use of a corner reflector to reduce the power requirements for the radar.

5.1.2 Reflector Return Link Budget for Pulsed Radar

Excessive peak and average powers required of long range radars to work with skin return necessitate considerations of augmenting the target return with a passive reflector. An alternative, of course, would be to use a beacon (transponder) but this presents a different problem which is discussed in Section 5.2.

* Coherent integration assumed here. Noncoherent integration will result in lower gains.

For a pulsed radar using skin return only,

For radar the Signal-to-Noise Ratio is:

$$(S/N) = \frac{P_T G^2 \lambda^2 \sigma L_T}{(4\pi)^3 R^4 (NF)(kT)BL_R}$$

where

P_T = Transmitter power (peak), W

G = Antenna gain

λ = Wavelength (meters)

σ = Target crossection ($meter^2$)

L_T = Transmitter losses

R = Range (meters)

NF = Receiver noise figure

B = Receiver bandwidth (Hz)

L_R = Receiver losses

$(kT) = -204$ dBW/Hz

The link budget (in dB) becomes:

P_T	= TBD	$(4\pi)^3$	= 33 dB
G^2	= 89 dB (1°x1°)	R^4	= 252 dB (2000 km)
λ^2	= -30.5 dB-m^2 (10 GHz)	NF	= 3 dB
σ	= 10 dB	KT	= -204 dBW/Hz
L_T	= -1 dB	L_R	= 2
		B	= 50 dB-Hz (10 μsec pulse)
	+67.5 dBW		+136 dBW

$(S/N)^*$ = 14.2 dBW = P_T (dBW) + 67.5 dBW - 136 dBW

P_T = 14.2 dBW - 67.5 dBW + 136 dBW = 82.7 dBW

or approximately 200 Megawatts!

*For P_d = 0.90

$P_{fa} = 10^{-8}$

Figure 5-1 Link Budget for Detection of Skin Return Target at 2000 Km (Pulsed Radar)

For baseline calculations that follow, we have considered a corner reflector return of 1 meter on a side. The details pertaining to corner reflector return are given in Appendix A. At X-band (10 GHz) the return from this corner refector is +36.7 dB above the return from a 1 square meter target. As indicated by the link budget in Figure 5-2, the use of a corner reflector makes pulse radar operation more feasible. Assuming again as in the previous case that one could integrate 1000 pulses, we obtain:

$$P_T \text{ (peak)} = \frac{40 \text{ kW}}{1000} = 0.4 \text{ kW or } 400 \text{ watts}$$

$$P_{AVE} = \frac{300 \text{ watts}}{1000} = 0.3 \text{ watts or } 300$$

5.1.3 Reflector Return Link Budget for FM/CW Radar

The FM/CW radar permits long signal integration times without summing up large numbers of individual pulses. Furthermore, 100% duty cycle of the FM/CW radar lowers the requirements for peak power. The latter feature is particularly attractive if one is considering utilization of shuttle orbiter's existing Ku-band radar system.

Figure 5-3 is a link budget for the FM/CW radar working with a corner reflector (1 meter on a side) at 2000 km. From this link budget it is evident that a reasonable margin exists if one utilizes the existing Ku-band radar tube for the long range radar.

Specifically for a 50 watt CW tube (Shuttle Ku-band radar) the margin is:

$$\text{Margin (dB)} = 100 \log \left(\frac{50W}{4W} \right) = 10 \log (12.5) = 11 \text{ dB}$$

It must be pointed out, however, that with a CW radar the transmitter is on all the time and thus means for minimizing the effects of this leakage on the receiver must be provided. Such means do exist but their discussion is postponed until subsequent reports when a better idea of implementation requirements is obtained.

For a pulsed radar with a corner reflector, the Signal-to-Noise Ratio is:

$$(S/N) = \frac{P_T G^2 \lambda^2 \sigma L_T}{(4\pi)^3 R^4 (NF)(kT)BL_R}$$

where

P_T = Transmitter power (peak), W
G = Antenna gain
λ = Wavelength (meters)
σ = Target cross-sectio(meter^2)
L_T = Transmitter losses
R = Range (meters)
NF = Receiver noise figure
B = Receiver bandwidth (Hz)
L_R = Receiver losses

(kT) = -204 dBw/Hz

The link budget (in dB) is:

P_T	= TBD	$(4\pi)^3$	= 33 dB
G^2	= 89 dB (1°x1°)	R^4	= 252 dB (2000 km)
λ^2	= -30.5 dB-m^2(10GHz)	NF	= 3dB
σ	= 36.7 dB-m^2(Corner Reflect)	T	=-204 dBW/Hz
L_T	= -1 dB	L_R	= 2dB
		B	= 50 dB-Hz(10 μsec pulse)
	+ 94.2 dBW		+136 dB

$(S/N)^*$ = 14.2 dBW = P_T (dBW) + 67.5 dBW - 136 dBW
= P_T (dBW) - 41.8 dBW

*P_d =0.90
$P_{fa}=10^{-8}$

P_T = 14.2 dBW + 41.8 dBW = 56 dBW or 400 kW peak power

P_{AVE} = (Peak power)x(Duty cycle)
= (400 kw)(0.00075)=0.300kw or 300 watts

Figure 5-2. Link Budget for Detection of a Corner Reflector at 2000 Km. (Pulsed Radar)

For the FM/CW radar using a corner reflector, radar the Signal-to-Noise Ratio is:

$$(S/N) = \frac{P_T G^2 \lambda^2 \sigma L_T}{(4\pi)^3 R^4 (NF)(kT)BL_R}$$

where

P_T = Transmitter power (peak),
G = Antenna gain
λ = Wavelength (meters)
σ = Target cross-section (meter^2)
L_T = Transmitter losses
R = Range (meters)
NF = Receiver noise figure
B = Receiver bandwidth (Hz)
L_R = Receiver losses

(kT) = -204 dBW/Hz

The link budget (in dB) is:

P_T	= TBD	$(4\pi)^3$	= 33 dB
G^2	= 89 dB (1°x1°)	R^4	= 252 dB (2000 km)
λ^2	= -33.3 dB-m^2 (13.9 GHz)	NF	= 3 dB
σ	= 39.4 dB-m^2 (corner Reflect)	KT	= -204 dBW/Hz
L_T	= -1dB	L_R	= 2 dB
		B	= 0 dB-Hz (1 Hz BW)
	P_T+94.1 dBW		+86 dBW

$(S/N)^*$ = 14.2 dBW = P_T (dBW) + 94.1 dBW - 86 dBW

= P_T (dBW) + 8.1 dBW

P_T = 14.2 dBW - 8.1 dBW = 6.1dBW or 4 watts (CW Power)

*For P_d = 0.90, P_{fa} = 10^{-8}

Figure 5-3 Link Budget for Detection of Corner Reflector Target with FM/CW Radar

Another area of implementation trade-off is the requirement for 1 Hz signal detection bandwidth. Such detection bandwidth must be implemented by digital techniques not only because of bandwidth but also because a large number of filters will be required. Such techniques as DFT and/or FFT can be utilzed, however. Also, in conjunction with the 1 Hz detection bandwidth assumption, there is a question of spectral linewidth at Ku-band. Specifically, a bandwidth of 1 Hz requires an extremely "clean" signal to provide reliable detection. Again, the implementation questions will be relegated to a subsequent report.

Despite all of the above-mentioned implementation considerations, the FM/CW radar appears a highly viable candidate for long-range radar, particularly if the Shuttle Ku-band radar can be modified to perform this function. Preliminary considerations along these lines are given in section 5-3 of this report.

5.2 Active Transponder (Beacon) Radar Performance

Use of a transponder on a free flyer is an alternative to using a corner reflector of large aperture. When considering a transponder, two links must be defined: 1) radar-to-transponder link and 2) transponder-to-radar link. In general, having two links provides for flexibility of optimizing each link. In the baseline examples considered below, however, the assumption is made that the two links operate within the same band and thus the same wavelength can be assumed for both links. It is also assumed that both links utilize the same pulse widths. Of specific importance is our baseline assumption that the beacon-based long range radar is to operate in the Ku-band as a modified Ku-band radar system of the Space Shuttle. This is the reason for using 13.9 GHz as the baseline frequency for both link budgets presented below.

5.2.1 Radar-to-Beacon Link Power Budget

Figure 5-4 shows the power budget for the radar-to-beacon link at 2000 km. An omni antenna and a mixer receiver are assumed for the beacon transponder. From the link budget we see that within the assumptions shown the peak power required is 15.5 watts. Considering that the Ku-band Shuttle radar TWTA produces 50 watts peak, the margin is:

$$\text{Margin} = 10 \log \left(\frac{50 \text{ W}}{15.5 \text{ W}} \right) = 10 \log (3.23) = 5.1 \text{ dB}$$

This is not what one may call a "generous" margin. One may keep in mind that we are dealing with a single pulse detection budget. Normally one would consider integration of several pulses thus, improving the margin and increasing link reliability. The important fact is that the 50 watt peak power capability of the present Ku-band system appears to be adequate for radar/beacon operation at 2000 km.

5.2.2 Beacon-to-Radar Link Power Budget

Figure 5-5 shows the baseline power budget for the beacon-to-radar link. As stated previously, we have made an assumption that the transponder reply has the same 10 μsec pulse width as the interrogating radar.

This link budget indicates that about 3 watts peak transmitter power is required from the transponder. If one were to increase this power to 10 to 15 watts, margins of about 5 dB and 7 dB, respectively, could be realized. Additional margin could be realized from multiple-pulse integration of the beacon reply.

The important conclusion indicated from the baseline link budget is that the peak power required is within the capability of solid state devices at Ku-band. Furthermore, the relatively low average power requirement is compatible with beacon operation on a free-flyer or another vehicle which is limited in its capacity to provide large amounts of prime power.

The Radar-to-Beacon Link Signal-to-Noise Ratio is:

$$(S/N)_B = \frac{P_r\, G_r\, G_b\, \lambda^2\, L_r}{(4\pi)^2\, R^2\, (NF_b)(kT)(B_b)L_b}$$

where

P_r = Radar Tx power

G_r = Radar Antenna Gain

λ = Wavelength

G_b = Beacon Antenna Gain

L_r = Radar Tx losses

R = Range (meters)

NF_b = Beacon Rx Noise Figure

B_b = Beacon Receiver Bandwidth (Hz)

L_b = Beacon R_x losses

kT = -204 dBW/Hz

P_r = TBD	$(4\pi)^2$ = 22 dB
G_r = 44.5 dB (1°x1°)	R^2 = 126 dB (2000 km)
G_b = 0 dB (Omni)	NF_b = 10 dB (Mixer receiver)
λ^2 = -33.3 dB-m^2 (13.9 GHz)	kT = -204 dBW/Hz
L_r = -3 dB	B_b = 50 dB-Hz (100 kHz, 10 μsec pulse)
	L_b = 2 dB
+ 8.2W	+6 dBW

$(S/N)^*$ = 14.2 dBW = P_T (dBW) + 8.3 dBW - 6dBW = P_T (dBW) + 2.3 dBW

*For P_D = 0.90, $P_{fa} = 10^{-8}$

P_r = 14.2 dBW - 2.2dBW = 12.0 dBW or 15.9 watts (peak)

P_r(ave) = (Peak Power) x (Duty cycle)

= (15.9w)(0.00075) = 0.012 watts or 12 millwatts

Figure 5-4 Radar-to-Beacon Link Budget for 2000 Km Range (Pulsed Radar)

The Beacon-to-Radar Link Signal to-Noise Ratio is:

$$(S/N)_R = \frac{P_b\, G_b\, G_r\, \lambda^2\, L_b}{(4\pi)^2\, R^2\, (NF_r)(kT)(B_r)L_r}$$

where

P_b = Beacon Tx Power (Peak)
G_r = Radar Antenna Gain
G_b = Beacon Antenna Gain
λ = Wavelength
L_b = Beacon Tx losses
R = Range (meters)
NF_r = Radar Rx Noise Figure
B_r = Radar Rx Bandwidth
L_r = Radar receiver (Rx) losses

and kT = -204 dBW/Hz

P_b	= TBD	$(4\pi)^2$	= 22 dB
G_b	= 0 dB	R^2	= 126 dB (2000 km)
G_r	= 44.5 dB (1°x1°)	NF_r	= 3 dB
λ^2	= -33.2 dB-m^2 (13.9 GHz)	kT	= -204 dBW/Hz
L_b	= -2dB	B_r	= 50 dB-Hz (100 khz, 10 μsec pulse)
		L_r	= 3 dB
	+9.2 dBW		0 dBW

$(S/N)^*$ = 14.2 dBW = P_b(dBW) + 9.2 dBW + 0 dBW *For P_d = 0.9

P_b = 14.2 dB-9.2 dBW = 5.0 dBW or $\frac{3.2 \text{ watts}}{\text{(peak)}}$ $P_{fa}=10^{-8}$

P_b(ave) = (Peak Power) x (Duty Cycle)

= (3.2W)(0.00075) = 0.0024 W or 2.4 milliwatts

Figure 5-5. Beacon-to-Radar Link Budget for 2000 Km Range (Pulsed Beacon)

5.3 Potential Application of Present Shuttle Orbiter Ku-Band System

From the baseline analysis presented in the previous sections it is evident that, at least within the framework of the assumptions used, there could be a utilzation of a 50 watt peak and average power transmitter at Ku-band for radar operation up to 2000 km. This fact points to potential utilization, with some modifications of course, of the currently operational Shuttle orbiter Ku-band radar/communication system.

At this point of the study it is too early to specify detailed modifications to be performed on this system. However, we can outline a possible approach towards modifying the present system for long range operation with either a corner reflector (passive mode) or a transponder (active mode). Preliminary ideas on this subject are listed below.

1) Retain with modifications the DEA (Deployed Electronics Assembly), DMA (Deployed Mechanical Assembly), EA-2 (Radar Assembly), and the EA-1 (Antenna Control Electronics) and possibly the SPA (Signal Processing Asseembly)

2) Increase the antenna dish size to 5-foot diameter and, if possible, retain the α and β - axis drive system without modifications.

3) Improve the antenna feed efficiency by simplifying to single polarization. Another possibility may be to replace the rotary joints by sections of flexible waveguide to minimize losses.

4) Consider removing the monopulse capability to simplify system and to improve the efficiency of the RF subsystem. The removal of the monopulse capability may be permitted by the fact

that no monopulse tracking is required of the long range radar. The tracking to be performed can be of the track-while-scan type which may obtain angular information on targets without requiring the monopulse capability.

These changes and/or modifications are only qualitative. It will be one of the objectives on this program to identify the possible adaptations of the Shuttle Ku-band system in a quantitative manner and to determine the true utilzation potential of the present Shuttle Ku-band system.

5.4 Radar Operating Frequency Trade-offs

In considering a radar system design, the operating frequency may be a trade-off parameter which will permit optimizing the performance of the planned system. In the previous sections we have baselined link budgets for X-band (10 GHz) and Ku-band (13.9 GHz) operation. At this point it may be worthwhile to consider tradeoffs, if any, which can be gained from operating at other frequencies. Some facts, however, are obvious and can be stated as follows:

1) Operation with a Corner Reflector

Operation with corner reflector is frequency independent from the standpoint of the range equation in that the λ^2 terms cancel. Specifically, the decrease in radar receiver antenna aperture at higher frequencies is cancelled by the increase in the effective cross-section of the corner reflector. Thus, frequency of operation must be determined by factors other than the range equation. Such factors are: availability of RF components, physical dimensions of antennas and corner reflector, noise figure, frequency allocations, etc.

2) Operation with a Transponder

Operation with a transponder beacon, however, is dependent on operation frequency. The dependence enters as the effective cross-sections of both the beacon receiver antenna and as the antenna aperture of the radar receiver. Figure 5-6 shows the dependence of radar peak power and the radar antenna size on frequency. From this figure it becomes evident that at frequencies below Shuttle Ku-band radar operation (13.9 GHz) antenna dimensions become excessive and peak power must be increased to reduce dish size and to provide for margin. Other methods for achieving this may be to provide multiple pulse integration.

On the other hand, reducing the size of the antenna by operating at frequenencies above 15 GHz places a demand on transmitter power. The latter is not easily obtained at higher frequencies with solid state devices.

3) Doppler Rate Considerations

Doppler rate enters into the radar operating frequency consideration if one contemplates the use of doppler shift for velocity measurement of the target. This is particularly true if pulse doppler radar is used instead of CW radar. Figure 5-7 shows the relative doppler shift vs. radar operating frequency and the relative orbits of the possible targets. Although the plot is for coplanar orbits and thus shows only the minimum dopplers without cross components, it never-the-less is of value for determining the PRF requirements for a pulse doppler radar.

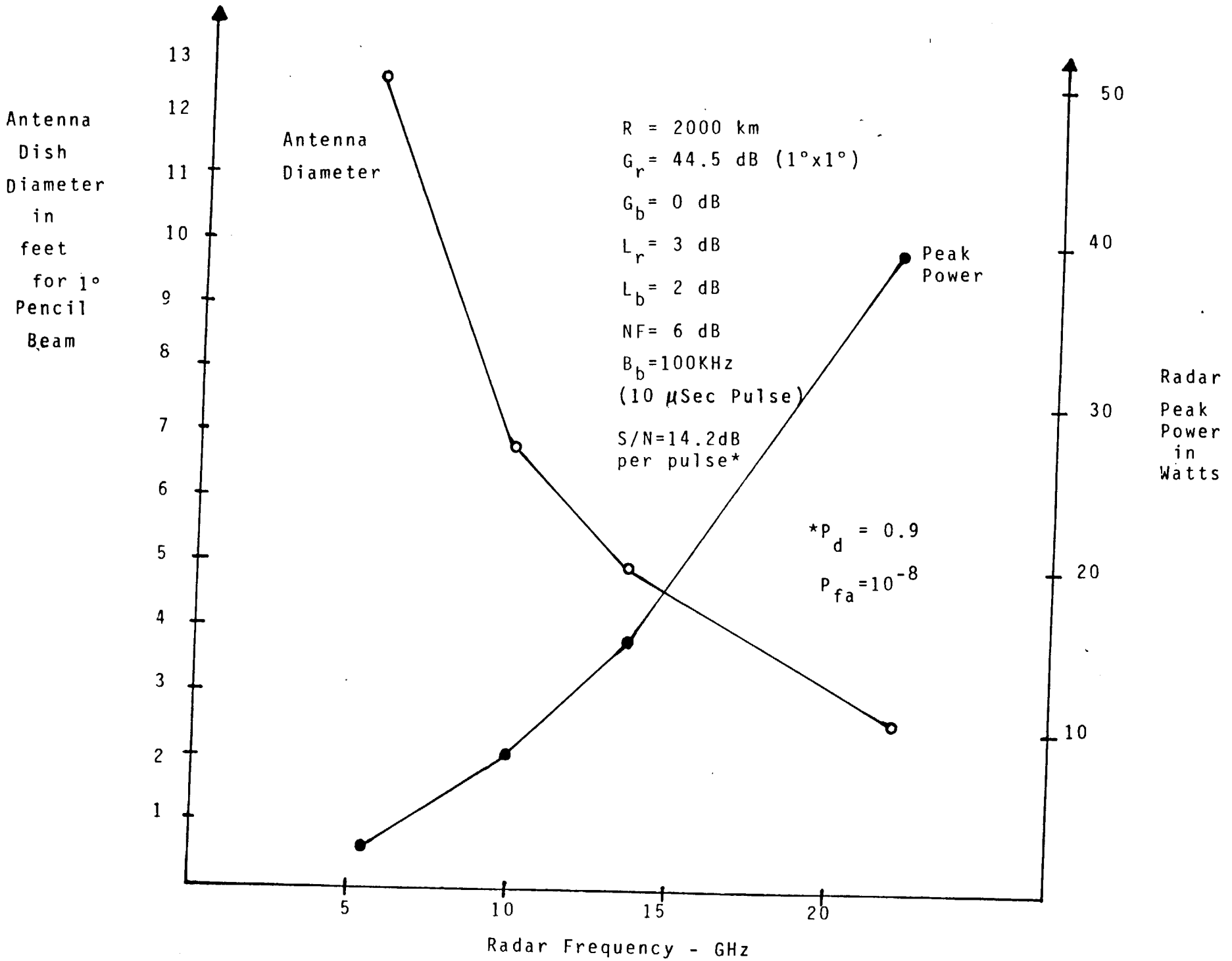

Figure 5-6 Radar Power and Antenna Size Requirements for Radar/Transponders System vs. Frequency (R = 2000 Km)

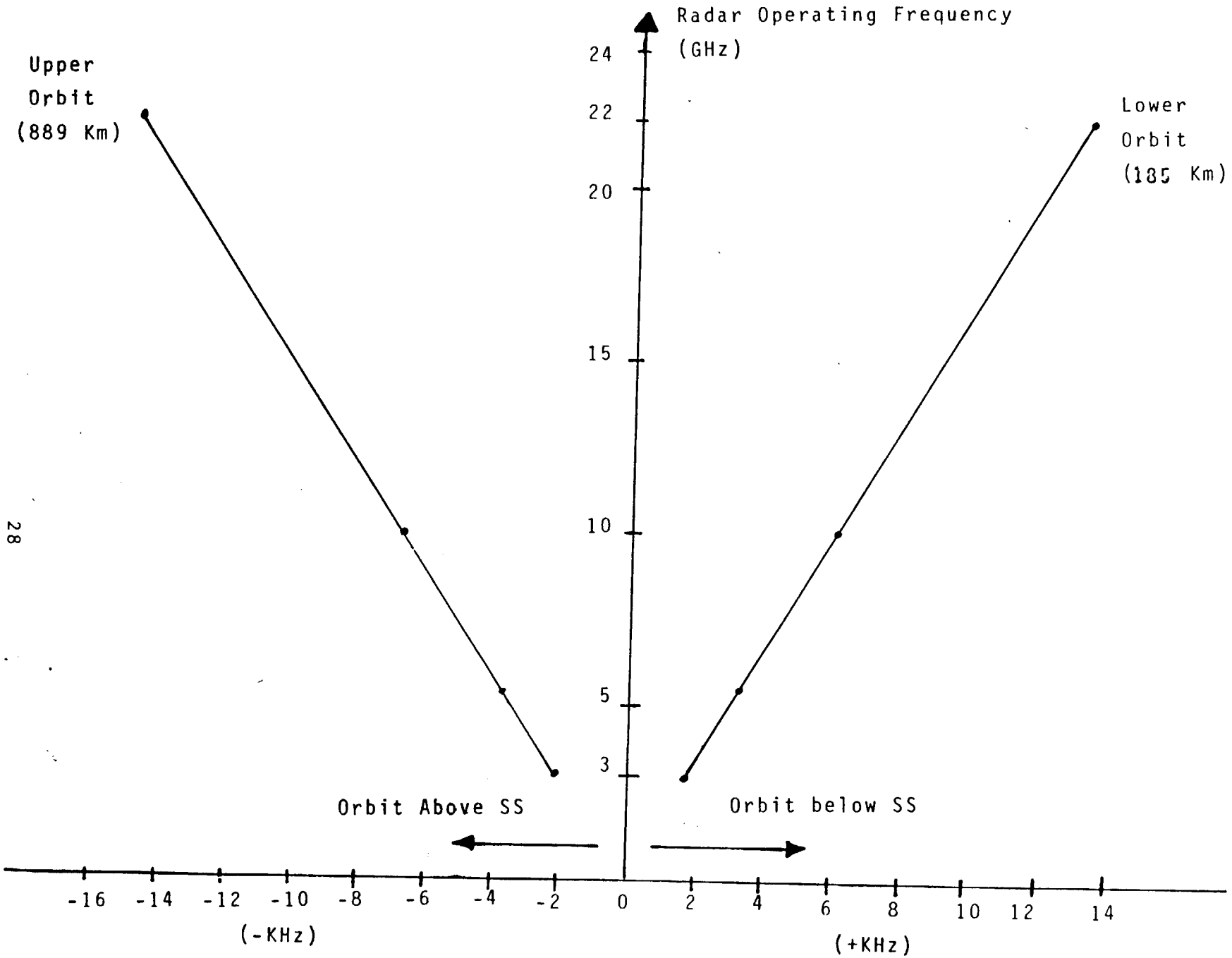

Figure 5-7 Relative Doppler Shift vs Orbit and Operating Frequency

5.5 Long Range Radar Potential Candidates Summary

Table 5-1 provides the summary of the potential candidates for the long range radar to cover the 185 km to 2000 km range of the co-orbital zones.

Table 5-1 Long Range * Radar Potential Candidates

RADAR TYPE	TARGET	ADVANTAGE	DISADVANTAGE
PULSED (LOW PRF)	SKIN RETURN	• NO REQUIREMENTS ON TARGET COOPERATION • ORIENTATION OF TARGET NOT CRITICAL	• PEAK POWERS IN MEGAWATT RANGE ARE REQUIRED • FREQUENCY DIVERSITY REQUIRED TO REDUCE FLUCTUATION LOSS • AVERAGE POWERS IN KILOWATT RANGE
PULSED (LOW PRF)	CORNER REFLECTOR (1 METER SIDE)	• PEAK POWER REDUCED TO 100 KW RANGE • AVERAGE POWER ON ORDER OF 100 W • FREQUENCY DIVERSITY NOT REQUIRED • SIMPLICITY	• PEAK POWER STILL EXCESSIVE FOR SS ENVIRONMENT • RETURN STRENGTH IS FUNCTION OF REFLECTOR ORIENTATION

*LONG RANGE: 185 KM TO 2000 KM (CO-ORBITAL ZONES)

Table 5-1 Long Range Radar Potential Candidates- continued

RADAR TYPE	TARGET	ADVANTAGES	DISADVANTAGES
PULSED, COHERENT (HIGH PRF)	CORNER REFLECTOR (1 M SIDE)	• PROVIDES FOR REDUCTION OF PEAK POWER TO KW RANGE OR UNDER • ACCURATE VOLOCITY TRACKING	• MULTIPLE PRF MUST BE USED TO RESOLVE RANGE AMBIGUITIES • RETURN STRENGTH IS FUNCTION OF REFLECTOR ORIENTATION
FM/CW	CORNER REFLECTOR (1 M SIDE)	• 50 W CW POWER ADEQUATE FOR REFLECTOR DETECTION AT 2000 KM • ACCURATE VELOCITY TRACKING • ACCURATE RANGE TRACKING	• REQUIRES TRANSMITTER (TX) LEAKAGE SUPPRESSION • REQUIRES TX SIGNAL OF HIGH PURITY • LONG INTEGRATION TIME (UP TO 1 SEC) IS REQUIRED • RETURN STRENGTH IS FUNCTION OF REFLECTION ORIENTATION
PULSED (LOW PRF)	BEACON (TRANSPONDER)	• 50 W PEAK POWER ADEQUATE FOR TARGET REPLY AT 2000 KM • WITH OMNI BEACON ANTENNA USER ORIENTATION NOT CRITICAL • GROUND RETURN IS NOT A PROBLEM	• REQUIRES BEACON (TRANSPONDER) ON EACH USER VEHICLE • SIDELOBE INTERROGATION MAY BE A PROBLEM AT CLOSE RANGES

6.0 CONCLUSIONS

As the result of our intitial effort to determine the feasibility of long range radar operation to cover the co-orbital zones extending from 185 km to 2000km, the following conclusions have been reached:

- Several candidates have been identified as workable radars with passive reflectors
- Cooperative target (beacon) radar is also a viable solution with low-power (50 watts peak) radar
- Detailed trade-offs are being considered

Appendix A

Corner Reflector Effective Area Considerations

Appendix A

Corner Reflector Effective Area Considerations

The corner reflector can make it possible to detect targets at long ranges with moderate amounts of transmitted power. In this appendix we consider quantitatively the performance of the trihedral corner reflector consisting of triangle sides as shown in Figure 1-A.

The effective radar cross-section of a trihedral reflector is

$$= \frac{4\pi a^4}{3\ \lambda^2} \qquad \text{(A-1)}$$

where

σ = effective cross-section

a = edge length

λ = wavelength

For example, at 10 GHz the wavelength $\lambda = 0.03$ meters (3 cm). Assuming an edge length of 1 meter, one obtains for σ :

$$\sigma = \left(\frac{4\pi}{3}\right)\frac{(1\text{m})^4}{(0.03)^2} = (4.19)/(9\text{x}10^{-4}) = 2656\text{m}^2 \text{ or } 36.7 \text{ dB with respect to } 1\text{m}^2 \text{ target.}$$

Figure A-1 shows the effective cross-section of a corner reflector as a function of edge length and operating frequency.

Figure A-2 shows the effect of corner reflector orientation upon the strength of the return. The surface shown in the figure is for a corner reflector that peaks at 40 dB. From this figure,, it is evident that within a cone defined by $\pm 20^\circ$ (i.e. 40° total) the corner reflector return decreases by no more than 5 dB.

Figure A-1 Corner Reflector Effective Crossection vs. Edge Length and Frequency

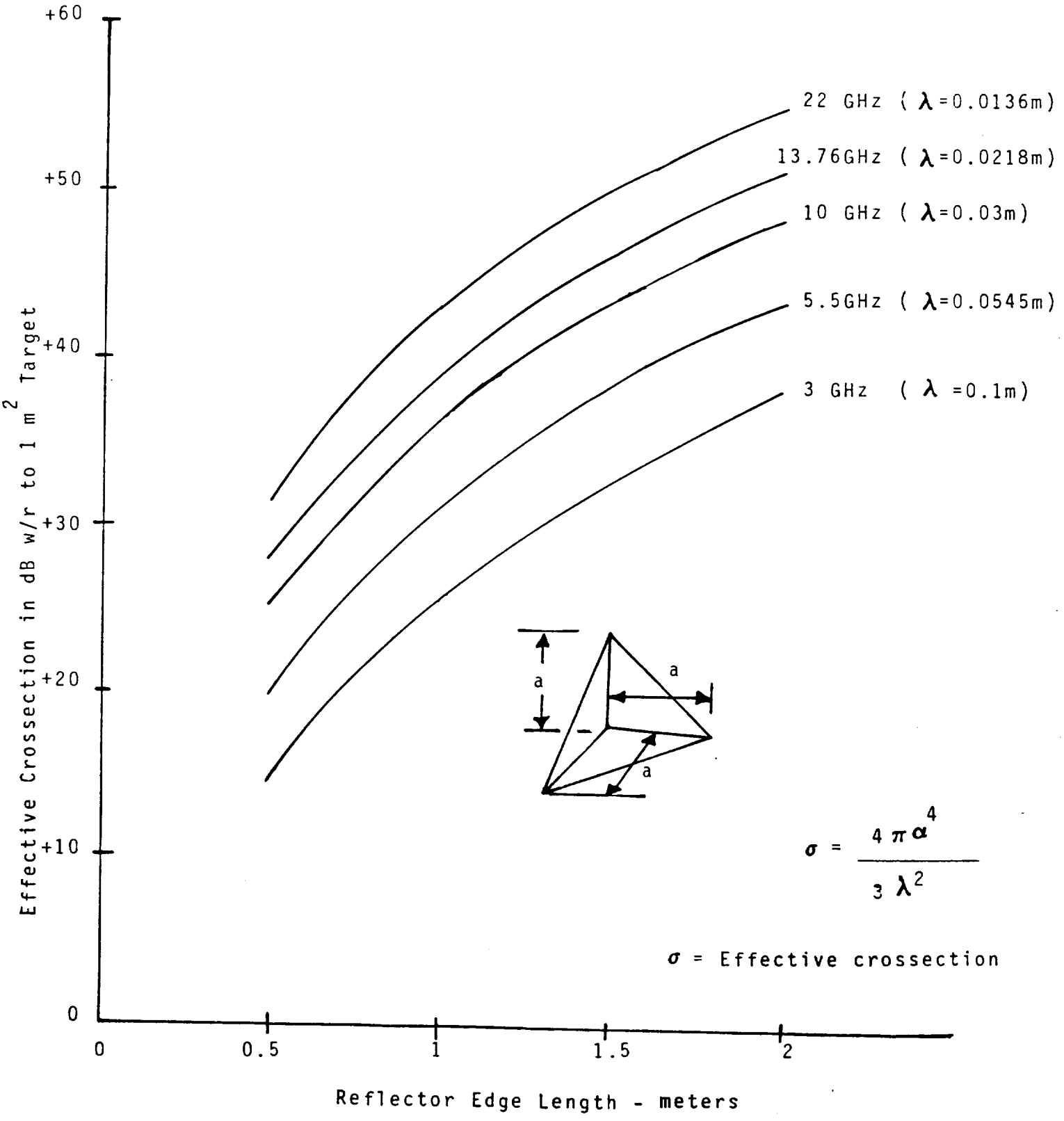

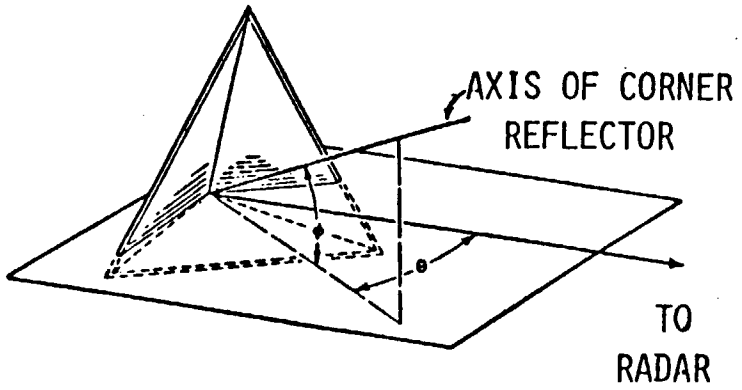

ANGLES BETWEEN THE AXIS OF CORNER REFLECTOR AND THE DIRECTION TO A DISTANT RADAR.

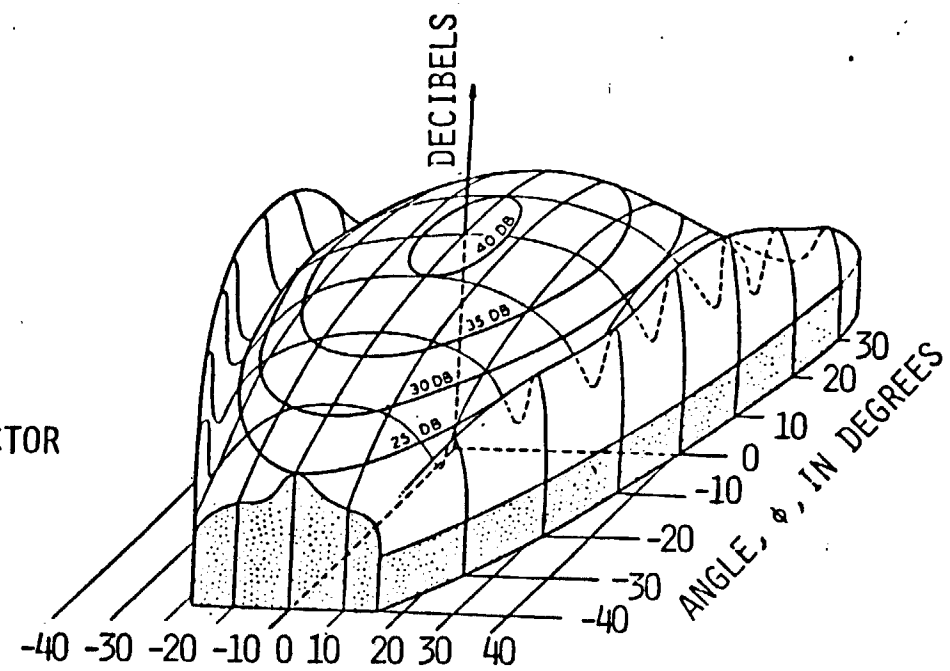

COMPOSITE SURFACE REPRESENTING SIGNAL LEVELS RETURNED BY A TYPICAL CORNER REFLECTOR

BOTTOM LINE: WITHIN A CONE DEFINED BY ±20° (40° TOTAL) THE RETURN DOES NOT DECREASE BY MORE THAN 5 dB

Figure A-2. Corner Reflector return vs. Orientation

Reference

[1] Space Station Reference Configuration Description; JSC-19989, Systems Engineering and Integration Space Station Program office/JSC, August 1984.

APPENDIX F

SPACE STATION RADAR CONSIDERATION

SPACE STATION RADAR CONSIDERATION

S. UDALOV
AXIOMATIX

APRIL 22, 1986

SPACE STATION RADAR REQUIREMENTS

Axiomatix

	SPACE STATION SPECIFICATIONS	CONTRACTOR SUGGESTED VALUES
MAXIMUM RANGE	20 NM (37 km)	
MINIMUM RANGE	1640 FT. (500 m)	
ANGULAR COVERAGE	4 PI STERADIANS	
REQUIRED FUNCITONS : (A) SEARCH AND ACQUISITION (B) TRACKING		
TARGET TYPES:		
NON-COOPERATIVE TARGETS MINIMUM RADAR CROSS SECTION	1 SQ. METER	
*SEARCH TIME (2 PI STERADIANS)		1 MINUTE
*TRACKING UPDATE RATE		10 Hz
NO. SIMULATIONS TRACKS/HEMISPHERE	4	
RANGE ACCURACY (ONE SIGMA)	328 FT. OR 1%	
RANGE RATE ACCURACY (ONE SIGMA)	1 FT./SEC. OR 1%	
ANGLE ACCURACY (ONE SIGMA)	10 MILS	
* PROBABILITY OF DETECTION (SINGLE DWELL)		0.9
*EXPECTED FALSE ALARMS/MINUTE		20
GROWTH CAPABILITY (TARGETS/HEMISPHERE)	8	

*ALL REQUIREMENTS, EXCEPT THESE, TAKEN FROM RFP OR REFERENCE CONFIGURATION DESCRIPTION. THESE REQUIREMENTS ADDED, CONSISTENT WITH RFP AND RCD, TO PROVIDE COMPLETE SET OF REQUIREMENTS FOR TRADEOFF ANALYSIS.

KU-BAND RENDEZVOUS RADAR LOCATION ON SPACE STATION

Axiomatix

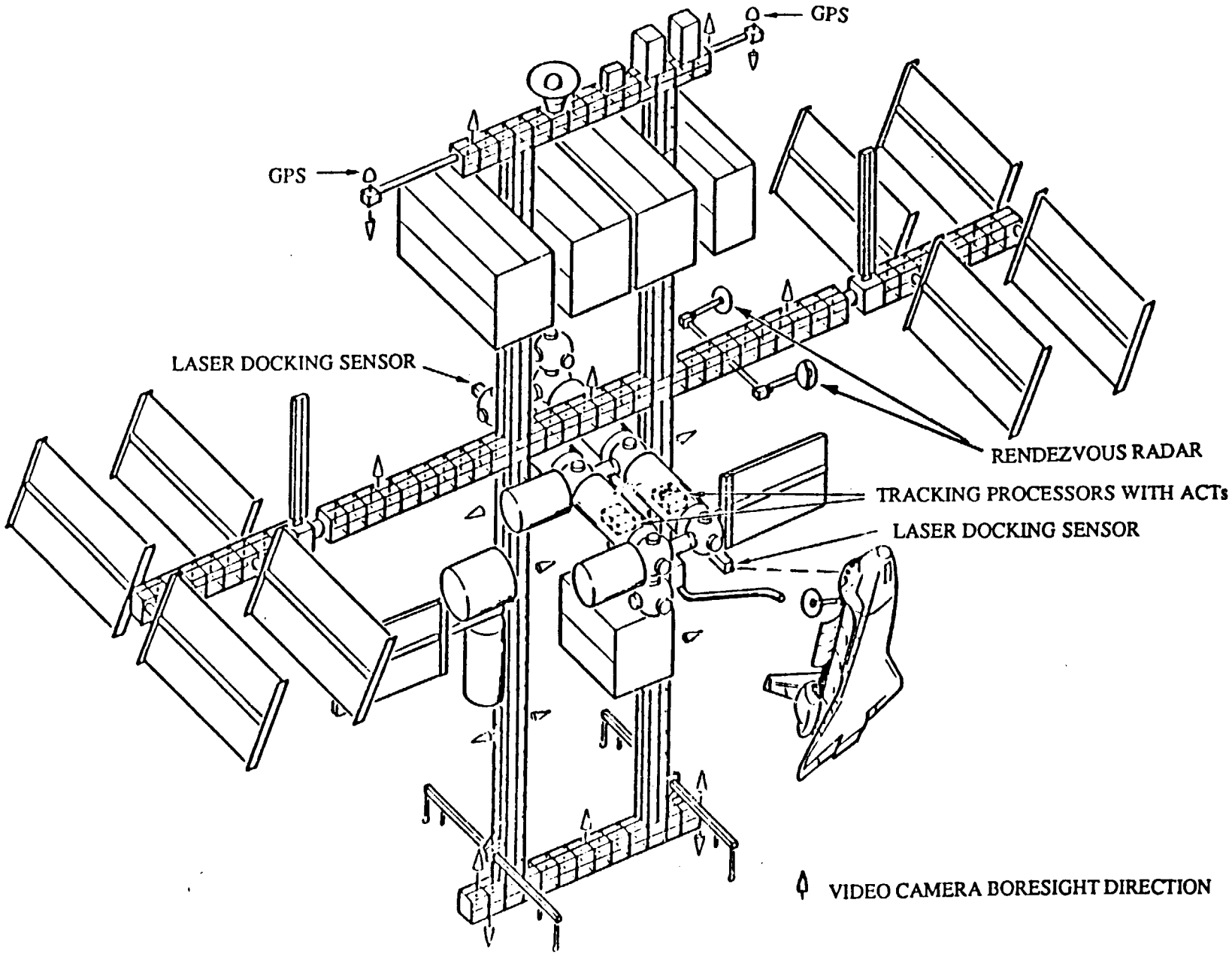

MODIFIED SHUTTLE KU-BAND RADAR COVERAGE FOR SPACE STATION

Axiomatix

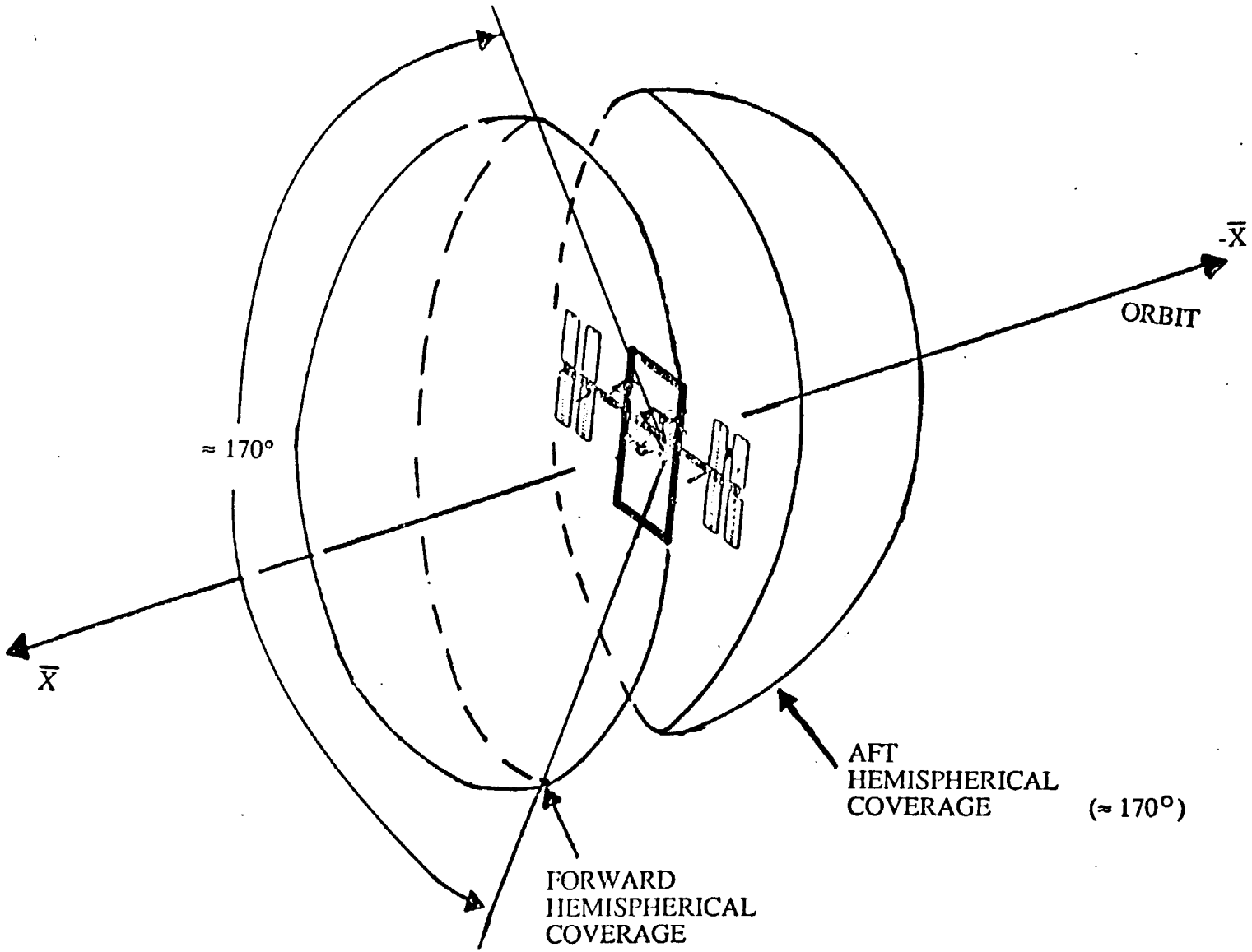

MODIFIED KU-BAND RADAR TARGET DETECTION DWELL TIME REQUIREMENT VS. SYSTEM LOSSES

Axiomatix

DETECTION CRITERION: (SINGLE SCAN)

Pd = 0.9, $P_{fa} = 10^{-6}$

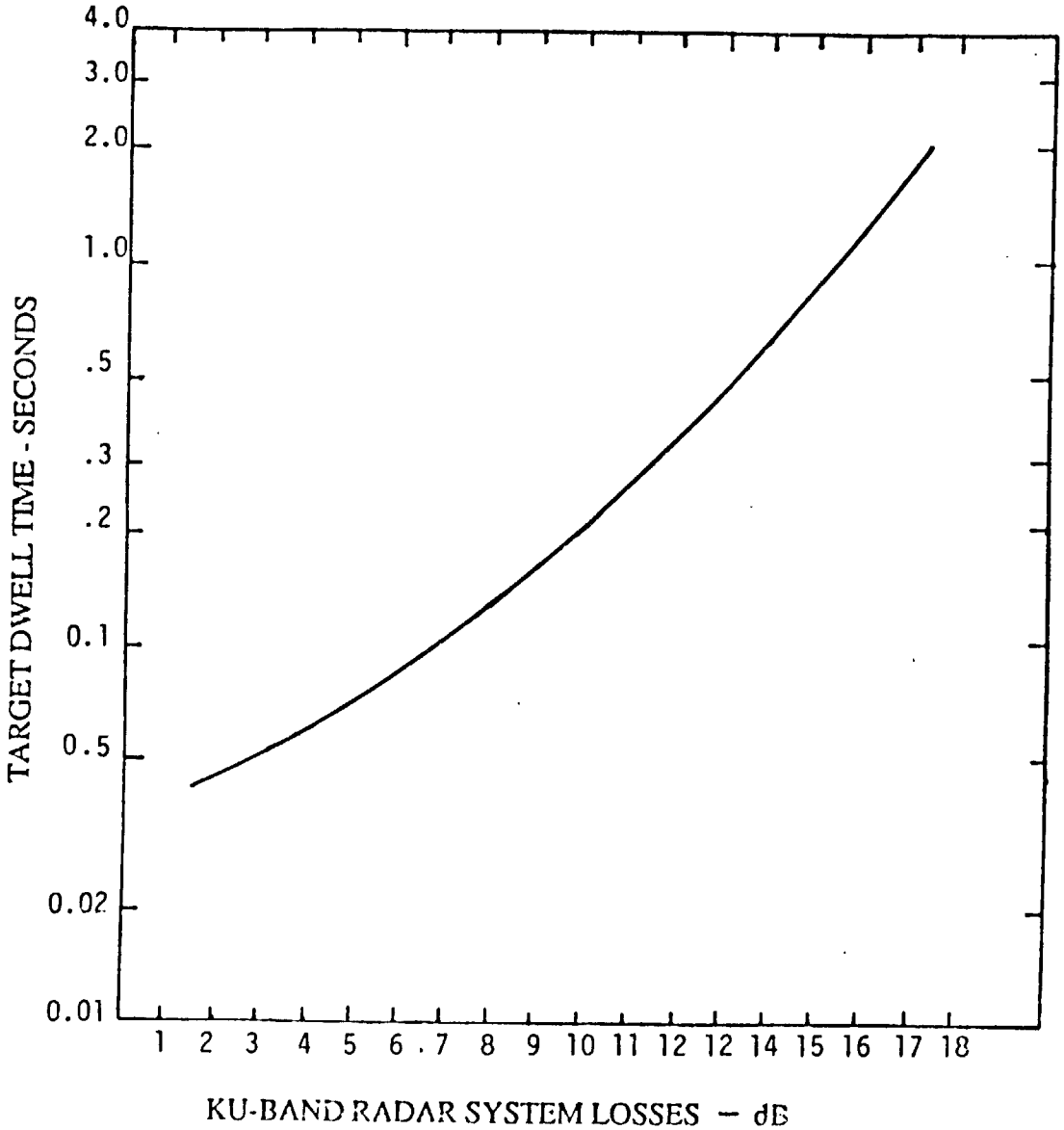

RADAR PARAMETERS

P_p = 50 Watts

PRF = 2985 Hz

R_{max} = 20 nmi (37 km)

τ = 66μ sec (pulse width)

d_t = 0.197 (duty factor)

G_A = 37.7 dB

σ = 1 m^2

λ = 0.0216 m (f = 13.89 GHz)

T_s = 1500° K

N_c = 64 (coherent int. pulses)

RADAR BEAM ANGULAR RATES DUE TO ORBITAL VELOCITY DIFFERENCE

Axiornatix

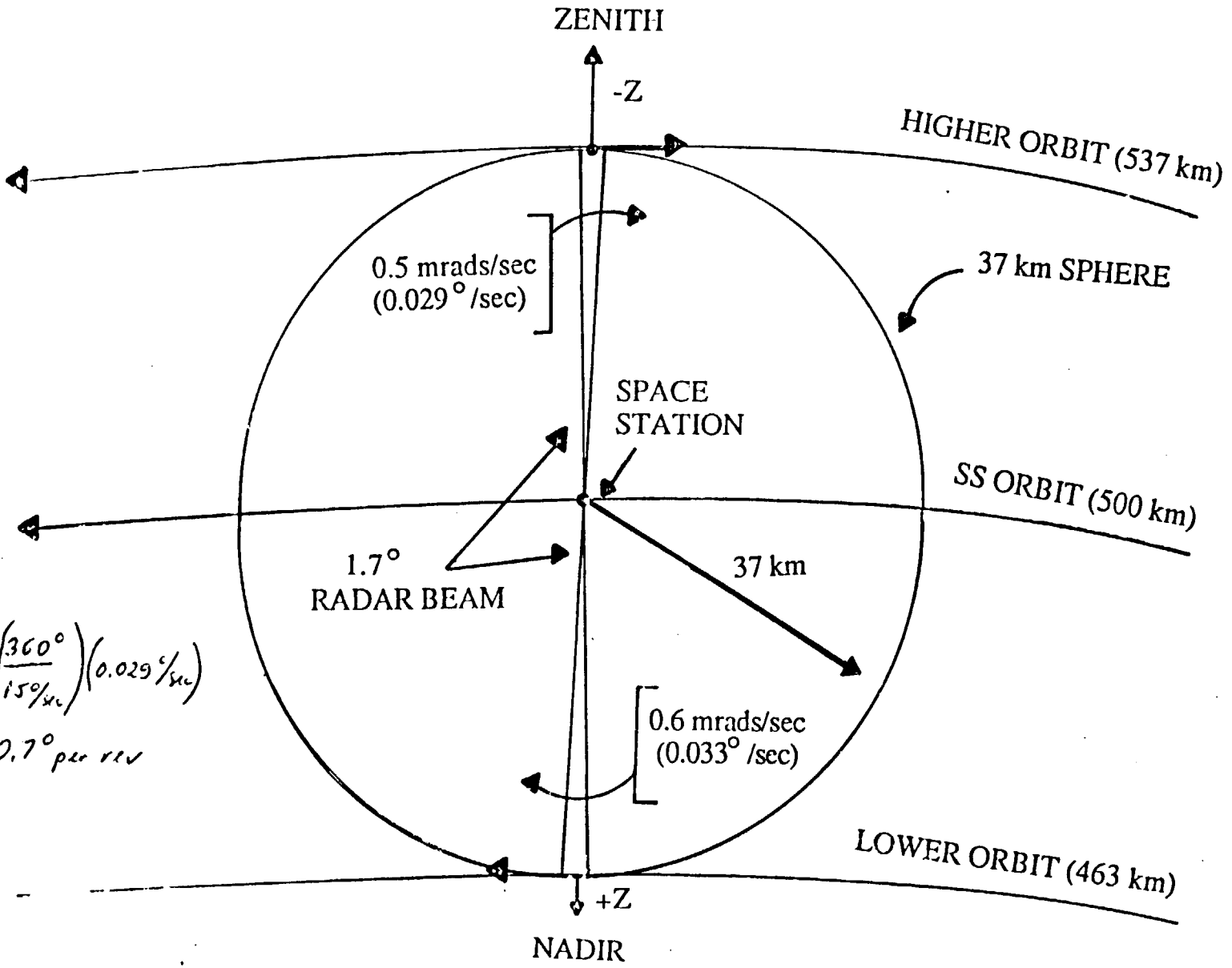

Relative Target motion $= \left(\frac{360°}{15^{\circ}/\text{sec}}\right)\left(0.029^{\circ}/\text{sec}\right)$

$= 0.7°$ per rev

ANGULAR SEARCH TIME WITH MODIFIED KU-BAND RADAR VS. ANGULAR COVERAGE AND DWELL TIME REQUIRED

Axiomatix

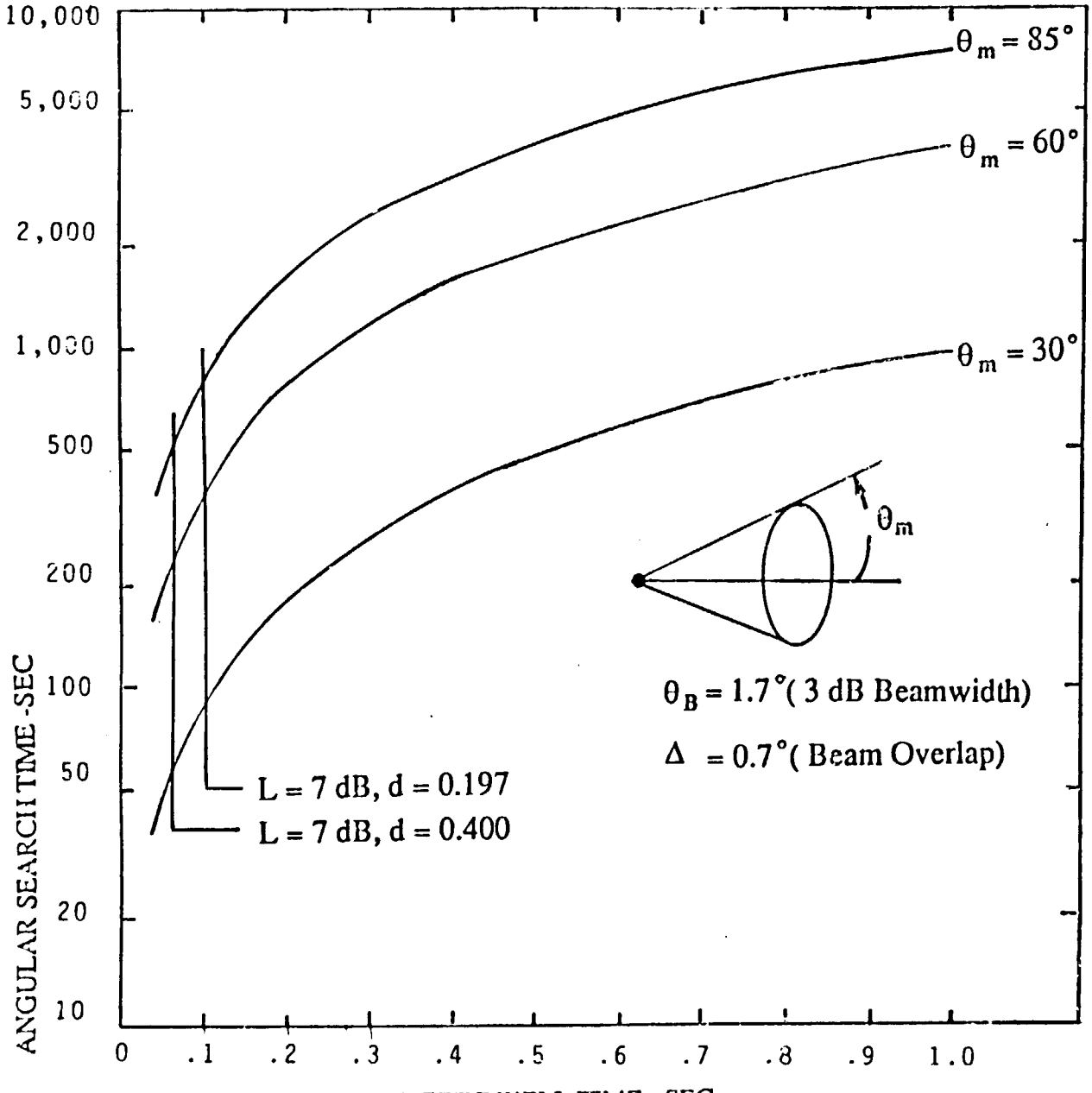

DETECTION CRITERION: Pd = 0.9, $P_{fa} = 10^{-6}$ (SINGLE SCAN)

RADAR PARAMETERS

P_p = 50 Watts

PRF = 2985 Hz

R_{max} = 20 nmi (37 km)

τ = 66μ sec (pulse width)

d_t = 0.197 (duty factor)

G_A = 37.7 dB

σ = 1 m^2

λ = 0.0216 m (f = 13.89 GHz)

T_s = 1500° K

N_c = 64 (coherent int. pulses

RANGE TRACKING ACCURACY (1σ) OF UNMODIFIED SHUTTLE KU-BAND RADAR

Axiomatix

Conclusion : Range Accuracy Spec can be met with unmodified Ku-band radar

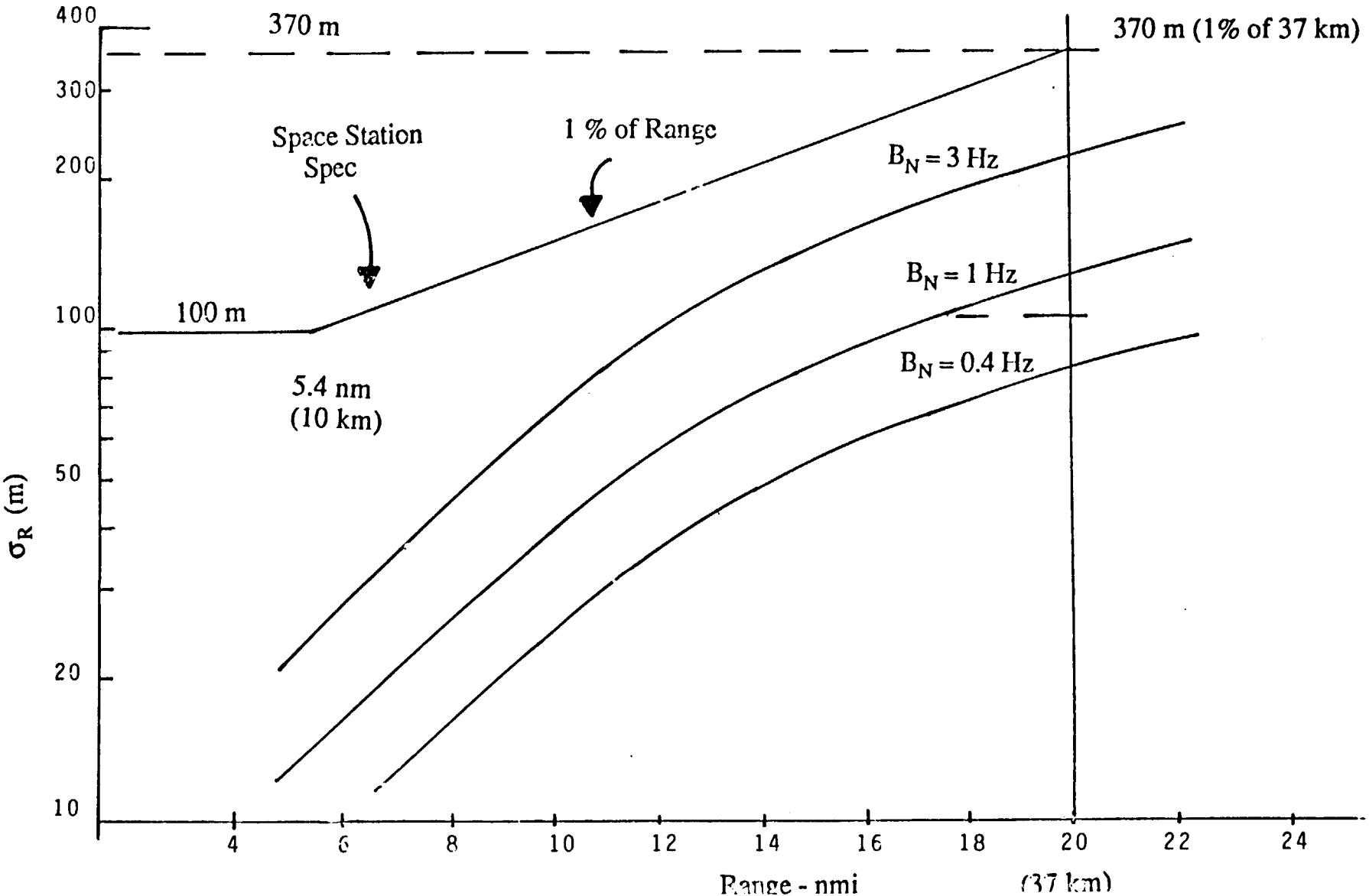

RANGE RATE TRACKING ACCURACY (1σ) OF UNMODIFIED KU-BAND RADAR

Axiomatix

Conclusion: Range Rate Accuracy Spec can be met with unmodified Ku-band radar

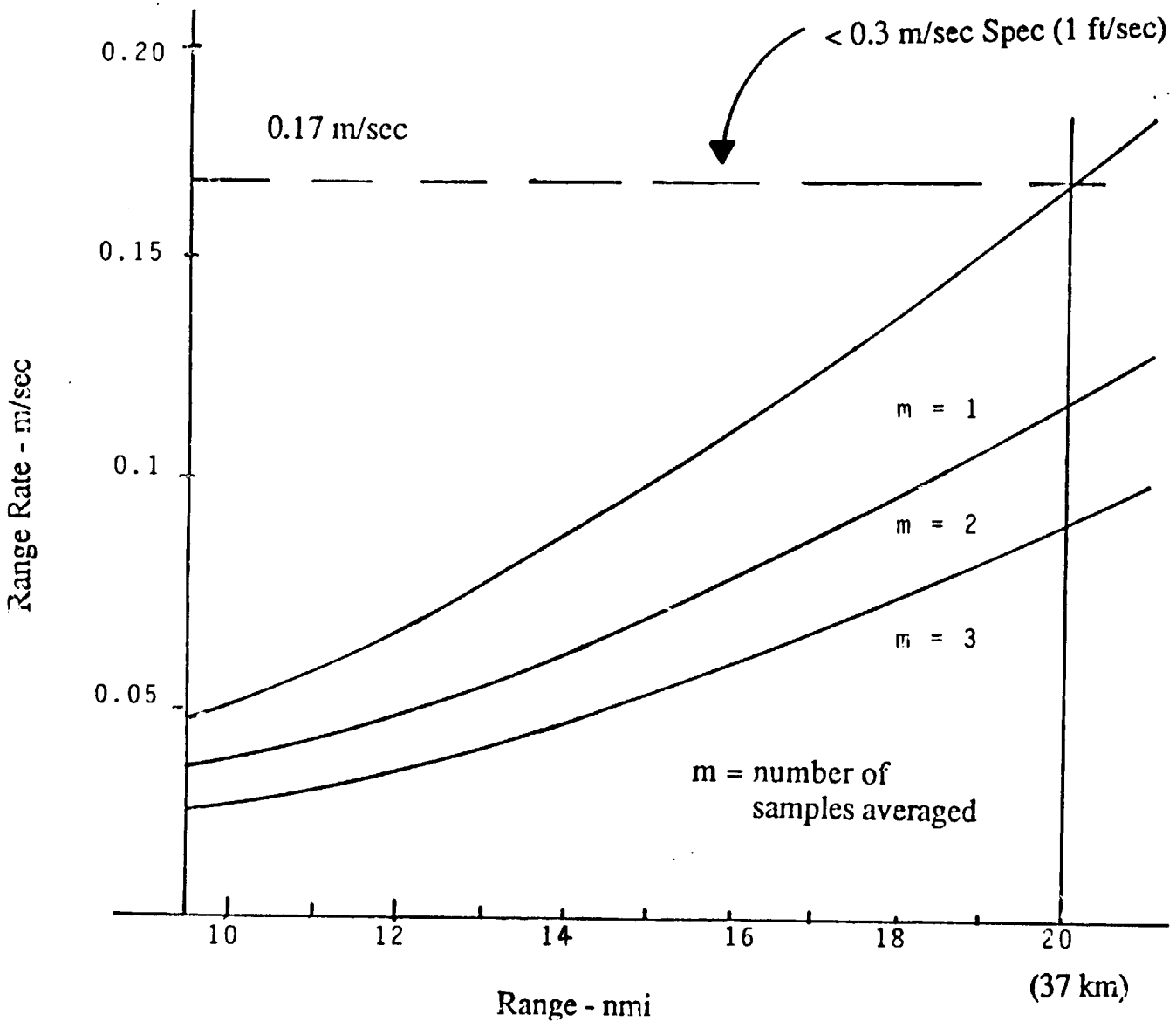

ANGLE TRACKING ACCURACY (1σ) OF UNMODIFIED SHUTTLE KU-BAND RADAR

Axiomatix

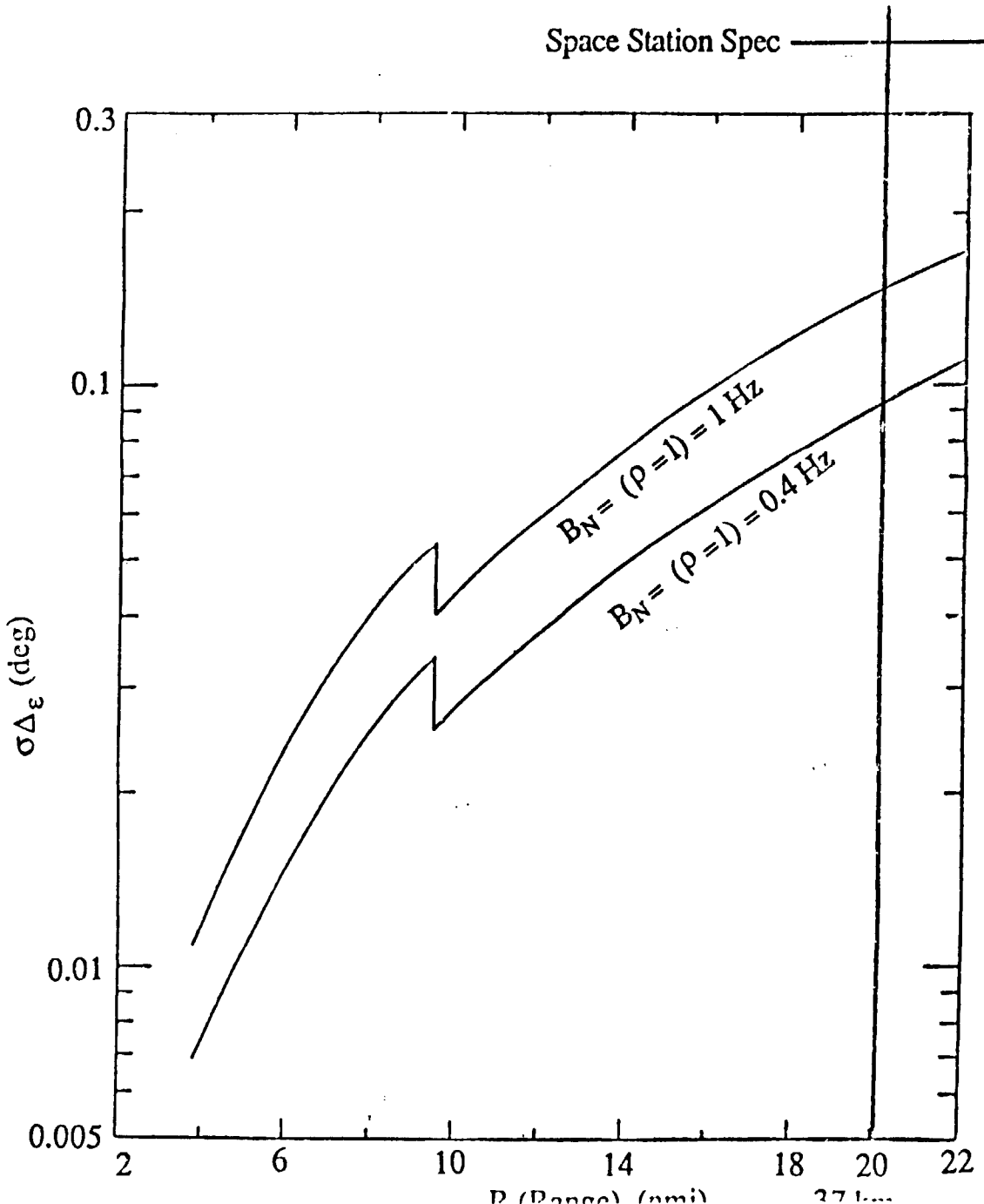

Conclusion: Angle accuracy can be met with unmodified Ku-band radar

CANDIDATE LOCATION OF SPACE STATION
RADAR ARRAY FACES ON SPACE STATION

Axiomatix

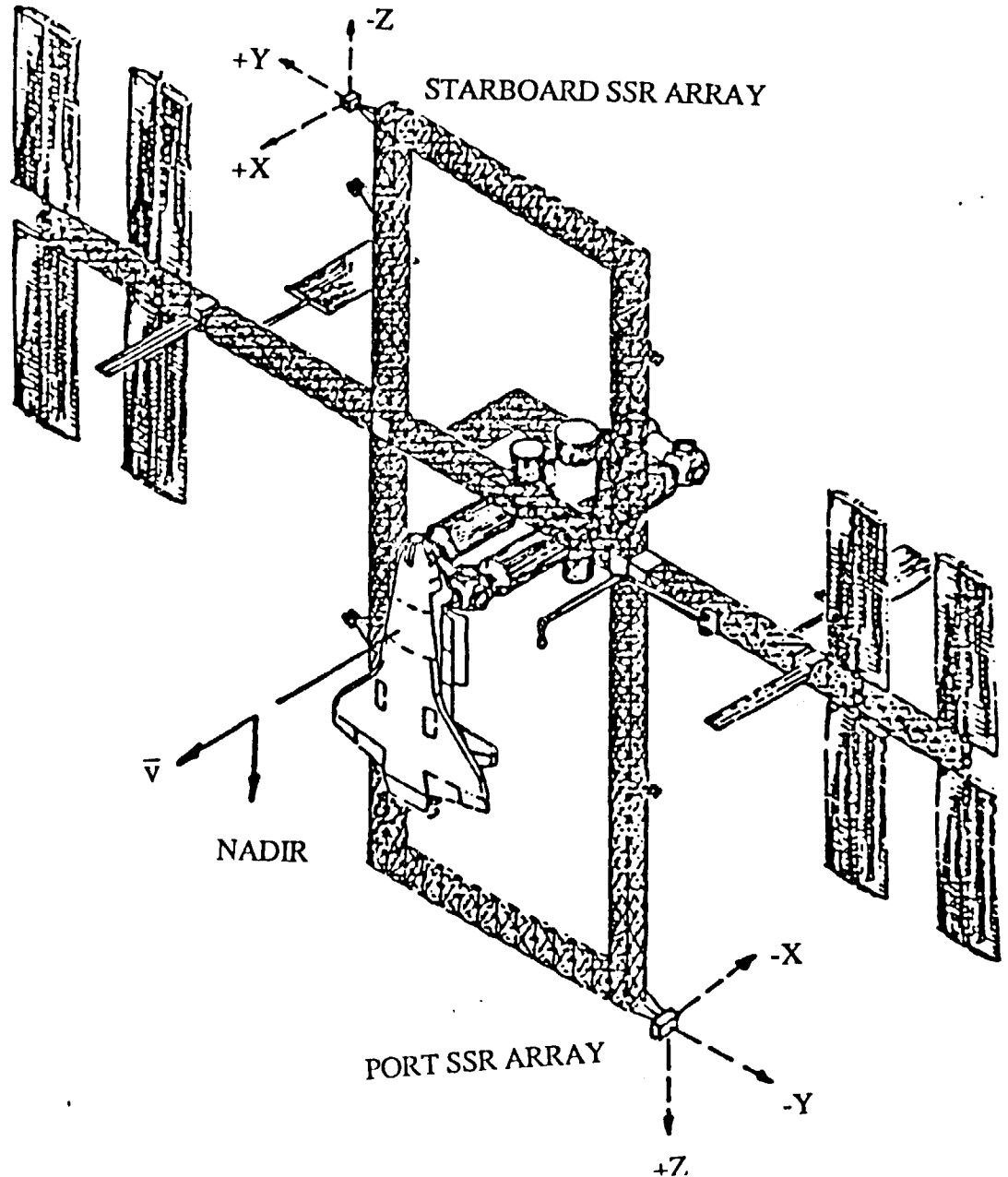

SPACE STATION PHASED ARRAY RADAR COVERAGE

Axiomatix

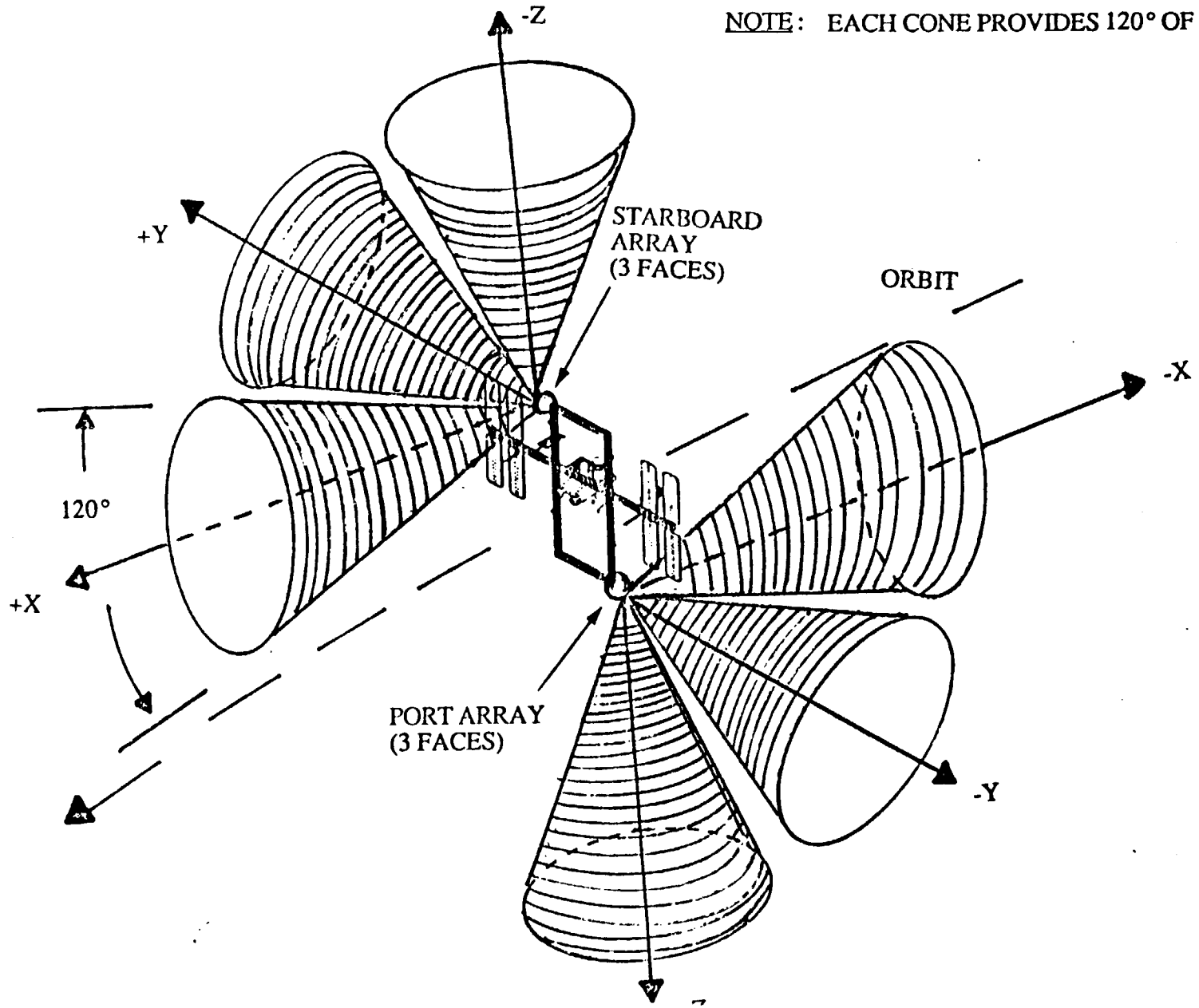

SPACE STATION SIX-FACE PHASED ARRAY COVERAGE

Axiomatix

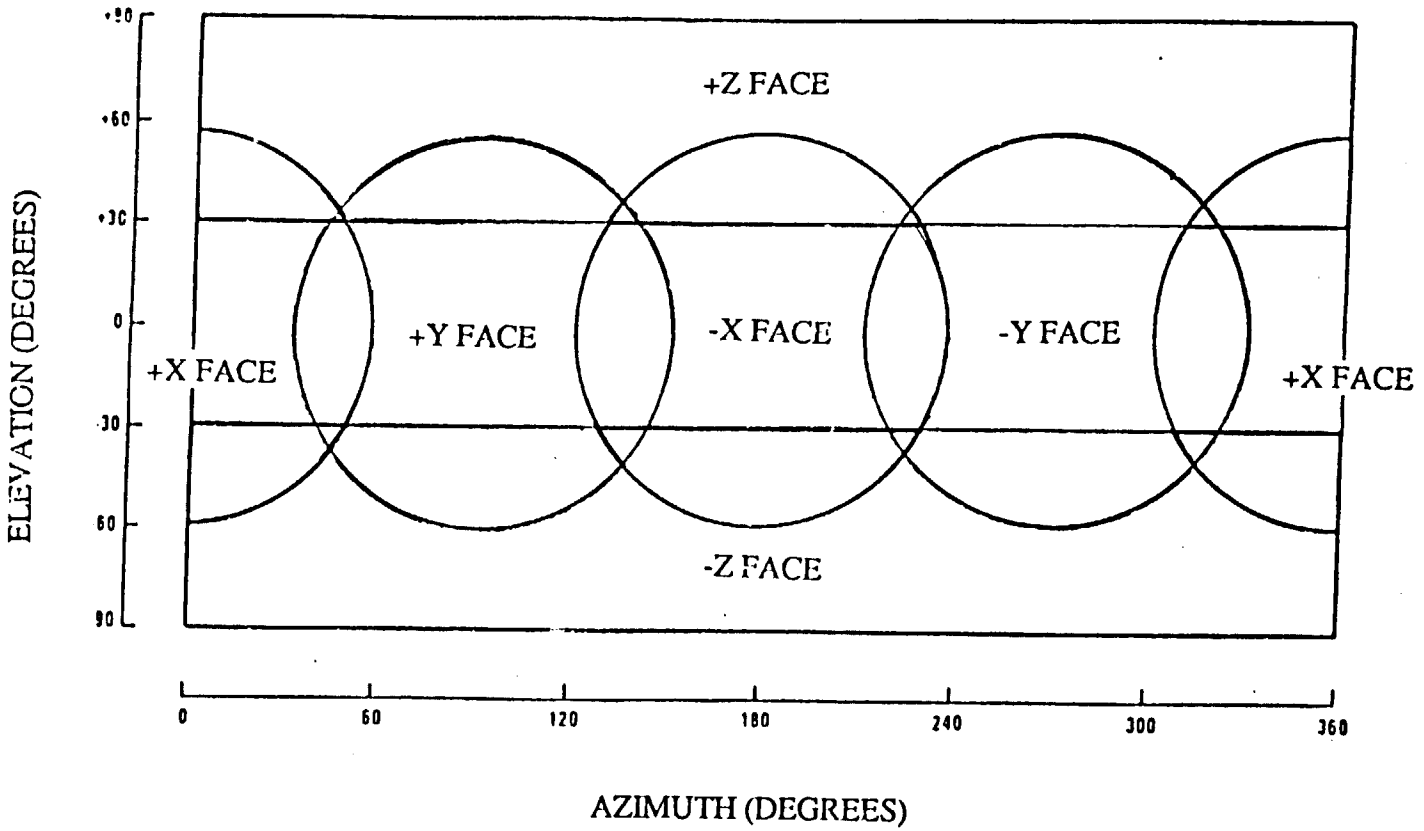

COMPARISON OF PHASED ARRAY AND SHUTTLE KU-BAND RADAR PERFORMANCE

Axiomatix

CHARACTERISTIC	PHASED ARRAY RADAR S-BAND	C-BAND	X-BAND	UNMODIFIED SHUTTLE RADAR KU-BAND[2]
OPERATING FREQUENCY (GHz)	3.1-3.5	5.2-5.6	9.8-10.2	13.9
ANTENNA DIAMETER (FT.)	3.2	2.77	2.2	3
NO. ARRAY ELEMENTS/FACE	256	512	1024	N/A
ANTENNA BEAMWIDTH (DEG.)	6.4	4.5	3.2	1.7
ANTENNA DIRECTIVE GAIN (dBI)	28	31	34	37.7
SYSTEM NOISE FIGURE (dB)	4.2	4.5	4.8	7.9
TRACK LOSS (dB)	14	15	15.7	15.1
PEAK POWER (WATTS)	647	543	517	50
AVERAGE POWER (WATTS)	150	126	120	9.85
OPERATING WAVELENGTH (M)	0.091	0.056	0.030	0.021
SEARCH TIME/HEMISPHERE (SEC)	51	102	220	820
RANGE ACCURACY (FT.)[1]	18.4	18.4	18.4	67
RANGE RATE ACCURACY (FT/SEC)[1]	1	0.66	0.33	0.56[3]
ANGLE ACCURACY (mrad)[1]	4	3.1	2	1.57[3]

NOTE 1: ONE-SIGMA VALUE AT MAXIMUM RANGE.

NOTE 2: TWT TRASMITTER AT KU-BAND

NOTE 3: $B_N = 0.4$Hz

MODIFIED SHUTTLE KU-BAND RADAR VS. PHASED ARRAY RADAR COMPARISION

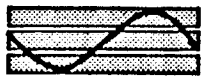

- CONCLUSIONS:

1. WITH THE EXCEPTION OF LONGER ACQUISITION TIME KU-BAND RADAR MEETS REQUIRED TRACKING ACCURACY IN RANGE, RANGE RATE AND ANGLE IN ITS UNMODIFIED STATE.

2. LONGER ACQUISITION TIME MAY NOT BE A LIMITATION FOR SPACE STATION RADAR BECAUSE OF SLOW RELATIVE TARGET MOTION.

3. ANTENNA SLEW TIME WILL BE THE LIMITING FACTOR FOR THE TRACK DATA UPDATE TIME FOR THE KU-BAND RADAR.

REMAINING ISSUES:

1. KU-BAND ANTENNA GIMBAL PERFORMANCE AND RELIABILITY UNDER THE REQUIREMENT TO MOVE FROM TARGET TO TARGET WHILE TRACKING.

2. COMPARATIVE PERFORMANCE OF THE TWO CANDIDATES (PHASED ARRAY VS. KU-BAND) WITH MANEUVERING TARGETS.

APPENDIX G

TRACKING PERFORMANCE OF THE MODIFIED KU-BAND SHUTTLE RADAR FOR THE SPACE STATION

TRACKING PERFORMANCE OF THE MODIFIED KU-BAND SHUTTLE RADAR FOR THE SPACE STATION

Contract No. NAS9-17414

Prepared for
NASA Lyndon B. Johnson Space Center
Houston, Texas 77058

Prepared by

Charles L. Weber
Andreas Polydoros

Axiomatix
9841 Airport Boulevard
Suite 912
Los Angeles, California 90045

Axiomatix Report No. R8604-3
MAY 28, 1986

1.0 System Evaluation

The tracking performance of the Ku-band Shuttle Radar has been estimated for the Space Station application. The performance is based on the requirement of being able to track a target of average radar cross section equal to one square meter which has Swerling I fluctuations at a range of 37 km (20 nmi.).

Suggested Specs:	(3 sigma)
Angle tracking	± 10 mrad
Range tracking	± 100 m or 1% of range
Range rate tracking	± 0.4 m/sec

Some nominal modifications of the existing Ku-band Shuttle radar are being considered in order to enhance the range tracking capability at maximum range, so as to meet the suggested specifications. These are summarized in Table 1, where the notation is analogous to the Ku-band radar performance predictions developed in [1] and is repeated below.

Table 1: Waveform Parameters

τ	d_t	N	$\tau_{FD}^{acq} = NT_p$	$\tau_{FD}^{tr} = 4NT_p$	T_s	Case
66 μsec	0.2	16	5.36 msec	21.44 msec	107.2 msec	1
66 μsec	0.2	32	10.72 msec	42.88 msec	214.4 msec	2
66 μsec	0.2	64	21.44 msec	85.76 msec	428.8 msec	3
Unchanged Parameters PRF = 3000 Hz T_p = 335 μsec						

τ = pulse width, which is increased from 33 to 66 μsec.

T_p = pulse period = $(PRF)^{-1}$

d_t = duty factor which increases from 0.1 to 0.2

N = number of pulses in a coherent integration period. The Shuttle system has N = 16. In addition N = 32 and 64 are being considered, which increases the coherent integration time accordingly.

τ_{CI} = coherent integration time = $N\tau$

τ_{FD} = dwell time at each of the five Ku-band RF frequencies. Depending on the mode (i.e., "acquisition" or "tracking"), τ_{FD}^{acq} and τ_{FD}^{tr} equals NT_p and $4NT_p$ respectively.

T_s = system update time, i.e. the time between samples into the various tracking loops.

The various changes enumerated in Table 1 evolve from changing N while keeping the PRF fixed. These changes will increase the SNR at the output of the DFT in the signed processing unit. Specifically, $\tau_{FD} = B_F^{-1}$, where B_F is the one-sided noise bandwidth of the DFT filter, and the SNR at the output of the DFT is

$$SNR = \frac{P_{pr}\, d_t\, \tau_{FD}}{N_o}$$

where P_{pr} is the peak received power. Since the pulse width is increased by a fraction of two, d_t is also increased by a factor of two. When N = 32, $\tau_{FD}$is also increased by a factor of two. Hence, there is an increase in SNR for each of the candidate waveform on the Ku-band Shuttle radar, as enumerated in Table 2.

To obtain a preliminary assessment of tracking performance we use the predictions for the Ku-band Shuttle radar in [1], and adjust the DFT output SNR as given in Table 2. This is sufficiently accurate for a preliminary assessment of system performance feasibility, as all other waveform and system parameters are assumed unchanged.

Table 2

Increase in SNR over Ku–band Shuttle Radar

Case	Increase in SNR
1	3 dB
2	6 dB
3	9 dB

2.0 Angle Tracking

From Figure 11 of Appendix C in [1] the one-sigma RMS angle tracking even at 37 km (20 nmi.) is, as shown in Figure 1:

$$\sigma_{\Delta c}\,(\text{deg}) = 0.15 \text{ degrees}$$
$$= 2.6 \text{ mrad}$$

Hence, the three sigma value is $3\sigma_{DE}\,(\text{deg}) = 8$ mrad which is below the suggested spec of 10 mrad without any alternations. All three cases would increase the design margin appropriately.

Thus, angle tracking is not a critical issue when assessing the feasibility of the Ku-band radar for the Space Station.

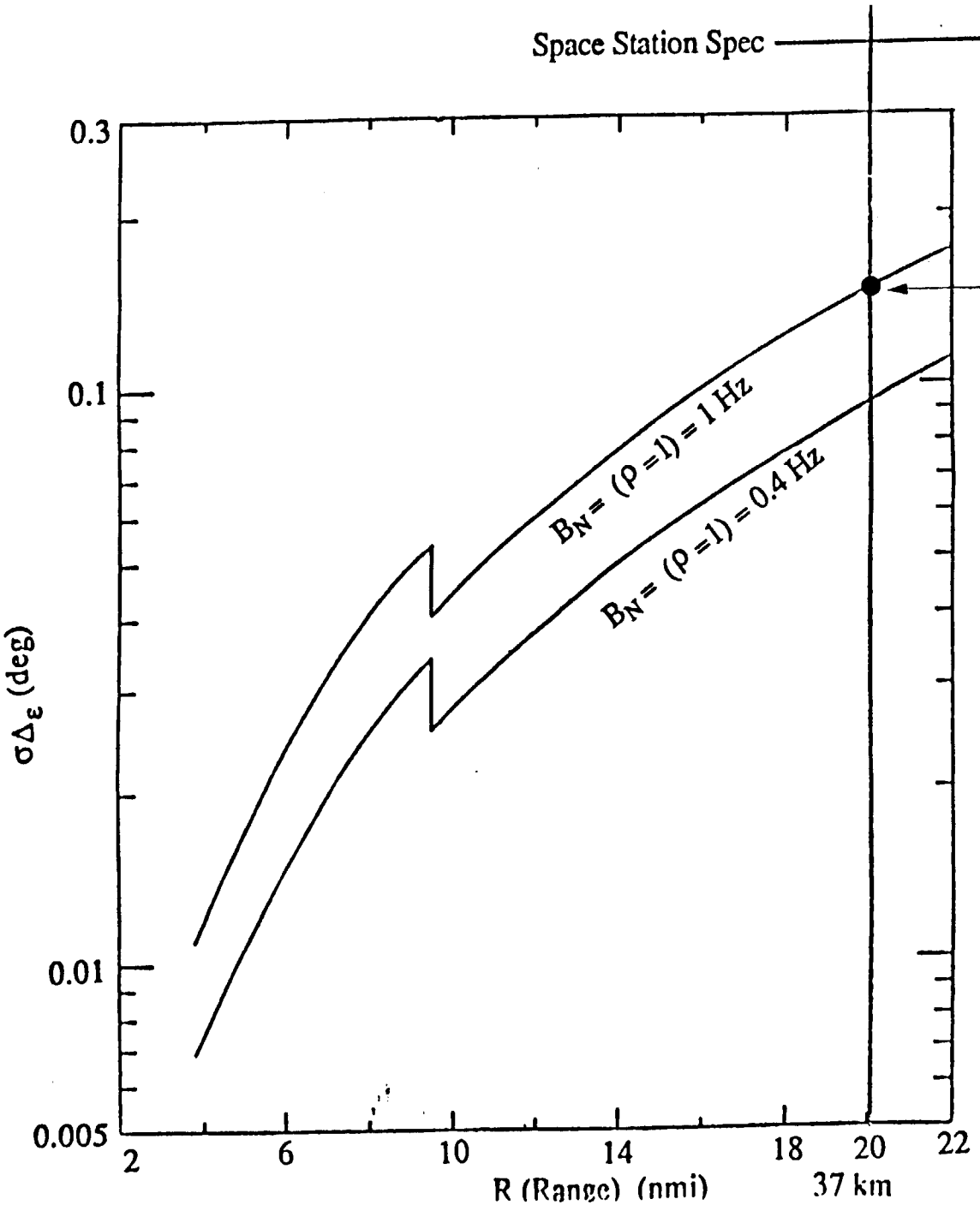

Conclusion: Angle accuracy can be met with unmodified Ku-band radar

Figure 1. Angle Tracking Accuracy (1σ) of Unmodified Shuttle Ku-Band Radar

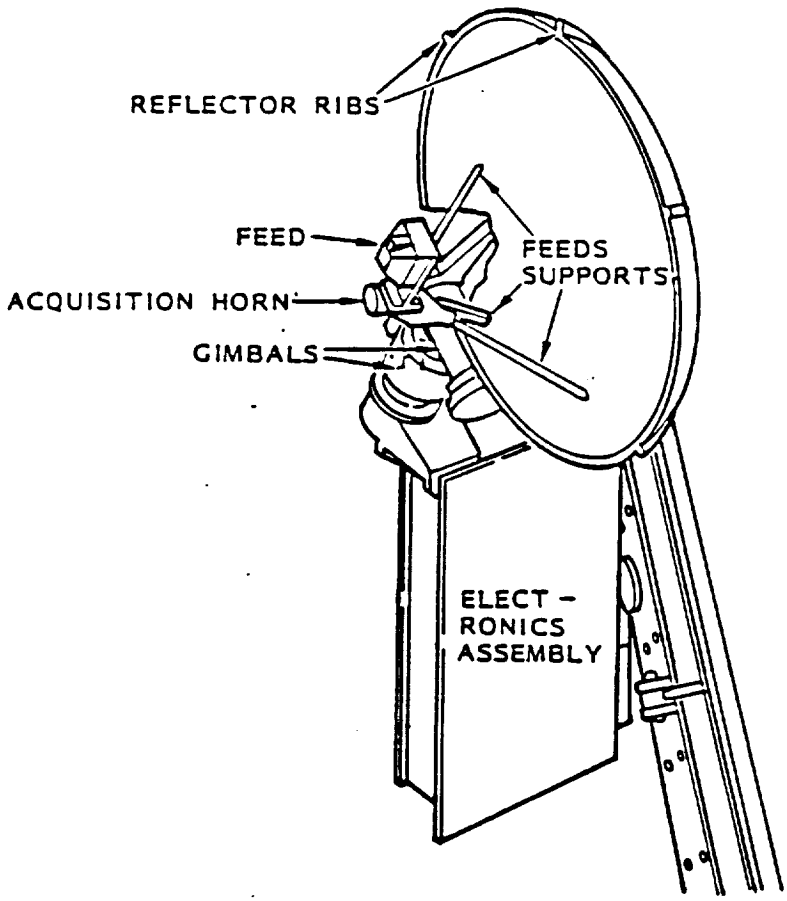

TRANSMIT POWER	50 WATTS
ANTENNA GAIN	37.7 dB
FREQUENCY DIVERSITY	5 CHANNELS KU-BAND
NUMBER OF PULSES	16 R < 22 KM
COHERENTLY INTEGRATED PER FREQUENCY	64 R > 22 KM
PULSE REPITION FREQUENCIES	7 kHz R < 15 KM 3 kHz R > 15 KM
PULSE WIDTHS	7 PULSEWIDTHS FROM 122 NSEC TO 66 μSEC
RANGE ACCURACY @ 37 KM	±21M (3σ)
RANGE RATE ACCURACY @ 37 KM	±0.29M/SEC
ANGLE ACCURACY @ 37 KM	±2mRAD (3σ)

Figure g.2.5.2.2-1. Gimballed Dish Design and Performance Parameters

"Communication and Tracking Report," Rockwell International, SS85-0191, Vol. II, December 6, 1985.

References

[1] C.L. Weber and W.K. Alem, "Study to Investigate and Evaluate Means of Optimizing the Ku-Band Combined Radar/Communication Functions for the Space Shuttle", Axiomatix Report No. R7710-5, October 28, 1977.

APPENDIX H

DWELL TIME ON TARGET AT MAXIMUM RANGE MODIFIED FOR THE MODIFIED KU-BAND FOR THE SPACE STATION

DWELL TIME ON TARGET AT MAXIMUM RANGE MODIFIED FOR THE MODIFIED Ku-BAND FOR THE SPACE STATION

Contract No. NAS9-17414

Prepared for
NASA Lyndon B. Johnson Space Center
Houston, Texas 77058

Prepared by

Andreas Polydoros

Axiomatix
9841 Airport Boulevard
Suite 912
Los Angeles, California 90045

Axiomatix Report No. R8604-6
MAY 28, 1986

We look here at the total dwell time on target required from the Ku-band Space Station radar in order to achieve a detection probability $P_D = 0.9$ and a false alarm of $P_{FA} \cong 10^{-6}$. We parametrize the dwell time τ_{ill} by the system loss factor L, i.e., we will show how τ_{ill} varies with L. The sytem parameters assumed here are shown in Table 1. The data is taken from [Ref.1. Figure g 2.5.5.2.2.-1):

Table 1: Fixed System Parameters

P_p = peak power= 50 Watts	τ = pulse time = 66 μsec
PRF = 2985 Hz	d_t = duty factor = 0.197
T_p = (PRF)-1 = 335 μsec	
N_{CI} = number of coherently integrated pulses per frequency = 64	t_{FDT} = dwell time per frequency = Nτp = 21.44 msec
R_{max} = maximum range = 20 nmi = 37 km	τ_{CI} = coherent integration time = 4.22 msec per frequency
G = antenna gain = 37.7 dB	σ = average cross section = 0 dBm
λ = 0.0216 m (f_o = 13.89 GHz)	Ts = system temperature = 1500° k

Furthermore, we will assume two types of targets, namely, Type 1 being a Swerling I model and Type 2 being a Swerling II model.

The ensemble-averaged, coherent-integration, peak-SNR R_p is given by

$$\overline{R}_p = \frac{G^2 \overline{\sigma} \lambda^2 \cdot [\, 2P_p \cdot \tau_{CI}\,]}{(4\pi)^3 R^4 \cdot K T_{sys} L} \qquad (1)$$

where K = Boltzman's constant = -228.6 dB (W/K/Hz). If the data from Table 1 is inserted into equation (1), we get (in dB)

$$R_p\,(dB) = 2(37.7) + 0 - 2(16.65) + 3 + 17 - 23.7 - 33$$
$$- 182.7 + 228.6 - 31.76 - L(dB)$$

or

$$R_p\,(dB) = 19.54 - L(dB) \qquad (2)$$

which is ploted in Figure 1. Note, that if τ is doubled to 132μsec R_p will pick up 3 dB.

Next, we note from DiFranco & Rubin [Ref. 1] that for $P_{FA} \cong 10^{-6}$, we can pick $n' \approx 10^6$, since $P_{FA} \approx 0.693/n'$ (see [1], Chapter 10), so that the results are actually exact for $P_{FA} = 0.69 \times 10^{-6}$. If we let N_{NCI} be the number of noncoherently integrated "pulses"* required to achieve $P_D = 0.9$ (in other words, N_{NCI} stands for the number of different frequencies which illuminate the target), we then have from [1] the following Table 2, which connects R_p, N_{NCI} and L (from equation 2)

Table 2: $\bar{R}_p$ Versus N_{NCI}

	Swerling I							Swerling II					
$\bar{R}_p$ (dB)	18	16.5	13.5	10	7.5	5	2	18	15.5	11.5	9.5	5.5	2
N_{NCI}	6	10	30	100	300	1,000	3,000	2	3	6	10	30	100
L (dB)	1.5	3	6	9.5	12	14.5	17.5	1.5	4	8	10	14	17.5

Now, the illumination time τ_{ill} is related to N_{NCI} as

$$\tau_{ill} = \tau_{FDT} \cdot N_{NCI} = 21.44 \cdot N_{NCI} \text{ msec} \qquad (3)$$

*Note that the word "pulse" here does not pertain to an acutal system pulse, but rather to the collection of coherently added pulses per frequency.

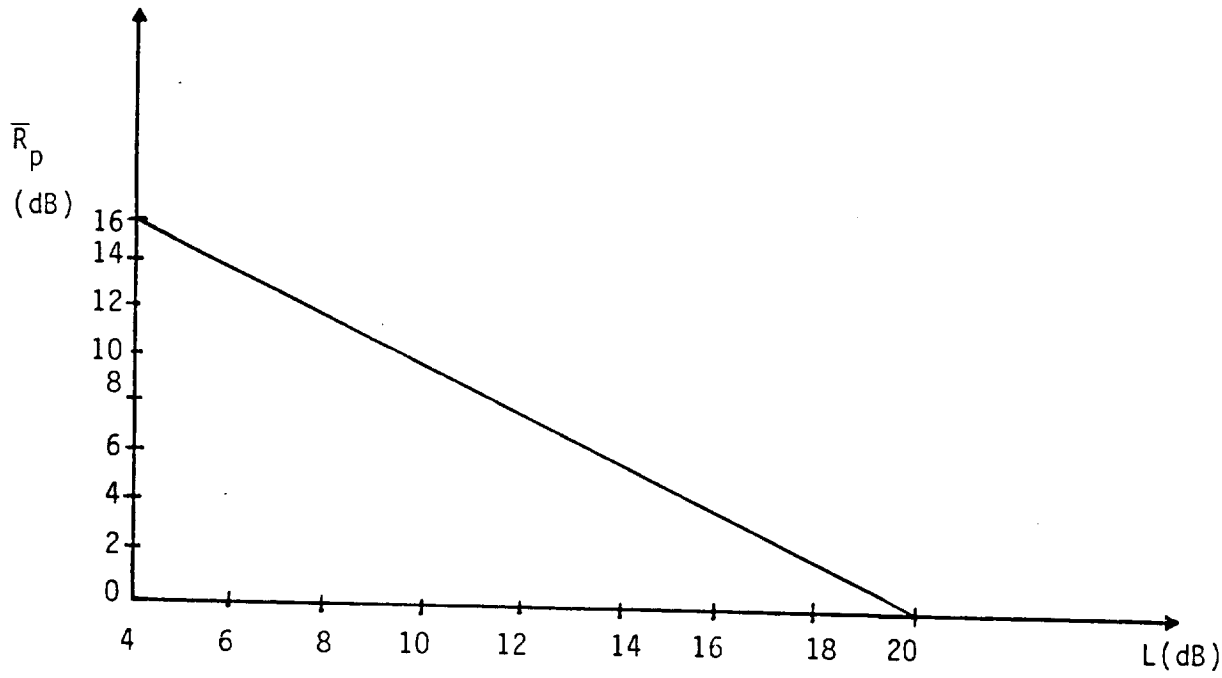

Figure 1: $\overline{R}_p$ versus L in dB

Therefore,putting Table 2 and equation (3) together results in the following Tables 3 and 4:

Table 3: τ_{ill} versus L (dB) for Swerling I

L(dB)	1.5	3	6	9.5	12	14.5	17.5
τ_{ill} (msec)	128	214	643	2,144	6432	21,440	64,320

while for Swerling II,

Table 4: τ_{ill} versus L (dB) for Swerling II

L(dB)	1.5	4	8	10	14	17.5
τ_{ill} (msec)	42.8	64.3	128.6	214.4	643	2,144

We see that the model assumption makes a tremendous difference on the required illumination time. For instance, if L = 14 dB (a reasonable figure all around), Swerling II requires a little more than half a second, while Swerling I requires 21 seconds, i.e, about forty times more!!

APPENDIX I

A CANDIDATE ACTIVE ELECTROMAGNETIC SYSTEM DOCKING SCHEME

A CANDIDATE ACTIVE ELECTROMAGNETIC SYSTEM DOCKING SCHEME

Prepared for
Contract No. NAS9-17414

NASA Lyndon B. Johnson Space Center
Houston, Texas 77058

Prepared by
Dr. Richard Iwasaki

Axiomatix
9841 Airport Boulevard
Suite 912
Los Angeles, California 90045

Axiomatix Report No. R8602-3
February 26, 1986

1.0 Abstract

Axiomatix has studied some optical docking proposals for the Space Station, and, noting the complexity of their design, investigated other techniques which may be applicable in solving the optical docking problem. The key issue for one proposal, it appears, is the spectral analysis of minute quantities of retroreflected light from a distant vehicle. Another is the multiple ranging to three retroreflectors to define a plane in space. Rather than follow the retroreflected light approach, a more direct method was conceived, one which would actively align a docking vehicle to a desired attitude and bearing and accurately monitor the closing rate during the docking maneuver. Remote control can be maintained by modulating (e.g., amplitude modulation) the same laser beam used to align and move the docking vehicle to send simple commands. Many of these techniques are readily compatible with similar RF techniques and therefore can be developed using comparable millimeter and submillimeter quasi-optic systems.

2.0 Summary of the Active Optical Docking Scheme

Initial acquisition of the docking vehicle is readily achieved by video means. Once acquired, the docking station aims a laser beam at a retroreflector on the docking vehicle, and photoconductive tracking sensors monitoring the retroreflected beam at the laser provides continuous tracking of the retroreflector. The laser beam is reflected off of a conical reflector to create a circularly symmetric beam of light to define a plane in space and illuminates a number of photodetector arrays. The illumination position on these photodetector arrays completely characterizes the alignment of the docking vehicle to the incident laser beam since it measures the degree of misalignment. This information in turn may be used to align the docking vehicle using an onboard computer.

However, it is also possible to dynamically correct this misalignment by an active technique that senses the direction of misalignment and uses the attitude control subsystem of the docking vehicle to immediately align itself to the laser beam. This novel technique

uses a complementary photoconductive pair of strips to provide the driving voltages to allow the attitude control system of the docking vehicle to align itself orthogonally to the incident laser beam. The laser beam, if normal to the plane of the docking vehicle, is reflected off the conical reflector to form a circular pattern centered on these photoconductive tracking sensors. If the docking vehicle is not orthogonal to the laser beam, the misalignment causes the reflected laser light to become offset from the centered position on the photoconductive tracking sensors, which in turn generate corrective driving voltages which realign the docking vehicle.

Furthermore, this same concept allows for the movement of the docking vehicle to follow the laser beam into the desired docking position by sensing the laser beam motion. The laser beam (increased in diameter by a beam expander) is larger than the conical reflector, and this spillover radiation incident on photoconductive tracking sensors can similarly drive the docking vehicle in the direction of movement of the laser beam.

The roll attitude can be measured precisely, although with a 180 degree ambiguity, by exploiting the linear polarization of the incident laser beam and using polarization cancellation to establish two ambiguous roll positions accurately. This ambiguity may be visually resolved or other techniques used to differentiate the correct position. This roll position can either be measured directly on the docking vehicle by using a photodetector behind a fixed crossed polarizer. On the docking station the roll attitude is determined by measuring the polarization of the reflected light from a flat mirror surrounding the conical reflector, once alignment is achieved, which retains the original polarization orientation. By incorporating a polarization rotator on the laser which effectively rotates the linear polarization (effectively rotating the laser), the polarization cancellation position and therefore the roll attitude can be established.

Active roll attitude control can be implemented such that the docking vehicle rolls with the orientation of linear polarization. If a tracking sensor is placed behind two adjacent polarizers oriented at + and -45 degrees to the laser beam polarization, the incident

illumination on both photoconductive sensors are identical and therefore balanced. Any deviation from this condition will generate driving voltages which will cause the docking vehicle to follow the orientation of linear polarization of the laser.

The accurate measurement of the closing rate is very crucial in a docking maneuver. A scheme has been developed to to measure the relative velocity, both on the docking vehicle and docking station, extremely accurately using interferometric techniques such that the resolution is of the order of the wavelength of the laser light.

Remote command capabilities may be incorporated into this active docking scheme by simply modulating the laser beam. Amplitude modulation, for example, can use the same laser beam to communicate commands which are received by a photodetector demodulation subsystem. FM may be considered for a similar millimeter wave system.

Thus, it is possible to have an active laser beam control system (or comparable active control system using millimeter waves) on the Space Station which can completely control the attitude and bearing of a docking vehicle, monitor the closing velocity, and remotely command the docking vehicle independent of a separate communications link.

3.0 Alignment Measurement Technique

In order to achieve high angular accuracies, optical leverage has often been used in the early days of physics, most notably in the measurement of the gravitational constant. In a related manner, a measurement scheme based on the detection of reflected light over a relatively long distance will enhance the accuracy, especially with the ready availability of optical lasers whose light is both coherent and collimated. Thus a beam of laser light will be used to illuminate a 45 degree inclined mirror such that the reflected light will be detected by a linear array of photodetectors, and the position of the light beam on the photodetectors is a direct measurement of the direction cosine to the laser beam, which therefore establishes the attitude of the docking vehicle.

Figure 1a shows this basic right angle configuration, where the measurement of one direction cosine is simply determined by the detection of the highest intensity reflected beam of laser light at a particular photodetector element. The laser light is reflected off the mirror inclined 45 degrees to the normal vector of the docking plane and, if the laser beam was oriented along this normal, orthogonal reflection would occur and the central photodetector element would be illuminated.

If the laser beam was slightly inclined to this normal vector, as seen in Figure 1b, then the angle of reflection would also deviate from this orthogonal reflection since the angle of reflection is equal to the angle of incidence. This basic law of optics is the only physical principle used in this scheme.

The resolution that can be achieved with this technique is limited only by the number and placement of these photodetector elements. For example, if a photoconductive element is 0.1 inches in diameter and located ten inches away, then the angular resolution is 0.57 degrees. Even greater resolution may be obtained by using smaller photodetectors or longer distances from the reflector to the photodetector array.

Since three direction cosines are the minimum required to establish a plane, this process must be repeated three times approximately symmetrically about the normal vector, which explains the use of an equilateral triangular base pyramid as sketched in Figure 2. Note, that symmetry is not critical to the placement of the reflecting pyramid nor the photodetector arrays since the direction cosines can be readily scaled for asymmetrical placements due to vehicle design.

4.0 Conical Reflector

Because of the possibility of blockage, it is apparent that more reflective surfaces besides the three in an equilateral triangular base pyramid might be useful, especially since any deviation from the normal vector of the docking plane introduces a lateral "squint" in the docking plane, although the direction cosine itself is nearly constant. In order to

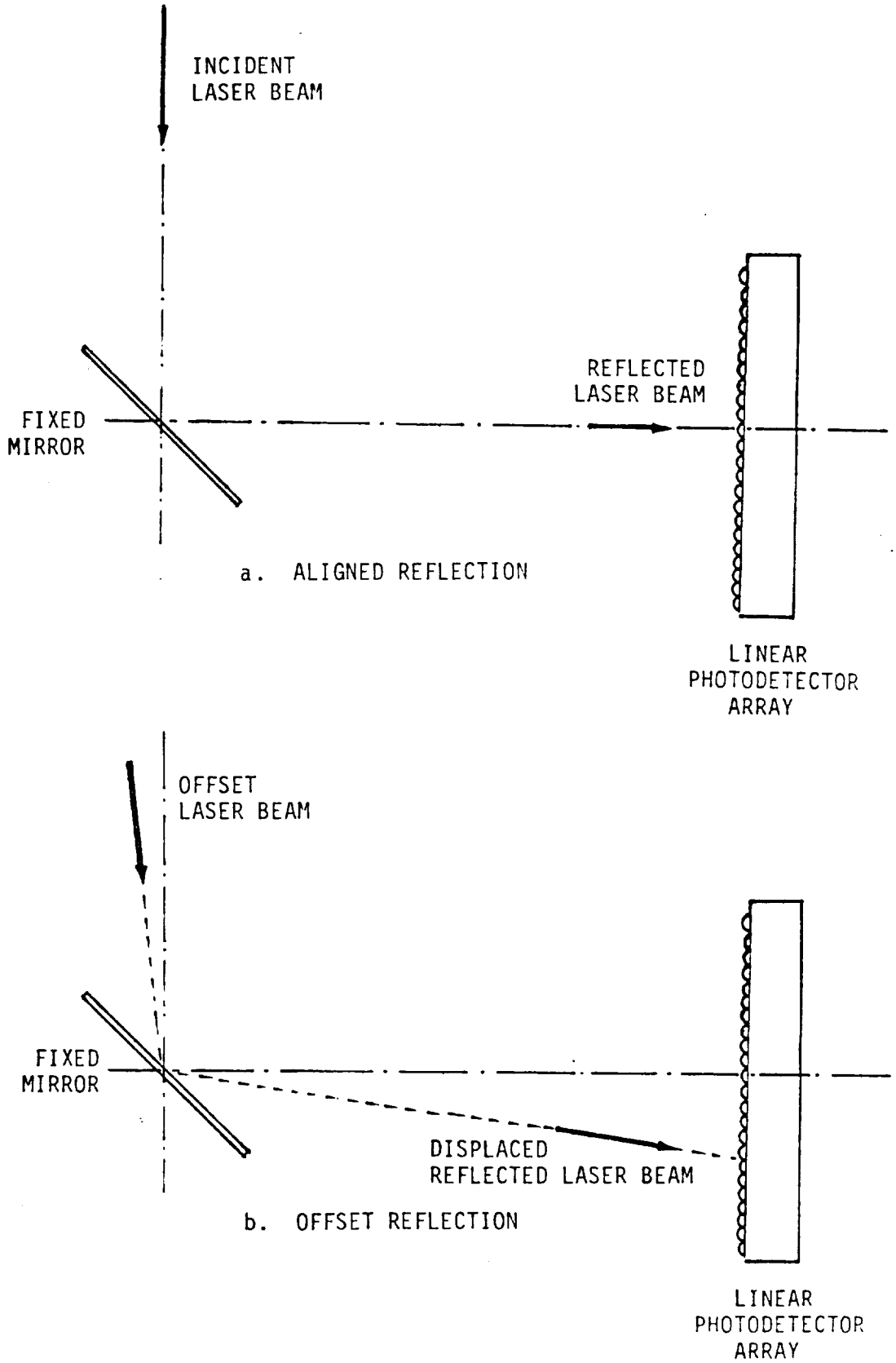
INCIDENT
LASER BEAM
REFLECTED
LASER BEAM
FIXED
MIRROR
a. ALIGNED REFLECTION
LINEAR
PHOTODETECTOR
ARRAY
OFFSET
LASER BEAM
FIXED
MIRROR
DISPLACED
REFLECTED LASER BEAM
b. OFFSET REFLECTION
LINEAR
PHOTODETECTOR
ARRAY

Figure 1

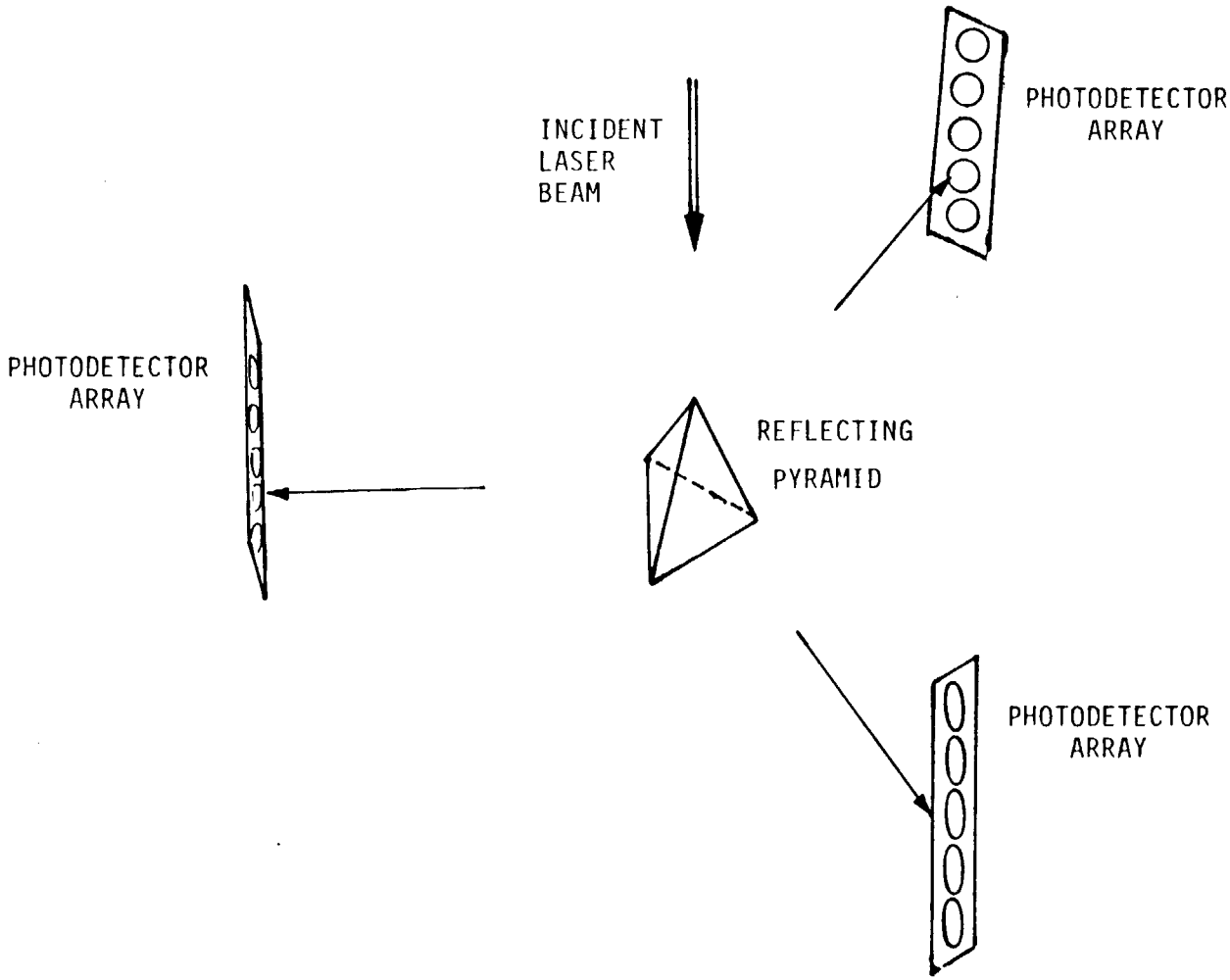

THREE ANGULAR ALIGNMENT MEASUREMENTS WITH A
REFLECTING PYRAMID

Figure 2

compensate for this lateral squint, a multifaceted surface (which in the extreme is a cone) can replace the pyramid such that the incident laser beam is transformed into a tilted pattern about the conical reflector, with the tilt reflected by the displacement of the beam along the photodetector arrays, as seen in Figure 3. This continuous beam of light about the conical reflector removes alignment considerations and permits the use of as many redundant photodetector arrays, fiber optic visual aids, and photoconductive tracking sensors as desired. It can be argued that a beam expander should be considered to decrease pointing problems and to ensure adequate illumination of the conical reflector, even though beam divergence is inherent to all practical systems.

5.0 Passive Alignment Measurement

The outputs of these photodetector arrays are used by the docking vehicle to measure its alignment with respect to the laser beam, since the position of each array is known. This particular method only measures the degree of misalignment but is not capable of initiating alignment maneuvers. These passive measurements can be readily incorporated into an active alignment scheme using the attitude control system on the docking vehicle itself with its navigation computer, or the data may be relayed to the docking station, such as the Space Shuttle or the Space Station, and the corrective maneuvers communicated back.

6.0 Visual Alignment Aids

Another useful passive visual aid, that may be employed to ensure alignment, is an array of optical fiber strands which are mounted such that the position of the circular beam pattern on the linear photodetector array is transmitted to the docking surface such that an observer would actually see the effective beam position and would, therefore, obtain visual verification of alignment. Figure 4a shows such a fiber optic array coupled to a display, and Figure 4b depicts perfect alignment when the circular beam is centered on the

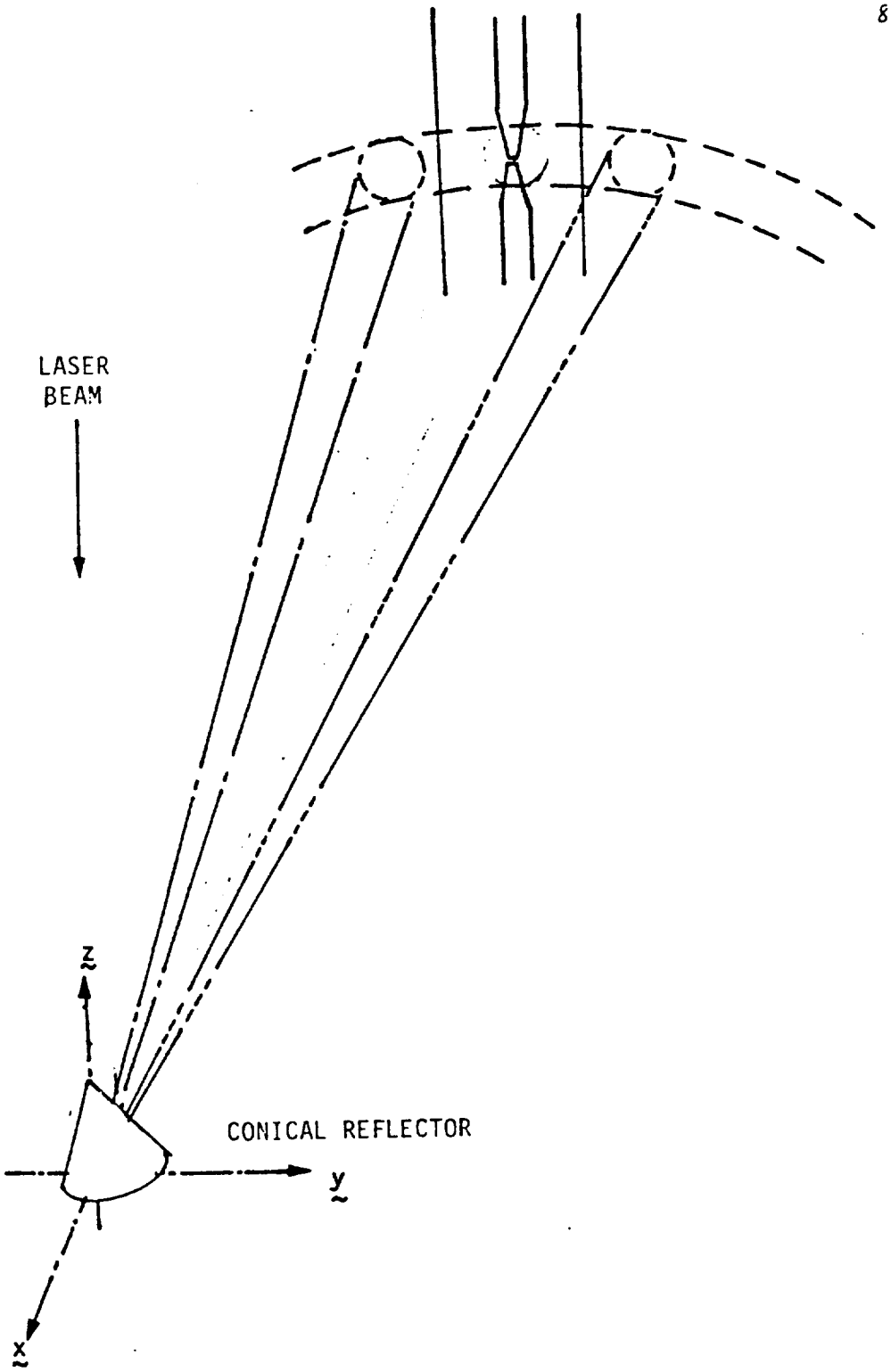

CIRCULARLY SYMMETRIC BEAM FROM CONICAL REFLECTOR
INCIDENT ON PHOTOCONDUCTIVE SENSOR

Figure 3

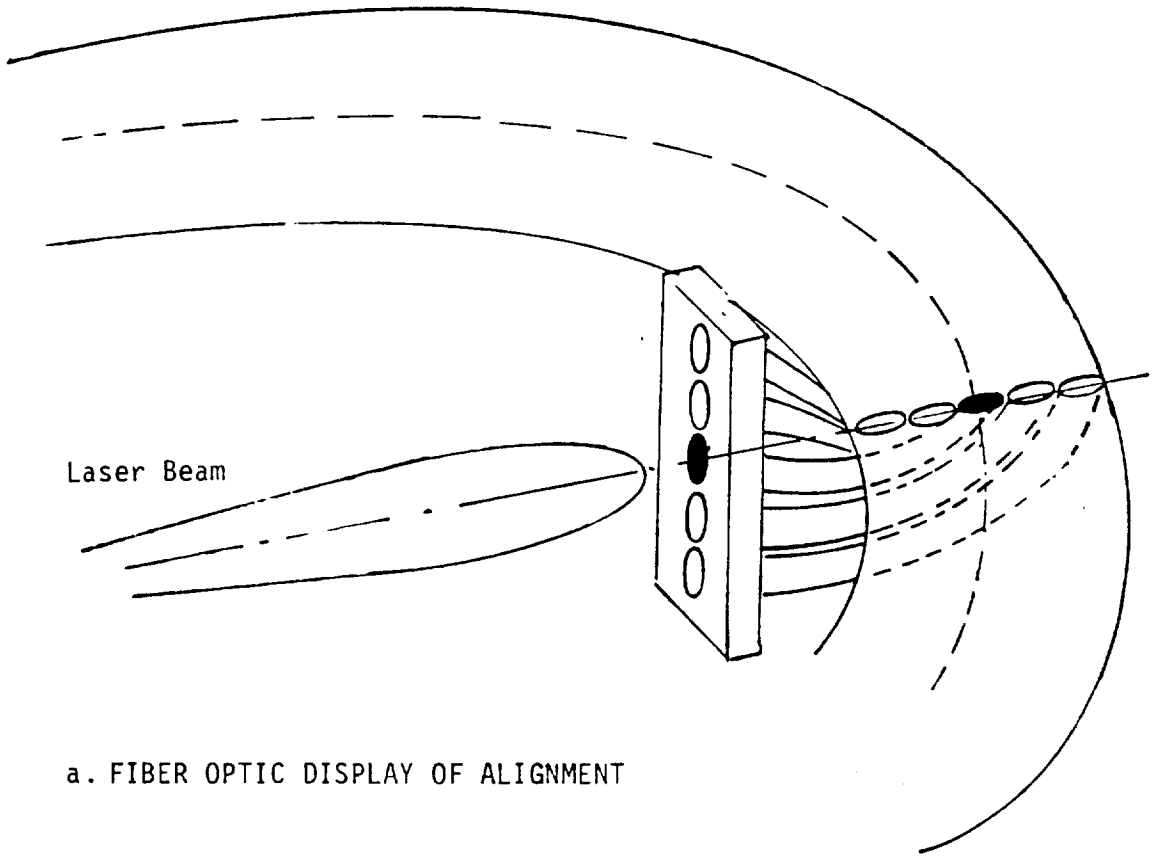

a. FIBER OPTIC DISPLAY OF ALIGNMENT

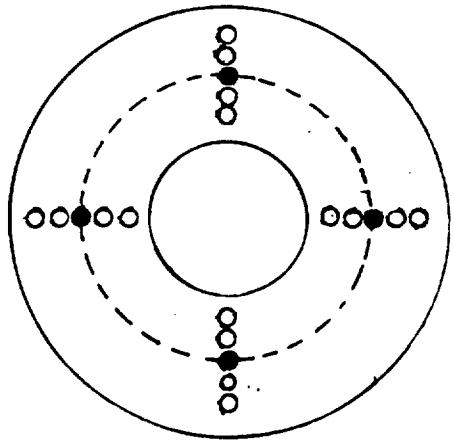

b. TOP VIEW OF FIBER OPTIC DISPLAY

Figure 4

photodetector array. This technique may even be expanded in the case that an invisible infrared CO2 laser is selected if the photodetector array is electronically coupled to corresponding colored light emitting diodes.

7.0 Photoconductive Tracking Sensors

There are some other types of photodetectors which may be useful in providing active alignment of the docking vehicle. One is the photoconductive strip bridge arrangement that provides voltage polarity information for alignment, which will be referred to as the photoconductive tracking sensor. The basic configuration is shown in Figure 5a; note, that the central tips of the photoconductors are tapered to increase the changes in resistivity due to illumination in the critical balancing position. The Wheatstone resistive bridge and the two photoconductive strips are shown in Figure 5b, and the effects of balanced and slightly unbalanced illumination are illustrated in Figure 5c. When both tips of the photoconductive strips are equally illuminated, the bridge is balanced and because of the null condition, no driving voltages exist.

The requirement that the photoconductive sensor be mounted normal to the circularly symmetric beam from the conical reflector introduces the possibility that a replaceable redundant photoconductive sensor design might be considered. One version of this replaceable unit is shown in Figure 6. The unit itself is plugged into a multiple pin socket accommodating the many redundant Wheatstone bridge electrical connections. The photoconductive strips are vapor deposited onto the flat glass surface of a cylindrical section which is reflectively coated on the back surface to collect and focus the incident laser light onto the photoconductive sensors so that illumination occurs both in front and behind the photoconductor. Restraining collars or clamps can ensure that the unit remains firmly attached.

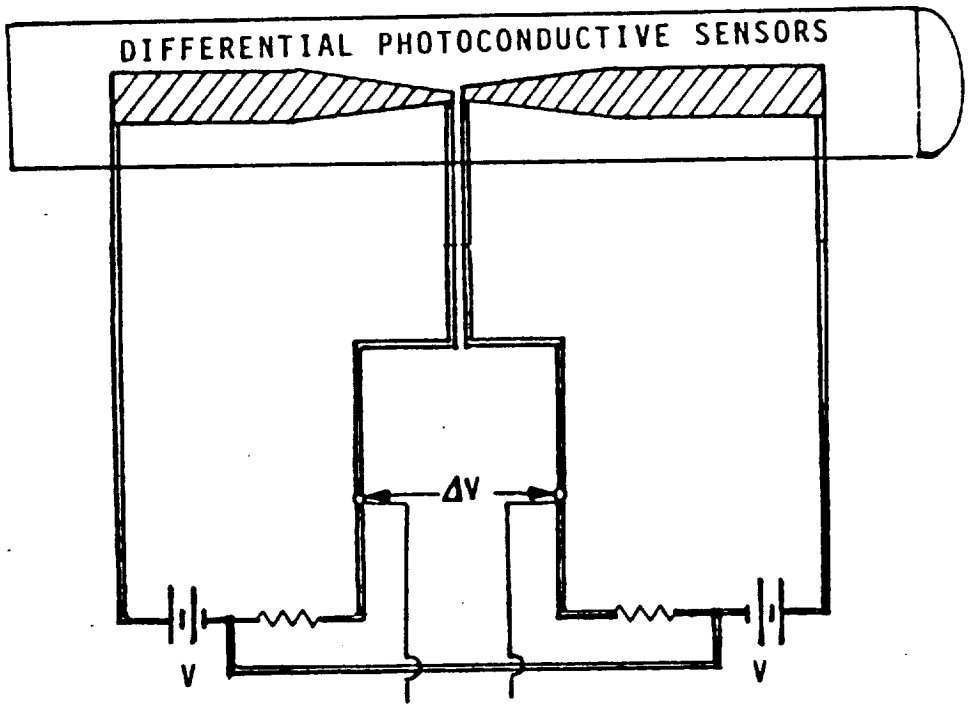

PHOTOCONDUCTIVE TRACKING SENSOR

Figure 5a

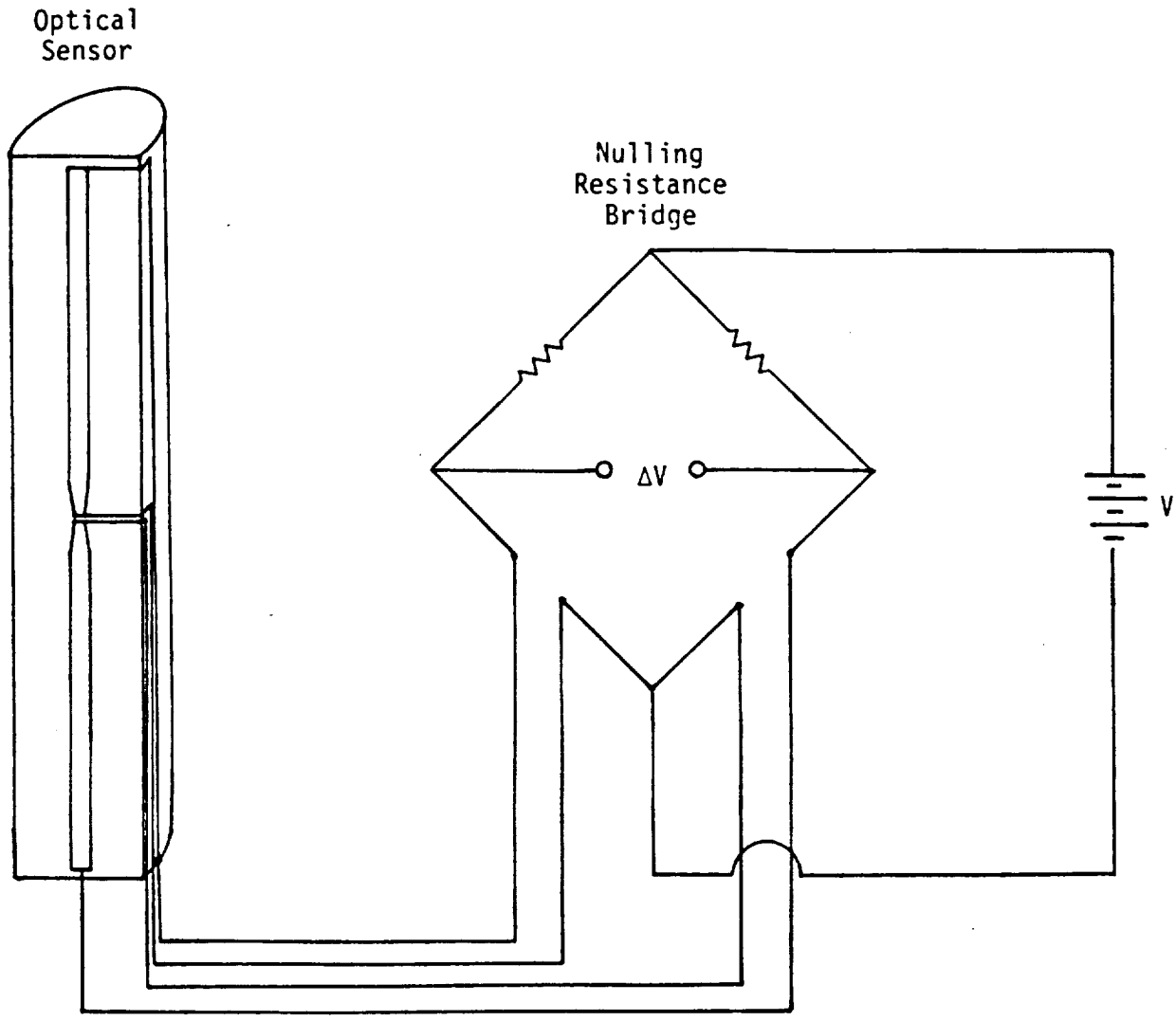

DIFFERENTIAL VOLTAGE DERIVED FROM A COMMON VOLTAGE SOURCE

Figure 5b

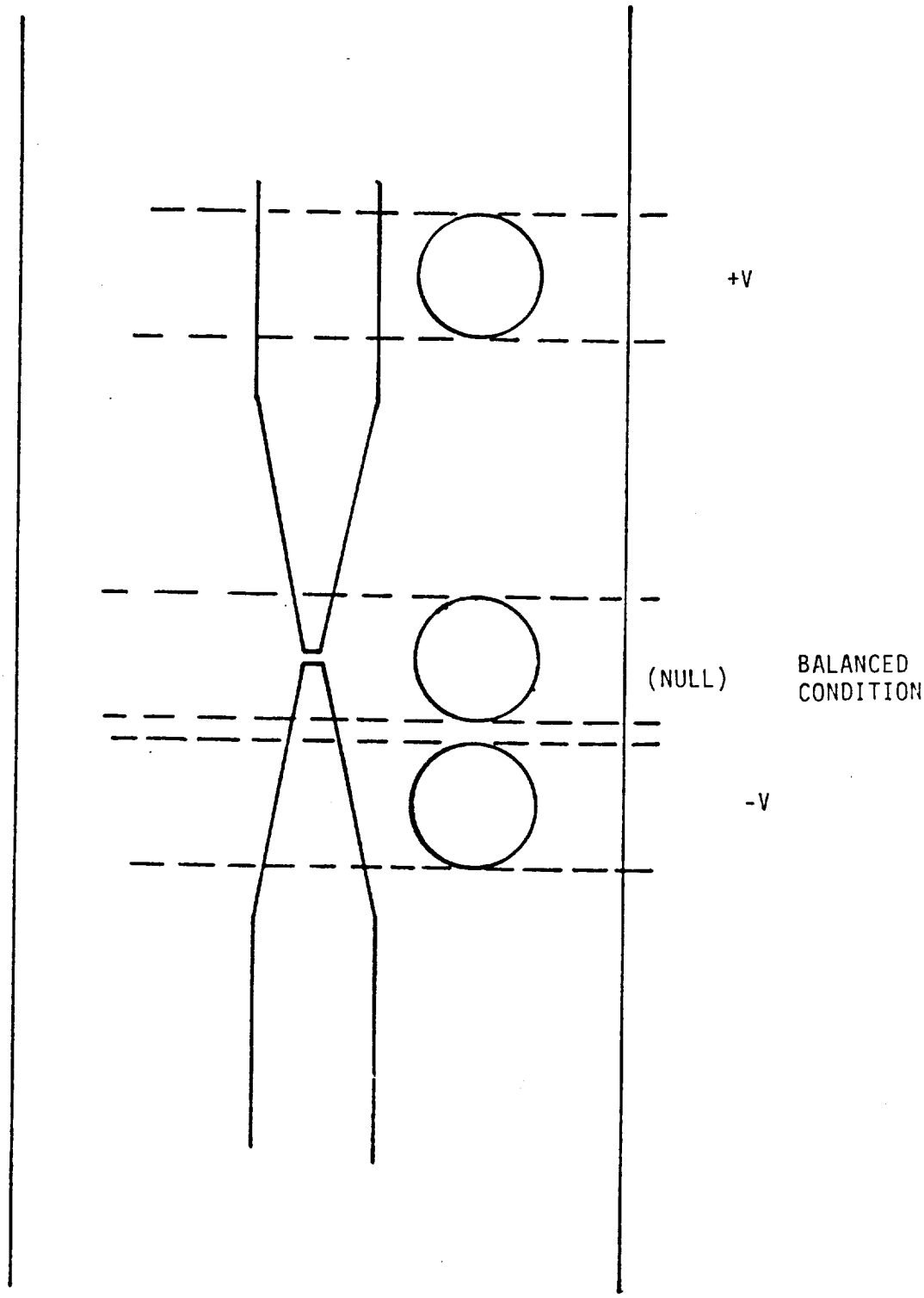

CIRCULARLY SYMMETRIC BEAM INCIDENT ON THE PHOTOCONDUCTIVE TRACKING SENSOR AT VARIOUS POSITIONS, INCLUDING NULL

Figure 5c

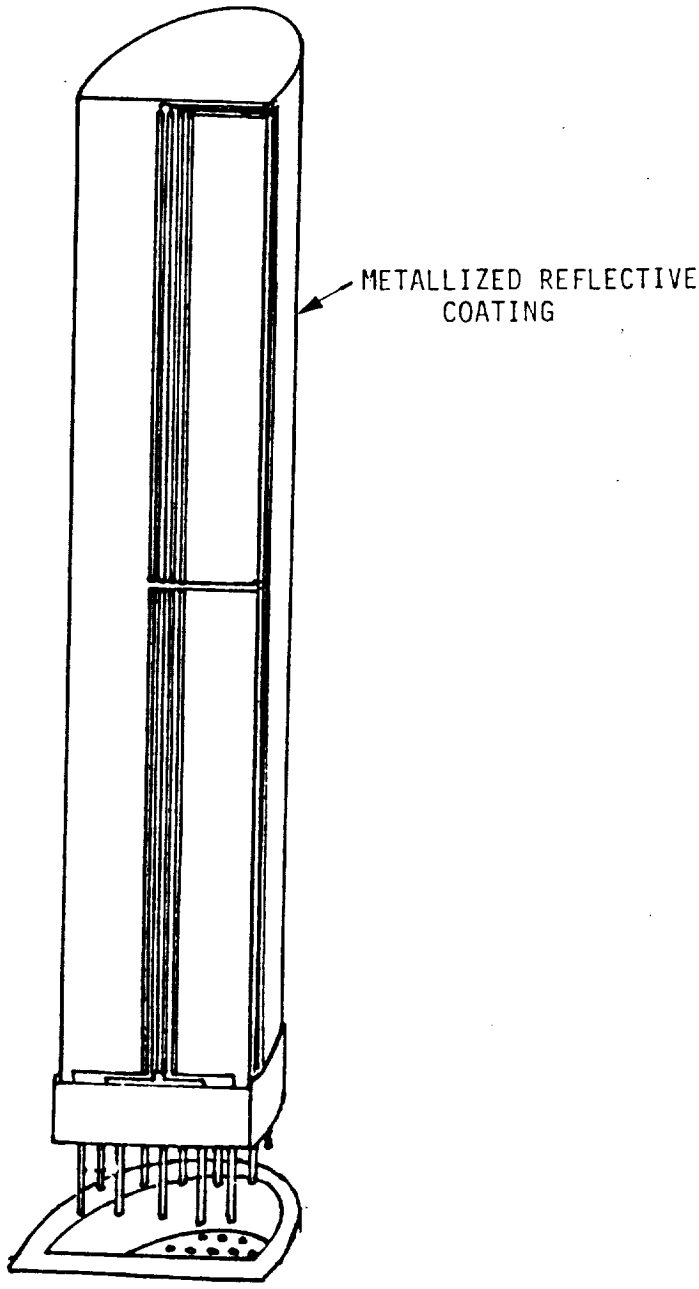

REMOVABLE PHOTOCONDUCTIVE TRACKING SENSOR WITH MULTIPLE REDUNDANT SENSORS AND REFLECTIVE REAR COATING

Figure 6

8.0 Active Alignment Scheme

The photoconductive tracking sensors can be used to provide the driving voltages to actively align the docking vehicle. When perfectly aligned, the circular beam from the conical reflector defines the orthogonal plane and will be centered on these sensors. A minimum of three sensors, spaced approximately equally about the docking vehicle, will establish the alignment plane. When these three sensor bridges are balanced, the docking vehicle is aligned normal to the laser beam. Since the circular beam is reflected symmetrically about the conical reflector, there are many possible locations for sensors and visual aids so that critical optical alignment is not required.

9.0 Docking Vehicle Maneuvering Scheme Using Beam Tracking

This photoconductive tracking sensor technique may also be used to maneuver the docking vehicle to the proper bearing since the laser beam can slowly be moved such that the active maneuvering scheme tracks the laser beam and attempts to continuously center the laser beam on the photodetector tracking sensors. If, for example, these same photoconductive tracking sensors are mounted in pairs orthogonally to the beam and to each other and aligned adjacent to the attitude control jets, as sketched in Figure 7, then the movement of the laser beam will provide a driving voltage in the direction that the laser beam moves, and the attitude control system of the docking vehicle will follow the movement of the laser beam to the proper stationkeeping position prior to docking.

10.0 Roll Attitude Measurement

Once the bearing and the alignment of the docking vehicle is established, the roll attitude must be known. By using a fixed polarizer in front of a photodetector, the transmitted laser light is a function of the roll attitude. If the polarizer orientation is orthogonal to the linear polarization of the laser, the maximum reduction of the intensity of the laser beam incident on a photodetector defines a specific orientation of the docking

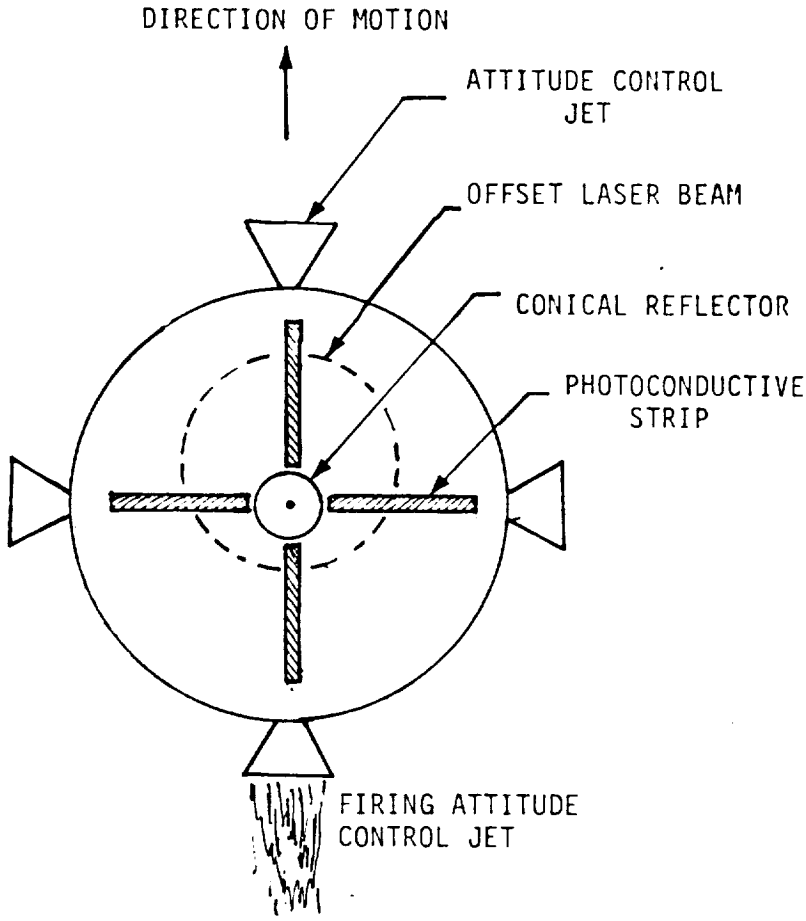

LASER BEAM TRACKING SYSTEM USING
PHOTOCONDUCTIVE TRACKING SENSORS

Figure 7

vehicle. For example, as the laser beam polarization rotates, there are two ambiguous extinguishing positions where the orthogonal polarizer completely blocks the laser beam transmission. This polarization cancellation measurement is the most sensitive roll information that can be remotely determined and can be accomplished both on the docking vehicle and the docking station, assuming the identical polarization is maintained upon reflection. A vertical reference plane is therefore defined, which can be related to two possible roll orientations of the docking vehicle.

11.0 Active Roll Axis Alignment

This polarization balancing phenomenon can also be exploited by using orthogonally oriented adjacent polarizers mounted on a photoconductive tracking sensor such that at the + and -45 degree orientations, the transmitted laser light on each photoconductor is equal, thereby creating a balanced condition. Figure 8a shows the light transmission for relative polarizer angles and Figure 8b tries to show how the two + and -45 degree polarizers attain the balanced condition. If the laser beam polarization is rotated slightly, simulated in Figure 8c, then the unbalanced condition generates a driving voltage whose polarity and magnitude is a function of the angular orientation from the balanced condition of the linear polarization of the laser beam. Thus, the docking vehicle can sense the offset of the laser beam polarization and roll in the appropriate direction to align itself to the balanced condition once again. Essentially, the docking vehicle tracks the linear polarization of the laser beam. Equivalently, the laser beam can control the roll attitude of the docking vehicle. If the laser is rotated, for example, the docking vehicle will undergo a corresponding roll. Since there are two ambiguous cancellation positions and therefore two possible roll positions, the docking vehicle can end up in an inverted position. This condition can be rectified in a number of ways. First, the laser itself can be slowly inverted such that the docking vehicle rotates to the proper position. Second, a polarization rotator mounted at the laser can perform the same gradual rotation function. And third, the laser

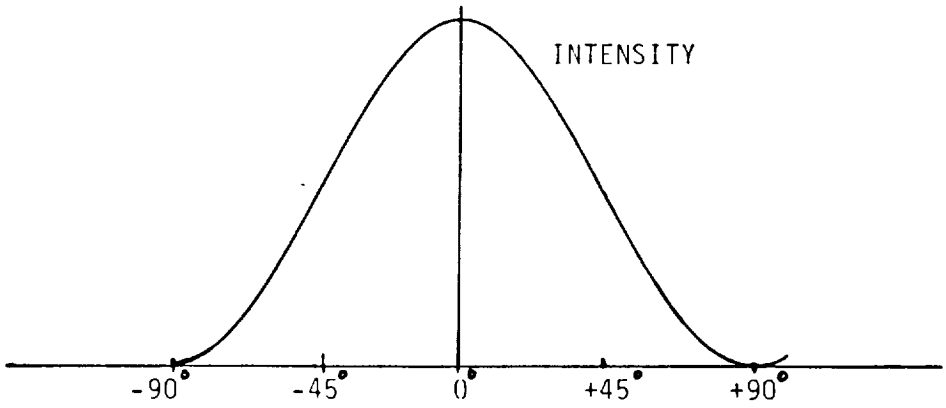

a. LIGHT TRANSMISSION vs. RELATIVE POLARIZER ANGLE

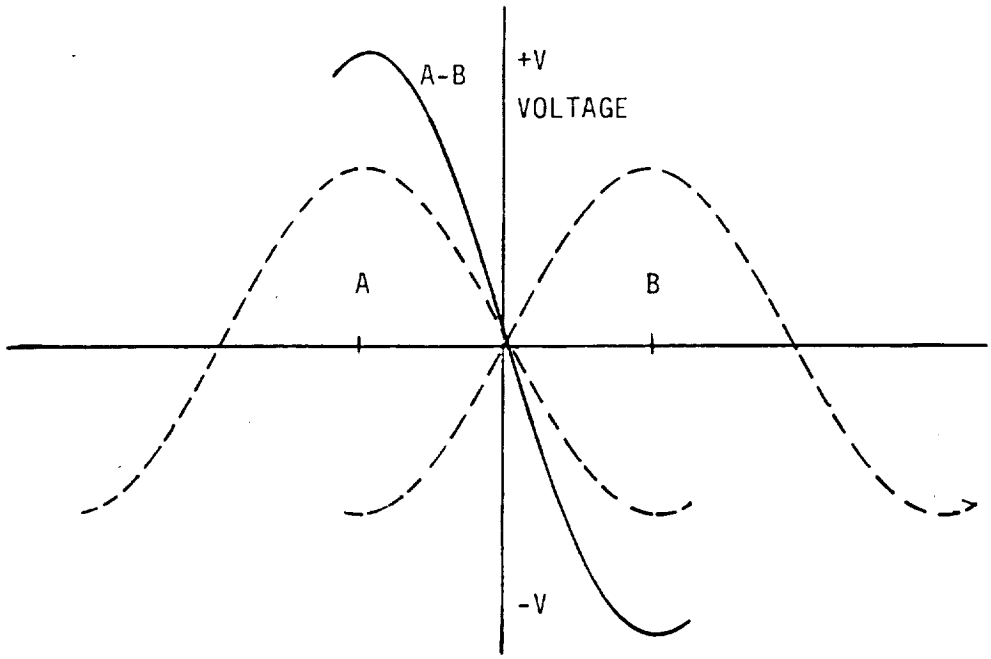

b. DIFFERENTIAL VOLTAGE FOR +45 POLARIZERS

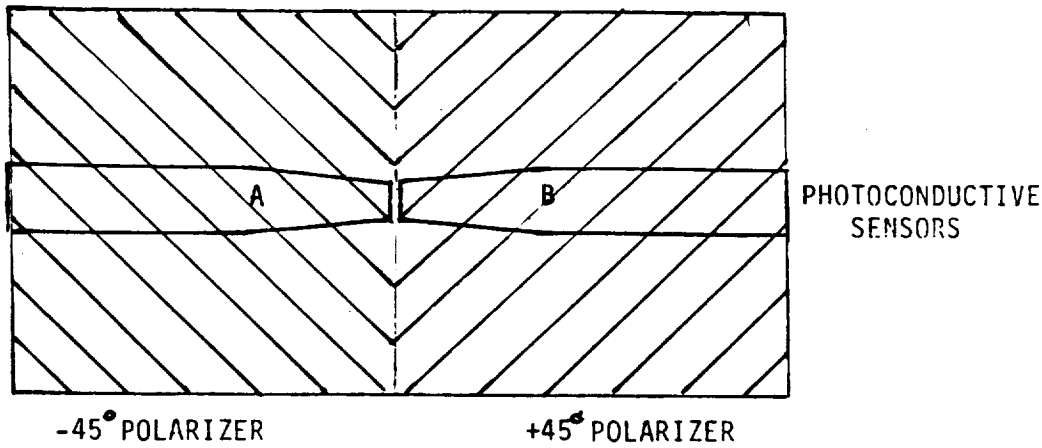

c. CONFIGURATION FOR POLARIZATION TRACKING PHOTOCONDUCTIVE SENSOR

Figure 8

can slowly be rotated past 90 degrees, and the laser beam is interrupted temporarily. The laser is then quickly moved 180 degrees such that the polarization tracking capabilities of the polarized photoconductive tracking sensors can reacquire the laser beam in the opposite orientation.

12.0 Retroreflective Ranging

The ranging capabilities of a laser rangefinder is well understood, so it will not be discussed in detail. Tone ranging, FM CW, or pulsed techniques are common. However, a means for retroreflection must be provided for this measurement. There are a number of possible locations for a corner reflector, but an extremely attractive one is at the center of the conical reflector since it is the critical element of this alignment scheme. As proposed, a corner retroreflector is fitted within the conical reflector, as sketched in Figure 9, to provide a strong return which can also be optically tracked by the laser pointing system.

Since this reflected light is used for roll attitude determination and will also be used for relative velocity measurements to be discussed later, it is important that the orientation of linear polarization be retained upon reflection. Since this is difficult with existing retroreflectors, a flat mirror surrounding the conical reflector might be considered which, upon precise alignment by the photoconductive tracking sensors, will provide an adequate polarization reference. The conical reflector can be physically mounted on this flat mirror, This conical reflector/mirror combination, with the alignment photoconductive tracking sensors, can be adjusted in the lab prior to launch in order to ensure perfect optical alignment which is required to reflect the beam exactly back towards the laser source for both roll and relative velocity measurements.

13.0 Interferometric Relative Velocity Measurements

The range rate or velocity measurement can be derived from periodic multiple range measurements over defined time periods, but it is also possible to use interferometric

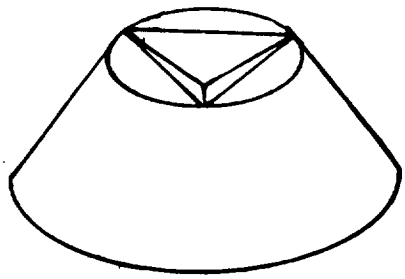

CONICAL REFLECTOR WITH CENTRAL CORNER RETROREFLECTOR

Figure 9

techniques that count interference fringes to determine relative velocity. A simple interferometer might be located at the laser source. By using a beam splitter as sketched in Figure 10, the interferometer measures the velocity of the moving flat mirror on the docking vehicle. The relative velocity, then, is directly related to the number of cyclic variations of intensity incident on a photodetector. Since a cyclic variation is of the order of a wavelength of the laser light, the velocity resolution capability is very high.

The availability of this relative velocity measurement on the docking vehicle itself, however, is desirable, especially if it is passive and doesn't require substantial additional equipment. One possible means of achieving this measurement might be an interferometric measurement using the orthogonal linear polarization, exploiting polarization isolation. Suppose the flat mirror at the base of the conical reflector reflects the laser beam back towards the laser. If there exists a polarized reflective grating at the laser output, it can reflect the orthogonally polarized component, as shown in Figure 11, to the docking vehicle. This orthogonally polarized reflected coherent light can be combined with an artificially created orthogonal component of the original incident of light, using an offset polarizer, to produce interferometric patterns characterizing the relative distances and, therefore, motion over a period of time. The magnitude of the orthogonal component of the reflected light at the polarized reflective grating can be controlled by the angular relationship of the grating to the original orientation of linear polarization, since the tangential component is reflected, creating an orthogonal component. Similarly, the magnitude of the orthogonal component of the original incident radiation can be controlled by the off-axis angular rotation away from polarization cancellation of a polarizer. The recombining of the orthogonal component of the incident coherent light from the off-axis polarizer and that reflected from the polarization grating will create orthogonal interference patterns, which can measure the relative velocity on the docking vehicle, a very attractive situation since the docking vehicle controls the closing velocity to the docking station.

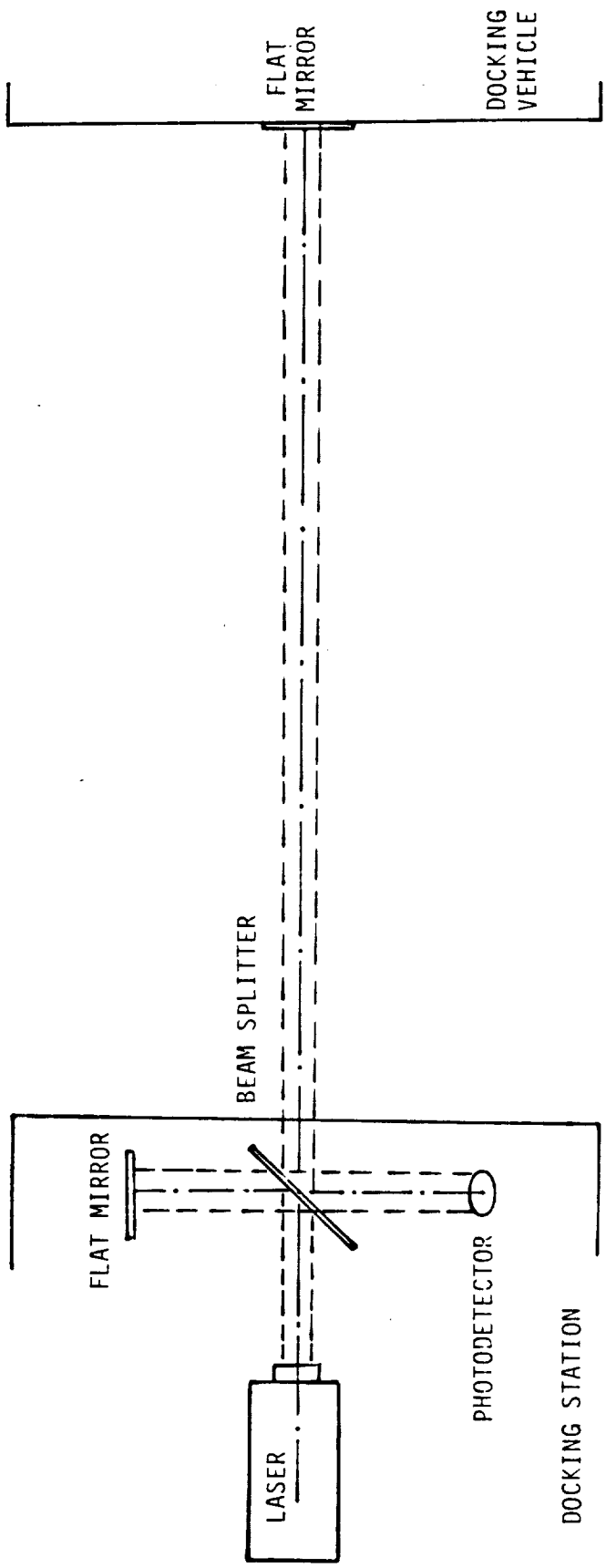

INTERFEROMETRIC VELOCITY MEASUREMENT ON THE DOCKING STATION

Figure 10

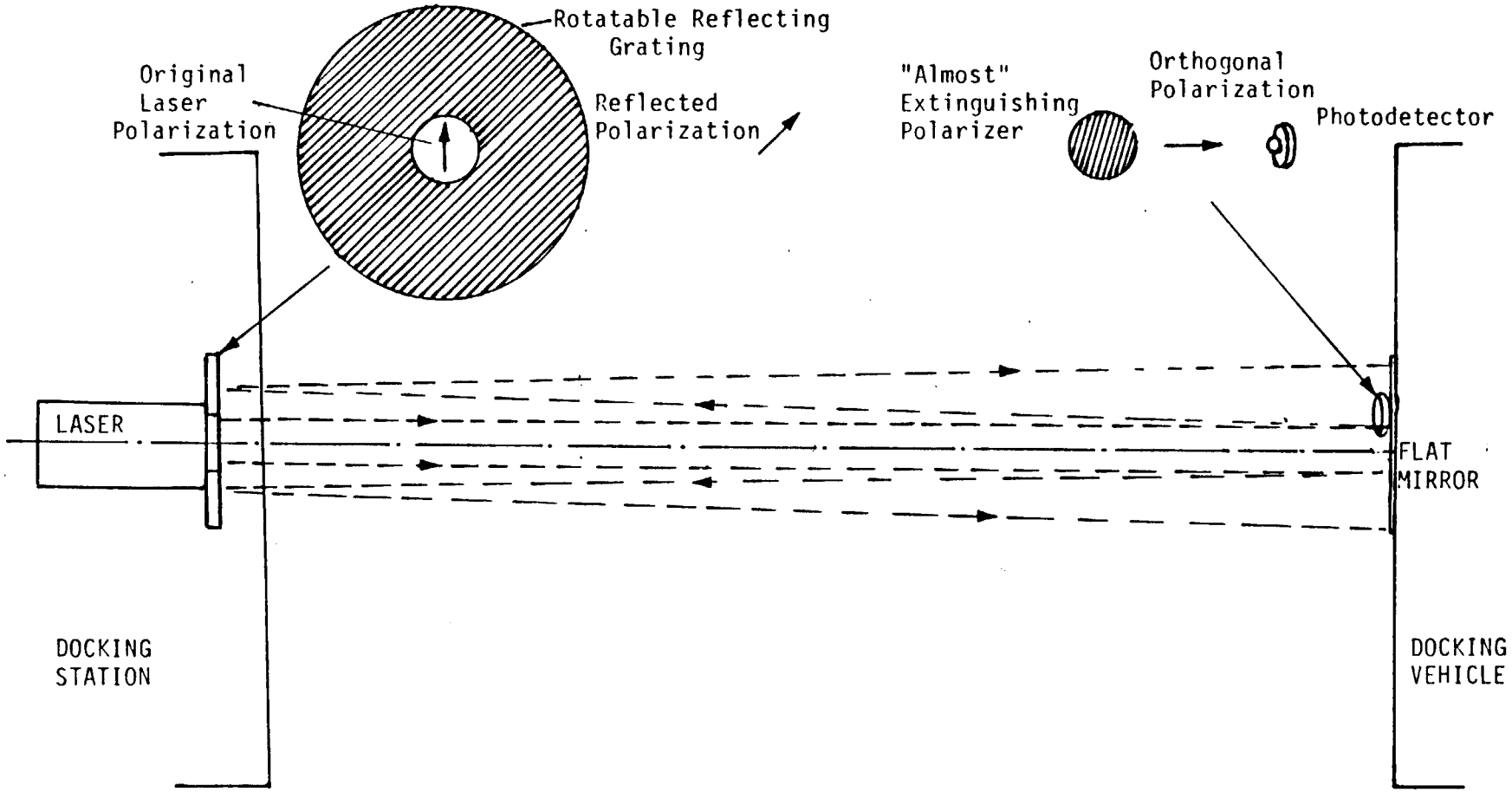

INTERFEROMETRIC VELOCITY MEASUREMENT ON THE DOCKING VEHICLE

Figure 11

14.0 Laser Communication Link

It is highly desirable to develop the capability to communicate with the docking vehicle to command it to move or stop during the docking maneuver. This may be accomplished by modulating the laser beam to transmit commands directly to the docking vehicle, thereby removing the necessity to add another type of link and associated equipment. Basically all that is required is a simple remote control link that would initiate and control closing and departing commands and rates. There are many modulation schemes, but simple amplitude modulation to a photodetector appears to be the most basic and compatible with the active laser beam control system described here.

15.0 An Active RF Docking System

Many of the techniques developed for the active laser beam docking system can be readily translated into the RF spectrum, especially millimeter and submillimeter waves. Quasi-optic techniques are widely used in the design of millimeter and submillimeter systems, and indeed are highly consistent with the laser techniques. The primary criteria for compatibility are coherency and polarization, which both RF and light share in the electromagnetic spectrum.

APPENDIX J

MSCS LINKS DESIGN CONSIDERATIONS

MSCS LINKS DESIGN CONSIDERATIONS

Contract No. NAS9-17414

Interim Report

Prepared for

NASA Lyndon B. Johnson Space Center
Houston, TX 77058

Prepared by

Sergei Udalov

Axiomatix
9841 Airport Boulevard
Suite 912
Los Angeles, CA 90045

Axiomatix Report No. R8607-1
July 10, 1986

Table of Contents

List of Figures

List of Tables

1.0 INTRODUCTION AND SUMMARY

This technical report considers the radio frequency (RF) links for the Mobile Service Center System (MSCS) formerly referred to as Mobile Remote Manipulator System (MRMS). The links analyzed are those between the MSCS and the Orbiter and also between the MSCS and the Space Station. It is assumed that only one link is active at any time.

The links considered are S-band links and Ku-band links. For the S-band case, we have assumed that, for IOC phase, the MSCS commands and telemetry requirements can be satisfied by treating the MSCS as a payload, thus allowing for utilization of the Payload Interrogator (PI) equipment on the Shuttle. We have also assumed that at S-band the 2.25 GHz Shuttle FM link frequency can be used for transmission of one TV channel in either an analog (FM) or in a digital (PSK or QPSK) format. For the Ku-band case, we are assuming that the multiple access (MA) Space Station equipment will be used ultimately for the MSCS as well as for the Shuttle/Space Station links.

The S-band and Ku-band link budgets for digital (22 Mbps) single channel TV transmission indicate that with a 1-watt transmitter and "omni" antennas at both ends adequate margin exists for either frequency. There is, of course, a significant margin advantage for the S-band link, because of the larger aperture of the S-band antennas (i.e., frequency dependence). But, this theoretical advantage of about 16 dB is offset by about 5dB due to exessive receive circuit losses at S-band.

In this report, we also address the problem of handling more than one TV channel at either band. The 'brute force" approach to this problem would be to utilize more RF channels for TV transmission. At S-band, however, this may be quite a problem because of frequency band limitation. At Ku-band, the problem may be less severe but still not trivial.

One way to reduce the total RF bandwidth required to transmit more than one channel (may be up to 5 channels) is to use video data compression on each channel. This, however, may not be acceptable from the standpoint of picture quality. Thus, methods which operate on a total bit stream of up to 5 digitized channels may have to be considered. Two possible methods are:

1) Adaptive Bit Sampling Multipexing (ABSMUX)

and

2) Multi-level, bandwidth conserving modulation such as M-ary PSK.

The first method (ABSMUX) takes advantage of picture statistics averaged over several channels. For example, if there is high activity in only one channel, and relatively low activity (i.e., little motion) in others, the total bit stream required for transmission may be far less than if the same constant bit rate was assigned to each channel. Note, however, that the bit rate is always higher than the bit rate of a single channel. Consequently, the RF bandwidth required is more than that required to transmit one digital TV channel. Furthermore, considerable amount of video signal processing is required at both ends of the ABSMUX link.

The second method, i.e., multi-level modulation such as M-ary PSK (MPSK), permits several digital data streams to be multiplexed into one RF channel having a bandwidth of a single channel. The penalty paid for such bandwidth conservation is, of course, the increased transmitter power. Because the use of MPSK falls into cathegory of RF transmission, we have considered a possiblity of using such modulation for MSCS link to Space Station.

Table 1-1 shows the summary of the link budgets.* From this table, it is evident that very good link margins exist for the command and telemetry links at all bands. For those telemetry links which are at Ku-band and which may be multiplexed with multi-channel digital TV, the margins were not computed, but it is assumed here that they (i.e., margins) are not worse than the margins for the multi-channel digital TV links.

*At maximum range of 100 meters.

Link	Band	Signal Transmitted	Origin	Destination	Rate	EIRP (dBm)	Link Margin (dB)	Comments
MSCS/ Shuttle Orbiter (SO)	S	CMD	SO	MSCS	2 kbps	30.4	64.5	Payload Interrogator Link
		TLM	MSCS	SO	16 kbps	15	37.8	Payload Interrogator Link
		Analog FM TV	MSCS	SO	Analog	25	15.8	Analog FM Receive
		Digital TV	MSCS	SO	25 Mbps	25	18.6	Requires Special Tx and Rx Equipment
	Ku	CMD	SO	MSCS	100 kbps	15	19.9	
		TLM	MSCS	SO	100 kbps	15	20.2	
		Digital TV	MSCS	SO	25 Mbps*	25	6.2	Single-Channel Digital TV
MSCS/ Space Station (SS)	S	CMD	SS	MSCS	2 kbps	30.4	64.5	
		TLM	MSCS	SS	16 kbps	15	37.9	
		Digital TV	MSCS	SS	25 Mbps*	32	9.6	5 Channels @ 25 Mbps via 32-level MPSK
	Ku	CMD	SS	MSCS	100 kbps	15	19.9	
		TLM	MSCS	SS	100 kbps	15	20.2	
		Digital TV	MSCS	SS	25 kbps	25	6.2	Single-Channel Digital TV
		Digital TV	MSCS	SS	25 Mbps*	42**	3.3	5 Channels @ 25 Mbps via 32-level MPSK

*Telemetry is assumed to be a small fraction of TV data rate, thus the multiplexing of TLM data stream with TV data is negligible on the link margin.

**Requires a 50 watts transmitter at Ku-band

Table 1-1. Link Budget Summary for MSCS/Orbiter and MSCS/Space Station Links (Range = 100 meters)

Most significant comparison of the S-band and Ku-band operation of the 5-channel links is that the larger aperture of the S-band omni antennas provides a significant transmitter power saving when compared to Ku-band operation. Specifically, it takes 5 watts of transmitter power at S-band with an omni antenna and 50 watts at Ku-band with an omni antenna.

This implies that for Ku-band operation either antenna gains have to be increased with concomitant directivity problems or the transmitter power has to increase accordingly if the 32-level MPSK approach is to be adopted for simultaneous transmission of 5 digital TV channels. But, 50 watts of Ku-band power is already equal to the capability of the TWTA which is currently used with the Orbiter Ku-band radar/communication system. Thus, requiring more power at Ku-band does not seem like a feasible approach.

The key remaining issue is the implementation of multi-channel digital TV links between MSCS and Space Station. We have baselined here an innovative approach, i.e, a 32-level MPSK for multiplexing of five digital TV channels within the bandwidth of a single 25 Mbps channel. We realize that we have to pay the penalty in power to stay within the bandwidth of a single channel. Such a trade-off is of particular importance for S-band utilization of multi-channel digital TV transmission if such utilization is considered as the only feasible alternative for multi-channel TV transmission. Also, if MPSK is to be adopted as a possible approach, there remains such technical issues as the effect of multi-path and the complexity of the equipment. Furthermore, MPSK equipment is different from the "baseline" Ku-band equipment, and thus the extra development cost must be considered. Consequently, further trade-offs are necessary to determine the most feasible approach to implementing simultaneous multi-channel digital TV transmission from MSCS.

2.0 LINK CONSIDERATIONS AND TRADE-OFFS

2.1 General Requirements

The Mobile Service Center System (MSCS) has been identified as a logistics/utility device required for both the assembly phase and the subsequent operation of the Space Station.

It is currently envisioned [1] that the MSCS be equipped with : 1) a spacecrane capability (i.e., Shuttle RMS) and 2) a pair of astronaut-foot restrained arms. During the initial Station assembly phase, the MSCS will be performing such functions as:

1) positioning astronauts for EVA functions

2) transporting modules and/or payloads from the Shuttle cargo bay

and

3) positioning the transport modules and/or payloads for attachment to the truss structure of the Space Station.

During the subsequent operational phases of the Space Station, the functions of the MSCS will include, but not necessarily be limited to the following:

1) maintenance and/or repair activities

2) providing construction capabilities for future Station growth

and

3) assembly and servicing of large spacecrafts.

Figure 2.1-1 shows the conceptual visualization of the MSCS. As indicated in the figure, the main body of MSCS consists of a mobile logistics platform to which are attached one Shuttle-type manipulator arm and two mobile foot restraint (MFR) arms.

The main manipulator arm has the same capability as the Shuttle RMS with the associated requirement for agility and dexterity. The function of the MFR is to position pressure-suited astronauts within their work envelope.

In contrast with the RMS the MFRs are controlled by the astronauts, who position themselves in a manner similar to the operation of a "cherry picker" bucket. Thus, the degrees of freedom available to MFR are determined by the "reachability" requirements of the specific EVA mission.

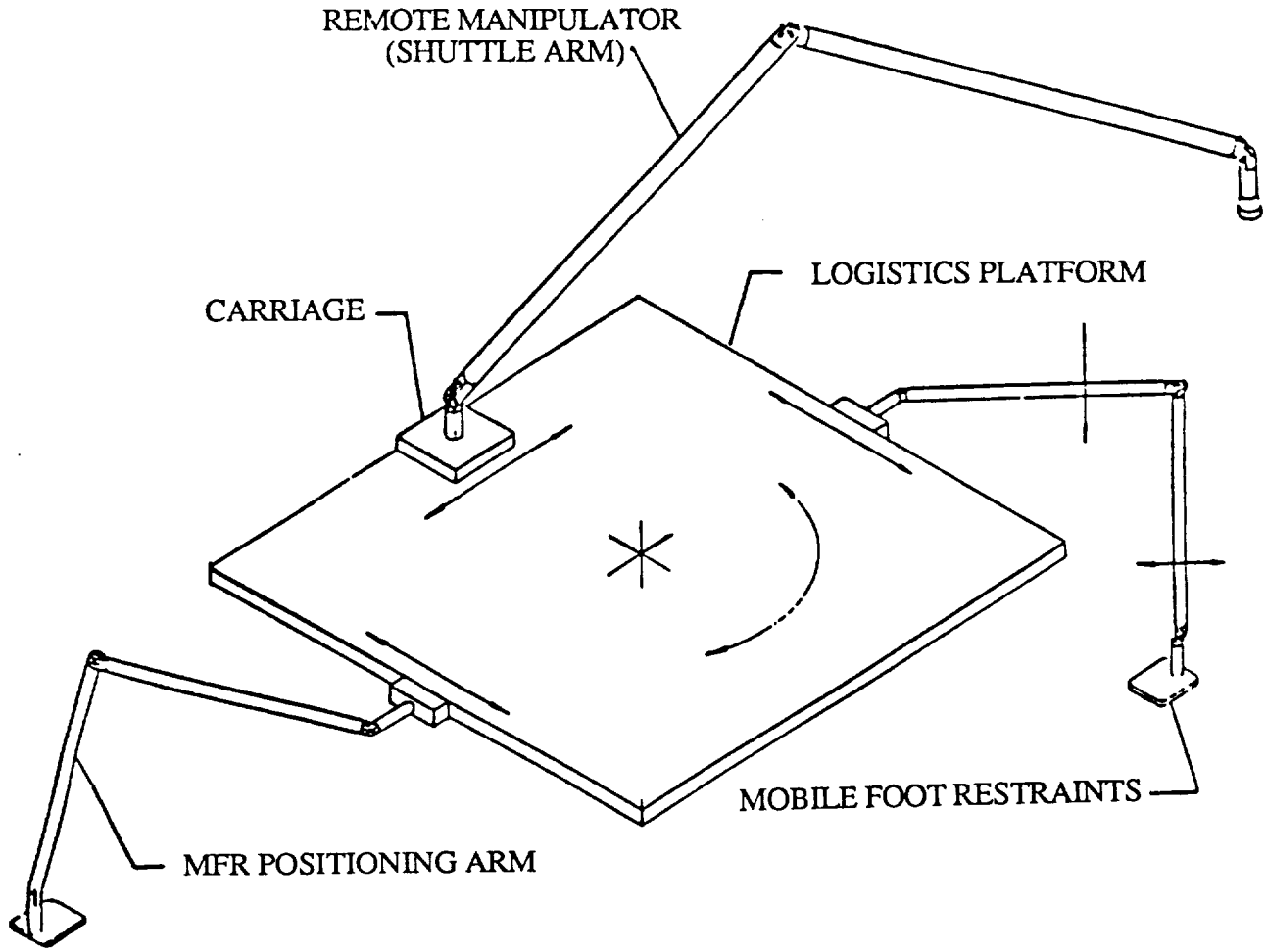

Figure 2.1-1. Mobile Service Center System (MSCS)

In view of these potential activities, the requirements on the C&T system of the MSCS can be conceptualized and defined.

Because the primary function of the MSCS is the support of the construction and maintenance of the Space Station, the RF link considerations for this device must take into account the interaction between all of the space vehicles envolved, i.e., the Orbiter, the MSCS and the Space Station.

To better understand the impact of the MSCS on the Orbiter (NSTS), we consider the time-phased profile of the communication requirement between the Orbiter, the MSCS and the Space Station. Figure 2.1-2 shows Shuttle Orbiter (NSTS) RF link interaction with MSCS, during the Space Station assembly phases.

During the first flight the transverse boom will be placed on orbit. Thus, the boom and the MSCS will be the two principal elements of the Space Station assembly in orbit. The C&T links will, thus, be between the MSCS and NSTS and the Space Station (boom). These links will consist of commands from the NSTS and the telemetry to the NSTS. One of these links will also carry TV from the MSCS to the NSTS.

During the second flight, the C&T capabilities will be expanded to permit full operational control of the MSCS by the crew aboard the NSTS. In addition, a link will be added which will also permit the full control of the MSCS by a crew onboard the Station.

At the time of flight #5 of the assembly, a Laboratory Module will be added to the Station. This module will be periodically inhabited by a crew. Thus, a two-way voice link between the Station and the NSTS will be added to the C&T capability at this point.

The important point of the discussion above is to show that the requirement for the direct interaction between the MSCS and the NSTS remain virtually unchanged from the first flight. The RF environment in which this interaction takes place, however,

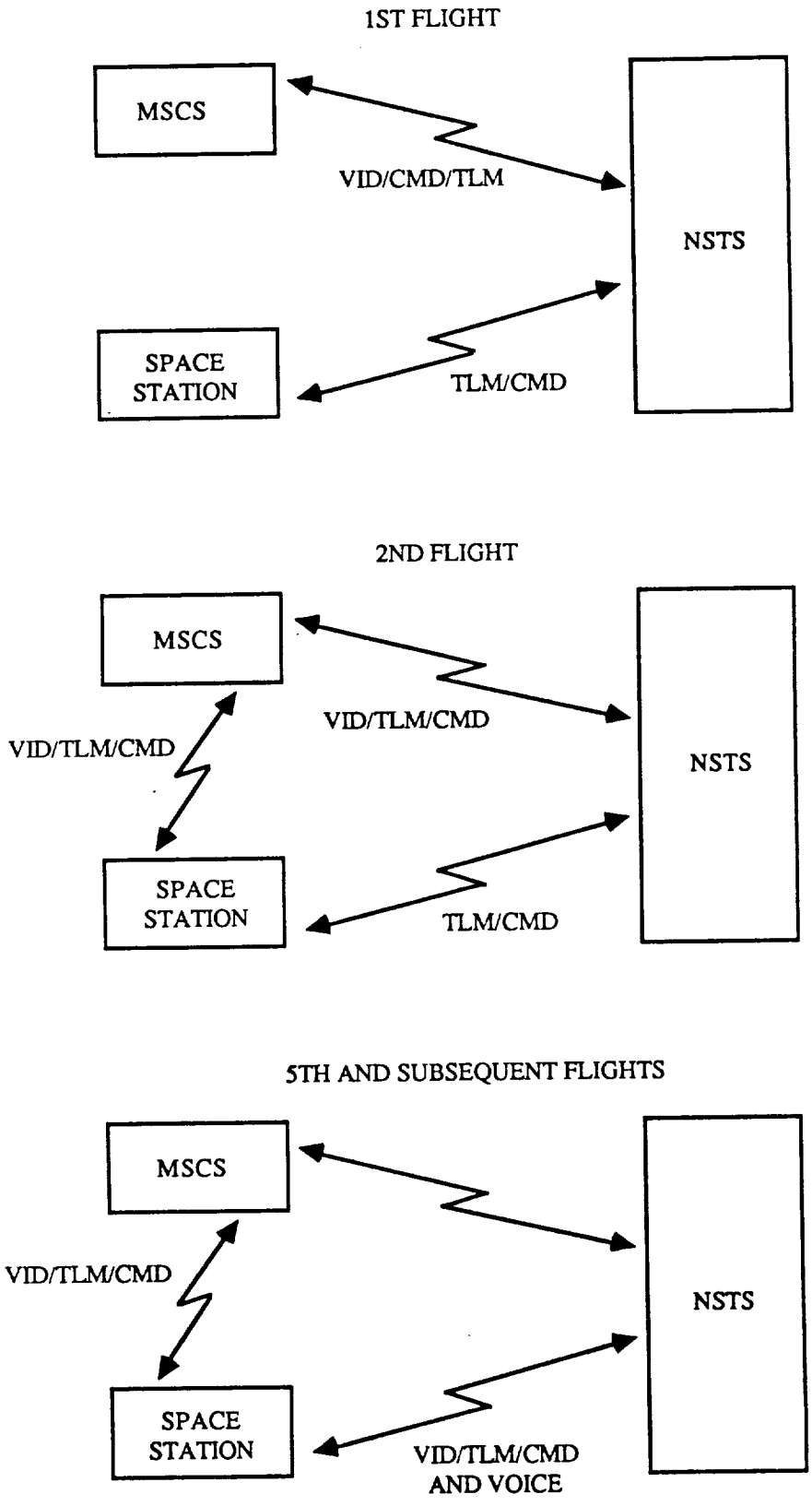

Figure 2.1-2. Shuttle Orbiter (NSTS) RF Link Interaction with MSCS during Space Station Assembly Phases

will be influenced by the requirements of the other links. Table 2.1-1 summarizes the RF link requirements for the NSTS, MSCS and Space Station interaction.

2.2 Video Requirements

The main driver on the RF link (or links) is the requirement to transmit TV video signals from MSCS to either the Orbiter or the Space Station. The number of video signals generated at any one time by the MSCS depends on the mission. Figure 2.2-1 and Table 2.2-1 show, respectively, the video component allocation and the corresponding MSCS element requirements. Figure 2.2-2 shows MSCS video subsystem reference architecture.

From Table 2.2-1, it can be seen that the Special Purpose Dextrous Manipulator (SPDM) may require as many as five (5) TV cameras.

If all of these cameras have to viewed simultaneously, then the RF link has to provide the necessary bandwidth. This presents a problem, particularly for the S-Band trasmission due to restricted bandwidth occupancy available to MSCS/Shuttle/Space Station communication. In sections that follow, we explore possibilities of using advanced modulation techniques for trading RF power for bandwidth conservation.

2.3 MSCS to Shuttle Orbiter Link

To obtain some quantitative idea with respect to the trade-offs between S-band and Ku-band operations of the MSCS/Orbiter links, we have postulated link budgets for both S-band and Ku-band operations. The S-band operation can be considered as starting point for two reasons: (1) It can be implemented with the existing S-band equipment and (2) it is the baseline operation defined for the MSCS/Orbiter and the MSCS/SS links in the Reference Configuration Document for the Space Station [1]. On the other hand, eventual utilization of the Ku-band multiple-access (MA) system baseline for the Space Station should be considered as a goal for these two links. The utilization of the Ku-band by the NSTS will have definite impacts on the latter.

Link	Range		Data Rate		Flight Number
	Min	Max	To	From	
NSTS/SS	0.1km	37km	2 kbps (CMD)	16 kbps (TLM)	1
NSTS/MSCS	0.01km	0.1km	2 kbps (CMD)	16 kbps + video	1
NSTS/SS	0.01km	0.1km	2 kbps (CMD) + 16kbps (Voice)	16 kbps (TLM) + (Voice) + Video	5
SS/MSCS	1m	100m	2 kbps (CMD)	16 kbps (TLM) + Video*	2

*May require up to 5 channels

Table 2.1-1. RF Link Requirements for NSTS, MRMS and Space Station Interaction

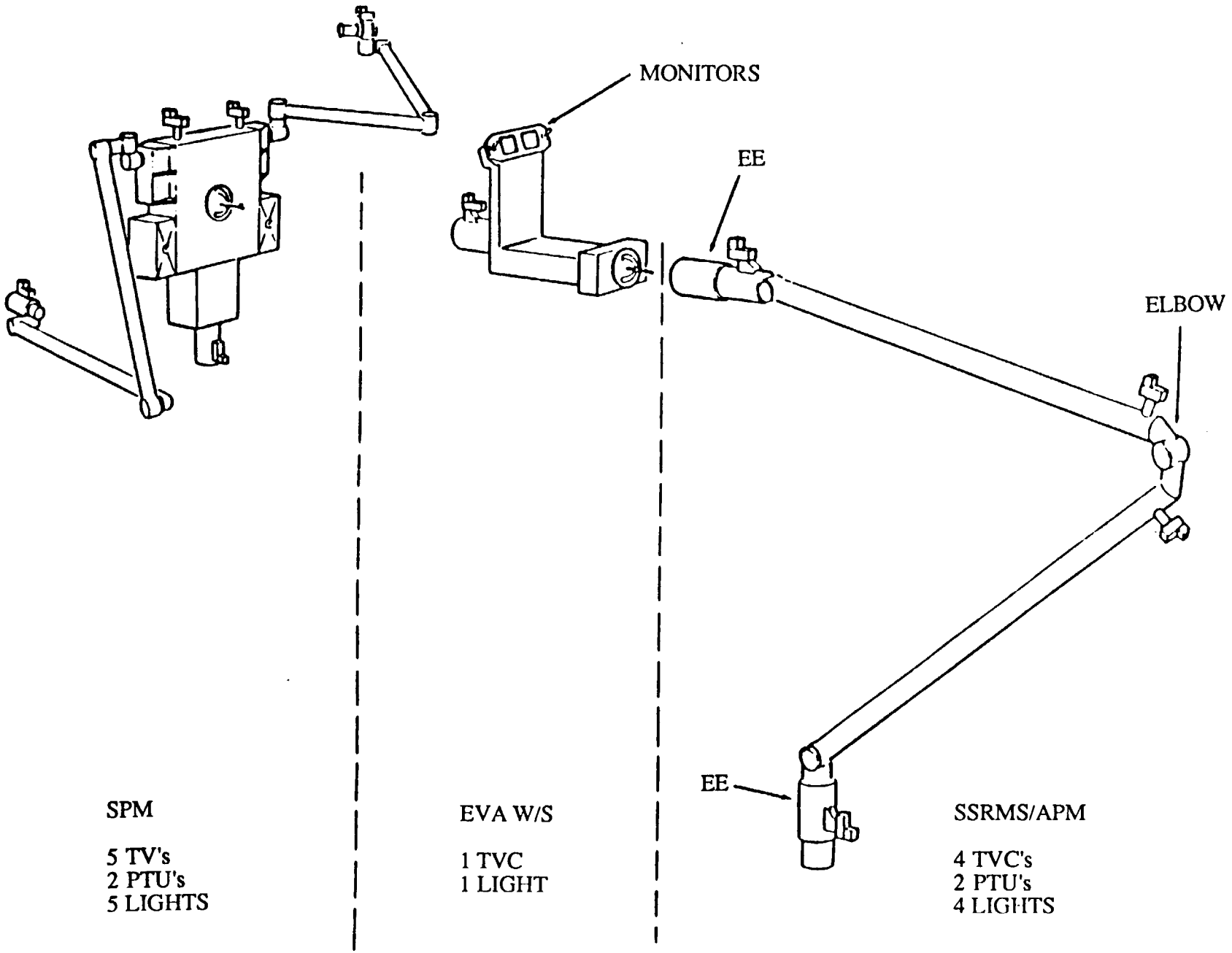

Figure 2.2-1. MSCS Video Component Allocation

MSCS VIDEO COMPONENT	SSRMS	APM	MBS AND P/O A	SPDM	EVA W/S	MMD	IVA C/S
TV CAMERA	4	4	3	5	1	1	NR
PAN & TILT UNIT	2	2	2	2	NR	NR	NR
LIGHT	4	4	3	5	1	1	NR
MONITOR	NR	NR	NR	NR	2	NR	3
VIDEO BUS INTERFACE UNIT	4	4	1	1	1	1	*
VIDEO CONTROL UNIT	NR	NR	1	NR	NR	NR	NR

NOTE: * SS INTERFACE UNIT REQUIRED

Table 2.2-1. MSCS Element Requirements

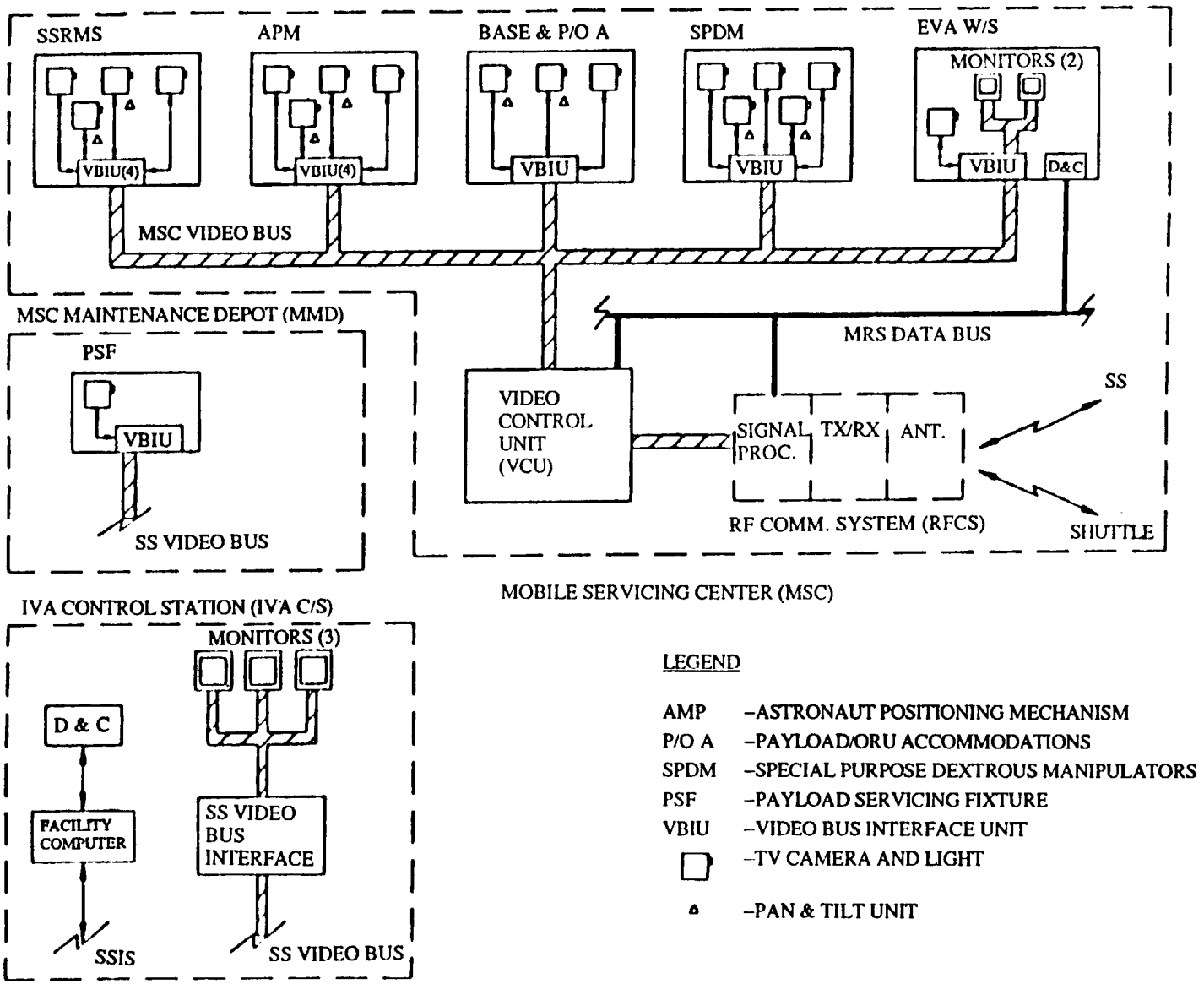

Figure 2.2.-2. MSCS Video Subsystem Reference Architecture

2.3.1 MSCS/Orbiter Links at S-Band

Table 2.3.1-1 shows a link budgets for a two-way CMD/TLM S-band link between the Orbiter and the MRMS. The budget assumes that the MSCS is treated as a payload and thus Payload Interogator can be utilized in its unmodified configuration. As indicated in the table, commands at the rate of 2 kbps are sent to the MSCS and the telemetry at 16 kbps is sent back to the Orbiter. Figure 2.3.1-1 shows a functional block diagram which uses FM transmission of a single analog video channel from MSCS. The commands and telemetry are handled by separate digital channel which is established at S-band between the PI and a transponder on MSCS. This transponder is assumed to be either the standard NASA payload transponder or equivalent.

Figure 2.3.1-2 shows the MSCS end of an S-band link which uses digital (25 Mbps) TV transmission instead of analog FM. The block diagram is similar to one shown in Figure 2.3.1-1 except for the addition of video processor for TV digitizing.

The S-band link budget for analog and digital TV trasmission forms the MSCS to Orbiter are given in Table 2.3.1-2 and 2.3.1-3, respectively. The operating frequency baseline for both of these links is at 2.25 GHz which is the frequency of the current FM link.

Consider first the analog FM link budget shown in Table 2.3.1-2. From that table, it is evident that the link margin is determined by the output signal-to-noise ratio if one assumes that 35dB SNR is required at the output. The margins, however, are adequate for both criteria used to define the threshold performance of the link. This allows for various parameter trade-offs if such trade-offs are required in the future.

Very good link margin is also indicated for the digital TV link at S-band as indicated by Table 2.3.1-3. It is important to note the criterion for the digital link is BER of 10^{-5} rather than the output SNR. Our experience with digital TV Δ-mod transmission indicates, however, that at 25 Mbps output SNR is not as good as that of an analog link for the same bandwidth.

	SO/MSCS CMD (2kbps) f = 2.125 GHz	MSCS/SO TLM (16kbps) f = 2.29 GHz	Comments
Transmitter power (dBm)	37(5w)	20 (0.1w)	
Transmit circuit loss (dB)	-8.1	-2	
Transmit antenna gain (dB)	2.5	0	
Transmit pointing loss (dB)	-1	-3	
EIRP (dBm)	30.4	15	
Path Loss (dB)	-78.9	-79.6	Range = 0.1km
Received antenna gain (dB)	0	-2.5	
Received pointing loss (dB)	-3	-1	
Polarization loss (dB)	-0.3	-0.3	
Received circuit loss (dB)	-2	-8.1	
Received signal power (dBm)	-53.8	-71.5	
System noise density (dBm/Hz)	-167	-167	NF = 7 dB at both ends
Carrier to noise density (dB-Hz)	113.2	95.5	
Modulation loss (dB)	-4.1	-4.1	β = 1.0 rad at both ends
Data rate (dB-Hz)	33	42	
Receive E_b/N_0 (dB)	76.1	49.4	
Theoretical E_b/N_0 (dB)	9.6	9.6	
Implementation loss (dB)	2	2	
Required E_b/N_0 (dB)	11.6	11.6	
Link Margin (dB)	64.5	37.8	

Table 2.3.1-1 Shuttle Orbiter/MSCS Links at S-band (CMD and TLM)

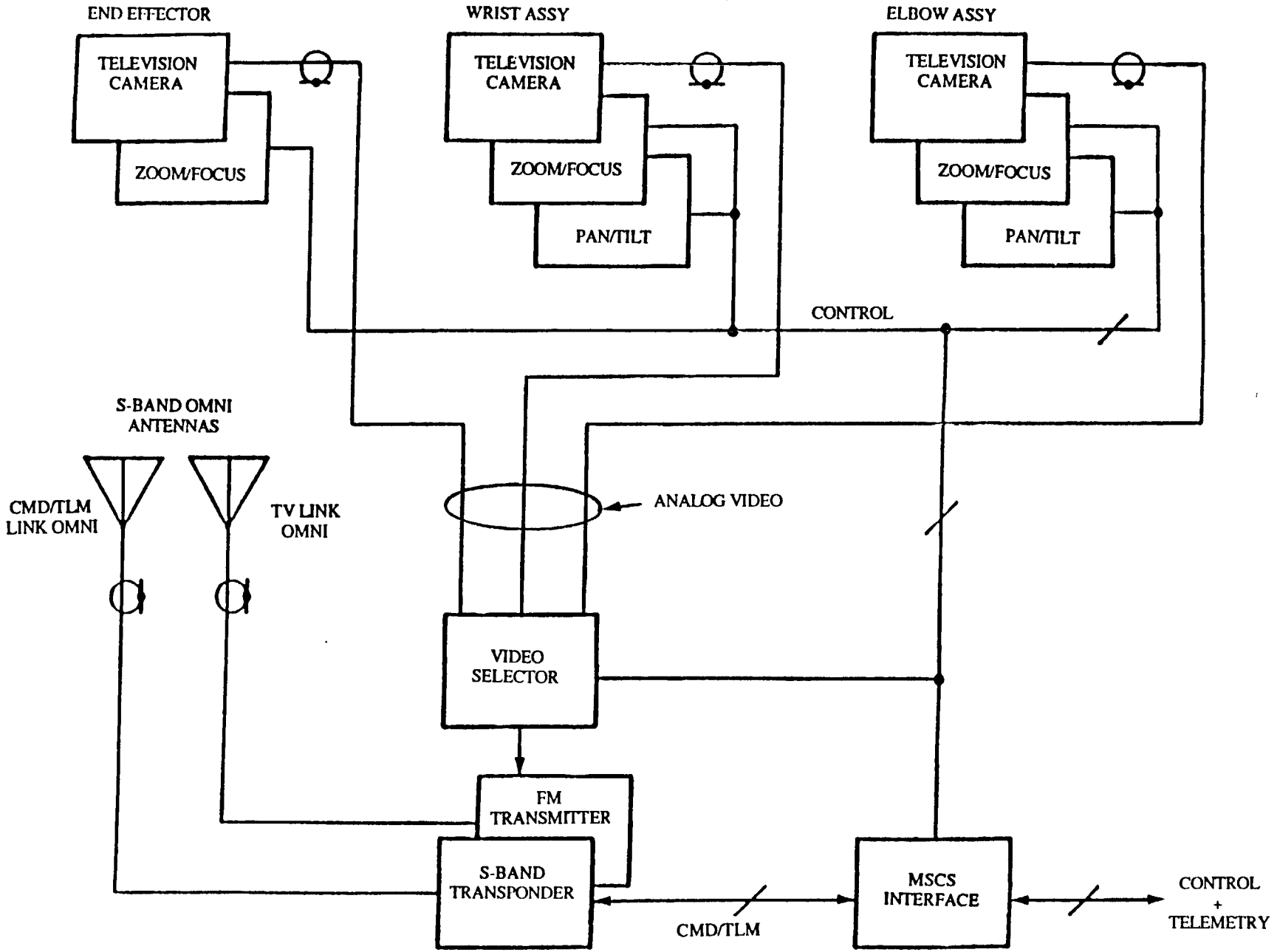

Figure 2.3.1-1 MSCS S-Band Analog TV Configuration

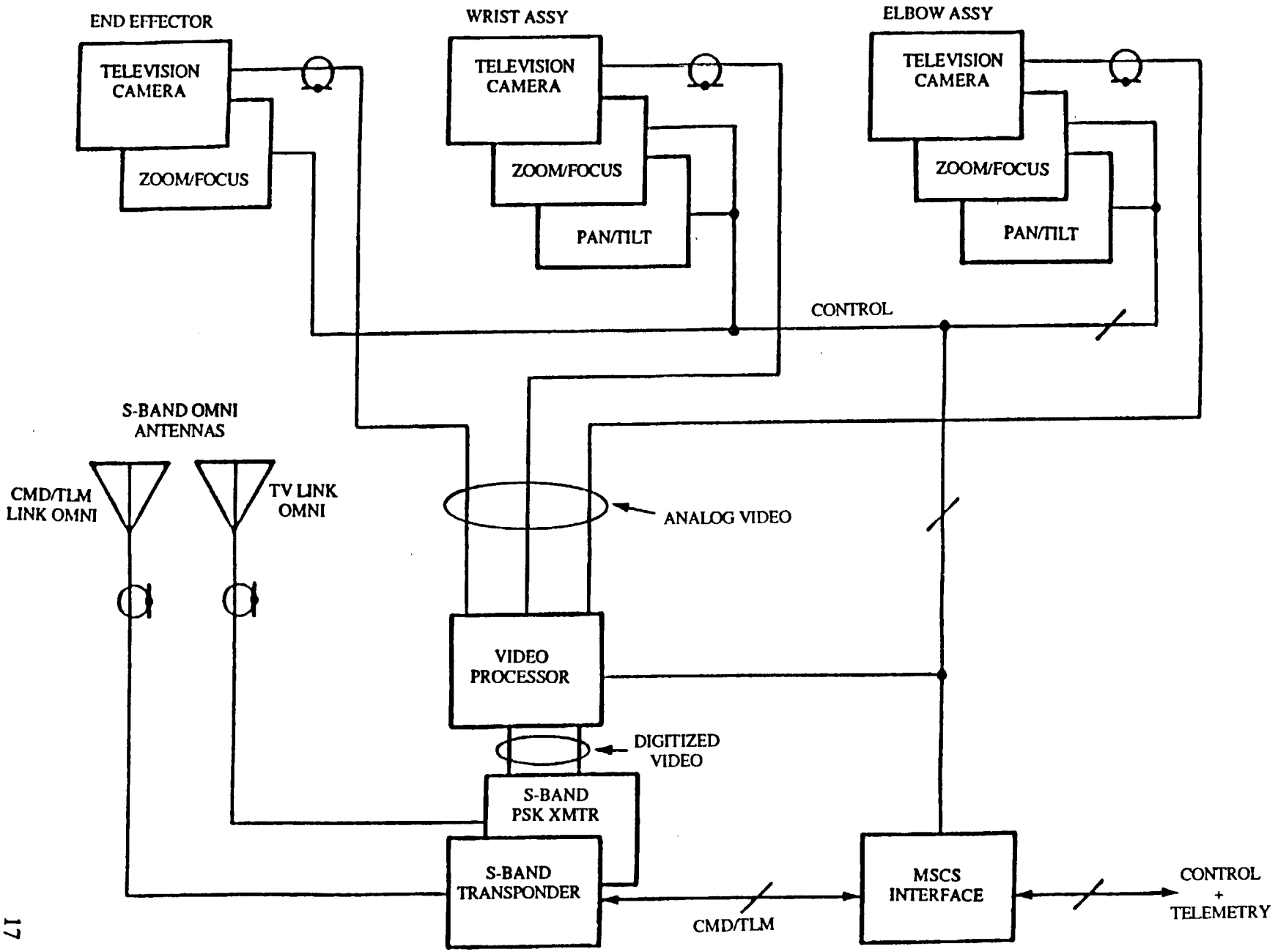

Figure 2.3.1-2. MSCS S-Band Digital TV Configuration

	MSCS/SO Analog TV FM Link	Comments
Transmitter power (dBm)	30	1 watt
Transmit circuit loss (dB)	-2	
Transmit antenna gain (dB)	0	
Transmit pointing loss (dB)	-3	
EIRP (dBm)	25	
Path Loss (dB)	-79.4	0.1km f = 2.25 GHz
Received antenna gain (dB)	1	
Received pointing loss (dB)	-3	
Polarization loss (dB)	-0.5	
Received circuit loss (dB)	-6.9	
Received signal power (dBm)	-63.8	
System noise density (dBm/Hz)	-168	6 dB NF
Carrier to noise density (dB-Hz)	104.2	
Predetection bandwidth (dB-Hz)	67	If BW = 40 MHz
SNR at discriminator input (dB)	28.2	
FM threshold (dB)	12	
FM threshold Margin (dB)	16.2	
Output SNR (dB)	50.8	Δf = 9 MHz, B_{out} = 5 MHz
Required SNR (dB)	35	
TV margin	15.8	
Link margin	15.8	Link Margin is determined by SNR output

Table 2.3.1-2 MSCS to Shuttle Orbiter Analog TV Link at S-Band

	MSCS/SO Digital TV Link	Comments
Transmitter power (dBm)	30	1 watt
Transmit circuit loss (dB)	-2	
Transmit antenna gain (dB)	0	
Transmit pointing loss (dB)	-3	
EIRP (dBm)	25	
Path Loss (dB)	-79.4	0.1 km f = 2.25 MHz
Received antenna gain (dB)	1	
Received pointing loss (dB)	-3	
Polarization loss (dB)	-0.5	
Received circuit loss (dB)	-6.9	
Received signal power (dBm)	-63.8	
System noise density (dBm/Hz)	-168	NF = 6 dB
Carrier to noise density (dB-Hz)	104.2	
Modulation loss (dB)	N/A	
Data rate (dB-Hz)	74	25 Mbps Δ-Mod
Receive E_b/N_0 (dB)	30.2	
Theoretical E_b/N_0 (dB)	9.6	BER = 10^{-6}
Implementation loss (dB)	2	
Required E_b/N_0 (dB)	11.6	
Link Margin (dB)	18.6	

Table 2.3.1-3 MSCS to Shuttle Orbiter Digital TV Link at S-Band

2.3.2 MSCS/Orbiter Links at Ku-Band

The Ku-band between the MSCS and the Orbiter will be established by means of the Ku-band Muliple Access (MA) equipment installed on the Orbiter. This equipment will be compatible with the Space Station MA equipment operating within the Ku-band.

Figure 2.3.2-1 shows the Ku-band Digital Configuration for the MSCS avionics. It must be noted that this configuration is essentially the same as that of the S-band digital configuration shown in Figure 2.3.1-2. The only difference is that with the Ku-band system, the commands and telemetry digital video data is multiplexed with the digital video data stream while with the S-band implementation shown in Figure 2.3.2-1, the digital video signal is handled by a separate RF link. Figure 2.3.2-2 clarifies some of the details of the Ku-band digital implementation of the MSCS.

Table 2.3.2-1 shows a link budget for MSCS/Orbiter Ku-band digital MA communication. As can be seen from this budget, the link margins are smaller for the Ku-band than they are for the corresponding links at S-band. Of particular important is the reduced margin for the digital TV. The main reason for this is the increased path loss at Ku-band which, of course, in actuality is the effect of the reduced antenna aperture at the receiver end of the link.

Considering the ratio of the Ku-band (14.15 GHz) to S-band frequency (2.25 GHz), the path loss difference is about 16 dB in favor of the S-band link. However, there are exessive receiver circuit losses at the S-band. Thus, the link margin difference is only about 12 dB in favor of S-band. The impact of this difference on the transition from the Ku-band digital MA operation of the Orbiter can not be ascertained until all of the operational considerations for the MSCS are fully defined.

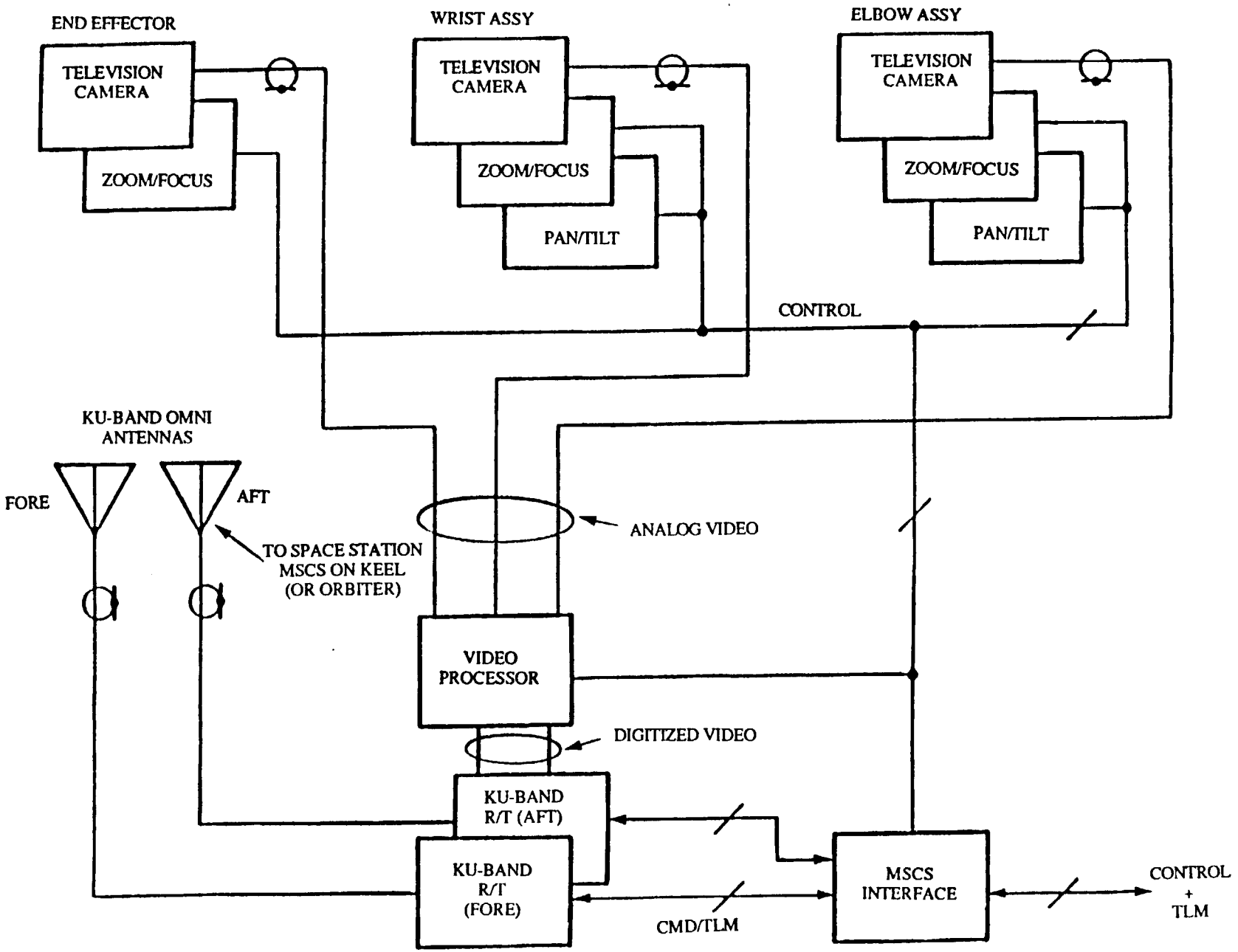

Figure 2.3.2-1. MSCS Ku-Band MA Digital Configuration

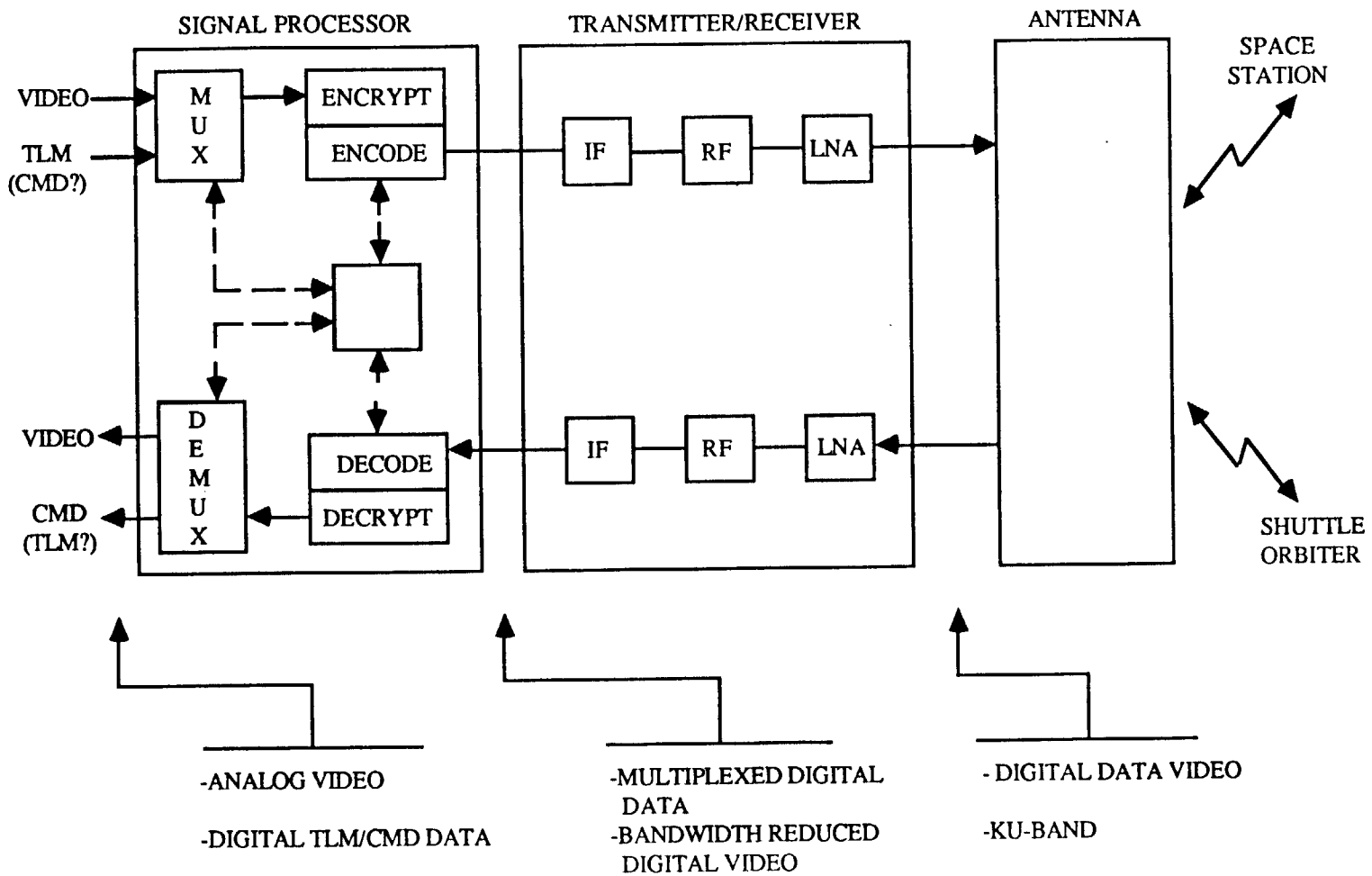

Figure 2.3.2-2. MSCS Communication Subsystem for Ku-Band MA Link

2.4 MSCS/Space Station Links

2.4.1 Bandwidth Conserving Multi-Channel TV Link

When the MSCS is operating on the Space Station, we may assume that all 5 TV channels may be required simultaneously. Thus means for transmitting all five channels should be addressed. Considering the fact that each digital TV channel consists of a 25 Mbps data stream, the RF bandwidth required would be at least 125 MHz, or more, unless some advanced modulation techniques, other than bi-phase, or QPSK are used.

For the baseline described below, we have chosen a 32-level Multiple-Phase Shift Keying (MPSK). The goal with this approach is to establish such 32-level MPSK link at either S-band or a Ku-band needs to be computed.

Figure 2.4.1-1 shows a functional diagram of a five-channel Multiplexer/Modulator which transforms the five (5) parallel digital TV channels into a single 32-level phase-shift modulated RF signal. As shown in the figure, the modulation can be accomplished at some intermediate carrier in the region of 100 to 500 MHz. Subsequent upconversion translates the PSK modulated carrier to either an S-band or Ku-band carrier frequency. The power amplifier supplies the require amplification to achieve the output power level (P_{out}) required by the link budgets.

Although the combined amplitude and phase modulation can provide a more efficient use of RF power, we have assumed that a constant level MPSK is used. Thus a limiting power amplifier can be assumed without a danger of distorting the composite RF signal.

2.4.2 MSCS/Space Station Links at S-band

Table 2.4.2-1 presents the link budgets for the MSCS/space Station links implemented at S-band. We have assumed here that commands and telemetry requirements can be satisfied by a S-band link which is based on utilization of a PI placed on the Space Station and a payload transponder placed on MSCS. Thus, it is the same link as is shown in Table 2.3.1-1

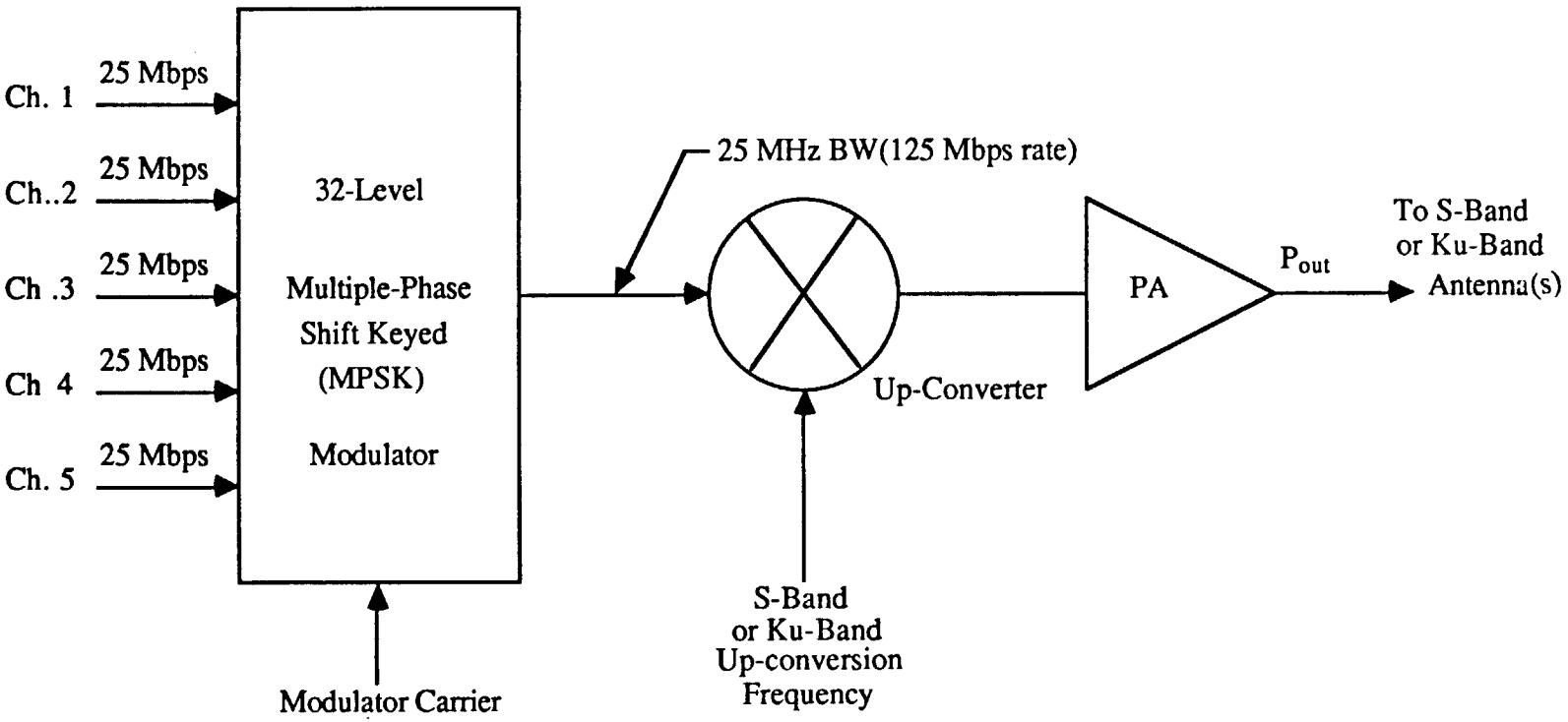

Figure 2.4.1-1 Five Channel Multiplexer/32-Level MPSK Modulator for MSCS/Space Station Digital TV Link(s)

	Space Station/MSCS CMD Link at 2.125 GHz		MSCS/Space Station TML Link at 2.29 GHz		MSCS/Space Station S-Channel MPSK Digital TV Link at 2.25 GHz	
	Value	Comments	Value	Comments	Value	Comments
Transmitter power (dBm)	37	5 Watts	20	0.1 watts	37	5 watts
Transmit circuit loss (dB)	-8.1	PI cable loss	-2		-2	
Transmit antenna gain (dB)	2.5		0		0	
Transmit pointing loss (dB)	-1		-3		-3	
EIRP (dBm)	30.4		15		32	
Path Loss (dB)	-78.9	R = 0.1km	-79.6	R = 0.1 km	-79.4	R = 0.1 km
Received antenna gain (dB)	0		2.5		0	
Received pointing loss (dB)	-3		-1		-3	
Polarization loss (dB)	-0.3		-0.3		0.5	
Received circuit loss (dB)	-2		-8.1	PI cable loss	-3	
Received signal power (dBm)	-53.8		-71.5		53.9	
System noise density (dBm/Hz)	-167	NF = 7 dB	-167	NF = 7 dB	-169	NF = 5 dB
Carrier to noise density (dB-Hz)	113.2		95.5		115.1	
Modulation loss (dB)	-4.1	β = 1.0 rad	-4.1	β = 0.1 rad	N/A	
Data rate (dB-Hz)	33	2 kbps	42	16 kbps	74	25Mbps (5-ch, 32 MPSK)
Receive E_b/N_0 (dB)	76.1		49.4		41.1	
Theoretical E_b/N_0 (dB)	9.6		9.6		29.5	32-level MPSK
Implementation loss (dB)	2		2		2	
Required E_b/N_0 (dB)	11.6		11.6		31.5	
Link Margin (dB)	64.5		37.9		9.6	
	PI Based Link				Special Link	

Table 2.4.2-1. Link Budgets for MSCS/Space Station Links at S-Band

The transmission of TV, however, is accomplished by a special 32-level MPSK link described in Section 2.4.1. Note that a range of 0.1 km (100 meters) the link margin with a 5-watt trasmitter is about 10dB for the 5-channel digital TV transmission.

The important accomplishment of the "special" link is that it allows operation within a 25 MHz bandwidth centered at 2.25 GHz. Thus the bandwidth occupancy is about the same as used for single analog and digital TV links at S-band.

2.4.3 MSCS/Space Station Links at Ku-band

Table 2.4.3-1 shows the link budgets for the MSCS/Space Station links implemented on Ku-band. The link is for a single digital TV channel, and thus it is the same as in Table 2.3.2-1 which is a link budget for the Orbiter/MSCS link. Thus, except for operational geometries, which may differ for the two links, this link is not unique in its implementation.

Table 2.4.3-2 gives a link budget which includes a five-channel digital TV link from MSCS to Space Station.

The most important fact shown by Table 2.4.3-1 is that 5-channel, 32-level MPSK requires up to 50 watts of Ku-band power to work over the distance of only 100 meters with a margin of only about 3 dB. This power level coresponds to a capability of the Shuttle Orbiter's Ku-band transmitter TWTA.

The comparison with a similar link implemented at S-band (see Table 2.4.2-1) clearly demonstrates the advantages of working at lower frequencies where antenna apertures are larger.* The bandwidth occupancy at S-band, however, is at preminium.

*This shows up as reduced space loss.

	SS/MSCS CMD 14.63 GHz	MSCS/SS TLM 14.15 GHz	MSCS/SS Digital TV 14.15 GHz	Comments
Transmitter power (dBm)	20 (0.1w)	20 (0.1w)	30 (1w)	
Transmit circuit loss (dB)	-2	-2	-2	
Transmit antenna gain (dB)	0	0	0	
Transmit pointing loss (dB)	-3	-3	-3	
EIRP (dBm)	15	15	25	
Path Loss (dB)	-95.7	-95.4	-95.4	0.1 km
Received antenna gain (dB)	0	0	0	
Received pointing loss (dB)	-3	-3	-3	
Polarization loss (dB)	-1.8	-1.8	-1.8	
Received circuit loss (dB)	-2	-2	-2	
Received signal power (dBm)	-87.5	-87.2	-77.2	
System noise density (dBm/Hz)	-169	-169	-169	NF = 5 dB at both ends
Carrier to noise density (dB-Hz)	81.5	81.8	91.8	
Modulation loss (dB)	N/A	N/A	N/A	
Data rate (dB-Hz)	50 (100 kbps)	50 (100 kbps)	74 (25 Mbps)	
Receive E_b/N_0 (dB)	31.5	31.8	17.8	
Theoretical E_b/N_0 (dB)	9.6	9.6	9.6	
Implementation loss (dB)	2	2	2	
Required E_b/N_0 (dB)	11.6	11.6	11.6	
Link Margin (dB)	19.9	20.2	6.2	

Table 2.4.3-1 MSCS/SS Link Budget for Ku-band Digital MA Communication (Single Digital TV Channel)

	Space Station/ MSCS CMD Link @ 14.63 GHz		MSCS/Space Station Digital TV Link @ 14.15 GHz	
	Value	Comments	Value	Comments
Transmitter power (dBm)	20	0.1 watt	47	50 watts
Transmit circuit loss (dB)	-2		-2	
Transmit antenna gain (dB)	0		0	
Transmit pointing loss (dB)	-3		-3	
EIRP (dBm)	15		42	
Path Loss (dB)	-95.7	R = 0.1 km	-95.4	R = 0.1 km
Received antenna gain (dB)	0		0	
Received pointing loss (dB)	-3		-3	
Polarization loss (dB)	-1.8		-1.8	
Received circuit loss (dB)	-2		-2	
Received signal power (dBm)	-97.5		-60.2	
System noise density (dBm/Hz)	-169	NF = 5 dB	-169	NF = 5 dB
Carrier to noise density (dB-Hz)	81.5		108.8	
Modulation loss (dB)	N/A		N/A	
Data rate (dB-Hz)	50	100 kbps	74	25 Mbp (5 Ch, 32-KPSK)
Receive E_b/N_0 (dB)	31.5		34.8	
Theoretical E_b/N_0 (dB)	9.6		29.5	32-level MPSK
Implementation loss (dB)	2		2	
Required E_b/N_0 (dB)	11.6		31.5	
Link Margin (dB)	19.9		3.3	

Table 2.4.3-2 MSCS/Space Station Links at Ku-band (5-Channel Digital TV)

3.0 CONCLUSIONS

The links between the MSCS and the Orbiter and between the MSCS and the Space Station have been examined from the standpoint of realizability and corresponding link budgets. We have considered both the S-band and Ku-band implementation of these links. Table 3-1 presents the summary of the link budgets.

From this table, it is evident that no link margin deficiencies exist for the command links at all bands and those telemetry links which are at S-band. For those telemetry links which are at Ku-band and are multiplexed with digital TV, the margins were not computed, but it is assumed here that they (i.e., margins) are not worse than the margins for the digital TV links.

Most significant comparison of the S-band and Ku-band operation of the 5-channel links is that the larger aperture of the S-band omni antennas provides a significant transmitter power saving when compared to Ku-band operation. Specifically, it takes 5 watts of transmitter power at S-band with an omni antenna and 50 watts at Ku-band with an omni antenna.

This implies that for Ku-band operation either antenna gains have to be increased with concomitant directivity problems or the transmitter power has to increase accordingly if the 32-level MPSK approach is to be adopted for simultaneous transmission of 5 digital TV channels. But, 50 watts of Ku-band power is already equal to the capability of the TWTA which is currently used with the Orbiter Ku-band radar/communication system. Thus, requiring more power at Ku-band does not seem like a feasible approach.

In comparison, if one were to use five parallel single-channel transmitters, the total Ku-band transmitter power would be 25 watts, i.e., 5 watts per channel. The bandwidth occupied would be at least 125 MHz. Furthermore, these multiple transmitters could be turned on when needed thus conserving power. This may not be a bad approach, afterall, for Ku-band operation.

Link	Band	Signal Transmitted	Origin	Destination	Rate	EIRP (dBm)	Link Margin (dB)	Comments
MSCS/ Shuttle Orbiter (SO)	S	CMD	SO	MSCS	2 kbps	30.4	64.5	Payload Interrogator Link
		TLM	MSCS	SO	16 kbps	15	37.8	Payload Interrogator Link
		Analog FM TV	MSCS	SO	Analog	25	15.8	Analog FM Receive
		Digital TV	MSCS	SO	25 Mbps	25	18.6	Requires Special Tx and Rx Equipment
	Ku	CMD	SO	MSCS	100 kbps	15	19.9	
		TLM	MSCS	SO	100 kbps	15	20.2	
		Digital TV	MSCS	SO	25 Mbps*	25	6.2	Single-Channel Digital TV
MSCS/ Space Station (SS)	S	CMD	SS	MSCS	2 kbps	30.4	64.5	
		TLM	MSCS	SS	16 kbps	15	37.9	
		Digital TV	MSCS	SS	25 Mbps*	32	9.6	5 Channels @ 25 Mbps via 32-level MPSK
	Ku	CMD	SS	MSCS	100 kbps	15	19.9	
		TLM	MSCS	SS	100 kbps	15	20.2	
		Digital TV	MSCS	SS	25 kbps	25	6.2	Single-Channel Digital TV
		Digital TV	MSCS	SS	25 Mbps*	42**	3.3	5 Channels @ 25 Mbps via 32-level MPSK

*Telemetry is assumed to be a small fraction of TV data rate, thus the multiplexing of TLM data stream with TV data is negligible on the link margin.

**Requires a 50 watts transmitter at Ku-band

Table 3-1. Link Budget Summary for MSCS/Orbiter and MSCS/Space Station Links (Range = 100 meters)

4.0 REMAINING ISSUES

The key remaining issue is the implementation of multi-channel digital TV links between MSCS and Space Station. We have baselined here an innovative approach, i.e, a 32-level MPSK for multiplexing of five digital TV channels within the bandwidth of a single 25 Mbps channel. We realize that we have to pay the penalty in power to stay within the bandwidth of a single channel. Such a trade-off is of particular importance for S-band utilization of multi-channel digital TV transmission if such utilization is considered as the only feasible alternative for multi-channel TV transmission. Also, if MPSK is to be adopted as a possible approach, there remains such technical issues as the effect of multi-path and the complexity of the equipment. Furthermore, MPSK equipment is different from the "baseline" Ku-band equipment, and thus the extra development cost must be considered. Consequently, further trade-offs are necessary to determine the most feasible approach to implementing simultaneous multi-channel digital TV transmission from MSCS.

5.0 REFERENCES

[1] "Space Station Reference Configuration Description," NASA/JSC Document No. JSC-19989, August 1984.